THE POCKELS' EFFECT IN LANGMUIR-BLODGETT FILMS

by

N Kalita B. Sc., M. Sc.

**A Thesis submitted in partial fulfilment
of the requirements for the degree of
Doctor of Philosophy**

Applied Physics Group

School of Engineering and Applied Science

The University of Durham

1991

DECLARATION

I hereby declare that the work carried out in this thesis has not been previously submitted for any degree and is not currently being submitted in candidature for any other degree

Signed.....

The work in this thesis was carried out by the candidate

Signed.....

Director of Studies

Signed.....

Candidate

DEDICATION

This thesis is dedicated to my parents

ACKNOWLEDGEMENTS

During my time at Durham I have become indebted to many people, whom I now wish to thank. Firstly, I am very grateful to my main supervisor Dr. Mike Petty for his time and effort in guiding my studies throughout my stay in Durham; also to Dr. Johnathan Lloyd for his direction during his stay at Durham. I have found working with them to be stimulating and rewarding. I am also indebted to everyone in the Department of Applied Physics and Electronics for their friendship, good humour and sharing of ideas. I wish to thank in particular the technical staff, headed by Mr Frank Spence; the mechanical workshop staff directed by Mr Brian Blackburn and the electronics workshop staff under Mr Peter Friend, who have all contributed their skills and knowledge. My thanks also go to Mrs Kay Cummings and Ms Julie Morgan for their efforts in preparing the diagrams. I am also grateful to the computer centre staff, headed by Brian Lander, for their instruction and speedy resolution of numerous computing difficulties, mostly of my own making.

I greatly appreciate the efforts of Dr Andrew McRoberts of the University of Hull, and Dr John Tsibouklis in synthesising the compounds described in this thesis, without which the work could not have been undertaken. I am also indebted to Drs Jack Brettle and Ian Stuart of Plessy Research (Caswell) for passing to me several materials and many ideas. The second harmonic generation measurements were performed with the collaboration of Drs Neil Carr and Martin Goodwin of Plessy Research (Caswell) and Dr Graham Cross, whose assistance has been very helpful to the research in this thesis. Thanks also to Dr Yuri Lvov of the Institute of Crystallography, Lebedev Institute, Moscow for his X-ray diffraction analysis. I gratefully acknowledge the financial support given me by the S.E.R.C. and Plessy Research (Caswell) Ltd. for the provision of a C.A.S.E. award.

Many personal friends have helped me in recent years, particularly the folks at the Parsonage; certain ladies, too numerous to thank individually here, it has been my delight to know whilst at Durham; and the University Sub Aqua Club, for much-needed extra-curricular activities above and under water. Lastly, but most importantly, thanks to my mother for her determination, support and encouragement over the years.

ABSTRACT

Simple, compact and inexpensive automated apparatus for recording surface plasmon resonance and the Pockels (or linear electro-optic) effect in Langmuir-Blodgett films has been used to estimate the thickness, permittivity and second order nonlinear susceptibility $\chi^{(2)}_{zzz}(-\omega;\omega,0)$ of several novel Langmuir-Blodgett film-forming materials. The results agree with estimates of nonlinear susceptibility obtained by second-harmonic generation.

The materials synthesised at Durham were all functionalised diaryl alkynes of the general formula $CH_3(CH_2)_n(Py^+)C{\equiv}C(Ph\text{-}R)$, wherein n =17 or 21 and R=H or OCH_3. Of these, that with n =21 and R=OCH_3 showed particularly promising Langmuir-Blodgett film-forming properties; its nonlinear susceptibility per monolayer, however, was approximately one hundredth that of a hemicyanine monolayer. The nonlinear susceptibility per monolayer, as measured by the Pockels effect and second harmonic generation, was inversely proportional to the square root of the film thickness. This indicated rapid deterioration of in-plane order with increasing film thickness.

Several novel polymeric materials synthesised at Hull and examined at Durham consisted of a siloxane spine of approximately 16 Si atoms, with randomly substituted bipolar chromophoric sidegroups. All were highly stable in floating film form. Of them, one known as AMCR23 showed promising optical nonlinearity when deposited on silver: a nonlinear susceptibility of -15+9.6i pm V^{-1} was recorded for a monolayer (cf. 94.5+49.9i pm V^{-1} for a hemicyanine monolayer).

CONTENTS

1 INTRODUCTION 5

2 THEORY 7

2.1 INTRODUCTION 7

2.2 SURFACE PLASMON RESONANCE 7

2.2.1 Historical Background 7

2.2.2 Theory 8

2.2.3 Interaction of light with surface plasmons 9

2.2.4 Effects Contributing to SPR 12

2.2.5 (a) Material Parameters 12

2.2.6 (b) Thermal Effects 13

2.2.7 (c) Piezoelectricity 14

2.3 NONLINEAR OPTICS 15

2.3.1 Introduction 15

2.3.2 Background 15

2.3.3 Physical Origins 15

2.3.4 Linear Susceptibilities 16

2.3.5 Nonlinear Phenomena and Applications 17

2.4 THE POCKELS EFFECT 18

2.4.1 Background 18

2.4.2 Relationship to Surface Plasmons 18

2.4.3 Effects Contributing to the Pockels' Effect 19

2.4.4 (a) The Converse Piezoelectric Effect 20

2.4.5 (b) Stark Effect (Electroabsorption) 20

2.4.6 (c) Contributions from the Substrate 21

2.4.7 (d) Cubic Responses 21

2.4.8 (e) Frequency Dependence 22

2.5 SUMMARY 22

2.6 REFERENCES 23

3 LANGMUIR- BLODGETT FILM TECHNOLOGY 26

3.1 INTRODUCTION 26

3.2 HISTORICAL BACKGROUND 26

3.3 BASIC CONCEPTS 27

3.4 MATERIALS 29

3.4.1 Classical Materials 29

3.4.2 Novel Materials from the Literature 31

3.4.3 Novel Materials used in this project 31
3.5 THE STANDARD LANGMUIR-BLODGETT TROUGH 32
3.5.1 Mechanical Construction 32
3.5.2 Instrumentation 32
3.5.3 Minimisation of Contamination 33
3.6 THE ROTARY LANGMUIR-BLODGETT TROUGH 34
3.6.1 Mechanical Construction and Instrumentation 34
3.6.2 Cross-Contamination 34
3.7 PROPERTIES OF THE FLOATING MONOLAYER 35
3.7.1 Pressure-Area Isotherms 35
3.7.2 Monolayer Stability 36
3.7.3 Monolayer Mobility 36
3.8 EXPERIMENTAL METHODS 37
3.8.1 Monolayer Spreading 37
3.8.2 Monolayer Compression 37
3.8.3 Langmuir-Blodgett Film Deposition 38
3.9 QUALITY ASSESSMENT 39
3.10 SUMMARY 40
3.11 REFERENCES 41

4 EXPERIMENTAL METHODS 43
4.1 INTRODUCTION 43
4.2 SAMPLE PREPARATION 43
4.2.1 Substrate Preparation 43
4.2.2 Thermal Evaporation 43
4.3 SURFACE PLASMON RESONANCE 44
4.3.1 Experimental Technique 44
4.3.2 Data Acquisition 45
4.3.3 Interpretation of Results and Curve Fitting 49
4.4 THE POCKELS EFFECT 51
4.4.1 Measurement 51
4.4.2 Analysis of Results 52
4.5 OPTICAL ABSORPTION SPECTRA 55
4.5.1 Introduction 55
4.6 ELLIPSOMETRY 56
4.6.1 Introduction 56
4.6.2 Theory 56
4.6.3 Experimental Arrangement 57

4.7 SECOND HARMONIC GENERATION FROM LB FILMS 58
4.8 SUMMARY 59
4.9 REFERENCES 61
5 CHARACTERISATION OF FLOATING MONOLAYERS AND MULTILAYER FILM DEPOSITION 63
5.1 MATERIALS 63
5.1.1 Hemicyanine and Nitrostilbene (4HANS) 63
5.1.2 Novel Polysiloxanes 64
5.1.3 Novel Bipolar Chromophores 65
5.2 PRESSURE-AREA ISOTHERMS AND STABILITY STUDIES 67
5.2.1 Exemplary Standards : Stearic Acid 67
5.2.2 Novel Polysiloxanes 69
5.2.3 Novel Bipolar Chromophores 70
5.3 FILM TRANSFER 71
5.3.1 Novel Polysiloxanes 71
5.3.2 Novel Dipolar Chromophores 74
5.4 RHEED and X-RAY DATA 74
5.5 SUMMARY 74
5.6 REFERENCES 76
6 LINEAR MEASUREMENTS: RESULTS AND DISCUSSION 77
6.1 INTRODUCTION 77
6.2 OPTICAL ABSORPTION 77
6.2.1 Background 77
6.2.2 Novel Materials 85
6.3 ELLIPSOMETRY 85
6.3.1 Introduction 85
6.3.2 Polysiloxanes and Diaryl Alkynes 87
6.4 SURFACE PLASMON RESONANCE 88
6.4.1 Equipment Calibration 88
6.4.2 Silver Substrates 88
6.4.3 Novel Materials 92
6.5 ELECTRON AND X-RAY DIFFRACTION 96
6.6 SUMMARY 97
6.7 REFERENCES 98
7 NONLINEAR OPTICAL TECHNIQUES: RESULTS AND DISCUSSION 99
7.1 INTRODUCTION 99

7.2 SECOND HARMONIC GENERATION 99
7.2.1 Background 99
7.2.2 Polysiloxanes 99
7.2.3 Diaryl alkynes 103
7.3 THE POCKELS EFFECT 105
7.3.1 Hemicyanine monolayers 105
7.3.2 Silver and Fatty Acids 108
7.3.3 Polysiloxanes 110
7.3.4 Diaryl Alkynes 112
7.4 SUMMARY 117
7.5 REFERENCES 118

8 CONCLUSIONS 120

9 SUGGESTIONS FOR FURTHER WORK 122

Appendix A Derivation of the Relationship between Permittivity and the Piezoelectric Coefficent 123

Appendix B Laser Beam Collimation 126

Appendix C Listing of the SPR and Pockels Data Acquisition Program Source Code 130

Appendix D Publications 163

Chapter I

INTRODUCTION

It is widely anticipated that nonlinear optical phenomena, in which electromagnetic fields interact to produce new waves with different propagation characteristics, will form the basis for high bandwidth logic and communication devices. The use of subtle methods of organic synthesis offers a broader and more precise range of material properties than is available through relatively well-established fabrication methods such as ion implantation, modulation doping, vapour phase growth and many other techniques common to the semiconductor industry. Synthetic methods for optimisation of molecular nonlinearities are currently under intense scrutiny, as are the techniques for improving other characteristics such as stability, ease of preparation, laser damage thresholds and compatibility with existing microelectronic fabrication methods. The enormous effort involved in such multidisciplinary research seems justified in view of the fact that molecular transition lifetimes can be as low as several femtoseconds, with a corresponding enormous bandwidth $\sim 10^{14}$Hz. Furthermore, as the interactions are essentially intramolecular, the typical scale of operations is on the order of nanometres. Bulk semiconductor devices, on the other hand, fall victim to detrimental effects such as crossover when their size becomes comparable to a Debye length, on the order of a micrometre.

The largest nonlinear effects are usually seen in bulk single crystals under intense coherent illumination. It comes as no surprise, therefore, that a lot of nonlinear optics is related to the use of bulk material for frequency conversion of high power laser beams. For device applications and initial evaluation, however, fabrication in thin film form is advantageous. One especially elegant method is that pioneered by Langmuir and Blodgett, which allows amphiphilic molecules to be deposited in oriented mono- and multilayers of precise thickness. Monolayer deposition and alternate deposition of two different materials leads to the noncentrosymmetric structure required for second order nonlinearity. The optical nonlinearities of such structures may be probed by a variety of methods. This thesis is largely concerned with the Pockels effect and second harmonic generation for evaluation of optical nonlinearities of Langmuir-Blodgett films. Relevant linear optical behaviour is also discussed.

A general introduction to surface plasmon resonance and nonlinear optics is presented in chapter two, which ends with a discussion on the Pockels effect. Chapter three is concerned with the instrumentation for fabrication of LB films; this deals with a description of the materials, experimental methods, rudimentary characterisation techniques and equipment associated with the fabrication process. Chapter four lists the various methods used to determine optical, structural, and dielectric properties. The bulk of the results is presented in chapters five to seven inclusive. Chapter five is concerned with the properties of floating Langmuir films. Chapter six contains information derived from linear measurements including ellipsometry, surface plasmon resonance, spectrophotometry and x-ray and electron diffraction. The final results chapter deals with optical nonlinearities as measured by the Pockels effect and SHG. The closing chapters list a summary and conclusions and suggestions for further work.

Chapter II

THEORY

2.1 INTRODUCTION

This chapter, in three major portions, contains an introduction to two of the characterisation techniques described in subsequent chapters. The first section on SPR describes the historical background and theory of surface plasmon resonance, its experimental realisation and its applications. The next portion deals briefly with the history and origins of nonlinear optics and the applications of nonlinear phenomena. The final portion on the Pockels effect describes its background, physical origins, relationship to surface plasmons and the elimination of undesirable contributory effects.

2.2 SURFACE PLASMON RESONANCE

2.2.1 Historical Background

Interest in surface electromagnetic wave (SEW) propagation began at the turn of the century, when a first definition of a SEW was formulated. Work on SEW propagation received a boost in the late 1950's, when the energy loss spectra of electrons on reflection from thin metallic films were first examined [Bohm et. al., 1953; Powell et. al., 1959 (two papers) ; Stern et. al., 1960]. It was found that certain loss peaks occurred at fixed energy irrespective of primary bombarding energy or scattering angle. More impetus was given to the work in the late 1960's when Otto, Raether and Kretschmann pointed out that SEWs could be excited by attenuated or frustrated total reflection (ATR and FTR respectively) methods [Otto, 1968; Kretschmann & Raether, 1968] which have since become common means of exciting SEWs. The theoretical work on the subject is mostly quite recent and relies largely on interpreting SEW propagation in terms of the behaviour of the oscillatory modes of a two-dimensional electron gas. Due to this, SEWs have come to be known as surface plasmons rather than surface electromagnetic waves.

Surface plasmons have remained very much a tool for the probing of layered structures and interfaces [Kovacs, 1982; Pockrand et.al., 1977; Pockrand, 1978; Wähling,

1978; Wähling et. al., 1979; Zhizhin et. al., 1982]; they may, however have a variety of applications outside of the laboratory as, for example, in biosensors and gas detectors [Roberts, 1990].

2.2.2 Theory

Several interpretations of the behaviour of two-dimensional plasmas have arisen since the 1950's. The two most fundamental theoretical approaches treat the electron gas at the interface between media of different permittivities either as a classical fluid moving against a background of positive charge, which is a hydrodynamic model [Boardman, 1982; Bohm et.al., 1953; Stern et. al., 1960], or as a collection of quasi-particles which may be treated quantum-mechanically using such methods as the random phase approximation [Dasgupta et. al., 1982]. These methods have been shown to be largely equivalent [Boardman, 1982]. Less detailed, although perhaps more meaningful to the experimentalist, is the electromagnetic wave approach to surface plasmons, in which the main features of the SEW are derived by adopting trial solutions to Maxwell's equations [Landau et. al., 1948]. Then, the major simplifying assumptions are that the interface between two semi-infinite isotropic media 1 and 2 is abrupt, that the magnetic permeabilities of the two media are both unity and that the (complex) dielectric functions ϵ_1 and ϵ_2 are independent of the wave vector in the absence of spatial dispersion. The assumed solutions to Maxwell's equations in this case are electromagnetic waves travelling parallel to the interface between the two media, and decaying exponentially normal to that interface. A schematic diagram of such an electric field is shown in figure 2.1. These waves can only exist at interfaces between media of dielectric functions of opposite signs, such as a metal and a dielectric. Application of the boundary conditions on the electric and magnetic fields at the interface shows that the SEWs are all TM modes (i.e. the SEW field is p- polarised). Accordingly, incident particles (be they photons or electrons) must have k-vector components in the plane of the interface in order to excite SEW modes. Taking the direction of SEW propagation to be along the positive x-axis between a metal of permittivity $\epsilon_2 = \epsilon$ and a vacuum ($\epsilon = 1$), it can be shown [Boardman, 1982] that the dispersion relation of the SEW field is

$$n^2 = \frac{1 - (\omega_p/\omega)^2}{2 - (\omega_p/\omega)^2} = \frac{\Omega^2 - 1}{2\Omega^2 - 1} \tag{2.1}$$

where $\Omega = \omega/\omega_p$ and $n = ck_x/\omega$ is a surface mode 'refractive index' , ω_p the plasma frequency and ω the angular frequency of incident light. The plasma frequency and

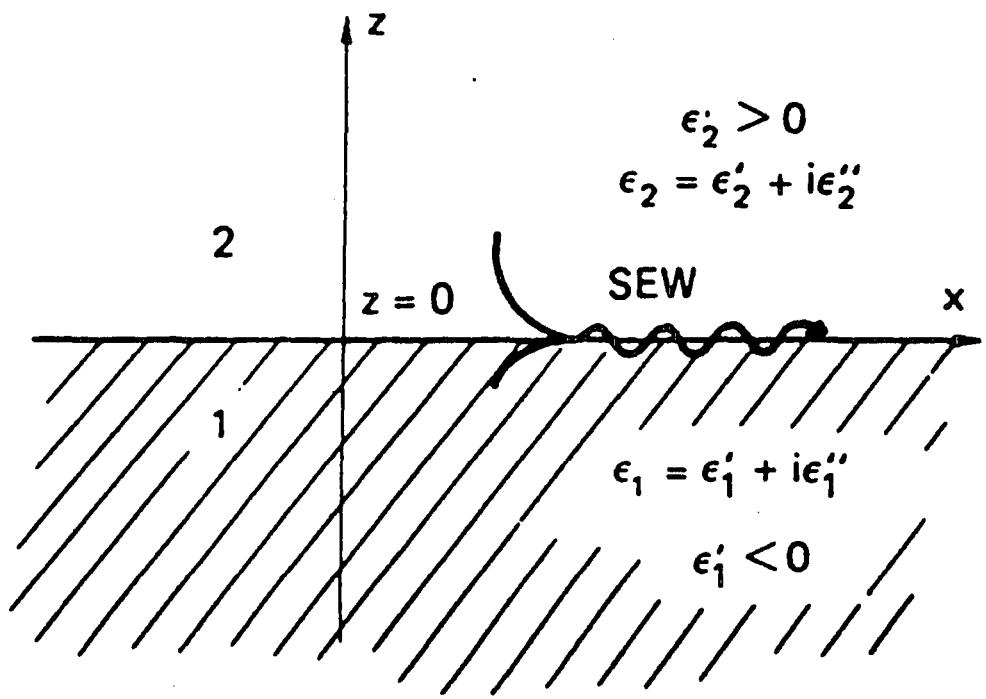

Figure 2.1 : SEW Electric fields

permittivity are related by $\epsilon = 1 - (\omega_p/\omega)^2$.

A typical dispersion relation is shown in figure 2.2 on the same axes as that for photons, which is the "light line ", given by $n^2 = 1$. The wavenumber k is represented by $K = ck/\omega_p$. The light line emphasises the difference between the two sets of SEW modes: the Brewster modes, for which $n^2 < 1$ and the Fano modes, for which $n^2 > 1$. Fano modes are nonradiative; Brewster modes are nonradiative only if the imaginary part of $\epsilon(\omega)$ is small [Boardman, 1982; Halevi, 1982]. As seen from figure 2.2 , Brewster modes are asymptotic to $ck\sqrt{2}$ while Fano modes are asymptotic to $\omega_p/\sqrt{2}$; we are concerned exclusively with the Fano modes. At this point, it is necessary to define the terminology pertaining to SEWs, prior to discussing the means by which they may be made to interact with other kinds of waves. A surface plasmon is a purely electromagnetic wave of the type described above. The term "polariton" originally designated "polarisation field particles analogous to photons" but has since come to denote the coupling of photons to the polar excitations of solids. Specifically, a surface plasmon-polariton denotes the coupling of light to a surface plasmon, and surface phonon-polaritons and magnon-polaritons have analogous meanings. From here on, we shall deal exclusively with surface plasmon-polaritons (SPPs) and the means by which they may be excited.

2.2.3 Interaction of light with surface plasmons

In considering the excitation of Fano mode SPPs of wavevector q_x by photons of frequency ω and $x-$component of wavevector k_x the laws of conservation of energy and momentum may be used to show that

$$\omega = \frac{c}{\sqrt{\epsilon}}\sqrt{k_x^2 + q_x^2} \tag{2.2}$$

The modes, however, obey the inequality [Mirlin, 1982]

$$\omega \leq \frac{c}{\sqrt{\epsilon}} q_x \tag{2.3}$$

The last two equations cannot be simultaneously valid for real k_x. Physically, this means that the light line does not cross the Fano mode dispersion curve, as can be seen from figure 2.2, and the light and SEW do not interact. In the case of imaginary k_x, however, the above two equations may be simultaneously valid. This happens when the SPP is excited by an evanescent wave. Then, the light line's

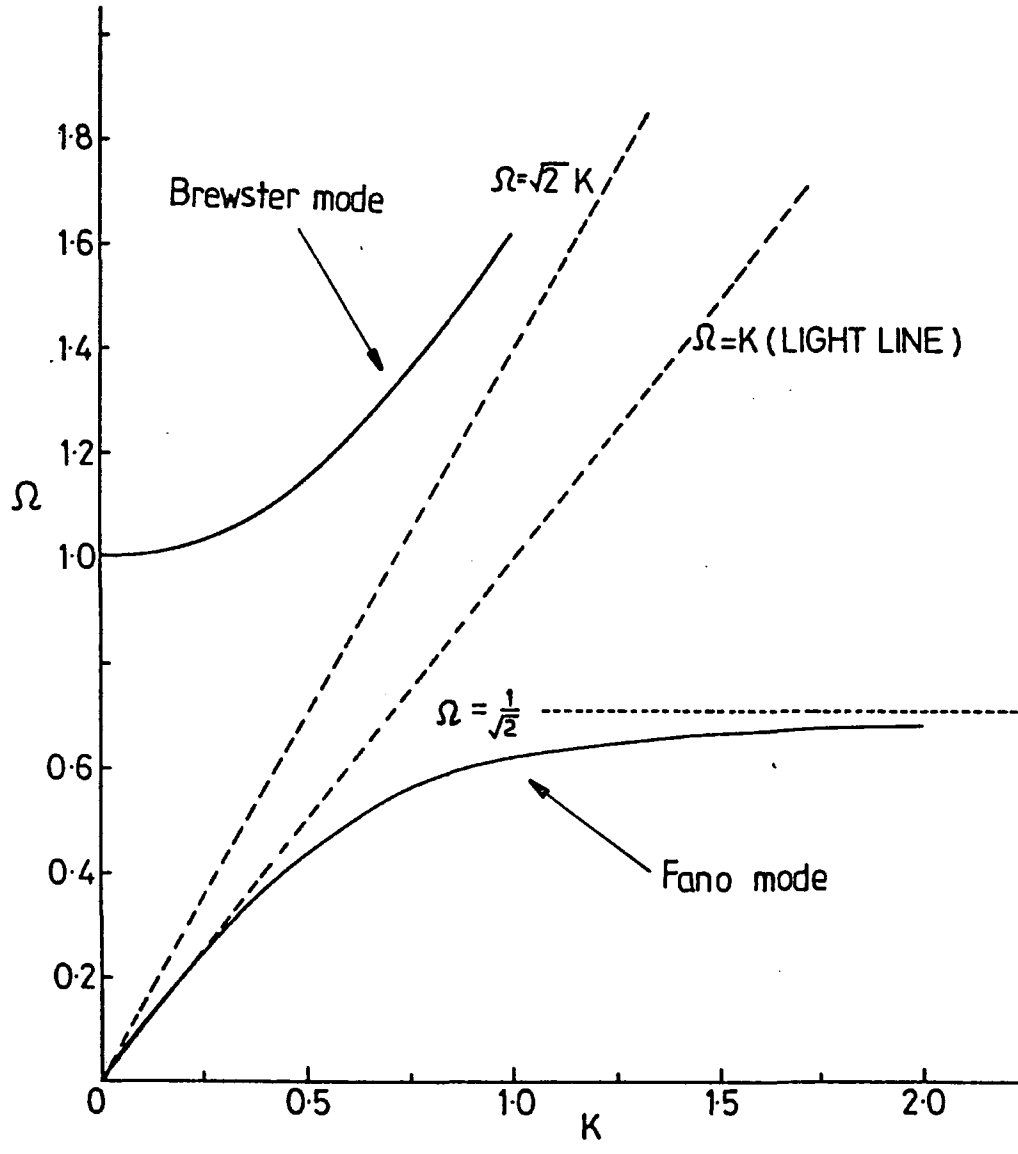

Figure 2.2 : SEW dispersion relation and the 'light line'

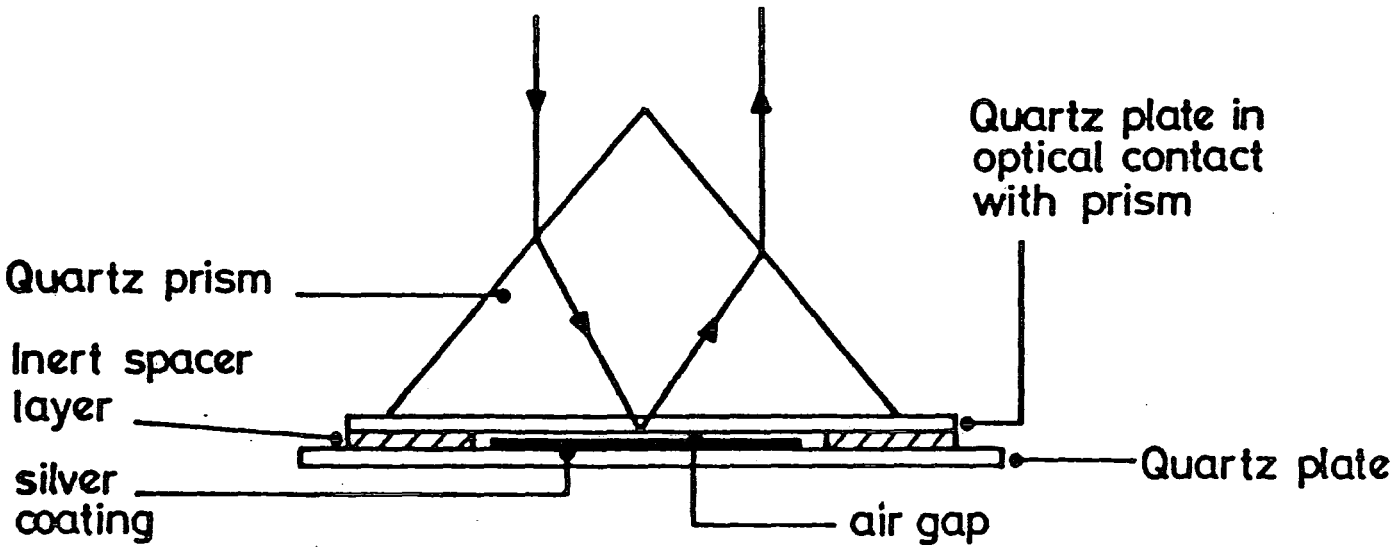

Figure 2.3 : The Otto configuration for SEW excitation

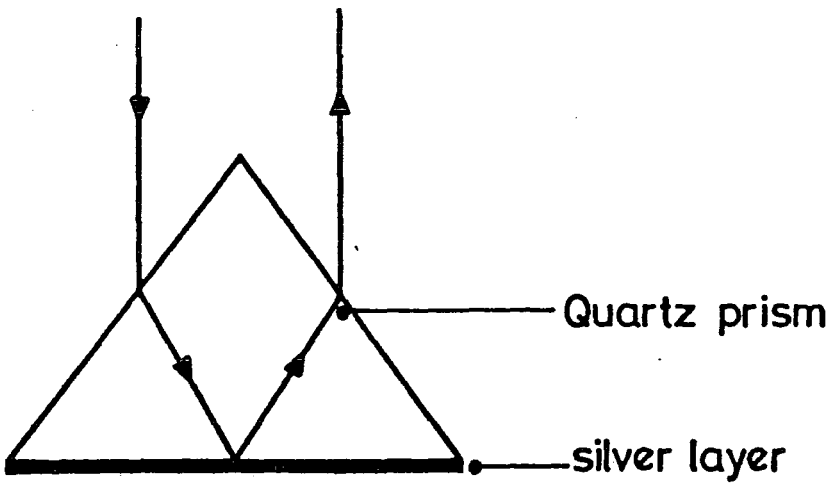

Figure 2.4 : The Kretschmann configuration for SEW excitation

slope is reduced by propagation through a high refractive index medium ($|k_x|$ is increased) and total internal reflection makes k_x imaginary. As k_x is increased, the slope of the light line decreases until a point is reached at which it crosses the SEW dispersion curve. This situation was realised by Otto, Raether and Kretschmann and led to the development of the two classical experimental arrangements for exciting SPPs in ATR geometries [Otto, 1968; Kretschamnn & Raether, 1968]. Schematic diagrams of the Otto and Kretschmann arrangements are shown in figures 2.3 and 2.4, respectively. The former relies on total internal reflection within a prism at a prism/air interface. Evanescent waves near the interface are coupled into SEW modes of a metal film separated from the prism by an inert spacer layer. In the latter case, the metallic film constitutes a spacer layer and the interface along which SEWs propagate is between the silver/dielectric boundary. In each configuration, the existence of SPPs is inferred from the reflectivity of the prism assembly: when the k_x component of incident light matches that of the SEW dispersion relation, SPPs absorb energy from the evanescent wave, leading to a sharp drop in reflectivity which is known as surface plasmon resonance (SPR). When the wavevectors do not match, the reflectivity of the assembly is close to unity. Clearly, there are two methods by which this can be observed: scanning the prism over a range of angles of incidence at fixed frequency, or scanning over a range of frequencies at fixed angle of incidence. The former corresponds to a section of the SEW dispersion relation parallel to the k_x-axis, the latter to a section through the $\omega-$axis; this work deals exclusively with scans at fixed frequency over a range of wavevectors. In that case, the reflectivity curves obtained closely resemble inverted log-linear distributions, as can be seen from the specimen plots for silver films overlaid with 22-TA shown in figure 2.5. The methods of data acquisition are discussed in chapter four.

2.2.4 Effects Contributing to SPR

2.2.5 (a) Material Parameters

Several phenomena influence the values of thickness and dielectric function derived from SPR. They include the adhesive qualities of silver and glass, moisture, surface roughness and sulphides. The former can be improved by rapid evaporation of silver overlayers onto the glass substrates; an evaporation rate of 4nm s^{-1} seems adequate in this respect. Moisture cannot be removed from any evaluation of silver layers which are to be used as substrates for LB films. Surface sulphides are kept to a minimum by using silver layers immediately after deposition.

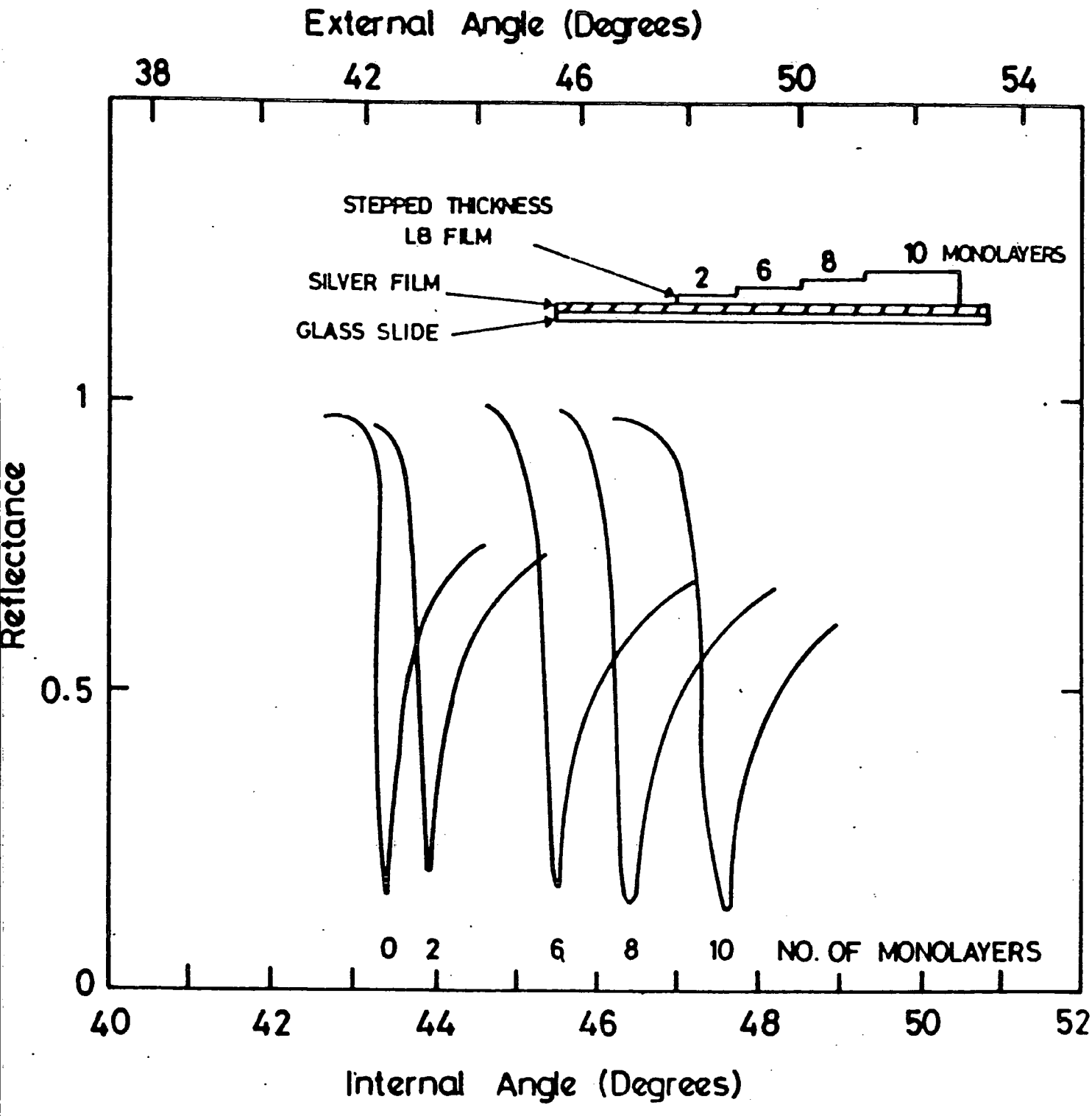

Figure 2.5 : Specimen SPR plots for a glass slide with a 50nm silver film coated with 0, 2, 6, 8, 10 monolayers of 22- TA

2.2.6 (b) Thermal Effects

As the SPR of silver layers is examined with a continuous-wave He-Ne laser, it is possible that local heating may alter the silver film properties through thermal expansion. To estimate the local heating at the laser spot we use the approach taken by Janossy et. al. in 1985 which predicts the temperature rise at the centre of a Gaussian input spot incident on a thin film on a semi-infinite substrate. For a spot temperature T_S an ambient temperature T_F, spot size w_0, film conductivity κ, absorption coefficient A and input power P,

$$T_S - T_F = \frac{PA}{2\kappa w_0 \sqrt{\pi}} \tag{2.4}$$

The beam input power is ~1mW with spot size ~1mm and the silver thermal conductivity is 418 $\mathrm{Wm^{-1}K^{-1}}$. The heating effect will be most pronounced at the SPR minimum where the absorption reaches a peak. Taking the minimum reflectivity as 0.01 sets A to approximately unity. This sets the temperature difference between the laser spot and the ambient medium as less than 10^{-3}K, which is too small to greatly influence the silver film properties. For instance, the thermal expansivity of silver is $19.2\times10^{-6}\mathrm{K^{-1}}$, so any change in silver film thickness can be safely ignored. Experiments treating the silver layer as one junction of a thermocouple have reported a thermoelectric voltage of 10μV, corresponding to a temperature rise of approximately 0.05K [Innes & Sambles, 1985].

2.2.7 (c) Piezoelectricity

There are two piezoelectric effects. The direct effect is a stress-induced electric displacement; the converse effect is an electric field-induced strain. As electric fields are applied when measuring the Pockels' effect, but not when measuring SPR curves, the discussion of the converse effect is delayed to a later section. The direct effect, on the other hand, may appear even though silver is not piezoelectric. As the silver substrate is heated, the differential expansion of LB film and silver induces stresses in the LB film. It may be shown (see appendix A) that if the LB film is piezoelectric, the permittivities at constant stress (ϵ^σ) and constant strain (ϵ^ε) are related to the piezoelectric coefficient d and the compliance s by

$$\epsilon^\sigma = \epsilon^\varepsilon - \frac{d^2}{s} \tag{2.5}$$

where the tensor nature of all quantities has been ignored. This represents an extreme case; an LB film on a heated substrate will generally be partly stressed and partly strained. No estimates of the piezoelectric coefficient are available in the literature for the nonlinear dyes used here. Other materials examined, however, include polyvinylidene fluoride (PVDF) with $|d| \sim 10 \mathrm{pCN}^{-1}$ and $|s| \sim 10^{-9} \mathrm{m}^2\mathrm{N}^{-1}$ [Nix, 1988], giving a contribution to permittivity of $\sim 10^{-13}$. Resorcinol crystals have been examined [Koptsik, 1952] and found to have $|d| \sim 0.1 \mathrm{pCN}^{-1}$ and $|s| \sim 10^{-10} \mathrm{m}^2\mathrm{N}^{-1}$, which amounts to a contribution of $\sim 10^{-16}$ to the permittivity. Presuming the piezoelectric coefficients and compliances of the materials described here to be of a similar order of magnitude in LB film form allows us to safely ignore any directly piezoelectrically-induced permittivity changes.

2.3 NONLINEAR OPTICS

2.3.1 Introduction

This section deals briefly with nonlinear optical effects and materials. A short section on the history and physical origins of nonlinear behaviour is followed by a list of nonlinear phenomena. Subsequent sections deal specifically with the Pockels' effect, phenomena which may mimic or obscure it and the methods used to eliminate them.

2.3.2 Background

Despite the discovery of nonlinear optical susceptibilities near the turn of the century and their expression in quantum-mechanical terms in the 1930's and 1940's, nonlinear optics received virtually no stimulus until twenty years later. This is because the field strengths required to observe nonlinear phenomena must be significant compared to those binding electrons to nuclei, which are $\sim 10^{10} \mathrm{Vm}^{-1}$. Compared to the field strength of bright sunshine, which is about $500 \mathrm{Vm}^{-1}$, this is enormous and was unattainable until relatively recently. Nowadays, pulsed Nd:YAG lasers with a peak power of $500 \mathrm{MWcm}^{-2}$ are by no means rare and have a corresponding field strength $\sim 10^{8} \mathrm{Vm}^{-1}$, making nonlinear phenomena accessible.

2.3.3 Physical Origins

Maxwell's equations describe completely the behaviour of macroscopic electric and magnetic fields. To describe the interaction of the fields with matter, another set of equations, the "constitutive relations" , between the field vectors and the moments

of charge and current distributions are required. These link the response of a medium with any incident electromagnetic wave; they are not linear. The electric polarisation in particular can be written

$$\frac{\mathbf{P}-\mathbf{P}_0}{\epsilon_0} = \chi^{(1)}:\mathbf{E} + \chi^{(2)}:\mathbf{EE} + \chi^{(3)}:\mathbf{EEE} + \ldots \tag{2.6}$$

where $\mathbf{P}_0$ is the polarisation with no applied field, ϵ_0 the permittivity of free space and $\chi^{(n)}$ is the nth order susceptibility tensor. Terms in the series beyond $\chi^{(3)}$ have to date been insignificant. The $\chi^{(n)}$ can be expressed quantum-mechanically [Shen, 1984; Bloembergen, 1965] and are always present unless symmetry properties of the interacting medium remove some or all of their components. Linear optics ignores terms beyond $\chi^{(1)}$. The following sections examine the various contributions to $\mathbf{P} - \mathbf{P}_0$.

2.3.4 Linear Susceptibilities

The linear susceptibility is responsible for refraction and attenuation. When the applied field is a wave of frequency ω, the linear polarisation is a radiative wave of the same frequency that modifies the propagation of the incident wave. The linear polarisation is given by

$$\mathbf{P}^{(1)} = \epsilon_0 \chi^{(1)} \mathbf{E} \tag{2.7}$$

while the electric displacement is

$$\mathbf{D} = \epsilon_0 \mathbf{E} + \mathbf{P}^{(1)} = \epsilon_0 (1 + \chi^{(1)}) \mathbf{E} = \epsilon_0 \epsilon_r \mathbf{E} \tag{2.8}$$

with ϵ_r as the relative permittivity. The refractive index is given by

$$\mathbf{n} = \sqrt{\epsilon_r} = \sqrt{1 + \chi^{(1)}} \tag{2.9}$$

which is generally complex. The real part of refractive index is responsible for propagation while the imaginary component causes attenuation of the electric field. When the optical field contains several waves at different frequencies, they propagate independently in the linear regime.

2.3.5 Nonlinear Phenomena and Applications

If an applied electric field consists of a dc and an optical frequency ac component

$$E = E_0 + E_\omega \cos(\omega t) \tag{2.10}$$

equation 2.6 may be used to find the induced nonlinear polarisation. It turns out to contain various harmonic and cross terms corresponding to different admixtures of the incident fields; all are listed in table 2.1. The first two components are due to linear susceptibility and have been described in the above section.

The dc hyperpolarisability is a quadratic contribution to the static electric field. The Pockels' effect, used for modulation and variable phase retardation, is discussed in later sections. Optical rectification can be seen as the interference of a pump wave with its phase-shifted counterpart to produce a static intensity-dependent polarisation. Second harmonic generation (SHG), which has no linear counterpart, is the mixing of two pump waves to produce a third wave at twice the pump frequency. It is commonly used to up-convert infrared laser lines to the visible region. This is a special case of sum- and difference-frequency generation, where pump waves at frequencies ω_1 and ω_2 combine to produce signal waves at $\omega_3 = \omega_1 \pm \omega_2$. If $\omega_3 > \omega_2 \gg \omega_1$, the same physical process is utilised in parametric oscillators, where ω_3 pumps a nonlinear material in a cavity resonant at ω_2 and ω_1. The signal at $\omega_1 \sim 0$ need not be provided explicitly, as it usually arises from spontaneous emission in the cavity. Parametric oscillation is a means of generating coherent tunable radiation between microwave and optical frequencies.

There is also a cubic contribution to the static electric field, known as the dc hyperhyperpolarisability. The dc Kerr (quadratic electro-optic) effect, is used for variable phase retardation and liquid crystal displays. The dc polarisation proportional to the optical field intensity resembles optical rectification and has similar applications in conversion of light signals to electrical ones. The dc-induced SHG arises from the resemblance of the term $\chi^{(3)}E_0^2$ to a second-order susceptibility. Third harmonic generation is used for up-conversion of infrared light into the far ultraviolet. The optical frequency Kerr effect has applications in high speed logic gates, optical bistability, phase conjugation, real time holography, amplification and amplitude chopping.

Term in P	Frequency	Phenomenon	Application
Linear Contributions to Polarisation			
$\chi^{(1)}E_0$	0	dc polarisability	
$\chi^{(1)}E_\omega \cos(\omega t)$	ω	Dispersion, refraction	Dispersion removal in e.g. optical fibres
Quadratic Contributions to Polarisation			
$\chi^{(2)}E_0^2 = (\chi^{(2)}E_0)E_0$	0	dc hyperpolarisability	$\chi^{(1)}$ modulation
$(2\chi^{(2)}E_0)E_\omega \cos(\omega t)$	ω	Pockels effect. Change in $\chi^{(1)} \propto$ dc field	Modulation, variable phase retardation
$\frac{1}{2}\chi^{(2)}E_\omega^2$	0	Optical rectification	Hybrid optical communication devices
$\frac{1}{2}\chi^{(2)}E_\omega^2 \cos(2\omega t)$	2ω	SHG	IR to visible conversion
Cubic Contributions to Polarisation			
$\chi^{(3)}E_0^3$	0	dc hyperhyperpolarisability	Cubic contribution to static polarisation
$(3\chi^{(3)}E_0^2)E_\omega \cos(\omega t)$	ω	dc Kerr effect. Refractive index change $\propto$(dc field)^2	Variable phase retardation, liquid-crystal displays
$(\frac{3}{2}\chi^{(3)}E_\omega^2)E_0$	0	dc polarisation; intensity-dependent refractive index	Hybrid optical communication devices
$((\frac{3}{2}\chi^{(3)}E_0)E_\omega^2)\cos(2\omega t)$	2ω	dc-induced SHG	$\chi^{(2)}$ modulation
$\frac{1}{4}\chi^{(3)}E_{2\omega}^3 \cos(3\omega t)$	3ω	THG	Deep UV up-conversion
$\frac{3}{4}\chi^{(3)}E_\omega^3 \cos(\omega t)$	ω	Optical Kerr effect	Self-focussing, bistability, phase conjugation, holography

Table 2.1 : Contributions to Optical Polarisation and their Applications

Nonlinear interactions are by no means limited to electromagnetic waves. For instance, Raman scattering is the result of mixing between optical and vibrational excitations; Brillouin scattering is the mixing of electromagnetic and sound waves; Rayleigh scattering deals with excitation of entropy waves and Rayleigh-wing scattering relates to molecular orientational excitation [Fabellinskii, 1968].

2.4 THE POCKELS EFFECT

2.4.1 Background

The electro-optic effect is one of the earliest optical nonlinearities to be observed [Pockels', 1906]. The subject of exhaustive study in the 1890's, it was soon established that under the influence of a sufficiently strong electric field, isotropic (cubic) crystals become uniaxial and uniaxial crystals may become biaxial through the Pockels' and related Kerr effect. Although this can be interpreted as a nonlinear polarisation within the crystal, it is conventionally expressed as a refractive index change described by a modification of the tensor components of the inverse dielectric constant matrix.

It is a confusing curiosity that the Pockels' effect is still frequently referred to as the linear electro-optic effect, despite the fact that the physics lies firmly in the field of nonlinear optics.

2.4.2 Relationship to Surface Plasmons

The Pockels' effect is usually thought of as electro-optic behaviour of uniaxial and biaxial crystals. Thin film structures lacking inversion symmetry, such as non-centrosymmetric LB overlayers, also show field-induced refractive index changes. To see how they are related to the nonlinear susceptibilities, consider the (scalar) optical dielectric constant $\epsilon(\omega, E)$, where $E = E(\Omega)$ is a weak low frequency ($\Omega \sim 0$) applied field. The permittivity can be expanded in a Taylor series

$$\epsilon(\omega, E) = \epsilon(\omega) + E\frac{\partial\epsilon(\omega)}{\partial E} + \frac{E^2}{2}\frac{\partial^2\epsilon(\omega)}{\partial E^2} + \ldots \tag{2.11}$$

but as

$$\epsilon E = \epsilon_0 E + P \tag{2.12}$$

and

$$\frac{P}{\epsilon_0} = \chi^{(1)}E + \chi^{(2)}E^2 + \ldots \tag{2.13}$$

evidently,

$$\epsilon_0(1 + \chi^{(1)}) = \epsilon(\omega) \tag{2.14}$$

$$\epsilon_0\chi^{(2)} = \frac{\partial\epsilon(\omega)}{\partial E} \equiv \frac{\Delta\epsilon_r(\omega) + i\Delta\epsilon_i(\omega)}{E} \tag{2.15}$$

In a noncentrosymmetric medium, wherein $\chi^{(2)} \neq 0$, the Pockels' effect is represented by the term linear in E. An oscillating applied electric field $E(\Omega \sim 0)$ thus appears as a permittivity modulation at the same frequency. The shapes and angular locations of surface plasmon resonance curves of LB films on silver depend in part on the LB film permittivity. So, any field-induced reflectivity changes provide an indirect indication of the nonlinear susceptibility $\chi^{(2)}$ [Cross, 1986; Loulergue et. al.,1988]. The way this is estimated is described in chapter four.

Writing the second-order component of induced polarisation as

$$P_i^{(2)} = \epsilon_0\chi_{ijk}^{(2)}E_jE_k \tag{2.16}$$

makes evident the tensor nature of the quantitites involved. In the given experimental arrangement, the low-frequency applied electric field $E(\Omega \sim 0)$ lies parallel to the substrate normal (z-direction). The optical field excites surface plasmons which are TM polarised with electric field vectors normal to the substrate; these undergo mixing with the applied low-frequency field at the silver/LB film interface. Clearly, the components of the nonlinear susceptibility mediating interaction between the two fields are $\chi_{xzz}^{(2)}$, $\chi_{yzz}^{(2)}$ and $\chi_{zzz}^{(2)}$; these give rise to second-order polarisations in the x- y- and z-directions, respectively. The p-polarised optical field, however, doubles as a probe of the nonlinear susceptibility. On reflection at the glass/silver interface, the in-plane components of the probe field interfere destructively while the normal components interfere constructively; the result is that the evanescent field at the silver/LB film interface is polarised predominantly in the z direction. Thus, the only measurable component of the nonlinear polarisation is in the z-direction, i.e. the method examines $\chi_{zzz}^{(2)}$ to the exclusion of all other components of the nonlinear susceptibility. For this reason, the above method alone cannot provide any indication of the LB film tilt angle.

2.4.3 Effects Contributing to the Pockels' Effect

As with SPR, numerous phenomena may contribute to the measurement of the Pockels' effect. Previous sections on surface plasmons have already mentioned material parameters, thermal effects and the direct piezoelectric effect. The following sections list contributions to the Pockels' effect from other sources.

2.4.4 (a) The Converse Piezoelectric Effect

The converse piezoelectric effect is an electric field-induced strain, which may alter the LB film thickness and thus affect the calculation of nonlinear susceptibilities. The strain in the LB film is given by

$$\varepsilon = Ed \tag{2.17}$$

where ε is the strain, E the applied electric field and d the piezoelectric coefficient and all quantities are taken as scalar. The electric field normal to the LB film plane is typically $\sim 10^7 \mathrm{Vm}^{-1}$, applied to a film up to 10nm in thickness. No estimates of the piezoelectric coefficient are available in the literature for the nonlinear dyes used here, but the information presented in section 2.2.7 [Nix, 1988; Koptsik, 1952] suggests a strain on the order of 10^{-4}. If the LB films described here have similar properties, this thickness change can be safely ignored, as it is two orders of magnitude smaller than the error in calculated estimates of film thickness.

2.4.5 (b) Stark Effect (Electroabsorption)

The Stark effect is the shift and splitting of spectral lines in an electric field weak compared to the internal atomic field of approximately $10^{10} \mathrm{Vm}^{-1}$ [Stark, 1919; Surdo, 1913]. Many materials, however, exhibit an absorption edge that varies exponentially with temperature. For low values of absorption coefficient, it can be shown [Franz, 1958; Keldysh, 1958] that the absorption change in an applied electric field can be expressed as

$$\frac{\Delta\alpha}{\alpha} = \frac{\beta^3 \hbar^2 E^2}{24 e m^\star} \tag{2.18}$$

where β is the logarithmic slope of the absorption edge, E the applied field, $m^\star$ the reduced effective mass and e the electronic charge. The absorption coefficient α and the imaginary part of the dielectric function are related by

$$\alpha = \frac{2\pi\epsilon_i}{n\lambda} \tag{2.19}$$

where n is the real part of refractive index and λ the wavelength of light. So,

$$\frac{\Delta\epsilon_i}{\epsilon_i} = \frac{\beta^3\hbar^2}{24em^\star}E^2 \tag{2.20}$$

This predicts a change in the imaginary part of the permittivity proportional to the square of the applied electric field. The observed dependence (see chapter seven) is linear; accordingly the presence of the Stark effect can be ruled out.

2.4.6 (c) Contributions from the Substrate

The lengthy expression for $\chi^{(2)}$, given in the literature [Shen,1984; Bloembergen, 1965] is nonzero for any system lacking inversion symmetry. An isolated boundary between two different media lacks inversion symmetry, therefore it has an associated susceptibility $\chi^{(2)}$. The nonlinear susceptibility of a thin silver film bounded on opposite sides by air and glass is observable in many ways [Sipe & Stegemann, 1982], including via the Pockels' effect as described in this thesis, and is presumed to be unaltered when the silver is overcoated by an LB film. Removal of this contribution from the gross differential reflectivity clearly places a limit on the sensitivity of the technique, as the remainder must be clearly identifiable as the LB film differential reflectivity. To date, the nonlinear susceptibility of silver has not been quoted in the literature. In practice, however, the contribution from silver is smaller than that of most LB film materials, and so contributions from the silver substrate have not been accounted for.

2.4.7 (d) Cubic Responses

For optical nonlinearities far from resonance, it may be shown [Shen, 1984] that

$$\left|\frac{P^{(3)}}{P^{(2)}}\right| \sim \left|\frac{E}{E_{at}}\right| \tag{2.21}$$

Typically, the atomic electric field E_{at} $\sim 10^8 \mathrm{Vm}^{-1}$. The electric field applied to the LB film is $\sim 10^6 \mathrm{Vm}^{-1}$, setting $|E/E_{at}|$ $\sim 10^{-2}$. All other things being equal, a signal one hundredth the size of that produced by the Pockels' effect is close to the

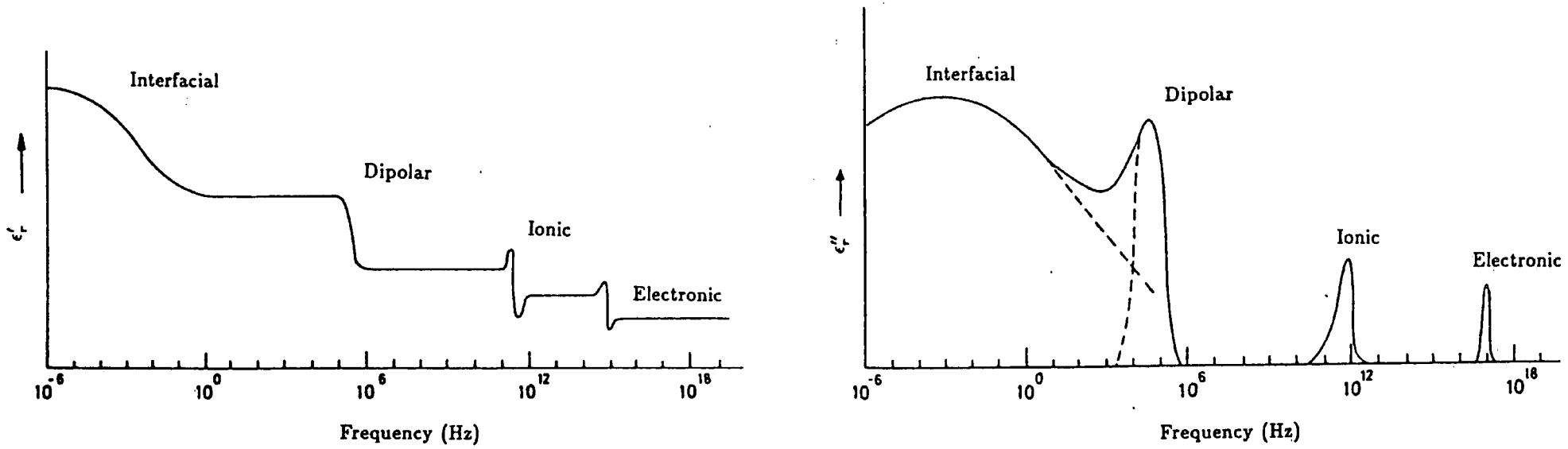

Figure 2.6 : Real and Imaginary Parts of Ideal Dielectric Permittivity Versus Frequency

limit of sensitivity of the detection equipment. It also appears at twice the frequency of the applied electric field.

2.4.8 (e) Frequency Dependence

The Pockels' effect in LB films can be thought of as an electric field-dependent component of permittivity. The film permittivity, however, is frequency-dependent; figure 2.6 shows the variation of the real and imaginary parts of an ideal dielectric's permittivity with frequency of applied electric field. In a measurement of the Pockels' effect, if the frequency of either of the applied fields overlaps with an absorption peak, the observed nonlinearity is resonantly enhanced. This is undesirable as it limits the useful bandwidth of any device based on this nonlinearity. The 3KHz electric field applied across the LB film is at a far lower frequency than the frequency of dielectric relaxation, which is higher than approximately 1MHz. Experimentally, the Pockels' effect is independent of the frequency of this field (see chapter seven). Likewise, as long as the laser frequency does not overlap with any LB film absorption bands, the nonlinearity remains nonresonant; this is also desirable from the point of eliminating contributions from the Stark effect (see above). The optical absorption spectra of the various dyes (see chapter six) are used to estimate whether this contribution is likely to be significant.

2.5 SUMMARY

This chapter has outlined the historical and physical origins of surface plasmons and their relationship to the Pockels' effect in LB films. Some effort is also made to demonstrate the enormous variety of nonlinear optical phenomena. Section two specifically explains how to estimate LB film nonlinear susceptibilities from induced permittivity changes. Piezoelectricity, thermal effects and electroabsorption, all of which may may provide spurious contributions to the Pockels' effect, are shown to be negligible. The nonlinearities are also frequency-independent provided the laser beam does not excite any LB film transitions.

2.6 REFERENCES

Bloembergen, N. : Nonlinear Optics , 1965 publ. W. A. Benjamin, Inc..

Bohm, D., Pines, D. : A Collective Description of Electron Interactions: III. Coulomb Interactions in a Degenerate Electron Gas ,*Phys. Rev.* **92** *3* , 1953 pp. 609-21.

Boardman, A. D. : Hydrodynamic Theory of Plasmon- Polaritons on Plane Surfaces ,*Electromagnetic Surface Modes* , 1982 pp. 1-76. publ. John Wiley. , ed. Boardman A D.

Cross, G. H. : Linear Pockels Response of a Monolayer Langmuir-Blodgett Film , *Electron. Letters* **22** *21* , 1986 pp. 1111-3.

Dasgupta, B. B., Beck, D. E. : Quantum- Mechanical Calculations of the Surface Plasmon Dispersion for Metals using the Random Phase Approximation ,*Electromagnetic Surface Modes* , 1982 pp. 77-118. publ. John Wiley. , ed. Boardman A D.

Fabellinski, I. L. : Molecular Scattering of Light , 1968 publ. Plenum, New York.

Franz, W. : ,*Z. Naturforsch* **13a** , 1958 pp. 484.

Halevi, P. : Polaritons at the Interface between two Dielectric Media , *Electromagnetic Surface Modes* , 1982 pp. 249-304. publ. John Wiley & Sons Ltd.. , ed. Boardman, A. D..

Innes, R. A., Sambles, J. R. : Simple Thermal Detection of Surface Plasmon-Polaritons ,*Solid State Communications* **56** *6* , 1985 pp. 493-6. publ. Pergamon.

Janossy, I., Taghizadeh, M. R., Gordon, J., Mathew, H., Smith, S. D. : Thermally Induced Optical Bistability in Thin Film Devices , *IEEE JQE.* **21** *9* , 1985 pp. 1447-52.

Keldysh, L. W. : ,*Sov. Phys. JETP.* **7** , 1958 pp. 788.

Koptsik V. A. : The Electrical and Elastic Parameters of Resorcinol Monocrystals *in Russian ,PhD Thesis, Lomonosov State University* , 1952

Kovacs, G. : Optical Excitation of Surface Plasmon- Polaritons in Layered Media ,*Electromagnetic Surface Modes* , 1982 pp. 143-200. publ. John Wiley. , ed.

Boardman A D.

Kretschmann, E., Raether, H. : Radiative Decay of Non Radiative Surface Plasmons Excited by Light ,*Z. Naturforsch* **23a** , 1968 pp. 2135-6.

Landau, L. D., Lifschitz, E. M. : Elektrodinamika Sploshnich Sred (Electrodynamics of the Continuum Media) , 1948 publ. Moscow.

Loulergue, J. C., Dumont, M., Levy, Y. : Linear Electro- Optic Properties of Langmuir-Blodgett Multilayers of an Organic Azo Dye , *Thin Solid Films Proc. 3rd Int. Conf. LB Films, Göttingen.* **160** , 1988 pp. 399-405.

Mirlin, D. N. : Surface Phonon Polaritons in Dielectrics and Semiconductors , *Surface Polaritons* , 1982 pp. 3-67. publ. North-Holland.

Nix, E. L., Nanayakkara, J., Davies, G. R., Ward, I. M. : Primary and Secondary Pyroelectricity in Highly Oriented Polyvinylidine Fluorid e ,*Journal of Polymer Science: Part B: Polymer Physics* **26** , 1988 pp. 127-40. publ. John Wiley and Sons.

Otto, A. : Excitation of Nonradiative Surface Plasma Waves in Silver by the Method of Frus trated Total Reflection ,*Z. Physik* **216** , 1968 pp. 398-410.

Pockels, F. : Lehrbuch der Kristalloptik , 1906 publ. Teuber (Leipzig).

Pockrand, I. : Surface Plasma Oscillations at Silver Surfaces with Thin Transparent and Absorb ing Coatings ,*Surf. Sci.* **72** , 1978 pp. 577-88.

Pockrand, I., Swalen, J. D., Gordon, J. G., Philpott, M. R. : Surface Plasmon Spectroscopy of Organic Monolayer Assemblies ,*Surf. Sci.* **74** , 1977 pp. 237-44.

Powell, C. J., Swan, J. B. : Origin of the Characteristic Energy Losses in Magnesium ,*Phys. Rev.* **116** *1* , 1959 pp. 81-3.

Powell, C. J., Swan, J. B. : Origin of the Characteristic Electron Energy Losses in Aluminium , *Phys. Rev.* **115** *4* , 1959 pp. 869-75.

Roberts, G. G. : Potential Applications of Langmuir- Blodgett Films ,*Langmuir-Blodgett Films* , 1990 pp. 317-401. publ. Plenum. , ed. Roberts, G. G..

Shen, Y. R. : The Principles of Nonlinear Optics , 1984 publ. Wiley.

Sipe, J. E., Stegemann, G. I. : Nonlinear Optical Response of Metal Surfaces ,*Surface Polaritions* , 1982 pp. 661-701. publ. North-Holland. , ed. Agranovich V M, Mills D L.

Stern, E. A., Ferrell, R. A. : Surface Plasma Oscillations of a Degenerate Electron Gas ,*Phys. Rev.* **120** *1* , 1960 pp. 130-36.

Stark, J. : ,*Annalen der Physik* **43** , 1919 pp. 965.

Surdo, A Lo. : ,*Accad. Lincei. Atti* **22** , 1913 pp. 665.

Wähling, G. : Arachidate Layers on Ag and Au Detected by the ATR Method ,*Z. Naturforsch* **33a** , 1978 pp. 536-39.

Wähling, G., Raether, H. : Studies of Organic Monolayers on Thin Silver Films using the Attenuated Total R eflection Method ,*Thin Solid Films* **58** , 1979

Zhizhin, G. N., Moskalova, M. A., Shomina, E. V., Yakovlev, V. A. : Surface Electromagentic Wave Propagation on Metal Surfaces , *Surface Polaritions* , 1982 pp. 93-184. publ. North-Holland. , ed. Agranovich V M, Mills D L.

Chapter III

LANGMUIR- BLODGETT FILM TECHNOLOGY

3.1 INTRODUCTION

This chapter deals with film- forming properties of classical and novel LB film materials as well as the Langmuir troughs required to fabricate specimens for study. After providing a brief summary of the history of floating monolayers in section 3.2, section 3.3 explains the basic concepts of LB film deposition, including the formation of a surface monolayer and its transfer to a suitable substrate. Section 3.4 compares various classical LB film materials, such as fatty acids, with the novel polymers and dipolar chromophores dealt with in this thesis. Sections 3.5 and 3.6 describe in some detail the designs of the two LB troughs used to fabricate the mono- and multilayer samples examined here. The former refers to the trough used to produce multilayers in which each monolayer has the same composition, while the latter outlines the design of a trough used for producing superlattice structures in which two different materials are deposited in alternating layers. The properties of the floating monolayer are described in section 3.7, while methods for spreading and compressing the monolayers,as well as different multilayer deposition modes, follow in section 3.8. The final section deals with techniques such as x-ray and electron diffraction which are at our disposal for structural assessment of LB films.

3.2 HISTORICAL BACKGROUND

The peculiar behaviour of oil on water has been known for many centuries. The earliest report is to be found on cuneiform tablets dating back to the Hammurabi period in the eighteenth century BC [Tabor, 1980] ; the spreading of oil was used by Babylonian seers as a means of practicing divinity. The earliest practical application of floating monolayers is believed to have been in Japanese printing: a dye consisting of proteins and colloidal carbon was spread onto a water surface; sprinkling the surface with gelatine converts the floating layer into a maze of light and dark regions, which can be preserved by lowering sheets of paper onto the surface [Terada et. al., 1984]. This art form, still popular today, is known as *suminagashi*.

The first attempt at scientific investigation of the properties of floating monolayers came with Benjamin Franklin's report of the calming effects of spoonfuls of

oil on the surfaces of various Clapham ponds [Franklin, 1774]. Lord Rayleigh must receive the credit for first suspecting in 1889 that the films thus formed were only one molecule thick. It was, however, only with the aid of Agnes Pockels' that he succeeded in directly measuring the thickness of a castor oil monolayer as one nanometre [Pockels', 1891]. This significant find was not exploited until after the First World War, when Irving Langmuir in the General Electric Company laboratories at Schenectady, New York, took up the study of floating monolayers and their deposition onto solid substrates. He initially hypothesised that highly stable molecular layers could form by adsorption of single layers of atoms onto an underlying substrate. Langmuir's Nobel Prize-winning experiments demonstrated the validity of this hypothesis by showing that stable organic monolayers could be formed on the water surface of his film balance, or trough, and transferred to solid substrates. This was first reported [Langmuir, 1920] using fatty acid salts; several years later, Katharine Blodgett reported sequential deposition of floating monolayers of the same materials onto solid substrates [Blodgett, 1935]. The floating monolayers have come to be known as Langmuir films, while the ordered multilayer assemblies are commonly referred to as Langmuir-Blodgett (LB) films. The pioneering work of these two intrepid investigators has been summarised in a comprehensive review of the subject [Gaines, 1966].

Following a period of relative inactivity in the field, interest in LB films has in recent years been rekindled by many European research groups, whose findings indicate that LB films may have profound and wide-ranging roles in electronics and optics. Interdisciplinary research groups the world over have made advances towards perfecting the deposition process for a wide variety of quite stable molecules. The proceedings of the Fourth International Conference on LB films, held in Tsukuba, Japan, in 1988 contain details of progress on all fronts of LB film research.

3.3 BASIC CONCEPTS

Langmuir films are invariably formed by depositing a small amount of a suitable material in a volatile solvent on the surface of a highly pure subphase, usually water, waiting for the solvent to evaporate then compressing the surface layer until it forms an ordered surface layer one molecule thick. To form LB films, a suitable substrate must be repeatedly passed through the surface layer. The process is illustrated in figure 3.1 for the first few monolayers. Under ideal conditions, the dipping process can be repeated indefinitely to form highly organised, structurally stable films of thickness ranging from approximately 2 nm (i.e. one monolayer) to fractions of a micrometre.

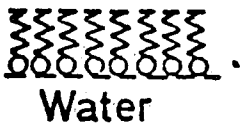

(a) Monolayer on the surface of the water.

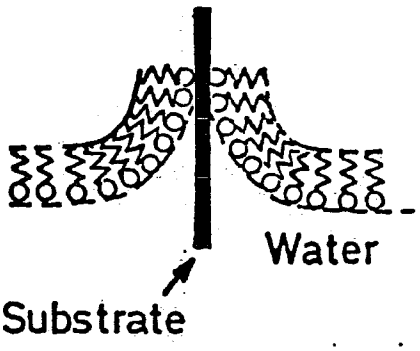

(b) First layer on withdrawal.

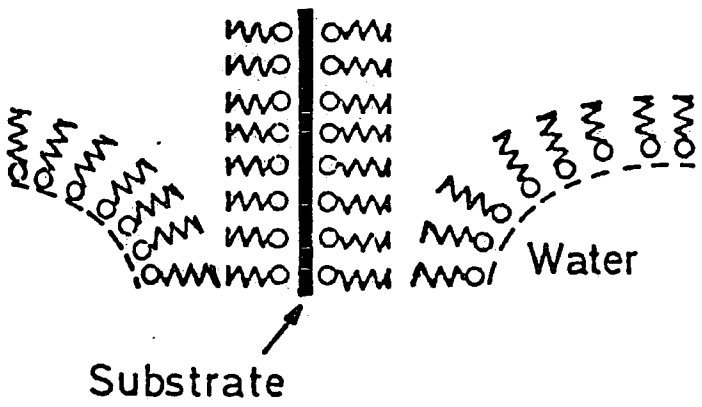

(c) Second layer (2nd Insertion)

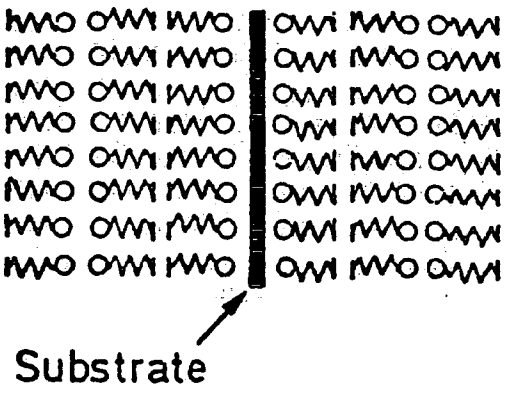

(d) Slide with three layers (after 2nd Removal)

Figure 3.1 : Stages in the deposition of an LB film

The method is simple in principle; unfortunately multilayer film deposition is rarely this successful due to the difficulty in meeting the experimental requirements for successful dipping. Furthermore, by no means all organic materials are capable of forming Langmuir films at all, and only a limited portion of these can form ordered LB multilayers. These factors are discussed in more detail in the following sections.

3.4 MATERIALS

The materials used in LB film formation can be regarded as either 'classical' or 'novel'. The former are those such as long chain fatty acids and their salts, which form the historical basis of LB film technology; the latter includes a wide range of compounds containing various combinations of chemical groups chosen because they are likely to impart specific properties to the formed LB film. For the purposes of this thesis, the novel materials are further subdivided into those described by other workers and those either bought in or 'designer synthesised' at Durham for their large expected optical nonlinearities.

3.4.1 Classical Materials

The materials used classically for LB film formation invariably have a hydrophilic head group and a hydrophobic tail. The hydrophilic group is required to ensure uniform orientation of floating monolayers and is usually a carboxylic acid. In the case of fatty acids the material solubility depends on the length of the hydrocarbon tail, all other things being equal, approximately twenty carbon atoms being necessary for negligible solubility. Accordingly, the materials which suggested themselves in early experiments on LB films are long-chain carboxylic acids, such as stearic and arachidic acids and their salts, whose structure is illustrated in figure 3.2.

The stability and solubility of Langmuir films depends on a variety of interrelated variables, including subphase pH, temperature, presence of ions, age and ambient lighting. For instance, Langmuir films of arachidic acid can be stabilised by adding doubly-ionised species such as Cd^{2+} to the subphase. Adjacent stearate ions share a single cadmium ion to form a salt at the water surface, which improves in-plane stability of the floating monolayer. Deposition of cadmium stearate will typically be carried out on a 10^{-4}M cadmium chloride subphase of pH 5.6. Another material finding wide use in LB films is 22- or $\omega-$tricosenoic acid (22-TA) , illustrated in figure 3.2. The terminal ethylene bond allows the possibility of polymerisation of such films by electron beams, resulting in a linear polymer. This feature, together with its insulating properties, prompted suggestions of its use as a possible electron

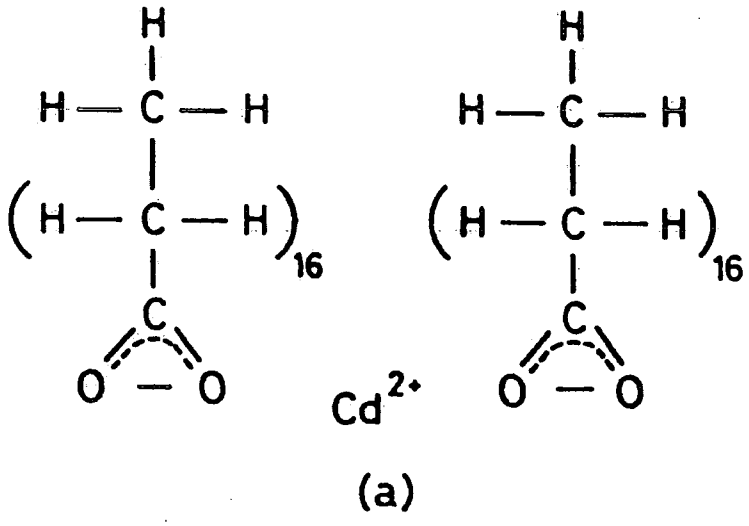

(a)

Cadmium stearate, Cd $(C_{17}H_{35}CO_2)_2$

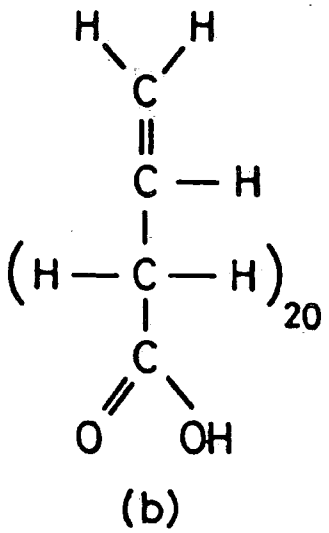

(b)

22-tricosenoic acid (22-TA)
$CH_2CH(CH_2)_{20}COOH$

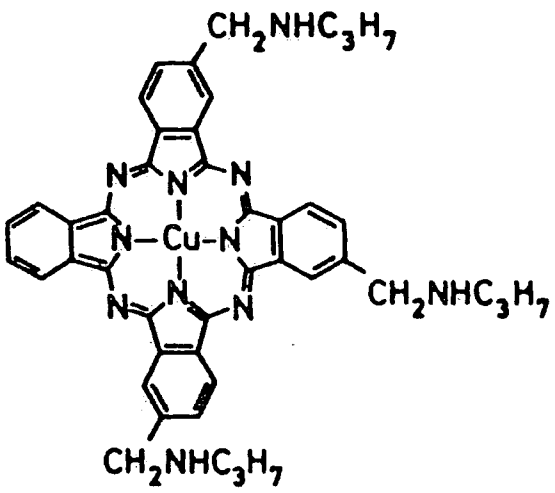

(c)

Asymmetric copper phthalocyanine

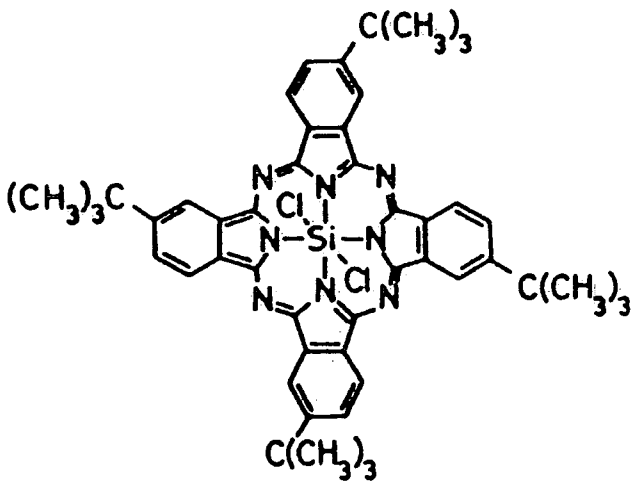

(d)

Symmetric silicon phthalocyanine

Figure 3.2 : Structural formulae of several classical and novel LB film-forming materials from the literature

beam resist material [Peterson, 1983]. Another useful property of fatty acids in general, and 22-TA in particular, is that they can be deposited very rapidly from pure subphases.

A variety of materials, having structures differing to a greater or lesser extent from that of a simple fatty acid, have been investigated with a view to LB film formation. They include anthracenes, diacetylenes, a range of polymers, and several biologically important materials such as chlorophyll A and phospholipids [Hann, 1990].

3.4.2 Novel Materials from the Literature

The previous section suggests that highly conjugated molecules are unlikely to be good candidates for LB film-forming materials unless they form a minor constituent of an otherwise aliphatic film. Such films are likely to resemble most closely films consisting exclusively of fatty acids. This is indeed unfortunate, as the electrical and linear and nonlinear optical properties of fatty acids are of minimal interest, whereas conjugated molecules having extended π-electron systems are of great interest in those respects. Furthermore, the greater stability and damage thresholds of conjugated systems makes them attractive for applications in integrated optics and electronics.

Recently, however, it has been shown that high-quality multilayers can be formed from materials containing aliphatic side-chains as short as four CH_2 units, such as substituted anthracene derivatives; more extreme examples of LB film-forming materials include the organic semiconductor perylene, which requires no hydrocarbon tail for film formation. Such films have no long range order and adjacent monolayers may not be distinct [Warren, 1989]. Regarding their aliphatic nature, most LB film materials fall somewhere between the two extremes of fatty acids and perylene. Many substituted dyes have been used in LB film formation, sometimes as homogeneous layers, often as layers of dye mixed with fatty acid to confer additionnal stability on the formed film. The list of conjugated materials used to form LB films includes merocyanine, rhodamine, hemicyanine, stilbenes, squarylium, anthraquinone, and azo dyes. In some cases, the molecule may contain more than one hydrocarbon chain to induce a preferred orientation of the dye chromophores.

3.4.3 Novel Materials used in this project

A variety of materials were examined in this project. Most of them were chosen according to standard guidelines [Meredith, 1983] outlined in the previous chapter, for producing molecules with a high second-order nonlinear susceptibility. These

have donor and acceptor groups separated by a conjugated system; their solubility is reduced by either the addition of a hydrocarbon chain to each molecule, or by mounting several molecules onto a polymer backbone. The materials used fall into two categories: modified di-aryl alkynes with hydrocarbon tails and polysiloxanes having dipolar chromophores as side groups.

3.5 THE STANDARD LANGMUIR-BLODGETT TROUGH

There are many variations on the original troughs used by Langmuir and Blodgett, including circular troughs with a radial barrier and those with a single movable barrier [Petty, 1990]. All troughs used in Durham are rectangular and have a constant-perimeter barrier. Those used for the work described in this thesis are described in the following sections.

3.5.1 Mechanical Construction

The least sophisticated trough used in Durham is shown schematically and pictorially in figures 3.3 and 3.4 respectively. The tank is made of glass and supported by a fixed steel framework. The constant-perimeter barrier consists of a PTFE-coated glass fibre belt held in place under its own tension by a set of PTFE rollers. The rollers are attached to movable cross-members which are pulled back and forth along steel runners by toothed belts driven by stepper motors. Barrier motion is limited by microswitches.

The deposition mechanism, or dipping head, is located above the central region of the trough and consists of a vertical motor-driven micrometer screw guage. Substrates are affixed to it by a metal screw clamp attached to the lower portion of the head. As in the barriers, dipping head motion is restricted by microswitches. The surface pressure is monitored by a Wilhelmy plate, which is a piece of filter paper of known dimensions attached to a microbalance. Changing surface pressure is equivalent to changing surface tension, i.e. effective weight of the paper plate, which is measured by the microbalance. The balance is housed in a draught-free cabinet, on top of a glass-doored cabinet containing the rest of the apparatus. The latter cabinet is ventilated by an extractor fan, used to aid solvent evaporation.

3.5.2 Instrumentation

A single electronic unit allows the user to control all the movements of the barriers and dipping head. The barriers can be moved in three modes : 'forward' , 'reverse' ,

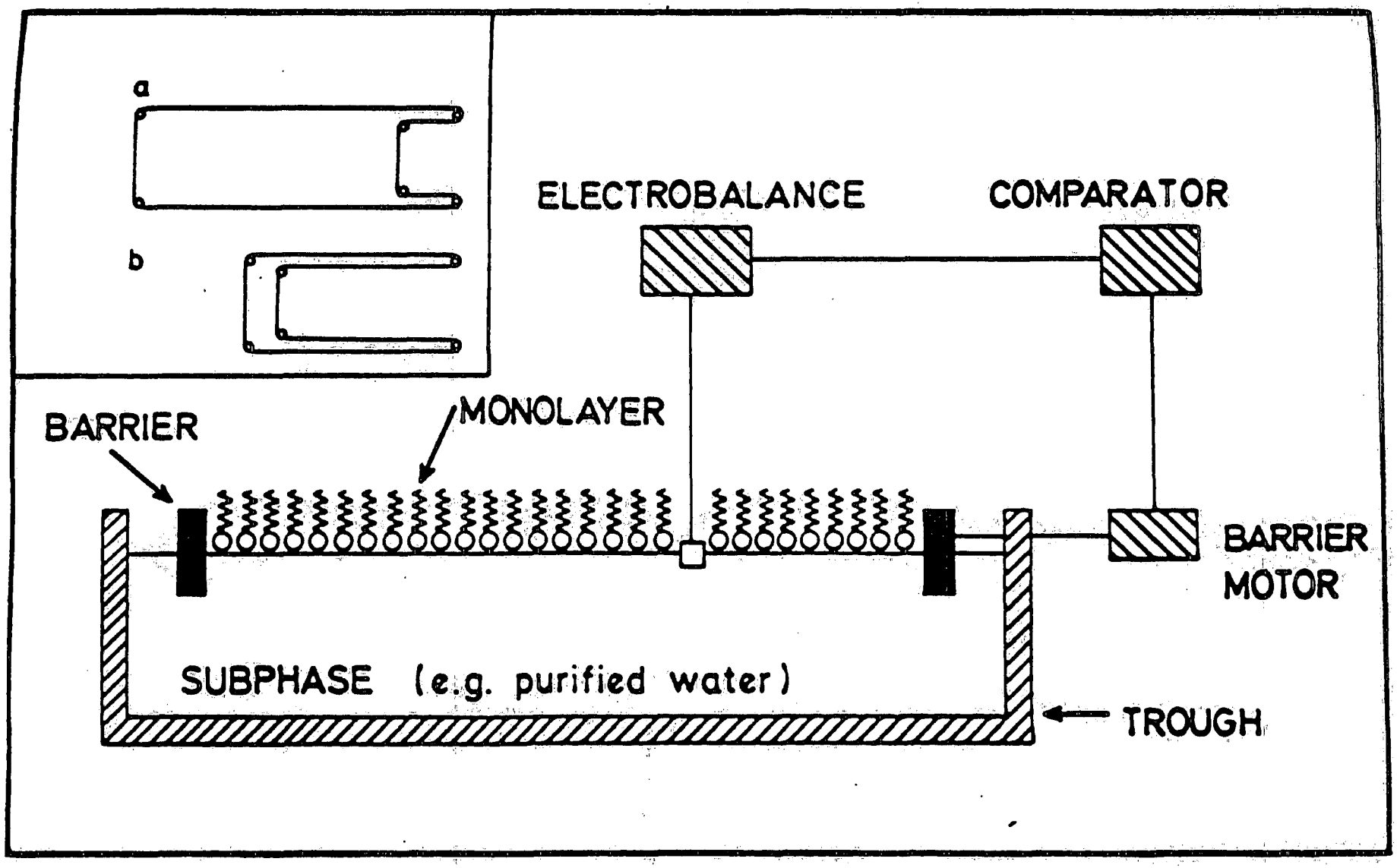

Figure 3.3 : Schematic diagram of a constant-perimeter barrier Langmuir trough. Inset: plan view of barriers (a) fully open (b) fully closed

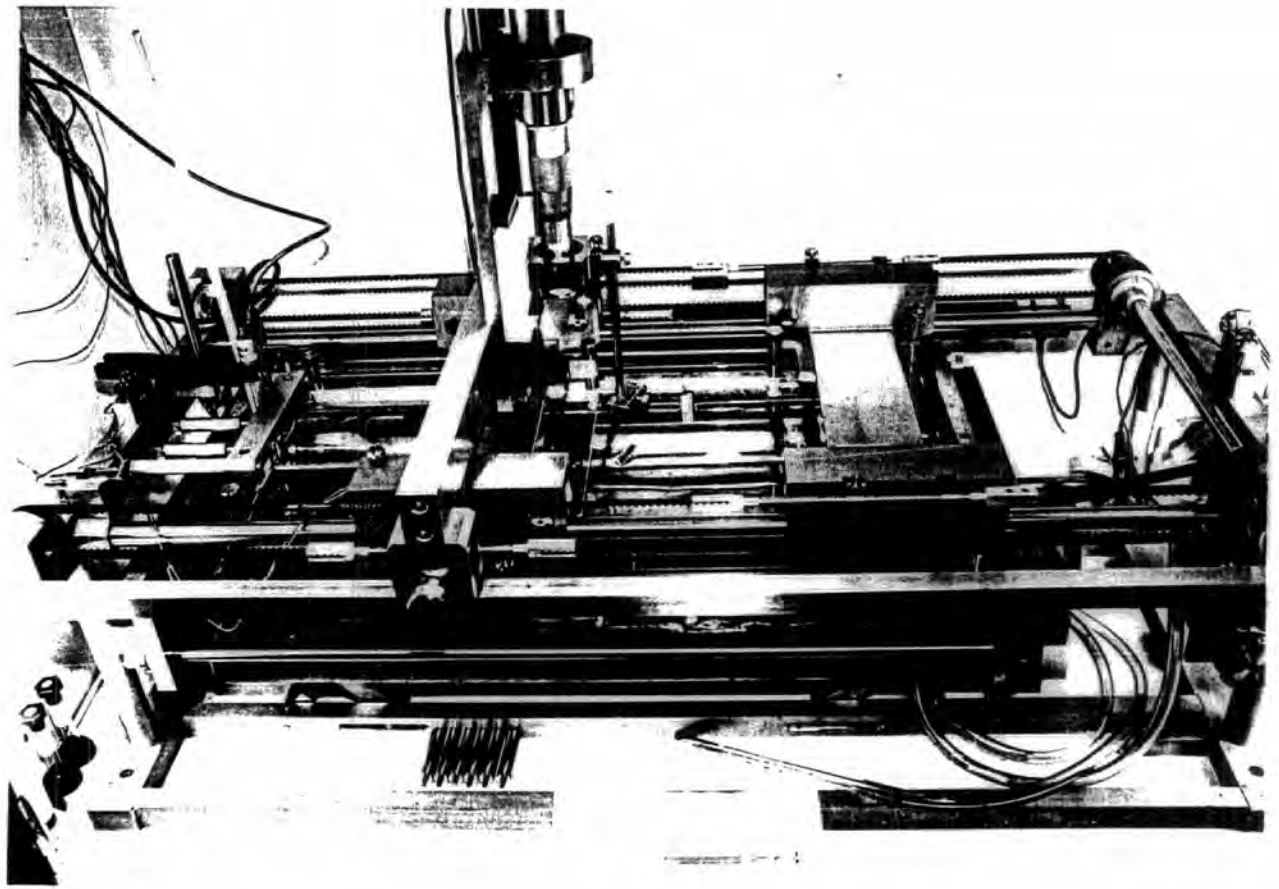

Figure 3.4 : A photograph of one of the standard Langmuir troughs used at Durham

and 'control' . In the first two, the barriers are compressed or expanded at a set speed regardless of any film on the surface. In the latter case, which is generally used in film deposition, the film is first compressed up to a preselected surface pressure. The dipping head is then programmed to move the substrate in and out of the Langmuir film a fixed number of times. As the film is picked up by the substrate, a feedback mechanism with variable gain compares measured and preset surface pressures and adjusts the barrier drive such that the difference is minimised.

Plots of surface pressure (i.e. microbalance output) versus film area can be measured on an attached X-Y recorder. Area and pressure may be recorded against time on a Y-t chart recorder to provide a 'dipping record' . Pye Unicam meters are used to continuously monitor subphase pH.

3.5.3 Minimisation of Contamination

Floating monolayers are highly susceptible to contamination from the ambient atmosphere. It is thus important that the LB trough be isolated as far as possible from any airborne particles. Hence the location of all Durham's LB troughs in a (nominal) class 1000* clean room and the use of appropriate anti-static clothing.

The weight of material spread onto the surface of a Langmuir trough is typically several hundreds of micrograms. The subphase volume is on the order of tens of litres. It is thus apparent that impurity concentrations of the order of fractions of a gramme per litre may seriously impair the quality of any floating and deposited films. To this end the Durham clean room is equipped with an 'Elga' recirculatory water system which cycles water through a reverse osmosis unit, a deionising cartridge and an ultraviolet steriliser, in that order. The water system is permanently in operation; the end product is water of resistivity consistently greater than 17MΩcm with a total organic content not greater than 20 ppb.

Even under ideal conditions, the subphase cannot be expected to remain pure indefinitely, and it becomes necessary to clean the LB trough sooner or later. This is generally done by rinsing twice with a suitable solvent, usually 'Aristar' grade chloroform, then rinsing twice with the purified water described above before refilling the trough and testing the surface for cleanliness as described in section 3.8.

* i.e. 1000 airborne particles not exceeding 0.2 micrometres in dimension per cubic foot

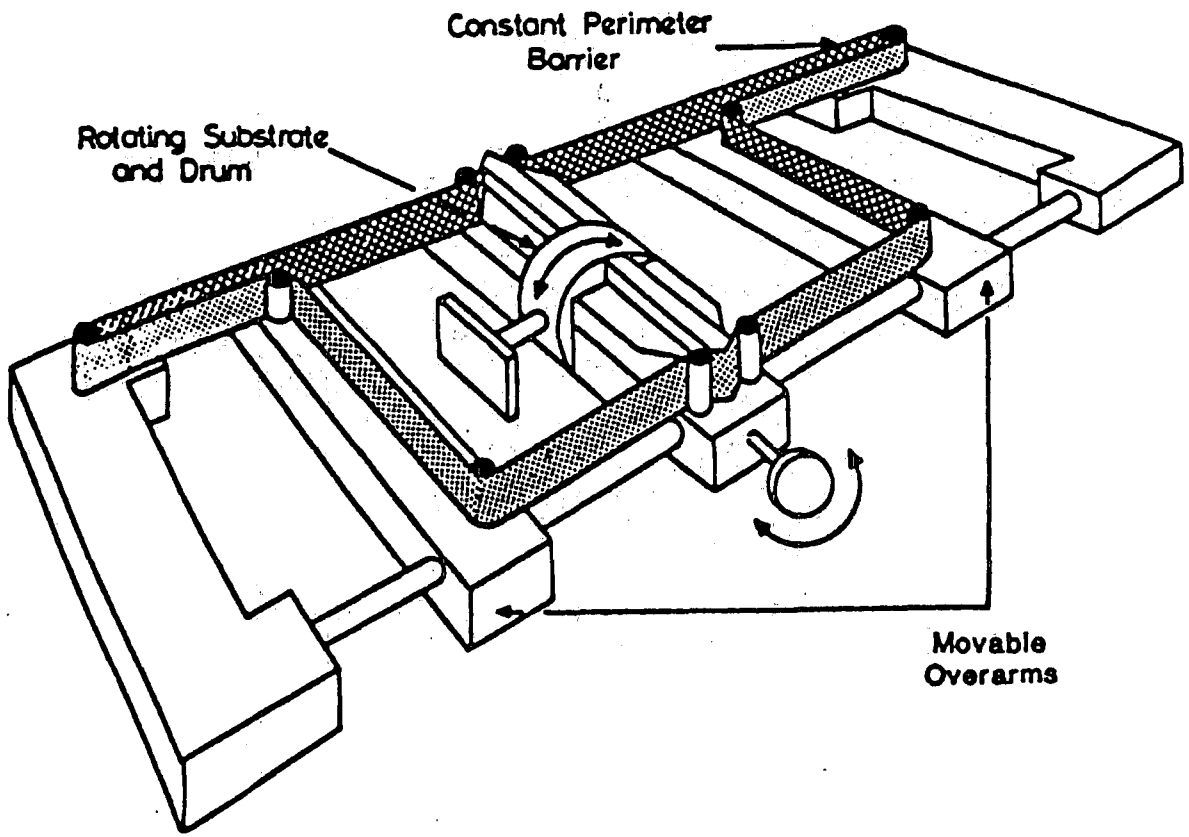

Figure 3.5 : Schematic diagram of the alternate-layer Langmuir trough used at Durham for fabrication of superlattices

3.6 THE ROTARY LANGMUIR-BLODGETT TROUGH

The following sections describe a rotary trough, designed and built in Durham, which is used to deposit two-component LB films in which alternate layers have the same composition. Such structures are commonly known as superlattices.

3.6.1 Mechanical Construction and Instrumentation

The alternate-layer Langmuir trough, shown in figure 3.5 , differs from the standard trough in several respects. First, the trough can be raised or lowered as required to adjust the relative levels of subphase and constant-perimeter barrier. Secondly, the constant-perimeter barrier is divided centrally to form two distinct regions on which Langmuir films may be spread. Third, each of these areas has its own Wilhelmy plate, barrier drive, feedback control and Y-t recorder, each of which are substantially the same as that described above in section 3.5.2. The control mechanisms differ in that the alternate layer trough barrier drive can be immobilised at any point by a 'stop' setting on the control box, and the dipping head cannot be programmed to deposit a fixed number of monolayers : it carries on regardless until switched off manually. Fourth, the dipping head is not simply a clamp at the end of a motorised vernier guage. Rather, it is a partially-submerged rotating drum mounted on the central divide between the two Langmuir film surfaces. A screw clamp stands proud of this drum; it is this that supports the LB film substrate in a plane parallel to the drum's long axis. Fifth and finally, there is no X-Y recorder on this trough for the recording of pressure-area isotherms, as only one area of Langmuir film is required for this process.

3.6.2 Cross-Contamination

Cross-contamination, that is movement of material between compartments of the alternate-layer trough, may arise by transfer from either the rotating cylinder or by the substrate. For floating monolayers of 22-TA and a squarylium dye, it has been found that cross-contamination between the floating layers remains negligible after twenty revolutions of the drum, although contamination has been observed for different monolayer materials with poor pickup ratios [Holcroft et. al]. It appears that cross-contamination occurs when material picked up by the rotating drum from one of the monolayers (with a poor deposition ratio) ceases to adhere to the drum on passing through the other floating monolayer.

Several of the materials, with high deposition ratios, used in this project were

spread as floating monolayers onto one side of the rotary trough, whilst the other side was kept clean. After fifteen revolutions of the drum, the clean side showed an increase in surface pressure of no more than 3mNm^{-1}.

3.7 PROPERTIES OF THE FLOATING MONOLAYER

The most important requirement for an LB film-forming material is that it be virtually insoluble in the water subphase. On account of their extreme ratio of surface area to volume, conventional wisdom regarding bulk solubility is not strictly relevant to Langmuir films. One must resort to studying the Langmuir film's behaviour in two dimensions. Then, the features of interest are the film pressure-area relationship and the variation in surface area with time at constant surface pressure; that is, the film stability.

3.7.1 Pressure-Area Isotherms

If a material forms an insoluble film at the subphase surface, then as the trough surface area is reduced, the surface pressure will rise. By plotting the microbalance output versus that of the barrier potentiometer, a plot of surface pressure versus area $(\pi - A)$, or an isotherm, may be obtained. Given that the amount of material spread is known, this is equivalent to a plot of pressure versus area per molecule. Such an isotherm is shown in figure 3.6 for stearic acid, one of the classic LB film materials. The plot shows three distinct regions which may be loosely identified with gas, liquid and solid phases. Broadly speaking, the first corresponds to a regime in which the average separation of fatty acid molecules is relatively large and the molecules are largely independent. The liquid phase represents the gradual development of short-range order with increasing surface pressure. The latter solid phase corresponds to a well-oriented monolayer which is relatively incompressible due to its close-packed structure. The steep linear portion of the isotherm may be extrapolated back to zero surface pressure to find the zero-pressure limit of the molecular area in the solid phase. This value may be compared with that deduced from computer simulations or mechanical models such as the Ealing CPK space-filling molecular modelling kit.

While few materials exhibit the above ideal behaviour, the shape and curvature of isotherms invariably aids understanding of molecular behaviour under compression. Many substances display a number of quasi-solid and/or 'liquid' phases; most display other features as well including hysteresis, peaks, troughs, flat portions (first order phase transitions), kinks (second order phase transitions) and spontaneous contraction or expansion [Stenhagen, 1955]. Hysteresis in particular can be interpreted as

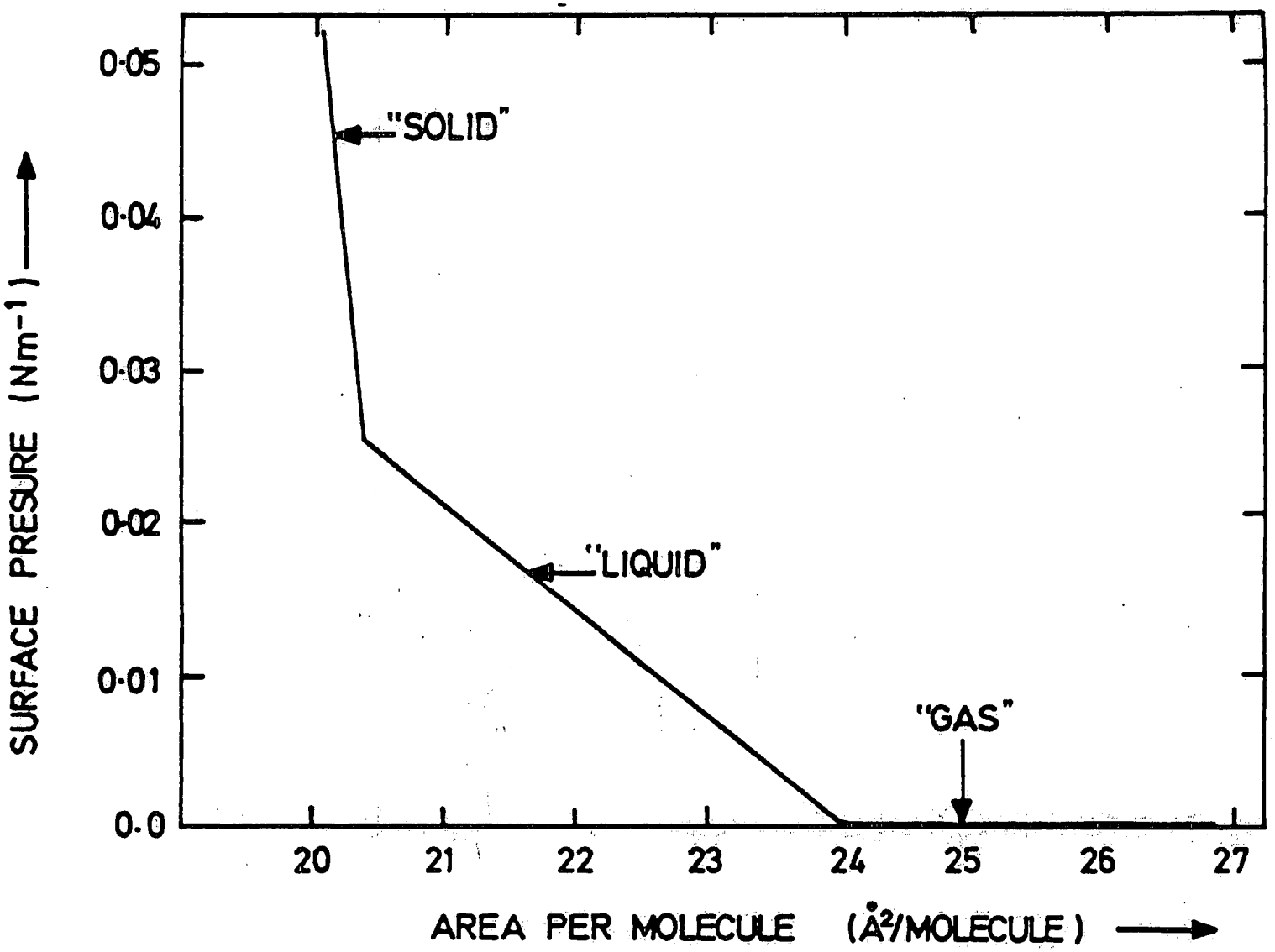

Figure 3.6 : A typical stearic acid isotherm

molecular rearrangement and interactions such as polymerisation and oxidation, as well as loss of film mobility. The latter is discussed in section 3.7.3

3.7.2 Monolayer Stability

Ideally, once spread, compressed to its quasi-solid phase and allowance has been made for any solvent to evaporate, a Langmuir film would cover a fixed area while the surface pressure is held constant. In reality, however, all floating monolayers show some shrinkage due to a combination of the following phenomena: evaporation, partial collapse (film buckling), solution into the subphase, molecular rearrangement, polymerisation or dissociation. The onset of some of these effects, particularly collapse, may be delayed by maintaining the surface pressure below some threshold value at which instability sets in, although in some cases this may be too low for successful monolayer deposition. The rate of solution of Langmuir films in the aqueous subphase depends on a variety of parameters, including pH and concentration of specific ionic species. In the case of the classic materials, monolayer solution can be almost totally halted by partial salt formation. These are very much a minority, and in the case of novel, more complex materials, solution can be quite rapid, and thus may become a major problem. Usually, dissolving Langmuir films decay in area in two stages: a rapid initial desorption followed by an exponential decay with time [Gaines, 1966]. The decay time represents the film half-life. This is consistent with the hypothesis that molecular rearrangement is followed by random dissolution of molecules into the subphase, the film half-life being proportional to the probability of solution. This probability generally exhibits a complex dependence on subphase parameters; it can generally only be optimised by experiment.

3.7.3 Monolayer Mobility

Although it is desirable that a Langmuir film be well-ordered and close-packed, it must also remain fluid in the plane of the air-water interface. If a film solidifies, then drawing a substrate through it causes fracture and tearing of the floating monolayer, with the result that the film is deposited in patches separated by large cracks, somewhat analogous to crazy paving.

The 'suction test' provides an indication of monolayer mobility: the film is held at constant pressure with the barrier feedback control set to maximum gain, and a small amount of material removed with a vacuum nozzle. A suitably mobile film will flow immediately to maintain the preset surface pressure. This test can be used to gauge crudely the mobility of a floating monolayer before or after transfer to a solid

substrate. A more precise method, however, of determining film rigidity is to record several pressure-area isotherms of a floating monolayer at regular intervals. Drastic changes in film fluidity will generally appear as irreversible changes in the form of the isotherm after some characteristic hardening time τ_h. Undesirable film rigidity can be circumvented by mixing the material with a fatty acid or by using a slowly-evaporating solvent. In some cases, rigidity sets in slowly and can be avoided by periodically replacing the film with a fresh monolayer, although it will be appreciated that this can be a tedious process.

3.8 EXPERIMENTAL METHODS

Having established a material as a good candidate for LB film formation, it becomes necessary to examine in detail the process of transfer of Langmuir films to solid substrates. The water subphase surface is first cleaned by compressing the barriers to their minimum area, removing surface detritus with a suction nozzle, expanding the barriers to their maximum area and comparing surface pressures before and after expansion. This is repeated until the surface pressure change on expansion falls within tolerable limits, usually 2 mNm^{-1}. The deposition process is continued by monolayer spreading, compression and deposition.

3.8.1 Monolayer Spreading

The solvent chosen for dissolving LB materials was 'Aristar' grade chloroform. A typical solution concentration was approximately 1 mg ml^{-1}, weights being determined accurately using an Oertling microbalance. The solution is invariably deposited onto the subphase a drop at a time from a height of approximately a millimetre using a microsyringe. The volume spread is accurately measured by a calibrated scale on the syringe body; approximately 100μl is typical.

3.8.2 Monolayer Compression

It is standard practice to record pressure-area isotherms for each new Langmuir film spreading solution, and to occasionally repeat the measurement for aged solutions to ensure they still form adequate floating monolayers. This is done by compressing the film at a fixed rate (in forward mode) and recording microbalance reading versus potentiometer output on an x-y plotter. Having done this, a fresh monolayer is spread and compressed in control mode to a pressure well into the solid phase, at which point the decay in surface area with time may be measured (section 3.7.2).

Otherwise, the film is left to stabilise for several minutes prior to deposition onto a suitable substrate.

3.8.3 Langmuir-Blodgett Film Deposition

There are three modes of LB film deposition [Blodgett, 1935], all of which are illustrated in figure 3.7. The eventual dipping mode will depend on a variety of parameters, the most important being the hydrophilic properties, or lack thereof, of the substrate, subphase pH and the amphiphilic nature of the Langmuir film. Most floating monolayers, including those of the classical LB film materials, dip in a Y-type manner, in which material is deposited regardless of direction of travel through the Langmuir film. In this case, the first monolayer is deposited on initial insertion of a hydrophobic substrate, or on the first withdrawl of a hydrophilic substrate. This deposition mode generally produces highly symmetrical structures. The film quality will, however, be inferior if different materials are chosen for succeeding alternate layers.

At high subphase pH, fatty acids may fail to deposit on the upstroke, leading to X-type films ; this is usually energetically unfavourable, and there is X-ray evidence to show that such films undergo rearrangement during and/or after deposition to essentially Y-type structures [Holley, 1938]. The other deposition mode, Z-type, in which case pickup only occurs on the upstroke, has been observed in many materials, for example phthalocyanines [Baker, 1985] and some materials synthesised at Durham [Tsibouklis et. al., 1989].

An important figure of merit for LB film deposition is the transfer ratio, which is the ratio of film area removed to substrate surface area; for ideal deposition the transfer ratio is unity. Unfortunately, the transfer ratio cannot be measured accurately on the alternate-layer trough used in Durham. The reason is that as the substrate passes through the Langmuir film, the rotating drum to which it is mounted also picks up some of the floating monolayer. In this case, the only way to estimate the deposition ratio is to subtract the rotating drum's contribution to the deposited film from the total amount removed from the subphase surface. This may be done using a dipping record, which always contains several sections in which only the drum surface passes through the floating monolayer.

Ultimately, successful multilayer deposition relies on the chemical and physical structure of the first layer, since any defects therein may propagate into subsequent layers. Furthermore, the first layer is the only one bonded directly to the substrate,

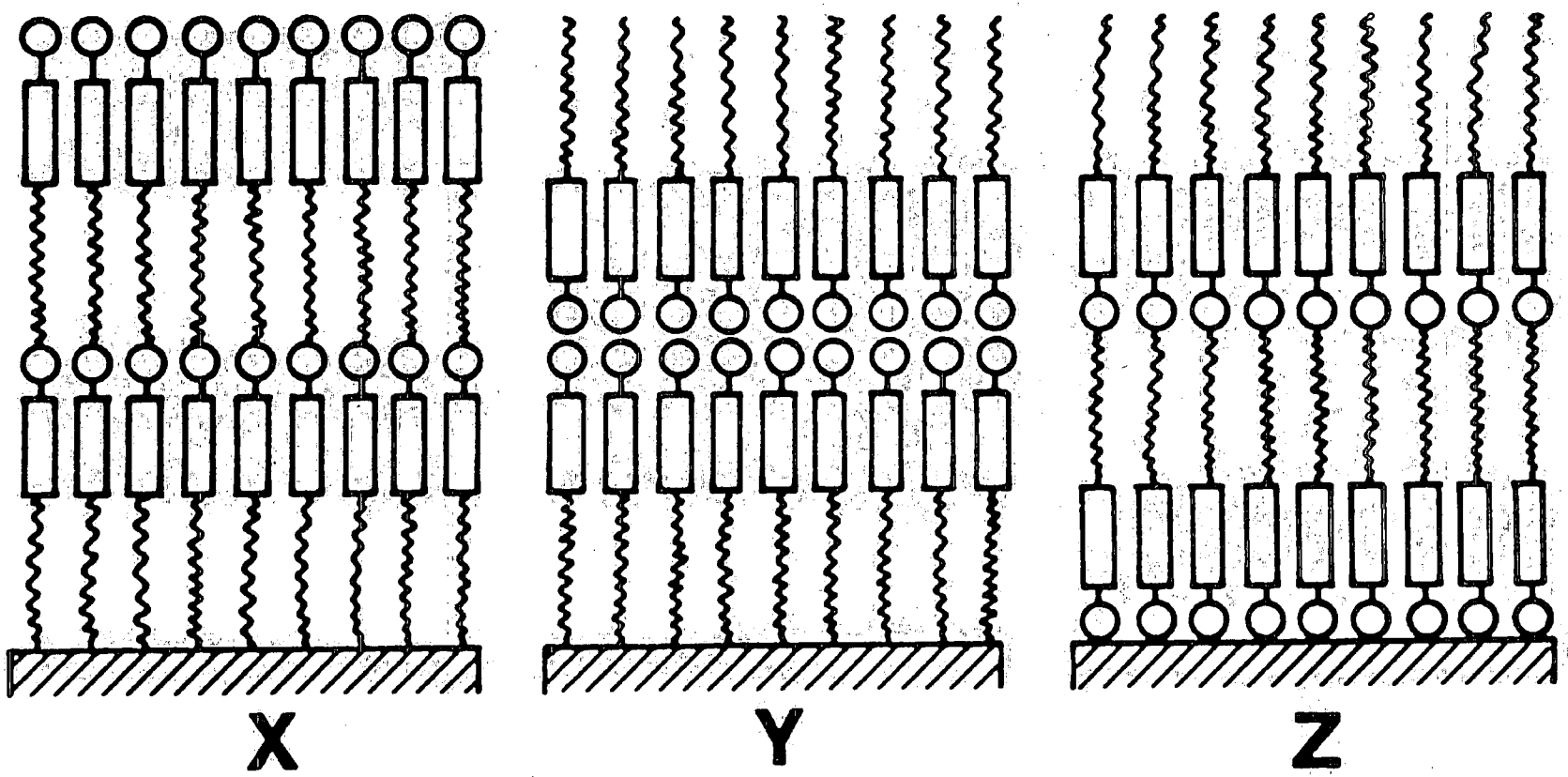

Figure 3.7 : X-, Y-, and Z-type modes of LB film deposition

and is thus fundamentally different from subsequent layers. Accordingly, particular care was taken when depositing the first of a number of layers. Slow (approximately 2mm min^{-1}) dipping commenced immediately after the final treatment of the substrate, and a drying time of at least a half hour was allowed before depositing any more layers.

In the case of Z-type multilayer deposition, the floating monolayer was expanded before the downstroke to reduce the possibility of deposition on initial immersion. Provision is made for this on another trough, not described here in detail, which has a control unit that performs the requisite tasks automatically. Ideally, however, the substrate would be immersed before spreading a Langmuir film.

3.9 QUALITY ASSESSMENT

Several features of LB films need examination in order to assess film quality. They include crystalline structure, defect density and the reproducibility of monolayers. Crystal structure can be thoroughly investigated by a variety of diffraction techniques including transmission electron, X-ray, neutron or reflection high energy electron diffraction (RHEED). The latter is adequate for an approximate identification of film structure and has the advantage of being quick and non-destructive.

Structural order in LB films is rarely described in terms of conventional crystalline symmetry groups; rather, LB films are generally described as having a particular average tilt angle with respect to the substrate normal. Tilt angles in the region of twenty degrees have been reported for various classic LB film-forming materials. Variations of tilt angle within a LB film tend to obscure any medium-range order which may otherwise have manifested itself in the film structure. Thus, the discovery of reproducible crystalline order in a LB film is quite rare, although some workers have reported success in this field [Neal, 1987].

The second feature, related to the above crystalline structure, is defect density. By this is meant the incidence of pinholes in the film, particulate contamination and other defects large enough to be seen by the naked eye or with the aid of an optical microscope. The last two types of defect can usually be observed with greater clarity by looking at a LB film in reflection between crossed polarisers [Peterson, 1984]. Relatively large crystallites ($\approx$500 nm) can be seen by this method. It has been reported that skew disclinations, a characteristic of liquid crystals, are also common to LB films, thus prompting a definition of LB films as a special class of liquid crystal [Bibo & Peterson, 1989]. Pinholes, on the other hand, are often first noticed when an

attempt is made to plot reciprocal capacitance versus number of layers in a metal-film-metal structure. A linear plot indicates good dielectric reproducibility from layer to layer. If the film is badly pinholed, however, the devices will be short-circuited and no such measurement will be meaningful.

Finally, film reproducibility can be tested in several ways. The first is to examine deposition ratios calculated for each layer from the appropriate dipping record. This is, however, not very accurate - especially in the case of substrates whose surface area is small compared to the trough area. A further drawback of this method arises when mixed (heterogeneous) monolayers are examined, as it is not possible to distinguish pickups of the different constituents. Most of the molecules examined in this thesis contain conjugated systems designed to optimise optical nonlinearities; they are also often brightly coloured. Thus, if optical absorption (usually measured at the dye absorption maximum) is linear with increasing number of monolayers, the Langmuir film pickup can be taken as uniform from layer to layer. This method also has applicability to mixed monolayers, since the relative intensities of absorption peaks belonging to all molecular species present should remain unchanged with increasing film thickness. Similar assessments can be made using other techniques, such as infra-red reflectance spectra, electroabsorption and attenuation of the x-ray photoemission.

3.10 SUMMARY

This chapter has reviewed the history, ideas, technology and materials relevant to LB film fabrication. Several methods for the analysis of the floating monolayer and the characterisation of formed LB mono- and multilayers have been described.

3.11 REFERENCES

Bibo, A. M., Peterson, I. R. : Disclination Recombination Kinetics in Water-surface Monolyers of 22- Tricosenoic Acid ,*Thin Solid Films* **178** , 1989 pp. 81-92. publ. Elesvier.

Baker, S. : Phthalocyanine Langmuir- Blodgett Films and their Associated Devices ,*Ph.D. Thesis, University of Durham* , 1985

Blodgett, K. B. : Films Built by Depositing Succesive Monolecular Layers onto a Solid Surface ,*J. Am. Chem. Soc.* **57** , 1935 pp. 1007.

Franklin, B. : ,*Phil. Trans. R. Soc.* **64** , 1774 pp. 445.

Gaines, G. L. Jr. : Insoluble Monolayers at Liquid- Gas Interfaces , 1966 publ. Interscience, N. Y..

Hann, R. A. : Molecular Structure and Monolayer Properties ,*Langmuir-Blodgett Films* , 1990 pp. 17-83. publ. Plenum. , ed. Roberts, G. G..

Holcroft, B., Petty, M. C., Roberts, G. G., Russell, G. J. : a Langmuir Trough for the Production of Organic Superlattices , *Thin Solid Films* **134** , 1985 pp. 83-8.

Holley, C. : X- ray and Optical Properties of Barium Copper Stearate Films ,*Phys. Rev.* **53** , 1938 pp. 534.

Langmuir, I. : ,*Trans. Faraday Soc.* **15** , 1920 pp. 62.

Meredith, G. R. : Design and Characterisation of Molecular and Polymeric Nonlinear Optical Materi als: Successes and Pitfalls , 1983 publ. ACS Symposium Series 233. , ed. Williams, D. J..

Neal, D. B. : Langmuir-Blodgett Films for Nonlinear Optics ,*PhD Thesis, University of Durham* , 1987

Peterson, I. R. : Optical Observation of Monomer Langmuir- Blodgett Film Structure ,*Thin Solid Films* **116** , 1984 pp. 357-66.

Peterson, I. R. : ,*IEEE Proc., Part 1* **130** , 1983 pp. 252.

Petty, M. C., Barlow, W. A. : Film Deposition , *Langmuir-Blodgett Films* , 1990 pp. 93-123. publ. Plenum. , ed. Roberts, G. G..

Pockels, A. : ,*Nature* **43** , 1891 pp. 437.

Stenhagen, E. : Determination of Organic Structures by Physical Methods , 1955 pp. 325- 71. publ. Academic Press (New York). , ed. Braude, E. A., Nachod, F. C..

Tabor, D. : ,*J. Colloid. Interface Sci.* **75** , 1980 pp. 240.

Terada, T., Yamamoto, R., Watanabe, T. : ,*Sci. Papers. Inst. Phys. Chem. Research (Tokyo)* **23** , 1984 pp. 173.

Tsibouklis, J., Cresswell, J. P., Kalita, N., Pearson, C., Maddaford, P. J., Ancelin, H., Yarwood, J., Goodwin, M. J., Carr, N., Feast, W. J., Petty, M. C. : Functionalised Diarylalkynes : A New Class of Langmuir-Blodgett Film Materials for Non-Linear Optics , *J. Phys. D.: Appl. Phys.* **22** , 1989 pp. 1608-12. publ. IOP.

Warren, J. G., Cresswell, J. P., Petty, M. C., Lloyd, J. P., Vitukhnovsky, A., Sluch, M. I. : Optical Properties of Highly Ordered Perylene Multilayers , *Thin Solid Films* **179** , 1989 pp. 515-20. publ. Elsevier.

Chapter IV

EXPERIMENTAL METHODS

4.1 INTRODUCTION

This chapter explains the methods of characterisation of mono- and multilayer LB film structures. Substrate preparation is discussed in section 4.2. Subsequent sections describe surface plasmon resonance (SPR) (4.3), the Pockels' effect (4.4), UV/visible spectrophotometry of solutions and LB films (4.5), ellipsometry (4.6) and second harmonic generation (SHG) from LB films (4.7).

4.2 SAMPLE PREPARATION

4.2.1 Substrate Preparation

The cleaning procedure for all substrate materials was broadly similar. Soda glass or quartz substrates were rinsed in cold iso-propanol to remove visible dust particles then cleaned for an hour in an ultrasonic bath containing deionised water (Elgastat Spectrum), Decon 90 and teepol. Next, the substrates were rinsed for an hour in an ultrasonic bath containing pure water. Finally, the substrates were left overnight in an iso-propanol reflux unit to remove any traces of grease. This procedure left hydrophilic surfaces; when a hydrophobic surface was required, the slides were first of all rinsed for half an hour in an ultrasonic bath containing chloroform plus 2% dimethyldichlorosilane. One other type of substrate was used regularly: n-type (111) orientation silicon, resistivity 10.5-17.5Ω cm (Dynamit Nobel). This was first etched in hydrofluoric acid to remove surface oxides, then cleaned as above. Wherever possible clean substrates were used immediately, although materials surplus to requirements were stored for as short a period as possible in a clean room grade glove or clean staining jar.

4.2.2 Thermal Evaporation

Soda glass substrates cleaned as described above were mounted inside a thermal evaporator unit evacuated to a maximum working pressure of 10^{-5} mbar. A molybdenum boat containing silver wire was heated within the evaporator by a large DC current; a typical evaporation rate was up to 6 nm s^{-1}. The film thickness and

evaporation rate were monitored by a quartz crystal driven at 6MHz and oscillating mechanically in a shear mode. As silver was progressively deposited onto the crystal, the shear mode frequency changed and the fractional change in frequency was used to calculate the thickness deposited. Once a preset thickness had been reached, the silver deposition was halted by a mechanical shutter controlled by an external film thickness monitor. The film thickness calculation requires the silver density, acoustic impedance and an empirical geometrical correction for the different separations of the substrate and crystal from the source and their differing orientations within the evaporator chamber. The first two are well-catalogued, while the latter, known as the tooling factor (TF), is given to first order by

$$\mathrm{TF} = \left(\frac{d_{sub}}{d_{cryst}}\right)^2 + \text{constant} \tag{4.1}$$

where d_{sub} and d_{cryst} are the boat-substrate and boat-crystal separations respectively. If the TF is incorrect, the film thickness monitor calculates a notional thickness which is indirectly related to the actual film thickness. The optimum TF is generally found by performing a series of evaporations at a fixed notional thickness for various tooling factors, fitting each resulting SPR curve to find the actual film thickness and adjusting the TF so that the notional and actual thicknesses correspond. This process is only successful up to a point since the silver film properties vary with silver quality, vacuum pressure, source dimensions, deposition rate, absorbed water (once removed from the evaporator) and other factors. A typical set of calibration data are presented in chapter six.

4.3 SURFACE PLASMON RESONANCE

4.3.1 Experimental Technique

The surface plasmon sensing apparatus is shown schematically in figures 4.1 and 4.2. The ITO-coated slide and phosphor bronze contacts were used for measuring the second-order susceptibility of LB films via the Pockels' effect; discussion of these topics is deferred to section 4.4. The following paragraphs explain the remaining components of the system. The next section describes the operation of the data acquisition program controlling the entire system.

The prism arrangement in figure 4.1 is a variant on the well-known Kretschmann configuration. The use of films deposited on microscope slides instead of directly

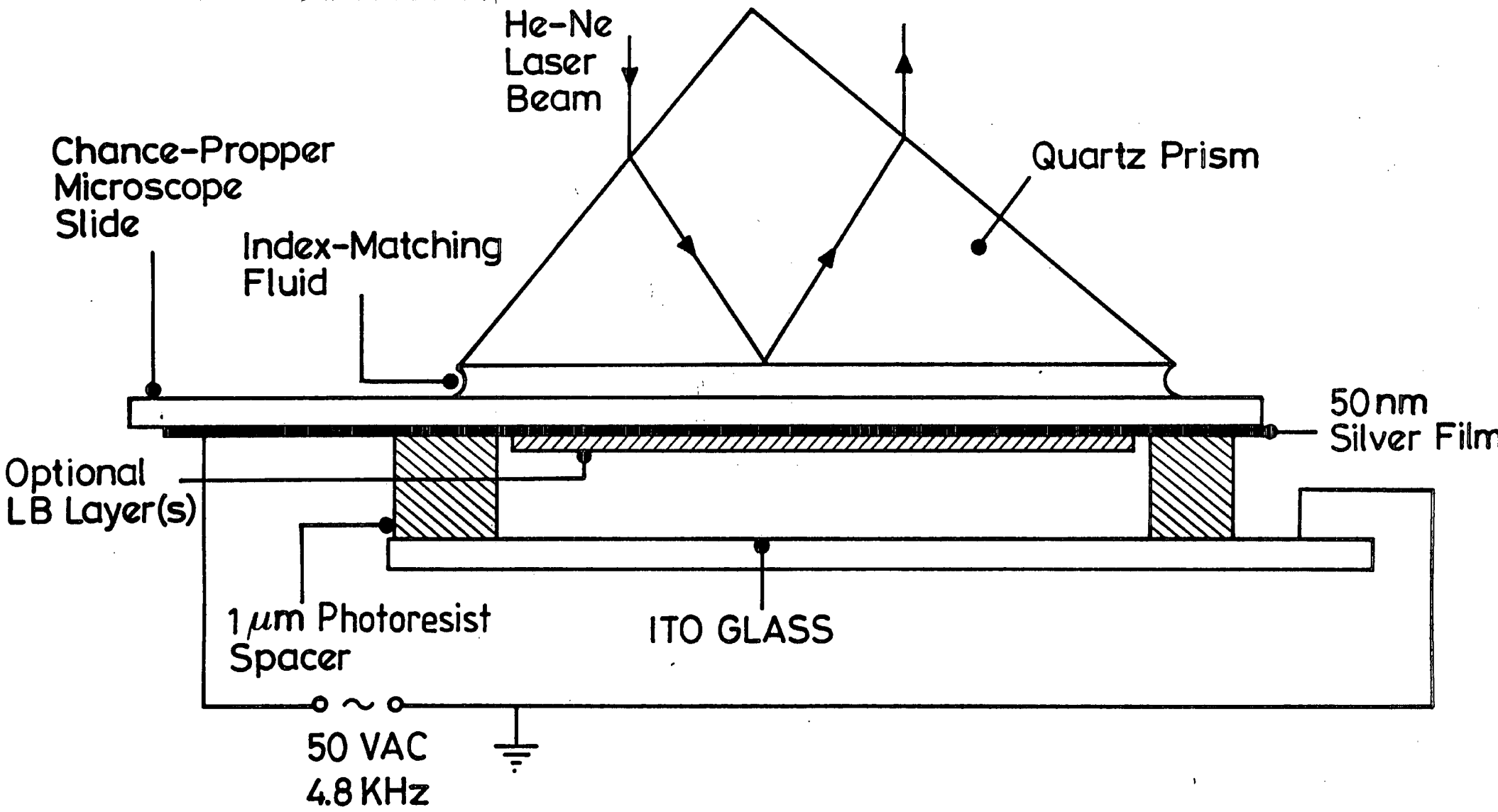

Figure 4.1 : The prism arrangement used for recording SPR and Pockels data

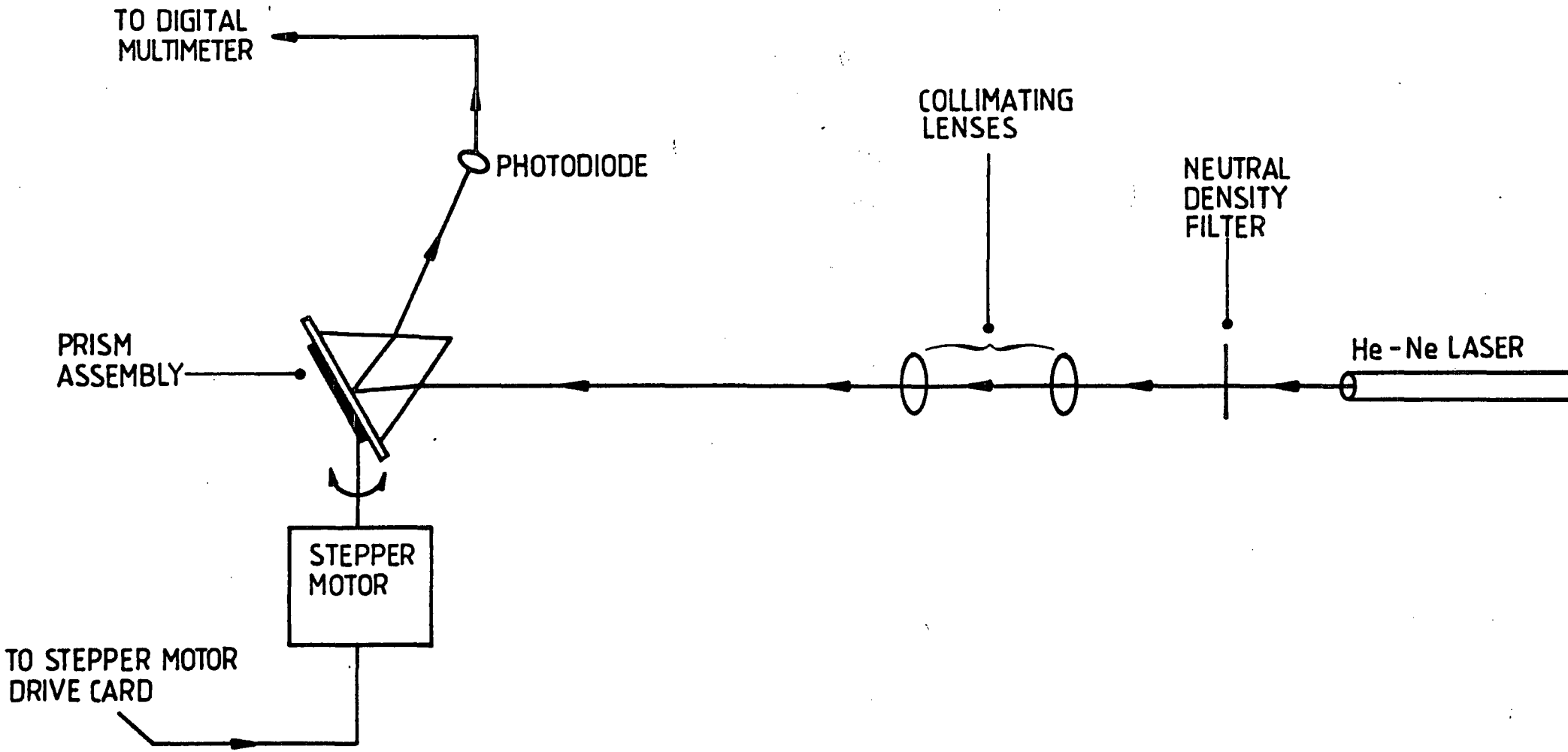

Figure 4.2 : Schematic diagram of the optics, detection apparatus and stepper motor

onto the prism allows straightforward transfer of samples between scans of reflectivity curves. The remaining optics are shown in figure 4.2. To avoid saturating the photodiodes, the prism arrangement was illuminated through a neutral density filter. The p-polarised He-Ne laser beam had a curved wavefront, so not all parts of the beam made the same angle of incidence with the prism; this placed an absolute limit on the accuracy to which the prism critical angle may be located. Because of the beam wavefront's curvature, the spread of $k-$vector components normal to the direction of propagation is not zero. Then, at a given angle of incidence, a degree of surface plasmon resonance may be observed where none is expected on account of this spread. The reasoning in appendix B, which is based on Gaussian optical theory that may be found in several standard texts [Yariv, 1985], suggests that the wavevector spread could be reduced by the lenses shown in figure 4.2. In practice, however, the collimating lenses made little measurable difference to the SPR and Pockels' data presented in chapters six and seven. Accordingly, the lenses were removed. The beam was then used to probe the prism assembly reflectivity, which was measured by silicon photodiodes in photoconductive mode, which assume a linear current response. The photodiode characteristics were: area 1 cm^2, dark current 1.5μA at 10V reverse bias, responsivity 0.4 A/W at 633nm, response time 500ns with a 50Ω load, and 0.1 pA rms noise current at zero bias. The reflectivity of the prism arrangement was proportional to the photodiode output. This was averaged by a digital multimeter (Keithley model 195A) until the standard error on the mean signal fell to less than some prescribed amount, usually set to less than one percent of the output signal. Angular scans were performed by rotating the prism by a five-phase stepper motor (Berger Lahr model RDM 564/50, resolution 0.004°) driven from a BBC Master series microcomputer via a commercially available drive card (Berger Lahr model D 380). As most SPR curves have halfwidths upwards of half a degree, this allowed acquisition of some 125 readings over the SPR minimum, which is more than enough to ensure reliable measurement of reflectivity over the SPR minimum.

4.3.2 Data Acquisition

Figure 4.3 shows the apparatus used to acquire automatically data on SPR and the Pockels' effect. The phase-sensitive detector and signal generator were used in measuring the Pockels' effect only (see section 4.4). The operation of the SPR data acquisition program, written in ISO Standard Pascal, is shown in the flow chart in figure 4.4 . After being presented with the choice of recording information on SPR or the Pockels' effect, the user is offered instruction on how to use the apparatus. If accepted, detailed instructions are displayed on the vdu screen. Next, the user is

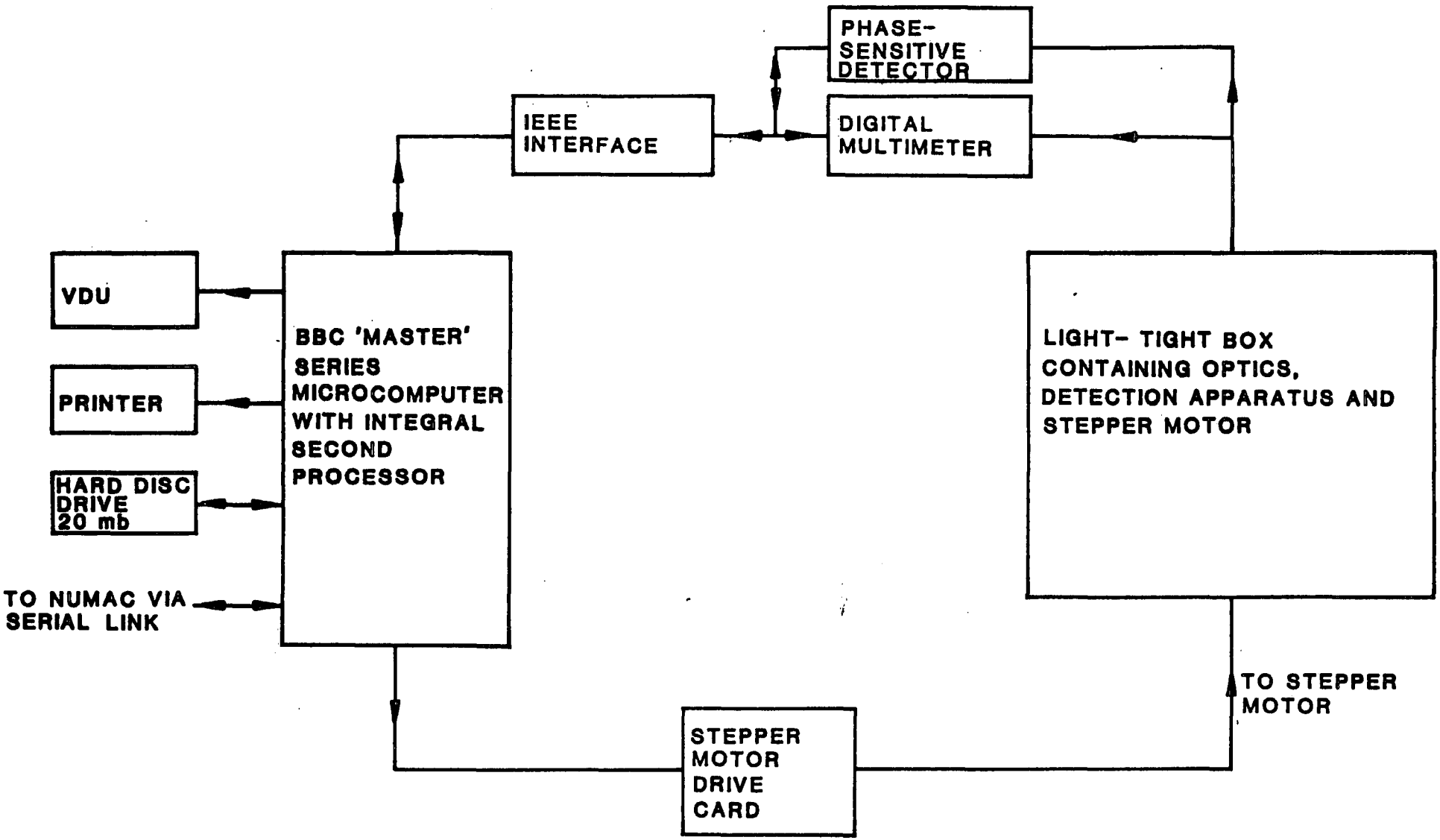

Figure 4.3 : Schematic diagram of the control equipment used in SPR and Pockels data acquisition

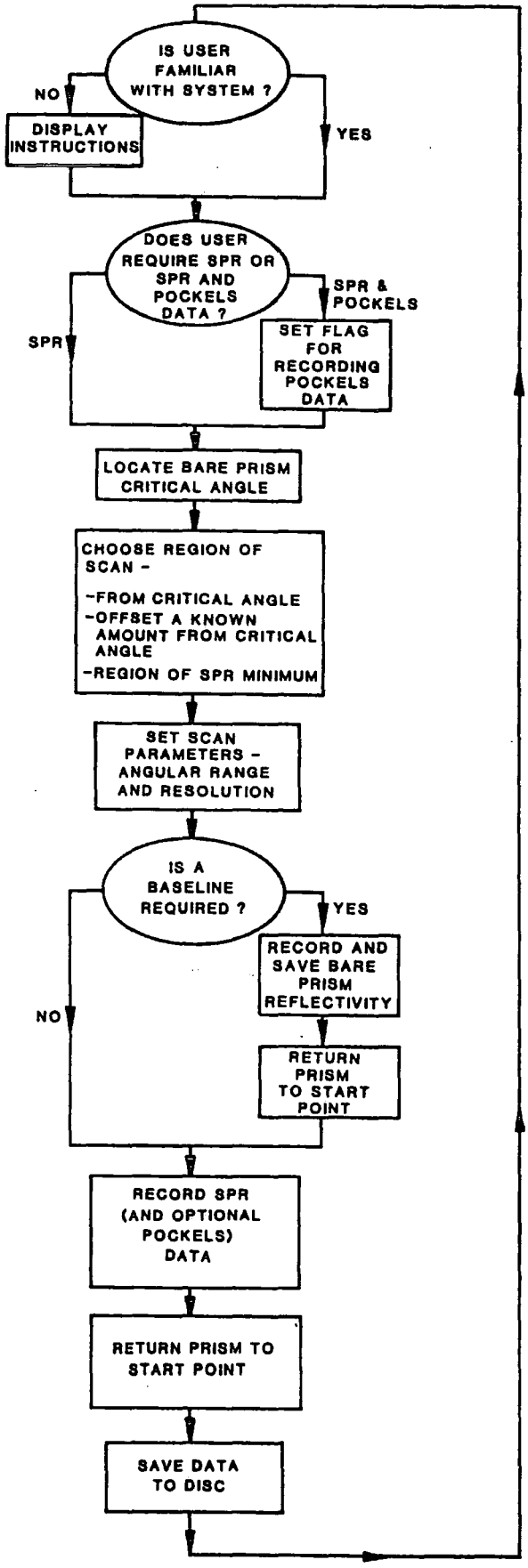

Figure 4.4 : Flow chart of the SPR data acquisition program

prompted for the refractive indices of the prism and clean glass substrate. This is in order that the program may calculate the internal critical angle of the prism assembly and subsequently allocate it to the right angular location. The user is prompted to rotate the prism in steps of half a degree until it is oriented fairly closely to the critical angle. Once this is done, the critical angle may be located more precisely. This is done by choosing a range of angles over which the reflectivity drops significantly, scanning that range, and locating the point of highest gradient of reflectivity by smoothing the measured reflectivity curve and fitting a quadratic equation to triplets of adjacent sample points. Several options for examining a coated sample are now available to the user. They permit angular scans from the present location (i.e. the critical angle), offsetting the photodiode by a known amount to either include the critical angle or exclude uninformative portions of the reflectivity curve between the critical angle and the SPR or locating the SPR minimum and scanning over the region of the SPR. A baseline curve, representing the reflectivity curve of a clean glass slide, can be first recorded if either of the first two options is chosen. Such a curve indicates the multiplicative calibration factors between the absolute prism reflectivity and the recorded photodiode output, including Fresnel losses at the diode faces, losses in wiring, and gain within the linearising circuitry. Once data acquisition has been completed, the prism is returned to the start of the scanning range and the program reboots the BBC microcomputer as from a cold start, and the user is forced to start from scratch. At this point the user has several text files containing the angles over which the scan was performed, the net reflectivity of the prism assembly at each angular location and an optional set of corresponding baseline reflectivities.

A listing of the reflectivity curve acquisition program is presented in appendix C. The main functional areas are in the last few hundred lines, which are the procedures responsible for locating the critical angle and performing reflectivity scans. The remaining three portions deal with: functions absent from Pascal but available in BASIC through standard reserved words, implementation of IEEE commands and automated control of a Keithley 195A digital multimeter (and a Brookdeal 5208 digital lock-in amplifier for Pockels' effect measurements), and stepper motor drive and initialisation via a dedicated drive card. Early versions of the program included a set of procedures known as a 'virtual memory driver', which act to convince the main computer that arrays of data held on a floppy disc are within its random access memory. This was later discarded since it was discovered that judicious choice of the angular range of the scans and their resolution allowed perfectly adequate SPR curves to be recorded within the limitations of the BBC microcomputer's small memory.

The curve acquisition program will run on any BBC microcomputer equipped with enough memory, Acorn Computer's Advanced Disc Filing System and the Acorn Computers ISO Standard Pascal operating system. The program contains an extensive commentary. The principal source of error in reflectivity data arises from the voltmeter. The sampled voltage at any particular angle can be made as precise as the BBC microcomputer's arithmetic and the researcher's patience permits by incorporating averaging procedures into the data acquisition program; this has been done. The multimeter also has a long response time to voltage changes, so the control procedures include a pause after each rotation of the stepper motor to allow the multimeter to arrive at a steady voltage reading. If this is omitted, data from previous readings can contribute to the reflectivity at the current angular location.

Another source of error lies in the angular positioning of the prism assembly. The means of location of the prism critical angle is by no means perfect, but it is quick and reliable. Inspection of the reflectivity close to the critical angle shows that the smoothed and interpolated reflectivity plots have gradients which rise steadily to a peak value close to or at the critical angle and decay to virtually nothing over less than 0.02°, or five motor steps. So, the prism is most likely to be located slightly below the critical angle, as that is the region in which the gradient of the reflectivity curve is largest. Errors of more than a few hundredths of a degree then become visible on reflectivity plots as a single kink at the low-angle end of a reflectivity scan. A problem related to the accuracy of location of the critical angle lies in the backlash in the gears between the stepper motor and the stage on which the prism is mounted. The gearbox (G & K Osborne Ltd.) is claimed to be backlash-free through having cogs immersed in fluid and pressed into good contact through a spring arrangement. Even if this were true, other gears in the rotation stage, some of which are made of PTFE, a very flexible material, are unlikely to be backlash-free. So any backlash was corrected for in the stepper motor driving procedures. No accuracy is lost in transfer of data to a mainframe via transfer programs such as KERMIT, as the data can be sent as character strings with trailing zeroes to far greater precision than the BBC microcomputer's arithmetical functions are capable of handling. The major subsequent source of error in reflectivity values is likely to arise from editing of the data prior to curve fitting.

Due to the above sources of error in angular location, the user is prevented from recording more than two reflectivity scans without relocating the critical angle, even though the program can record SPR curves *ad infinitum*. In any case, there is little

need to record copious SPR curves in series as the duration of each run of the program prohibits taking more than three SPR curves during one long working day.

4.3.3 Interpretation of Results and Curve Fitting

The SEW propagation can be described by the surface modes of a thin metallic film bounded on one side by glass and on the other by air. Strictly, the SEWs at each interface interact, but for silver films of the thickness used here, the modes are independent to a very good approximation [Shen, 1986]. Then, the form of the SPR curve can be predicted from solution of Maxwell's equations for the relevant electric fields at the interface between silver and air [Kovacs, 1982]. If one makes no assumptions regarding the functional forms of these fields, this becomes an exercise in satisfying the boundary conditions on the electric fields at the interfaces involved. Neglecting internal reflections allows individual films to be treated with Fresnel's equations [Heavens, 1955; McLeod, 1986]. In all approaches, choice of suitable optical constants of the film assembly can lead to extremely good correspondence of theory and experiment [Pockrand et. al., 1977; Wähling, 1978].

The detailed features of the reflectivity curves are influenced by a variety of factors, principally the dielectric function and thickness of each layer. Crudely, the angular locations of the reflectivity minima depend primarily on the real part of the film refractive index and their halfwidths depend strongly on the imaginary part, indicating the damping rate of the SEW. The depth of resonance depends strongly on the silver film thickness [Otto, 1968; Pockrand, 1978]. Two additional loss mechanisms influence the halfwidth of the resonance: internal damping within the metal film, which is proportional to the imaginary part of the metal dielectric function and radiation damping due to reradiation of energy back out from the SEW. The latter depends strongly on the thickness of the metal or spacer layer and any overlayers such as LB films, and disappears only when the metal film thickness is infinite. As far as this is concerned, it has been shown both theoretically and experimentally [Otto, 1968; Pockrand et.al., 1977; Pockrand, 1978] that the optimum thickness for pronounced SPR in a silver layer is approximately 50 nm at He-Ne laser wavelengths.

Other factors influencing the optical properties of such thin metallic layers include purity, method of deposition, absorption of water vapour, exposure to reactive gases and, of course, the presence of overlayers such as LB films. Each of these can alter the measured film dielectric function, leading to spurious and irreproducible results if the fabrication of the metallic film and/or overlayers is not carefully controlled. The method of deposition in particular has a marked effect on the film crystalline

structure and surface roughness, which in turn influence SEW propagation [Raether, 1982]. Also, exposure to air frequently leaves a thin (several nm) oxide coating on the film surface, which introduces an extra overcoating that has to be either treated as such or accounted for by absorbing its optical constants into those for silver.

It is clear that fitting of experimental data to theoretical models may turn out to be a worthless pursuit if the films examined have very different histories. Even if this is not so, the influence of the above factors is not readily quantifiable and the most that can be done is to show in a qualitative way the effect of different histories and preparation methods on SPR curves. From a survey of the literature [Lloyd, private communication], however, it appears that SPR is quite a reproducible phenomenon: discrepancies in angular locations of reflectivity minima tend to be less than a degree and resonance halfwidths agree to approximately a few tenths of a degree. If these errors are interpreted as arising from a hypothetical overcoating of, say, 22-tricosenoic acid, the worst discrepancies correspond to the presence of no more than one LB monolayer (thickness $\sim$2-3nm) - which is quite satisfactory as regards study of LB films on a previously-characterised substrate is concerned.

Finally, the role of anisotropy of LB overlayers on metallic substrates must be considered. As it consists of monolayers of oriented molecules which are themselves anisotropic, an LB film will have different refractive indices parallel and perpendicular to its plane, i.e. it will be uniaxial, at the very least. Furthermore, as the orientation of molecules of an LB film is rarely uniform, it will usually be biaxial. Herein lies an important limitation of fitting experimental SPR data to theoretical models of film reflectivity: in general, curve fitting assuming anisotropic films produces fits no better than those assuming isotropic films of slightly different refractive index [Pockrand, 1977]. The same applies to the differences in quality of fit between models of uniaxial and biaxial LB films. Accordingly, SPR studies alone cannot distinguish between isotropic and anisotropic coatings. The above also suggests that the interpretation of an LB film as a perfectly-ordered array of molecules oriented perpendicularly to their substrate cannot be established by fitting of SPR curves alone; other information such as infrared spectra or X-ray diffraction patterns are required.

The experimental arrangement used here is modelled as a multilayer structure (prism/silver/LB film/air, ignoring the index matching fluid and soda glass slide) supporting electromagnetic fields having positively- and negatively-travelling components within each homogeneous isotropic layer. So, with each layer are associated a pair of amplitudes, giving 2N unknown amplitudes for N layers. There are two

conditions on the electromagnetic fields per boundary and N-1 boundaries, i.e. 2N-2 conditions to satisfy. If we specify unit input intensity and and zero input intensity from the output side (light incident from one side only) the problem becomes one of generating a matrix of simultaneous equations and solving it by Gaussian elimination [Cresswell, J. P., private communication]. For fitting of experimental data to theoretical curves, initial estimates of film parameters are used to calculate a reflectivity-angle curve which is compared to the experimental data ; the difference is then minimised by a method of steepest descent and the appropriate film parameters extracted.

In principle, the SPR curve of a single layer can be curve fitted to give unique values of thickness and refractive index. Once an LB overlayer is added, however, an unambiguous free fit between theory and experiment is no longer possible [Sambles, private communications]: either the thickness or the real or imaginary part of the LB film permittivity must be known beforehand. In practice, substrate thickness and optical constants are first calculated, a film is deposited and either its thickness or real part of refractive index is measured. This is treated as known while the other two parameters are calculated. Figure 6.11 shows a reference SPR curve for uncoated silver, while figure 6.12 is a fitted SPR curve for a hemicyanine monolayer on silver. The relevant permittivities and thicknesses are shown in tables 6.4 and 6.5.

4.4 THE POCKELS EFFECT

4.4.1 Measurement

The permittivity modulation induced by optical mixing at the interface between silver and an electro-optic LB film is usually very small ($\sim 10^{-5}$). A sensitive method is needed to observe the resulting small intensity modulation of the reflected laser beam. The apparatus used for detecting the Pockels' effect is a slightly modified version of the surface plasmon sensing apparatus described in the previous section. The indium tin oxide (ITO) conducting top electrode shown in figure 4.1 is used for this. The photoresist is patterned to leave an air gap of approximately 10.5 μm between the ITO and LB film. This air gap has been verified by measurement of the impedance of the silver substrate/ITO electrode assembly. The electrode is clamped in place by a pair of grub screws protruding from an aluminium stage. Electrical contact is made to the conducting faces (ITO and silver) by a pair of sprung phosphor bronze leaves; through these a 30V pk-pk electric field, frequency 3kHz approximately, is applied across the air gap and LB film (if any) within the

cell. The reflected beam from the He-Ne laser is amplitude modulated near the SPR; the resulting sinusoidal intensity change is picked up by the detector photodiode and its in-phase and quadrature components are measured by a Brookdeal 5208 phase-sensitive detector (PSD) linked in series with the Keithley 195A digital multimeter responsible for measuring the SPR data.

The SPR data acquisition program contains procedures for measurement of Pockels' data by interrogation of the lock-in amplifier. For every DC measurement associated with surface plasmons there is a corresponding AC Pockels' effect measurement for the in-phase and quadrature components of the Pockels' signal. Prior to each angular scan, the phase of the PSD is set such that the entire signal appears only on one channel and the sensitivity, rolloff rate and time constant are 5mV, 12dB/octave and 100ms respectively. Signal averaging procedures similar to those for the digital multimeter are applied to the PSD. Also, a pause of several seconds is included between readings to allow the PSD to stabilise, as the stepper motor drive circuitry, while active, emits radio noise which disturbs the PSD. Data on the Pockels' effect are stored and transferred in exactly the same manner as for SPR.

4.4.2 Analysis of Results

Electro-optic modulation is due to field-induced changes in the real (ϵ_r) and imaginary (ϵ_i) parts of dielectric function. The peak change in reflectivity of the prism assembly at any angle can be written

$$\Delta R = \Delta\epsilon_r \partial R/\partial\epsilon_r + \Delta\epsilon_i \partial R/\partial\epsilon_i \tag{4.2}$$

Specimen plots of the angular dependences of the two derivatives are shown in figure 4.5 for a hemicyanine monolayer. The permittivity change can be found by using NAG routines to calculate the derivatives $\partial R/\partial\epsilon_r$ and $\partial R/\partial\epsilon_i$ from the thicknesses and permittivities of the silver substrate and LB overlayers [Cresswell, J. P. private communication]. Estimates of the permittivity changes $\Delta\epsilon_r$ and $\Delta\epsilon_i$ are used to generate curves of ΔR versus internal angle of incidence; these are subtracted from measured values to give a sum of squares to be minimised. The net second-order nonlinear surface susceptibility is related to the relative permittivity changes by

$$\epsilon_0 \chi_c^{(2)} = \frac{\Delta\epsilon_r + i\Delta\epsilon_i}{E_a} \tag{4.3}$$

where the applied electric field E_a is

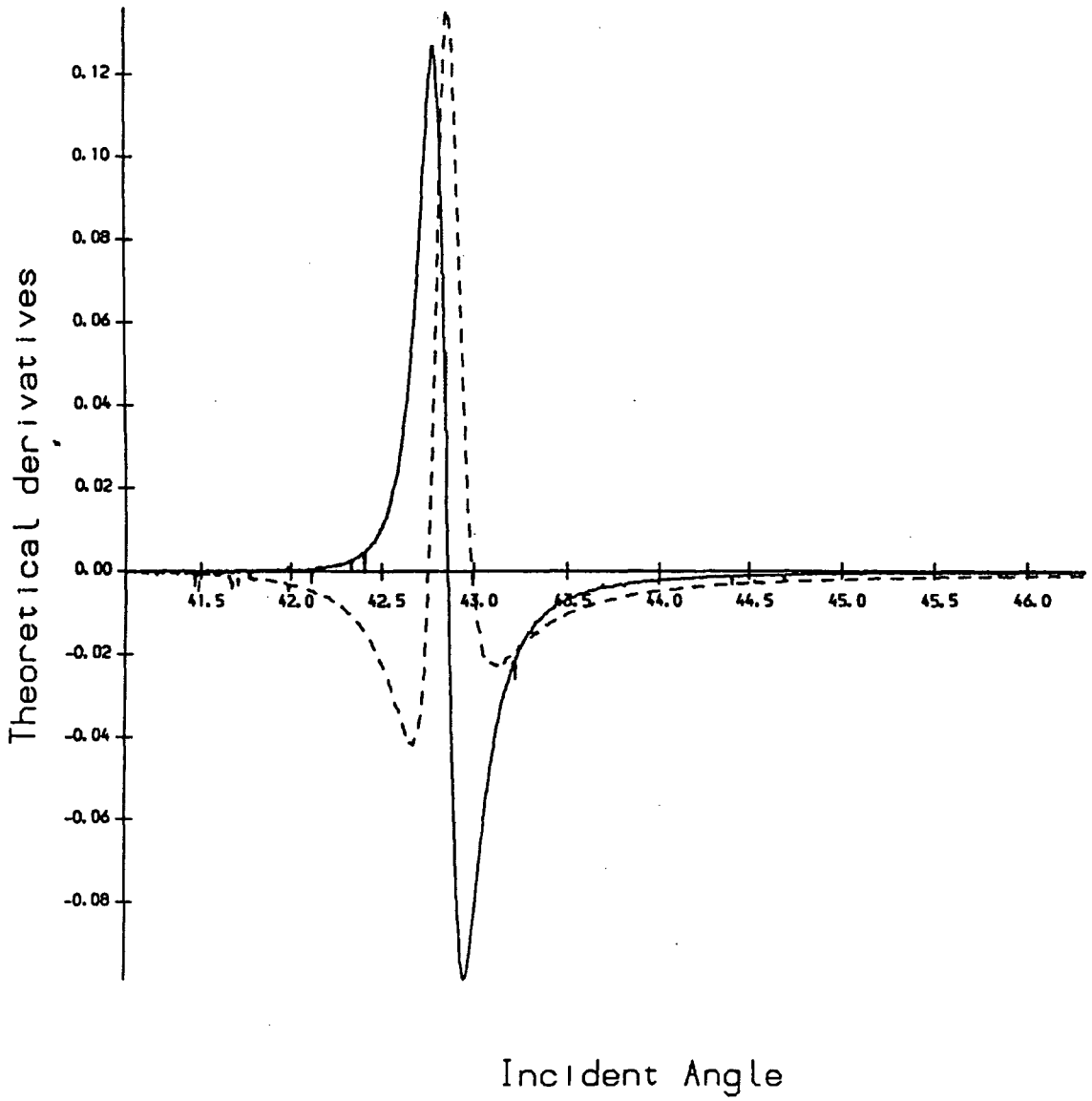

Figure 4.5 : Theoretical $\partial R/\partial \epsilon_r$ (full line) and $\partial R/\partial \epsilon_i$ (interrupted line) for a hemicyanine monolayer

Feature	SHG	Pockels' Effect
Equipment Cost	~£30,000	~£2,000
Laser required	Pulsed Nd:YAG	CW He-Ne
Safety precautions	As for Class 4 laser	As for class 2 laser
$\|\chi^{(2)}\|$	Yes	Yes
Phase of $\chi^{(2)}$	No	Yes
Sense of $\chi^{(2)}$	No	Yes
Background signal?	No	Yes
minimum $\frac{\chi^{(2)}}{\chi^{(2)}(\text{hemi})}$	~1/50	~1/50
Microscopic β	Yes	No
Tilt angle	Yes	No
Duration of experiment	A few hours	A few hours
Might it destroy samples?	Yes	No

Table 4.1 : A Comparison of SHG and the Pockels' Effect

$$E_a \simeq \frac{V_a}{d\epsilon_r} \tag{4.4}$$

d being the air gap and V_a the applied voltage. Note that this is a net nonlinear surface susceptibility related to the bulk susceptibility $\chi_V^{(2)}$ by

$$\chi_c^{(2)} = \int \chi_V^{(2)} dz \tag{4.5}$$

where the z-direction lies normal to the plane of the LB film. The bulk susceptibility may contain contributions from several other effects, which must be distinguished from genuine optical nonlinearities. These have been described in chapter two. Once this has been done, the estimate of $\chi^{(2)}$ produced by curve fitting contains the magnitude and phase of the second-order susceptibility as well as an indication of its direction with respect to the substrate. Chapter seven contains differential reflectivity curves of hemicyanine and 4HANS to illustrate the difference in the orientation of $\chi^{(2)}$.

The Pockels' effect cannot, unfortunately, yield any more information on LB film properties. Compared to the data produced by apparatus dedicated to SHG, for example, the Pockels' effect is a relatively crude technique for estimating the optical nonlinearities of LB films. Its strength, however, lies in its convenience, economy, comparative safety and the possibility of performing experiments in a light-tight box, as opposed to the dark room usually required for SHG. Table 4.1 summarises the difference between SHG and the Pockels' effect.

The usefulness of the Pockels' effect as a means for characterising the structure and nonlinear optical properties of LB films is limited. It is a convenient means of estimating optical nonlinearity. Second harmonic generation, on the other hand, provides additional information on microscopic film structure and nonlinearity.

4.5 OPTICAL ABSORPTION SPECTRA

4.5.1 Introduction

Several instruments were used for recording absorbances between the near ultraviolet and near infrared regions. The absorbance A is universally defined in terms of the transmission coefficent T:

$$A = -\log_{10}(T) \tag{4.6}$$

where T is on a scale of zero to unity. A Cary 2300 UV-VIS-NIR Spectrophotometer was used for some of the earlier measurements before it developed a host of minor and apparently irreperable faults. Subsequent measurements were performed on Perkin-Elmer S3 and $\lambda 2$ spectrophotometers. Where solution spectra were recorded, the solutions were placed in spectrosil B cuvettes; these were corrected for solvent absorption by placing identical cuvettes containing clean solvents into the path of the spectrophotometer reference beam. Where LB film spectra were recorded the substrate was usually a Chance-Propper soda glass microscope slide (for measurements to 400 nm) or a spectrosil B cuvette window (for measurements down to 180 nm); the reference signal was taken from an appropriate substrate prepared the same way as the sample substrate. All the spectra are recorded in transmission, so in the case of LB films, overlayers on both sides of the substrate contribute to the absorbance.

4.6 ELLIPSOMETRY

4.6.1 Introduction

Ellipsometry can be most broadly defined as the measurement of the polarisation state of a vector wave. It relies on the transformation of polarisation states of light on interaction with optical systems. Factors influencing the polarisation state of light include reflection or refraction, transmission and scattering. The corresponding fields of study are reflection or surface ellipsometry, polarimetry and scattering ellipsometry. Although other properties of the polarised light are usually altered too, such changes require analysis by formalism beyond the scope of ellipsometry. Its main attractions are three: it is non-destructive, provided that the wavelength and intensity of the incident light are properly chosen, and so suitable for *in situ* measurements; it is sensitive to miniscule interfacial effects, such as the presence of a single LB monolayer and measurements are perfectly feasable in media such as air, so that elaborate preparation of the immediate environment is unnecessary. The enormous variety of existing natural and artificial systems containing interfaces has led to the development of theory and application of ellipsometry in diverse fields of study [Azzam and Bashara, 1977; Moisil and Moisil, 1973]. The following is restricted to study of LB films on silicon substrates by reflection ellipsometry.

4.6.2 Theory

Numerous articles describe the theoretical basis and applications of reflection ellipsometry [Bashara, et. al., 1969]. Here we are concerned with the thickness (TU) and real part of refractive index (NU) of LB overlayers on a previously characterised substrate having complex refractive index NS+iKS. In reflection, we may resolve the incident electric fields of polarised light into s and p components. The theory of ellipsometry is beyond the scope of this thesis, but some of its results are quoted below to clarify the approach taken in calculating optical constants. The basic equation of ellipsometry is

$$\rho = (tan\Psi)\exp(i\Delta) \tag{4.7}$$

where ρ is the (complex) ratio of Fresnel reflection coefficents for s and p polarisations, Ψ is its magnitude, expressed as an angle, and Δ is ρ's phase angle, or the difference between the s and p polarisation phase changes on reflection. Note that Δ and Ψ are angles ranging from 0 to 90° and 0 to 360°, respectively.

4.6.3 Experimental Arrangement

A Rudolph Research Auto-EL-IV nulling ellipsometer was used for all measurements. It consists essentially of two parts: an optical system for measuring polarisation states and a dedicated computer for converting the angles Δ and Ψ to optical constants. The optical equipment is shown schematically in figure 4.6 and consists of a polariser, quarter-wave compensator, sample and analyser (PCSA) through which light passes in that order. The compensator is fixed at some at some known azimuthal angle with respect to the direction of propagation of light. The polariser can be rotated until the reflected beam is linearly polarised; the analyser can be rotated until the reflected beam is extinguished, hence the appellation nulling ellipsometer. The polariser and analyser azimuths are directly proportional to the ellipsometric angles Δ and Ψ. Several measurements over the different angular zones over which the nulling condition may be satisfied ensure that the accuracy of the ellipsometric angles is known.

The second portion of the ellipsometer is a computer dedicated to extracting meaningful optical constants from the ellipsometric angles and other information. For the bare substrate, Fresnel showed that

$$\Delta = f_1(\Phi, \lambda, NA, NS, KS) \tag{4.8}$$

and

$$\Psi = g_1(\Phi, \lambda, NA, NS, KS) \tag{4.9}$$

where Φ is the angle of incidence and reflection, λ is the wavelength of light, NA the ambient refractive index. As NS and KS are the only two variables, their actual values are unique solutions to the above equations. Furthermore, for transparent films on characterised substrates, Drude proposed that

$$\Delta = f_2(\Phi, \lambda, NA, NS, KS, NU, TU) \tag{4.10}$$

and

$$\Psi = g_2(\Phi, \lambda, NA, NS, KS, NU, TU) \tag{4.11}$$

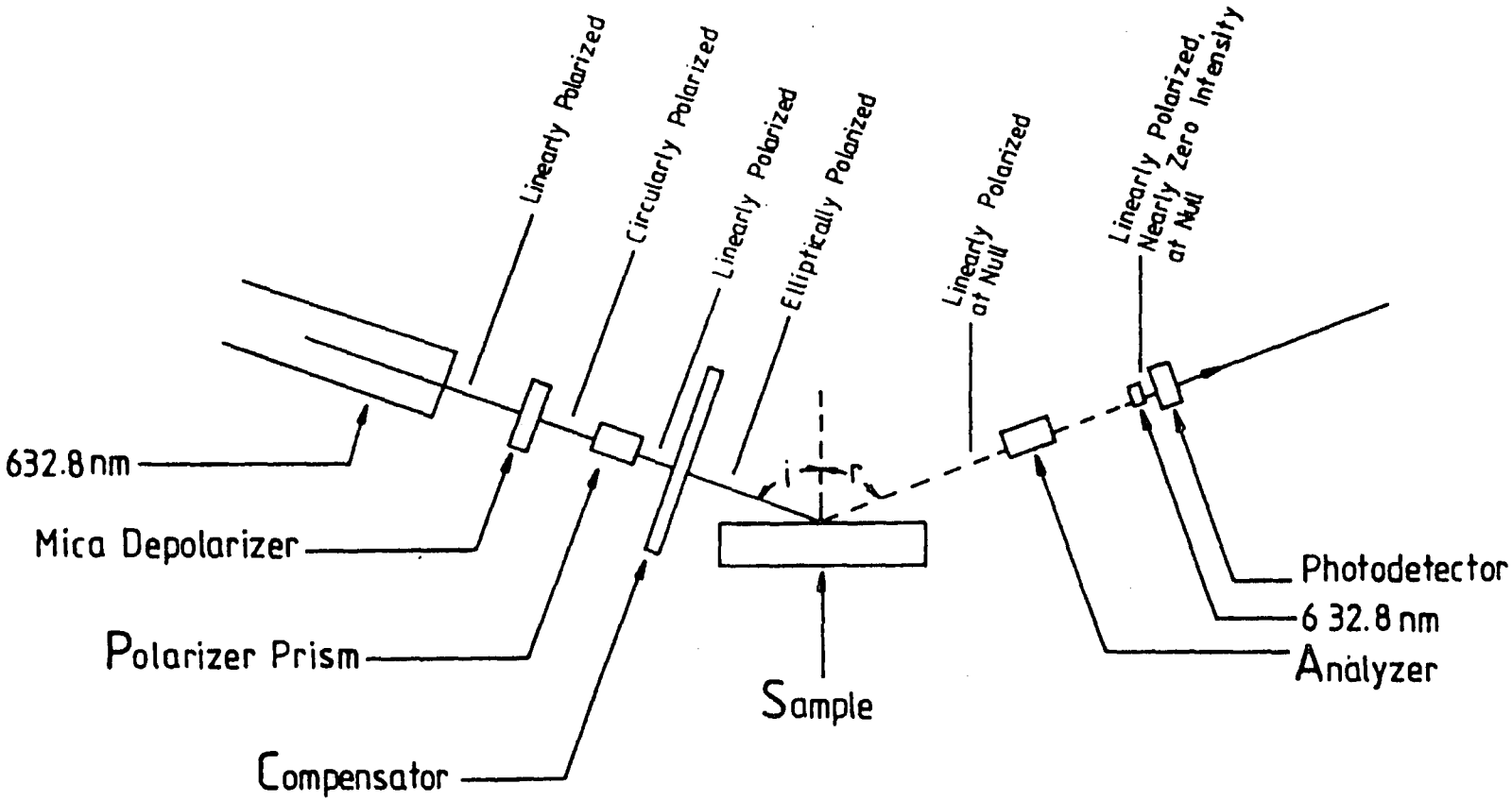

Figure 4.6 : Optical components of the Rudolph Auto-EL-IV nulling ellipsometer

where TU and NU are the thickness and real part of refractive index respectively. These equations cannot be inverted to provide unique solutions for NU and TU; numerical methods are used instead. The ellipsometer used here presumes that, for a single film, the ellipsometric angles arise entirely from the effects of reflection from the film surface and film-substrate interface, and transmission through the film. When the optical path taken by the light through the film is an integral multiple of the wavelength of light, constructive interference occurs between the beams reflected from the air/film interface and the film/substrate interface, with the results that the ellipsometric angles are as they would be if the film were absent. That is, Δ and Ψ are periodic functions of film thickness, each period corresponding to one cycle thickness. The cycle thickness d_c, given by

$$d_c = \frac{\lambda}{2\sqrt{(NU)^2 - sin^2\Phi}} \tag{4.12}$$

is always smaller than half the wavelength of light since light entering the film traverses the optically dense film twice at an oblique angle. One consequence of this is that if a film is thicker than d_c, the ellipsometer must be informed as to which cycle it is operating on if it is to produce the correct answer for film thickness. Another consequence is that in the unlikely event of the real film thickness being very close to a cycle thickness, iterative solution of equations 4.10 and 4.11 for thickness and refractive index is unlikely to succeed.

4.7 SECOND HARMONIC GENERATION FROM LB FILMS

The second-harmonic generation experiments described here were performed at Plessy (Caswell) with the collaboration of Drs. Neil Carr and Martin Goodwin. The equipment used is shown schematically in figure 4.7. The mono- and multilayer samples were deposited onto hydrophilic Chance-Propper soda glass or Corning 7059 slides. The optical equipment was aligned with a He-Ne laser so that the vertically mounted sample was inclined normally with respect to the Nd:YAG laser beam. The incident s-polarised beam was tuned to the 1.06μm Nd:YAG fundamental wavelength, with pulse energy 7.5 mJ and duration 30 ns and focussed down to its minimum spot size by inserting a hemicyanine monolayer sample into the beam path and adjusting the lens position until the second harmonic output power reached a maximum. The second harmonic at 532 nm was filtered out from the transmitted radiation and measured in intensity with a photomultiplier. The reference photodiode provided a convenient measure of input power at the fundamental wavelength. Measurements

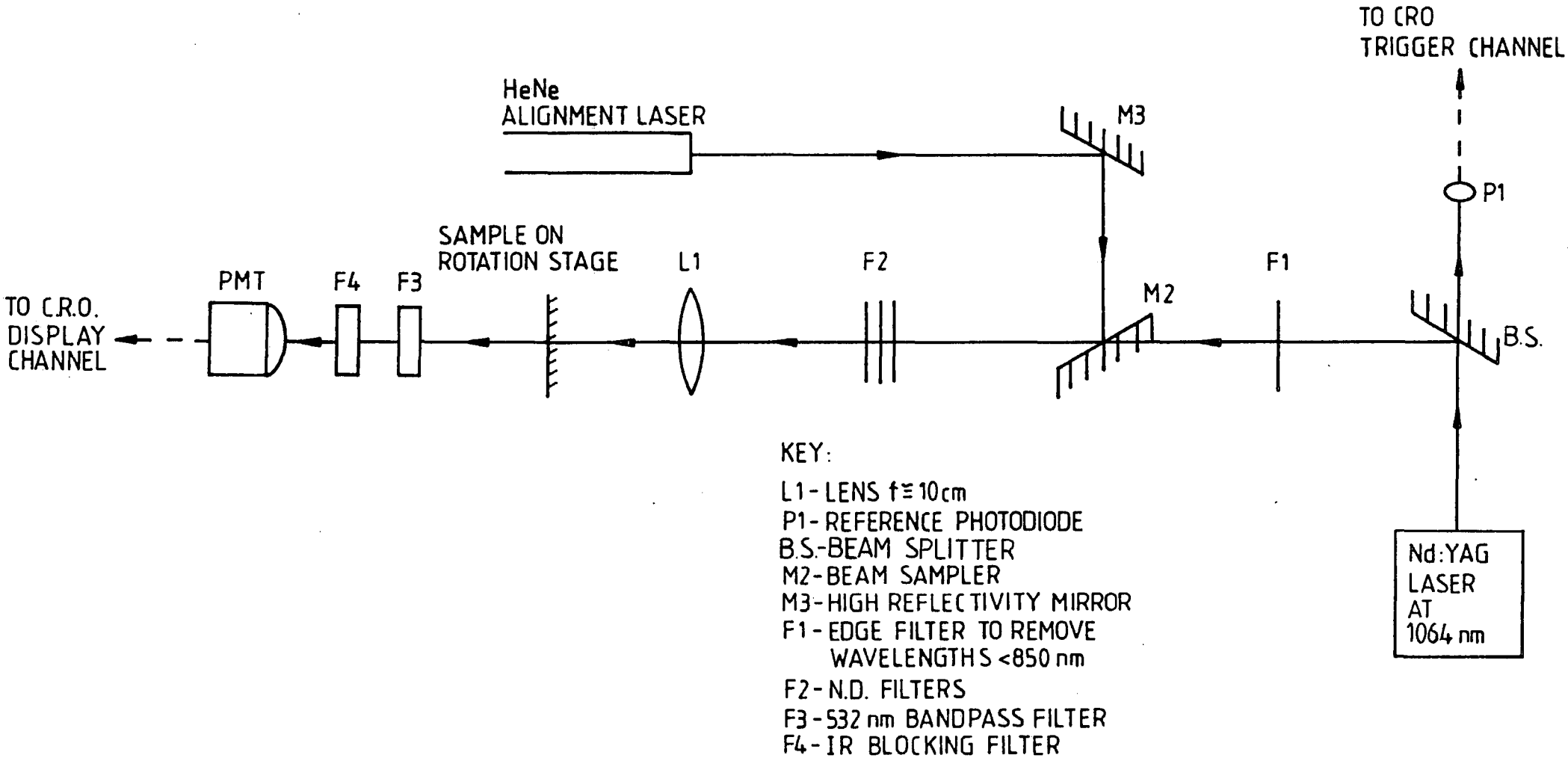

Figure 4.7 : Schematic Diagram of equipment used to observe SHG from LB films

were made by averaging pulse heights at a number of different locations on the sample and comparing them to the output pulse heights for a hemicyanine monolayer, all other factors being equal. The purpose of the experiments was to rank the samples investigated in order of second harmonic output power with respect to a hemicyanine monolayer.

The second harmonic output power in transmission through a thin sample (one too thin for the fundamental and second harmonic to develop significant phase mismatch) is given by [Bosshard, et. al., 1989]

$$I_{2\omega} = \frac{1}{2c\epsilon_0 n_{2\omega}} \left(\frac{\pi \chi^{(2)}(-2\omega;\omega,\omega) L I_\omega}{\lambda_\omega n_\omega} \right)^2 \tag{4.13}$$

where $I_{2\omega}$ =second harmonic intensity

$n_{2\omega}$ =refractive index at second harmonic

$\chi^{(2)}(-2\omega;\omega,\omega)$ = second harmonic susceptibility

L = sample thickness

I_ω = fundamental intensity

λ_ω = fundamental wavelength

n_ω = refractive index at fundamental

For constant input intensity and wavelength, ignoring dispersion,

$$\chi^{(2)}(-2\omega;\omega,\omega) = \chi^{(2)}_{hemi}(-2\omega;\omega,\omega) \sqrt{\frac{I_{2\omega}}{I_{2\omega}(hemi)}} \frac{L_{hemi}}{L} \sqrt{\frac{n^3}{n^3_{hemi}}} \tag{4.14}$$

This formula is used in chapter seven to calculate second order susceptibilities of novel materials. In normal-incidence transmission SHG using an s-polarised fundamental and collecting p-polarised second harmonic radiation, the only components of the nonlinear susceptibility tensor that may be probed are $\chi^{(2)}_{yxx}$ or $\chi^{(2)}_{xyy}$.

4.8 SUMMARY

This chapter has described the methods and equipment used for characterisation of LB films in this thesis. The procedures for recording and interpreting SPR and

Pockels' effect data have been described in detail. Ellipsometry, second harmonic generation and spectrophotometry have also been mentioned as relevent characterisation techniques, since they provide additionnal data to corroborate results obtained by SPR and the Pockels' effect.

4.9 REFERENCES

Azzam, R. M. A., Bashara, N. M. : Ellipsometry and Polarised Light , 1977 publ. North-Holland.

Bosshard, Ch., Tieke, B., Seifert, M., Günter, P. : Nonlinear Optical Y-type Langmuir-Blodgett Films of 2-docosylamino-5- nitropyridine (Presented at Int. Conf. Materials for Non-linear and Electro- optics, Cambridge, UK) ,*Inst. Phys. Conf. Ser. No 103 Section 2.3* , 1989 pp. 181-6. publ. IOP Publishing.

Barker, A. S. Jnr. : Optical Measurements of Surface Plasmons in Gold ,*Phys. Rev. B.* **8** *12* , 1973 pp. 5418-26.

Collected Authors : Proceedings of the Symposium on Recent Developments in Ellipsometry , *Surf. Sci.* **16** , 1969 publ. North-Holland, Amsterdam. , ed. Bashara, N. M., Buckman, A. B., Hall, A. C..

Connes, J. : PhD Thesis , 1961

Heavens, O. S. : Optical Properties of Thin Solid Films , 1955 publ. Dover.

Kovacs, G. : Optical Excitation of Surface Plasmon- Polaritons in Layered Media ,*Electromagnetic Surface Modes* , 1982 pp. 143-200. publ. John Wiley. , ed. Boardman A D.

McLeod, H. A. : Thin-Film Optical Filters , 1986 publ. Main Library.

Moisil, D., Moisil, G. : Teoria Şi Practica Elipsometriei (*in Romanian*) , 1973 publ. Editura Techniča, Budapest.

Otto, A. : Excitation of Nonradiative Surface Plasma Waves in Silver by the Method of Frus trated Total Reflection ,*Z. Physik* **216** , 1968 pp. 398-410.

Pockrand, I. : Surface Plasma Oscillations at Silver Surfaces with Thin Transparent and Absorb ing Coatings ,*Surf. Sci.* **72** , 1978 pp. 577-88.

Pockrand, I., Swalen, J. D., Gordon, J. G., Philpott, M. R. : Surface Plasmon Spectroscopy of Organic Monolayer Assemblies ,*Surf. Sci.* **74** , 1977 pp. 237-44.

Raether, H. : Surface Plasmons and Roughness , *Surface Polaritons* , 1982 pp. 331-403. publ. North-Holland.

Shen, Y. R. : The Principles of Nonlinear Optics , 1984 publ. Wiley.

Wähling, G. : Arachidate Layers on Ag and Au Detected by the ATR Method ,*Z. Naturforsch* **33a** , 1978 pp. 536-39.

Yariv, A. : Optical Electronics , 1985 publ. Holt, Rinehart and Winston.

Chapter V

CHARACTERISATION OF FLOATING MONOLAYERS AND MULTILAYER FILM DEPOSITION

5.1 MATERIALS

One of the major concerns of this project was to examine LB film assemblies having second-order optical nonlinearities measureable by the Pockels' Effect. To this end, the present chapter is dedicated to three classes of materials which have many of the characteristics expected of compounds having large molecular hyperpolarisabilities. The criteria for production of the latter hyperpolarisabilities have been elucidated in chapter two, and the resulting macroscopic nonlinear optical properties are detailed in following chapters. This chapter describes the formation, stability and deposition of monolayers of each of the above classes of material. The basic structure of the compounds examined here is that of donor and acceptor groups separated by a conjugated system, with added hydrophobic groups for improved floating monolayer stability.

5.1.1 Hemicyanine and Nitrostilbene (4HANS)

A variety of dipolar chromophores, synthesised in Durham, exemplify the use of donor and acceptor groups separated by conjugated systems to produce molecules with large second-order nonlinearities. A variety of styrylpyridinium and stilbene dyes was examined in Durham and elsewhere [Neal, 1987]. Several combinations of donor and acceptor groups were attached to the above two fundamental moieties, forming a range of molecules with predictable ranking of microscopic hyperpolarisabilities. The donor-acceptor assemblies hemicyanine and 4HANS, shown schematically in figure 5.1, have been culled from those experiments as the two molecules exhibiting a good combination of LB film-forming properties and optical nonlinearities. The hemicyanine pyridinium group is expected to act as an acceptor while the donor is the dimethylamino group. By contrast, the 4HANS acceptor is a nitro group while the donor is an amide group, putting its dipole moment in the opposite sense to that of hemicyanine. Both compounds have long hydrocarbon chains to render them highly water-insoluble.

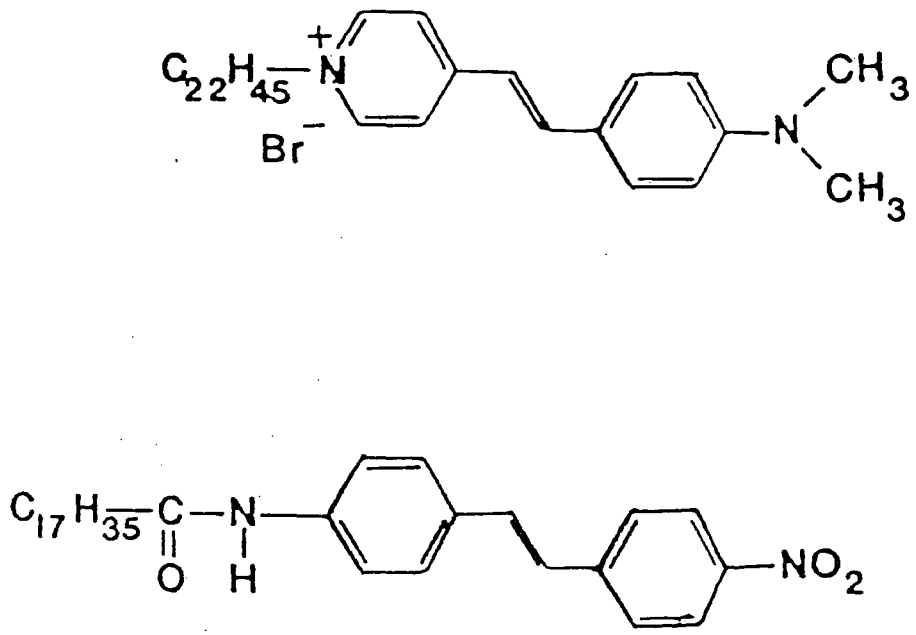

Figure 5.1 : Hemicyanine (upper) and 4HANS (lower). They are based on styrylpyridinium and stilbene moieties respectively

The hemicyanine dye, available in its pure form, has been characterised extensively at Durham and elsewhere [Neal, 1987]. By contrast, *pure* 4HANS has only been available at Durham since February 1990; batches of dye from previous synthesis are now known to contain approximately 50% 4HANS whilst the remainder is equal portions of stearic acid and water-soluble stilbene derivatives. Pure 4HANS dissolves in chloroform with difficulty and cannot be deposited in LB film form [Tsibouklis et. al., 1990]. As a result, the published data from Durham on 4HANS film formation applies not to the pure material, but to a mixture of 4HANS and fatty acid. The practical consequences of this are, fortunately, not severe. Film parameters such as area per molecule, molecular weight and collapse pressure have to be revised; estimates of the microscopic nonlinear susceptibility of 4HANS must be revised upwards, as the presence of the fatty acid will dilute macroscopic nonlinear effects [Neal, 1987].

5.1.2 Novel Polysiloxanes

New polymeric materials synthesised at Hull University [Carr et. al., 1987] have

been examined at Durham for their LB film-forming capabilities. In bulk form they are all dark red tar-like materials which disslove readily in chloroform. Their essential structure is shown in figure 5.2 and consists of a siloxane backbone to which are attached functional groups at random intervals. The siloxane spine amounts to a substitute for the conventional long hydrocarbon tail, preventing dissolution of the floating monolayer. It is also expected to confer a high degree of robustness onto the LB film. The average length of each polymer molecule corresponds to sixteen siloxane units; eight of these, on average, will attach to a dipolar chromophore. The polymethylene spacer units between the chromophores and the spine prevent excessive polymer rigidity, in the expectation that this eases film deposition. The limitation of chromophore substitution to no more than 50% avoids steric hindrance. The portions of the molecule responsible for nonlinear optical behaviour are the dipolar chromophores. The nitromethyl groups of AMCR22 and AMCR23 are strong donors while the carboxy group of AMCR24 and the azophenyl portions of all chromophores are acceptors. Thus, the dipole moment of AMCR24 is in an opposite direction to that of AMCR22 or AMCR23 with respect to the siloxane spine. Since each material is not one pure compound, but a mixture of hundreds of polymers of differing lengths and compositions, such characteristics as area per molecule and molecular weight cannot be known exactly. Another material fabricated by a similar method has been examined for its LB film-forming and nonlinear optical properties [Brettle et. al., 1987] with promising results.

5.1.3 Novel Bipolar Chromophores

Given the efficacy of hemicyanine and 4HANS as optically nonlinear materials in LB film form, it was considered worthwhile to vary several aspects of their structure while retaining their basic form. The chosen materials, shown in figure 5.3 and synthesised at Durham University's Department of Chemistry [Tsibouklis et. al., 1989], are all dark green chloroform-soluble crystals. Each is based on a diarylalkyne moiety terminating in a hydrocarbon chain. They all consist of a donor and an acceptor separated by a conjugated system. Those of particular interest to this thesis are JT1-JT4 inclusive whose terminal donor, if present, is a methoxy group while the acceptor is a pyridinium radical.

The structures and purities of the JT materials have been assessed by several methods. Foremost of these is nuclear magnetic resonance (NMR). There exists a vast body of information on the nature and applications of NMR, to which the interested reader is referred [Carrington & McLachlan, 1967]. Briefly, NMR has been

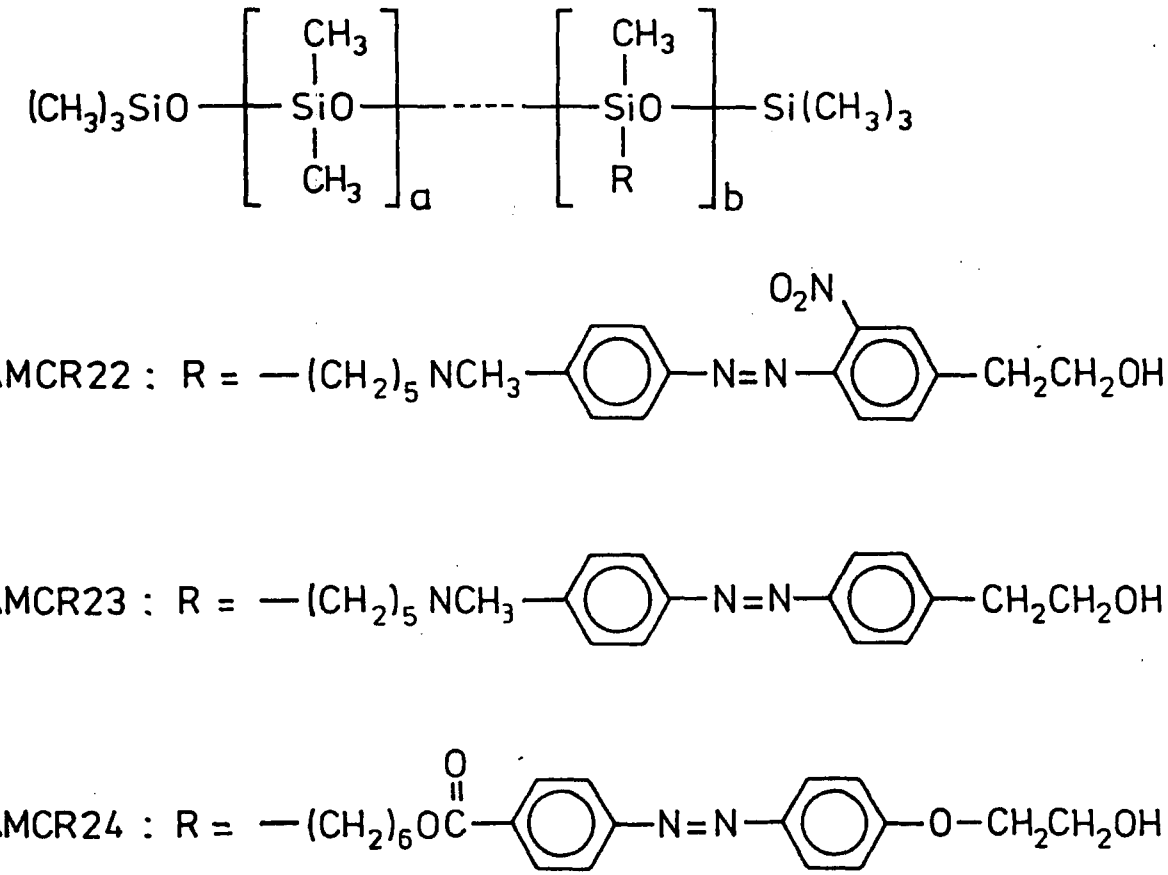

Figure 5.2 : Molecular Structures of the Hull Polymers AMCR22, AMCR23 and AMCR24

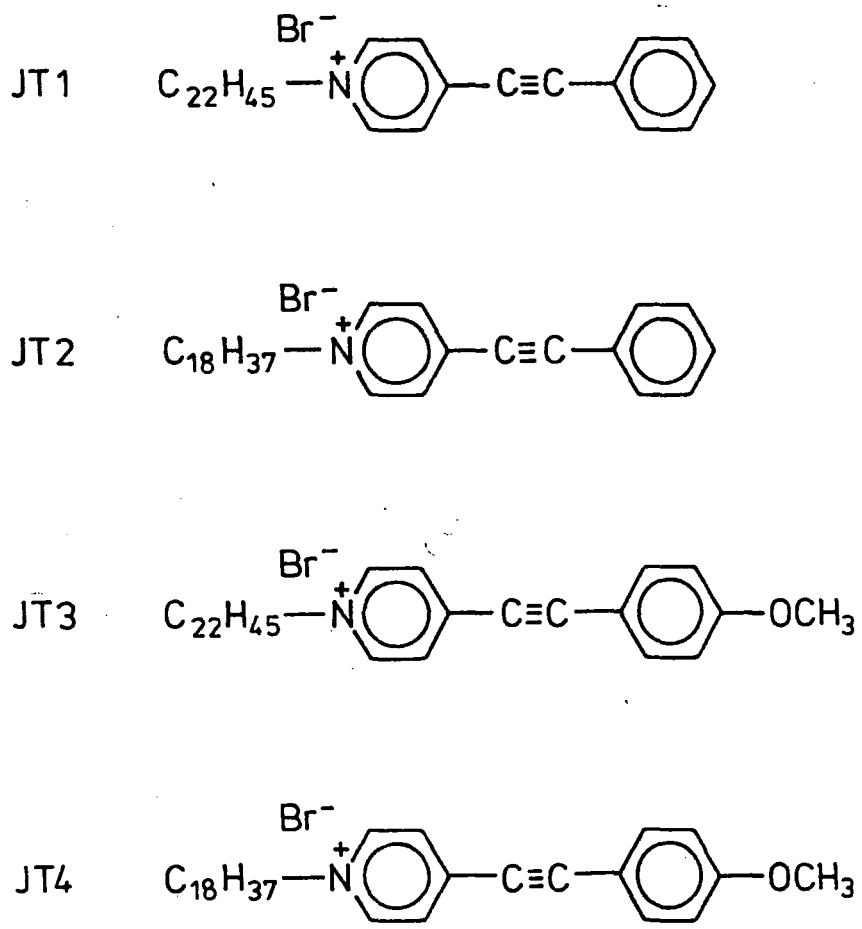

Figure 5.3 : The JT series of molecules

used here to identify the different chemical environments present in the vicinity of any particular nucleus, thus indicating the presence of impurities or degredation products. For example, examination of the carbon nucleus by NMR is a way of enumerating the different types of carbon bond present in any particular material. Applied to several nuclei, this method is a conclusive test of chemical purity.

5.2 PRESSURE-AREA ISOTHERMS AND STABILITY STUDIES

5.2.1 Exemplary Standards : Stearic Acid

The pressure-area (π-A) isotherm of a classic LB film-forming material, stearic acid, is shown in figure 3.6. This isotherm consists of several distinct sections, discussed in section 3.7, and is frequently used as a standard against which other materials are compared. On account of their simplicity, such isotherms are desirable in materials having commercial applications, although more complex isotherms may be more useful in fundamental structure studies [Stenhagen, 1955]. The less complex isotherms generally show only a small surface pressure prior to the most condensed phase, which should be sufficiently fluid to allow the film to be maintained at a set surface pressure with a precision greater than 1 mNm^{-1}. Films displaying a finite surface pressure at extremely large molecular areas, and whose isotherms have gentle slopes with increasing pressure almost invariably consist of molecules lying nearly flat on the subphase; film compression, then, gradually alters their orientation until the hydrophobic portions stand approximately vertically.

The isotherms are plotted with surface pressure (mNm^{-1}) as ordinate and area per molecule (nm^2) as abcissa. The latter is originally recorded as the area of water surface A enclosed by the trough barriers and is converted to molecular area a by the formula

$$a = \frac{AM}{cVN_A} \tag{5.1}$$

where c is the spreading solution concentration, V the volume spread, M the molecular weight and N_A Avogadro's number. The principal sources of error in molecular area arise from measurement errors in trough area, solution concentration and volume spread. These are each on the order of 5%, giving a net fractional error on the order of 11.5% in molecular area. It is, however, worth noting that the precision of the molecular area measurement may not be as high as the errors in A, c, V and M may suggest. Several reasons for this present themselves: soluble impurities in the bulk

material, notably water in the case of hygroscopic materials, lead to values for molecular areas which are too small, as do dissolution of the monolayer prior to compression and formation of films which are thicker than one monolayer; over-large values of molecular area arise from rigid films which do not spread to occupy every available space on the subphase. If the Langmuir film material is a mixture of polymers, the average molecular weight M may not be representative of the component molecules responsible for film properties. So, the above measurement is generally referred to as the "apparent "area per molecule. Two values of molecular area are particularly important: a_0, the condensed phase area per molecule in the zero-pressure limit, obtained by extrapolation of the steep linear portion of the isotherm to zero surface pressure, and a_c, the area at the point of monolayer collapse. The surface pressure π_c corresponding to the latter area is also often quoted.

It is informative to repeatedly compress a monolayer to just below its point of collapse and expand it out to its original area, observing any changes in the isotherm. The perfect isotherm would exhibit no hysteresis; in practice, classical LB film-forming materials show little change on repeated cycling of isotherms. Dissolution of monolayers becomes apparent in a shift of the isotherm towards smaller trough area. Film rigidity, on the other hand, usually appears as failure of surface pressure to drop significantly on expansion of the trough barriers.

The onset of monolayer collapse can be observed in two ways. Firstly, the isotherm slope decreases markedly at the collapsing pressure π_c and secondly, striations appear parallel to the moving portions of the barriers on the subphase. The latter are particularly noticeable when dealing with coloured dye materials, but are by no means difficult to espy in the case of clear materials. Langmuir film collapse is a catastrophic demise of film structure in which the film buckles and piles up on itself. Certain materials have a tendency to form floating multilayers under various degrees of coercion; these can be detected, if not by a suspiciously low molecular area, then by the formation of coloured islands visible to the naked eye. Such materials are rarely of any use in their pure form, but have to be diluted with stearic, arachidic or 22-tricosenoic acid to produce good quality LB films. The chosen molar ratio of dye to fatty acid is usually 1 : 1, but may be as small as 1 : 10, depending on the difficulty of film formation.

Given the above, it is clear that a pressure-area isotherm can be an invaluable aid to successful dipping. Aside from any information it may contain on the structure of the floating layer, its purpose is to indicate a range of surface pressures over

which deposition of monolayers is likely to succeed. This usually spans a steep part of the isotherm below the collapse pressure. In this respect, isotherms are most useful if the origins of their pressure axes are at the subphase surface pressure and their behaviour with time is known. Thus, the pressure-area plot of each material is presented, where possible, as a collection of isotherms recorded at various intervals after initial spreading of the Langmuir film. At the film pickup rates used in Durham to date, most floating monolayers are exhausted after an hour and a half from the time of spreading, so it was not considered worthwhile to record isotherms at times beyond approximately ninety minutes.

5.2.2 Novel Polysiloxanes

As can be seen from figures 5.4-5.6 these polymers exhibit isotherms having several distinct sections at different ranges of surface pressure. Bearing in mind, however, that these materials do not consist of one type of polymer chain of definite length, but of numerous chains of different sizes and compositions, and that the isotherms of any of these are unlikely to resemble those of the ideal materials, care must be taken in the interpretation of these isotherms. Initially, at surface pressures up to approximately 1 mNm^{-1}, the polymer molecules unwind and distribute themselves freely over the subphase surface. On compression up to approximately 22 mNm^{-1}, the polymer molecules are gradually forced to interdigitate until all available interstices are occupied. Given the apparent lack of order in LB films of the AMCR series of materials (see section 5.4), it is likely that the compressed monolayers resemble an array of comb-like molecules whose flexible spines and side chains lie more or less in the plane of the aqueous subphase. As the collapse pressure is approached, the molecules gradually abut onto each other until a continuous floating film is formed.

Beyond the collapse pressure films of AMCR22 and AMCR23 maintain their surface pressure but decrease in area. Exceptionally, AMCR24 has no well-defined collapse pressure. Although the floating films darken visibly at this stage, the striations characteristic of a collapsed film do not appear on the subphase surface; this is taken as an indication that the floating monolayers are piling up one on top of another to form stable multilayers. The fact that isotherms of these materials vary little on expansion and recompression (*vide* figures 5.4-5.6) indicates that any structural changes associated with collapse are either negligible or reversible. No attempt was made to deposit these films onto substrates owing to the uncertainty in film uniformity and the difficulty of holding the film area constant under feedback from the Wilhelmy plate pressure sensor.

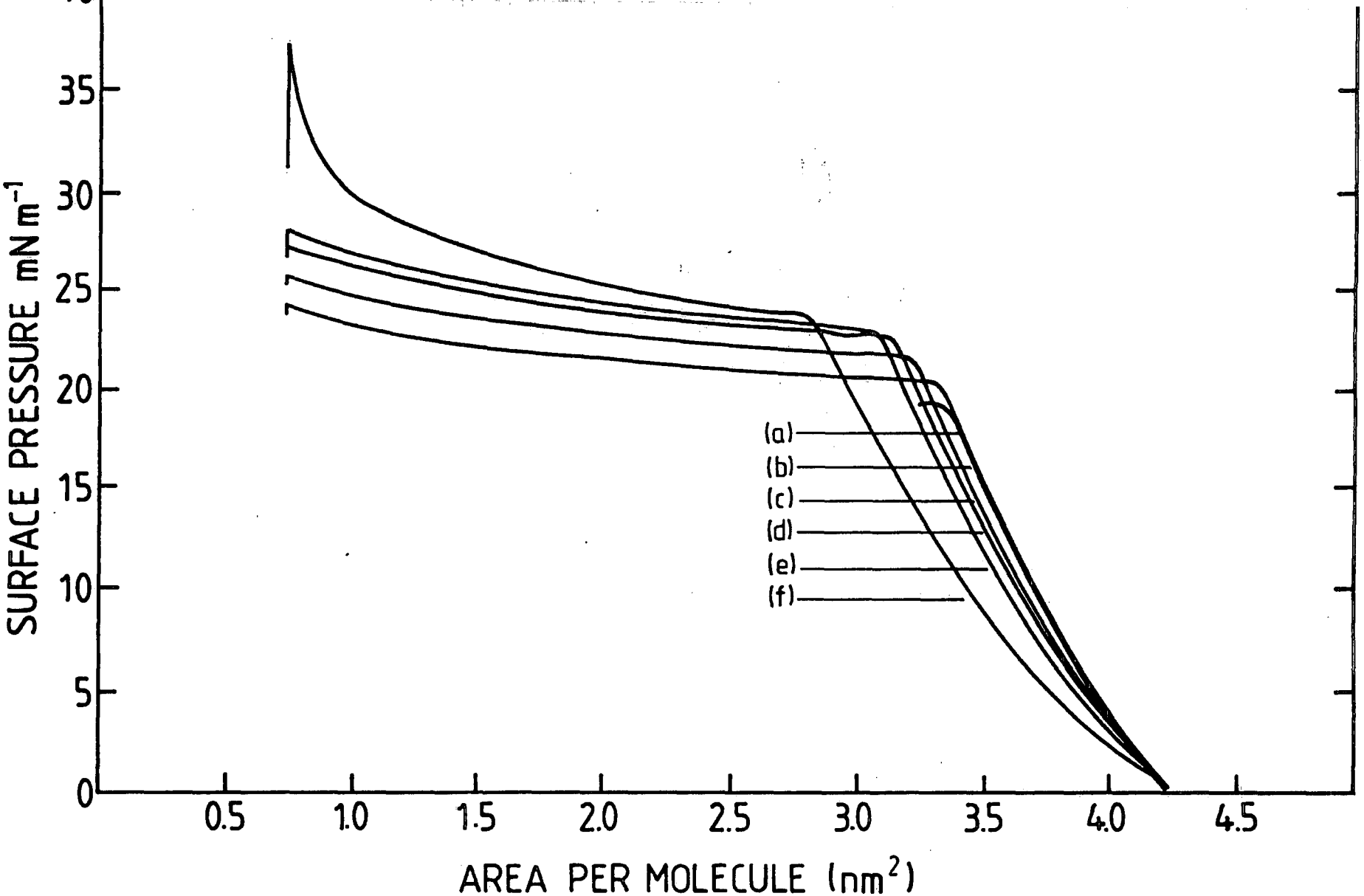

Figure 5.4 : AMCR22 Isotherm family. Curves a-f are isotherms at fifteen-minute intervals after spreading

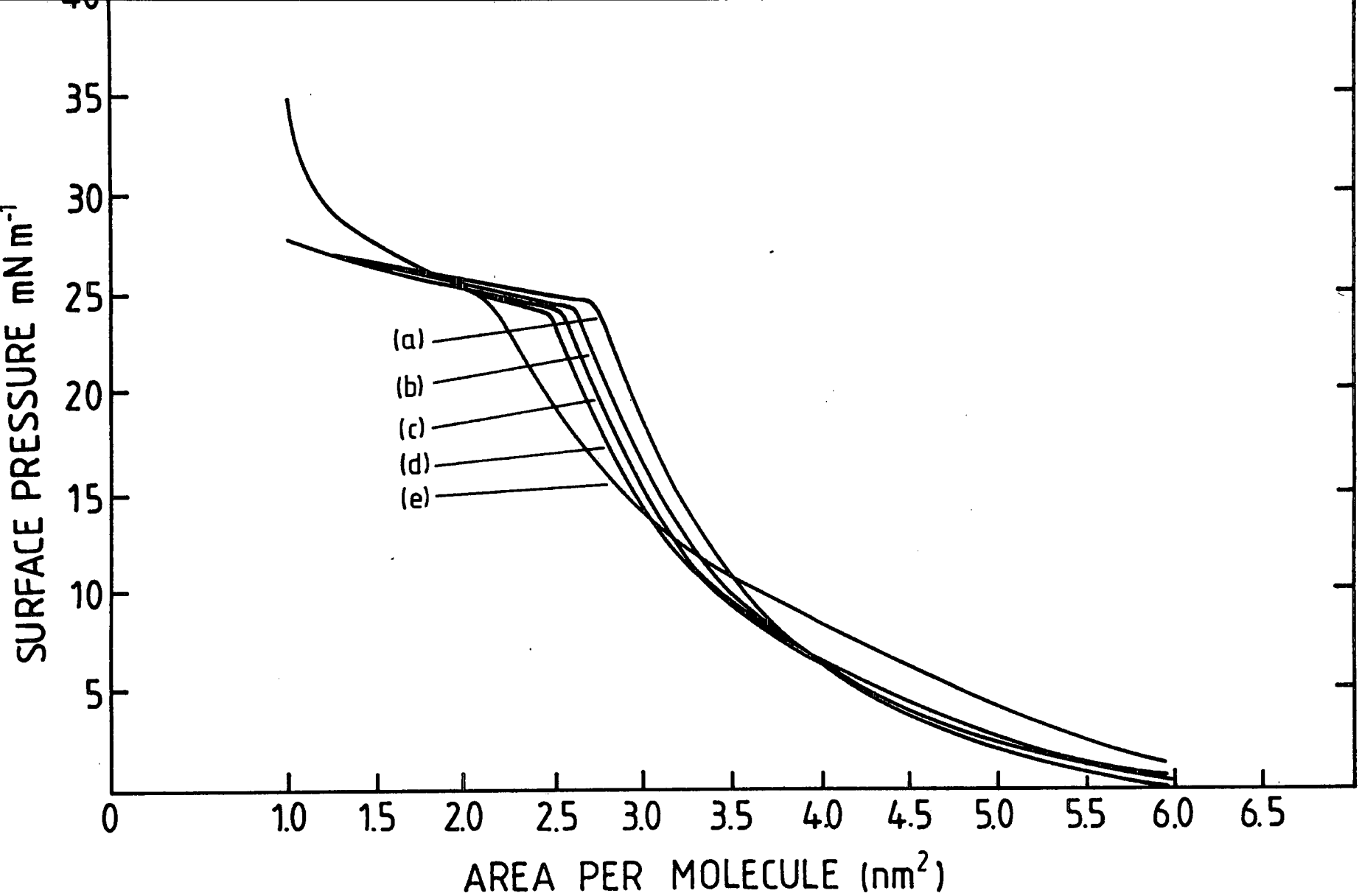

Figure 5.5 : AMCR23 Isotherm family. Curves a-e are isotherms at fifteen-minute intervals after spreading

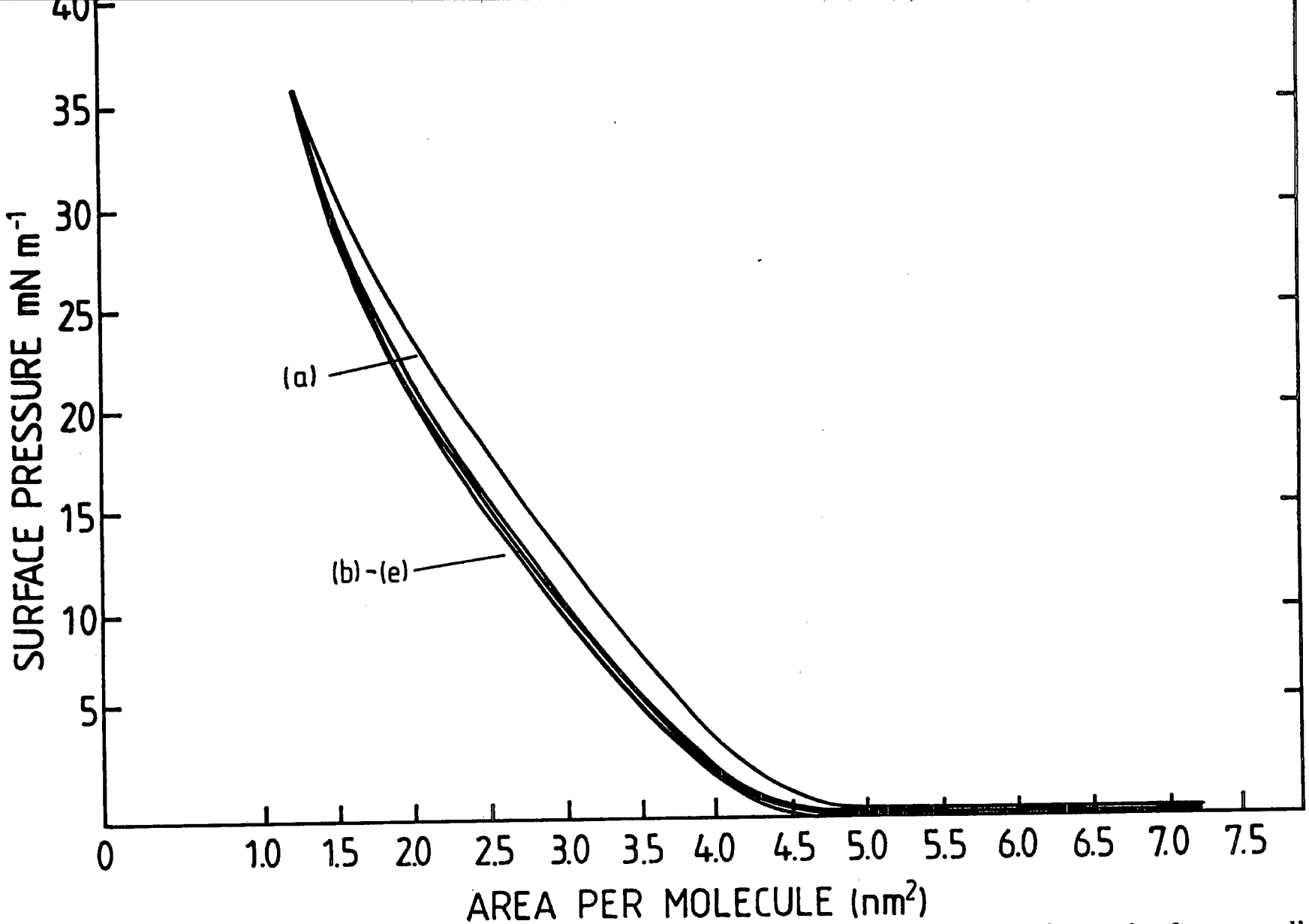

Figure 5.6 : AMCR24 Isotherm family. Curves a-e are isotherms at fifteen-minute intervals after spreading

When held below collapse pressure, monolayers of each material show a slow exponential decay of area with time, having a characterisitic half-life. Table 5.1 lists those floating monolayer properties, including film half-life, derived from isotherms and stability studies.

Although film half-lives are a good indicator of decay of an undisturbed floating monolayer, they provide no information on film mobility, and so cannot indicate whether film rigidity is likely to inhibit film deposition. From the film's property of respreading itself, described above, it is clear that these films do not harden sufficiently, on the timescale of the experiments described here, for monolayer rigidity to become a problem where film deposition is concerned. Furthermore, the suction test has been applied to monolayers spread and compressed on the previous day; the floating films of all materials responded well in every case.

5.2.3 Novel Bipolar Chromophores

Isotherm families for materials JT1, JT3 and JT4 are shown in figures 5.7, 5.8 and 5.9 respectively. The isotherm of JT2 is absent because the material dissolved in water too rapidly to record an isotherm. To record the isotherms, the material was first spread on a fully-expanded trough, the solvent was left to evaporate for fifteen minutes and the isotherms were then recorded at fifteen-minute intervals. It is immediately apparent that the largest change in the isotherms occurs between the first two compressions, probably as a result of evaporation of residual chloroform from the film after fifteen minutes. Otherwise, the form of the curves changes little over the next few compressions up to the last one, which reduces the film area to the limit imposed by the trough. The liquid and gaseous phases are largely contiguous, and no well-defined solid phase exists at high pressures. Instead, the films exhibit quite complex behaviour near the collapse pressure. JT1 and JT3 have in common a feature similar to the isosbestic point of absorption spectra: the isotherms all intersect at one point, indicating that no significant film dissolution has taken place; this observation is borne out by their long decay times. The behaviour of JT1, at 38 mNm^{-1} is clearer than that of JT3, at 36 mNm^{-1}. At pressures below that point, the films occupy progressively smaller areas with successive isotherms. This indicates that the structural order imposed at high pressure is to some extent retained on expansion of the film, even though the film can by no means be described as rigid. Beyond the point of crossover, each film undergoes partial collapse, as shown by the decrease in film area, and subsequently rallies to form a very incompressible phase at pressures above 40 mNm^{-1}. Although the isotherms of that region are steep enough

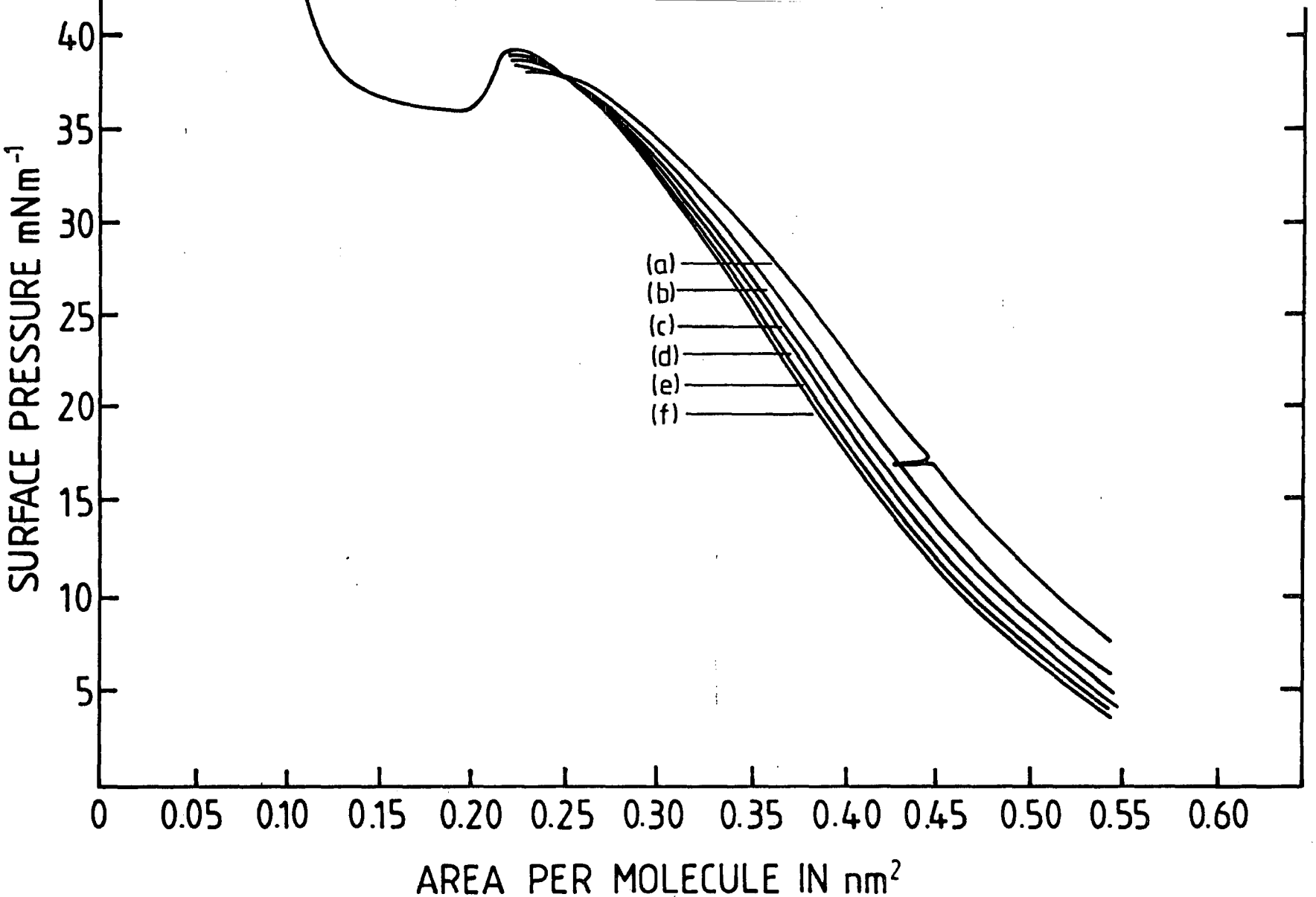

Figure 5.7 : A family of JT1 isotherms. Curves (a)-(f) are recorded at fifteen-minute intervals after spreading

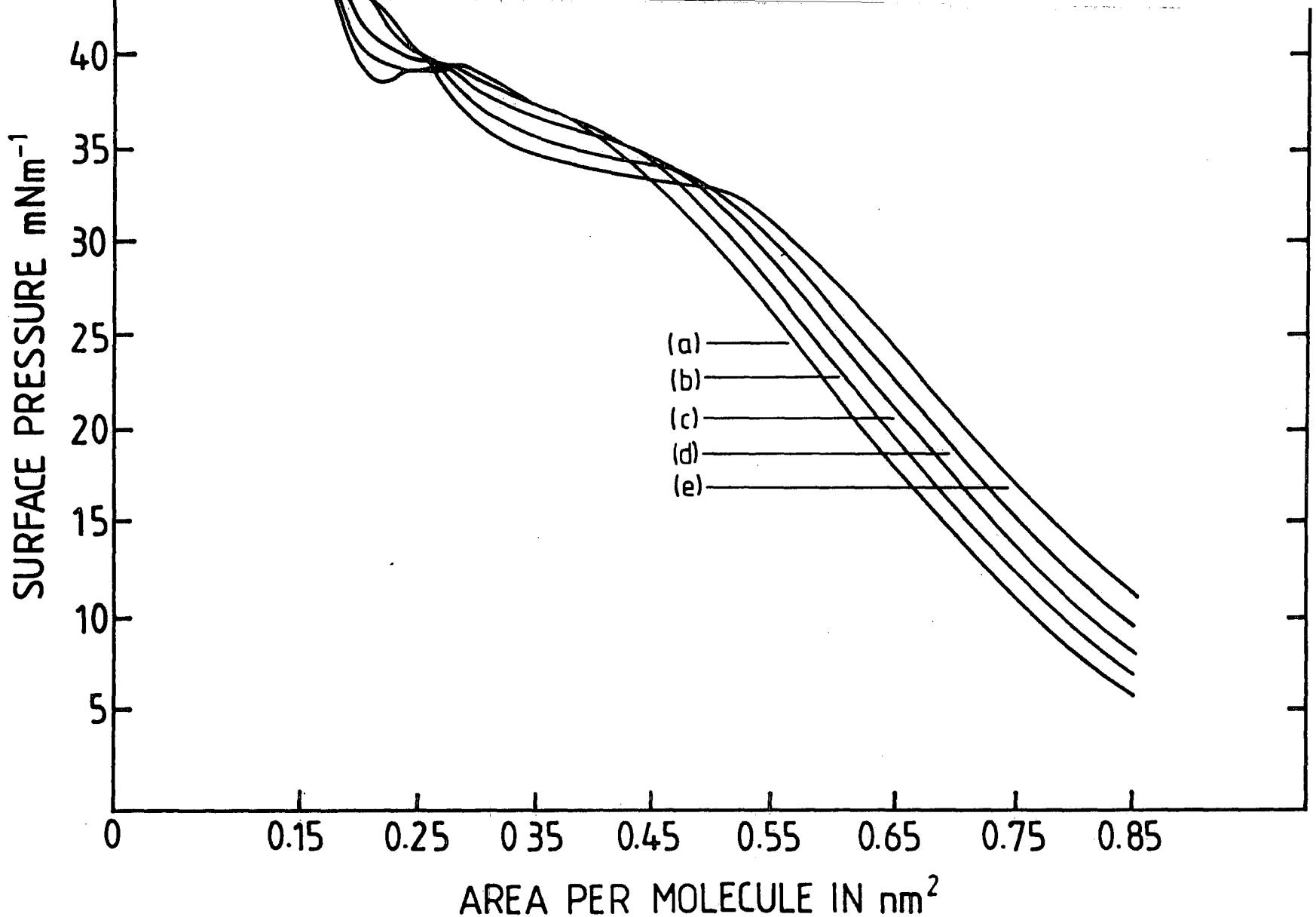

Figure 5.8 : A family of JT3 isotherms. Curves (a)-(e) are recorded at fifteen-minute intervals after spreading

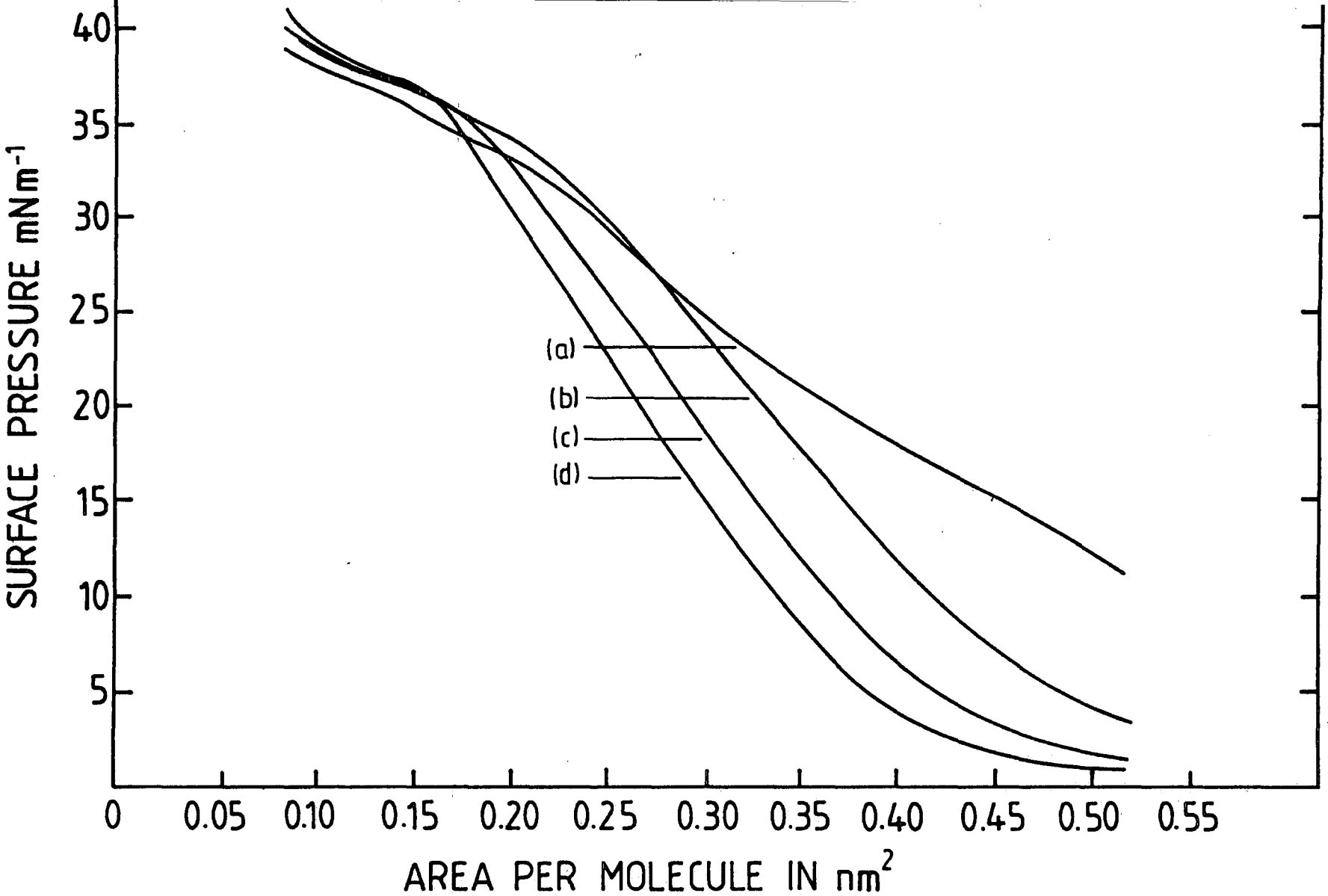

Figure 5.9 : A family of JT4 isotherms. Curves (a)-(d) are recorded at fifteen-minute intervals after spreading

to permit successful film deposition, the film is obviously not a monolayer; so dipping is performed below that pressure.

The JT4 isotherms shown in figure 5.9 have no such isosbestic point, and the large amount of material spread indicates that the monolayer is dissolving rapidly. The same applies to films of JT2, which dissolved so rapidly that the trough barriers could not be moved quickly enough to measure the film decay time. Evidently, the longer hydrocarbon chain of JT4, compared to that of JT2, defers film dissolution. This behaviour, though, is clearly not as significant as the effect of the terminal methoxy group. Comparison of film decay times of JT2 and JT4 with those of JT1 and JT3, respectively, suggests that the terminal polar methoxy group confers far greater insolubility onto the floating monolayer than the additional few methylene groups. The film properties derived from each isotherm are listed in table 5.1; $\tau_{1/2}$, the time taken for a compressed monolayer to halve in area, is also listed for each material.

5.3 FILM TRANSFER

Having examined the behaviour of the floating monolayers, the next step was to attempt to transfer them to solid substrates. The methods described in this section for assessment of film quality are quite simple; more refined techniques can be found in the following chapter. The transfer ratio was introduced in section 3.8.3; this figure of merit was the primary indicator of the consistency of LB film deposition. Where deposition was especially poor, examination with the naked eye would usually reveal patches where islands of collapsed film had been picked up. For thicker films ($\approx$20 layers) the same test could be used to check that the film colour was uniform over the entire sample. Finally, breathing lightly on the film will cloud the surface, giving an indication of the uniformity of deposition.

5.3.1 Novel Polysiloxanes

All of the polysiloxane materials have reproducible isotherms and are sufficiently stable to allow pickup of numerous layers from one floating film. Deposition onto hydrophilic substrates such as ordinary soda glass and silver is initially Y-type, becoming Z-type after the first three monolayers. Deposition onto soda glass was markedly more consistent than onto silver: several attempts were made to deposit monolayers onto silver, with indifferent success, although several samples were sufficently uniform to warrant further eaxmination (see chapters six and seven). Deposition onto hydrophobic substrates is firmly Z-type. In decreasing order of monolayer quality, the

Material	MW	Solubility	π_c	a_0	pH	τ_h	Suction Test	$\tau_{1/2}$ (min)
	(Kg mol)		(mNm^{-1})	(nm^2)		(min)	Response	at π_c
AMCR22	$\approx$4.13	Yes in $CHCl_3$	23	$\approx$3.9	5.6	N/A	Rapid after 14 hours	1320
AMCR23	$\approx$3.54	Yes in $CHCl_3$	24	$\approx$3.6	5.6	N/A	Rapid after 12 hours approx	850
AMCR24	$\approx$4.02	Yes in $CHCl_3$	$\geq$36	$\leq$2.7	5.6	N/A	Rapid after 4 hours	$\geq$10,000
JT1	0.568	Yes in $CHCl_3$	36	0.8	5.4	$\geq$120	Rapid after 3 hours	259
JT2	0.512	Yes in $CHCl_3$	N/A	N/A	5.4	—	N/A-water soluble	nil
JT3	0.598	Yes in $CHCl_3$	31-35	0.82-0.93	5.5	$\geq$200	Rapid after two hours	$\approx$454
JT4	0.542	Yes in $CHCl_3$	25-35	0.49-0.34	5.42	—	N/A - soluble film	$\approx$31

Table 5.1 : Properties of floating monolayers of AMCR and JT series materials

Material	π	Dip rate	Typical	Pickup Mode	Transfer	Max. no.	Substrate	Film Quality
	(mNm^{-1})	($mm\ min^{-1}$)	pH		Ratio (%±5)	of layers		
AMCR22	20	1	4.5-5	Z-type	93	30	hydrophobic glass	Initially patchy
AMCR23	21	1	4.5 5	Z-type	95	40	hydrophobic glass	Excellent
AMCR24	20	1	4.5-5	Z-type	85	10	hydrophobic glass	Very patchy
JT1	35	1	6.8-7	Y→Z-type	70	10	hydrophilic glass	Visibly uniform
JT2	-	-	-	N/A	-	None	-	
JT3	35	1	6.8	Z-type	86	37	hydrophilic glass	Visibly uniform
JT4	33	1	6.8-7	Z-type	60	8	hydrophilic glass	Patchy

Table 5.2 : Pickup properties of AMCR and JT series monolayers

materials rank as AMCR23, AMCR22 and AMCR24. Single monolayers of AMCR23 were invariably uniform to the naked eye and optical microscope. Occasionally, a defective film was streaked with drying stains. As indicated by the transfer ratios, these covered only a small portion of the total film area. Collapsed portions and pinholes on the monolayer were conspicuous by their absence.

5.3.2 Novel Dipolar Chromophores

Not all of the JT series of materials examined here dipped successfully. JT2 dissolved too rapidly to deposit any layers at all. Although JT4's monolayer decay time of half an hour permitted buildup of multilayers by spreading a fresh floating film between successive depositions, the film quality was clearly too poor to merit further investigation. Materials JT1 and JT3 were sufficently stable to allow deposition of several Z-type multilayers from a single floating monolayer. JT1 deposited initially on hydrophilic glass in a Z-type manner, becoming Y-type after the first few layers. JT3 was firmly Z-type on glass and silver.

5.4 RHEED and X-RAY DATA

A cursory examination of stepped structures of 10, 20, and 30 Z-type layers of AMCR22 and AMCR23 on Dynamit Nobel silicon by RHEED yielded no concrete evidence as to the structural order within the film, although Kikuchi lines from the silicon substrate were visible, as were one or two very diffuse rings ascribable to the polymer overlayers. Tubular glass substrates having twenty Z-type monolayers of AMCR22 and AMCR23 were subjected to low-angle X-ray scattering at the Lebedev Institute in Moscow [Y. Lvov., private communication]. This technique is designed to estimate the electron density in a direction normal to the glass substrate. The results indicated that the films were amorphous. The lack of well-defined crystalline structure within polymeric thin films, however, comes as no surprise.

5.5 SUMMARY

This chapter contains information on the isotherms, stability and pickup properties of floating monolayers of the siloxane polymers from Hull University and the JT series of material synthesised at Durham. Of the polymers, AMCR23 has the best LB film-forming properties, closely followed by AMCR22. The inadequacy of AMCR24 films precludes the need to examine it any further. Very cursory initial characterisation suggests that although the polymer films deposit well, they are dis-

ordered within the limits of sensitivity of RHEED and low-angle X-ray scattering. Of the JT series, JT3 produces by far the best LB films and merits further investigation.

5.6 REFERENCES

Brettle, J., Carr, N., Glenn, R., Goodwin, M., Trundle, C. : Polymeric Non-Linear Optical Waveguides ,*Proc. Int. SPIE. Conf., San Diego California* , 1987

Carr, N., Goodwin, M. J., McRoberts, A. M., Gray, G. W., Marsden, R., Scrowston, R. M. : Second Harmonic Generation in a Monomolecular Langmuir-Blodgett Film of a Preformed Polymer ,*Makromol. Chem. Rapid. commun.* **8** , 1987 pp. 487-93.

Carrington, A., McLachlan, A. D. : Introduction to Magnetic Resonance , 1967 publ. Chapman & Hall.

Neal, D. B. : Langmuir-Blodgett Films for Nonlinear Optics ,*PhD Thesis, University of Durham* , 1987

Stenhagen, E. : Determination of Organic Structures by Physical Methods , 1955 pp. 325- 71. publ. Academic Press (New York). , ed. Braude, E. A., Nachod, F. C..

Tsiboulkis, J., Cresswell, J. P., Feast, W. J., Mukherjee, S., Petty, M. C., : The Synthesis of 4-N-heptadecylamido-4- nitrostilbene (4HANS) ,*J. Molec. Electron.* **6** , 1990 pp. 221-3.

Tsibouklis, J., Cresswell, J. P., Kalita, N., Pearson, C., Maddaford, P. J., Ancelin, H., Yarwood, J., Goodwin, M. J., Carr, N., Feast, W. J., Petty, M. C. : Functionalised Diarylalkynes : A New Class of Langmuir-Blodgett Film Materials for Non-Linear Optics , *J. Phys. D.: Appl. Phys.* **22** , 1989 pp. 1608-12. publ. IOP.

Chapter VI

LINEAR MEASUREMENTS: RESULTS AND DISCUSSION

6.1 INTRODUCTION

This chapter contains the results of linear optical characterisation methods described in chapter four. The order of presentation is: optical absorption, ellipsometry and surface plasmon resonance (SPR). The final section mentions reflection high energy electron diffraction (RHEED) and small-angle X-ray diffraction.

6.2 OPTICAL ABSORPTION

6.2.1 Background

For any LB film designed for applications in optics, the optical absorption spectrum is an important characteristic, primarily because optical absorption spectra show which wavelengths may propagate through the film without significant attenuation. The optical absorption spectrum also influences the Pockels' effect: if the optical absorption is large over the SPR minimum, the curve is broadened and the magnitude of its slope either side of the minimum is reduced. When an electric field is applied to shift the SPR curve via the Pockels' effect, the reflectivity change is reduced and the efficiency of the device is also reduced. This is detrimental to the performance of the device as a modulator. Despite this, the LB film in question may have a high nonlinear susceptibility as, from equations 4.3 and 4.4, the susceptibility $\chi^{(2)}$ depends in part on the imaginary part of the film permittivity ϵ_i and its change $\Delta\epsilon_i$ under an applied electric field.

A collection of absorption spectra recorded as a function of film thickness is also useful as a test of film uniformity from monolayer to monolayer. Assuming the LB film obeys the Beer-Lambert law, and that interference effects between monolayers are negligible, it follows that a linear plot of absorbance versus film thickness indicates consistent film pickup. Compared to LB film spectra, solution spectra may show shifts in absorption peaks depending on the polarities of solute and solvent. Weakly polar compounds in polar solvents tend to show shifts of absorption peaks towards longer wavelength (bathochromic shift); strongly polar solutes, on the other hand show a shift to shorter wavelengths (hypsochromic shift). This is due to stabilisation

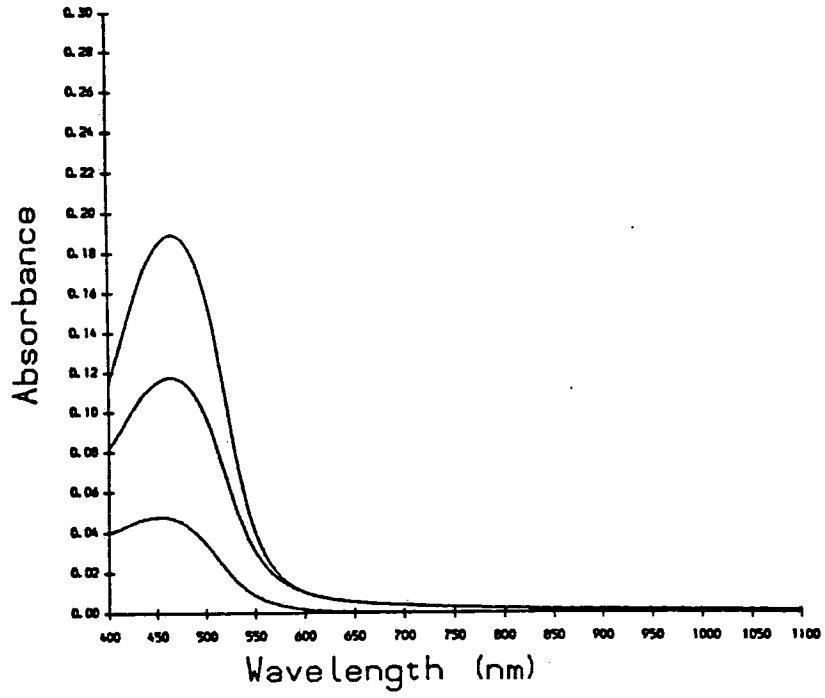

Figure 6.1 : Optical absorption of 20,40,60 Z-type monolayers of AMCR22 on soda glass

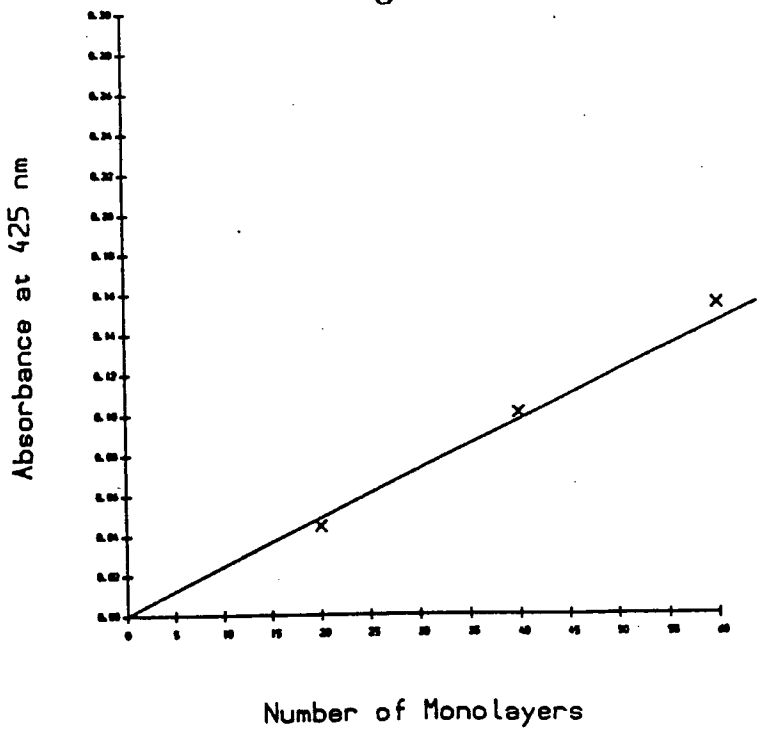

Figure 6.2 : Peak Absorbance of AMCR22 versus Number of Monolayers

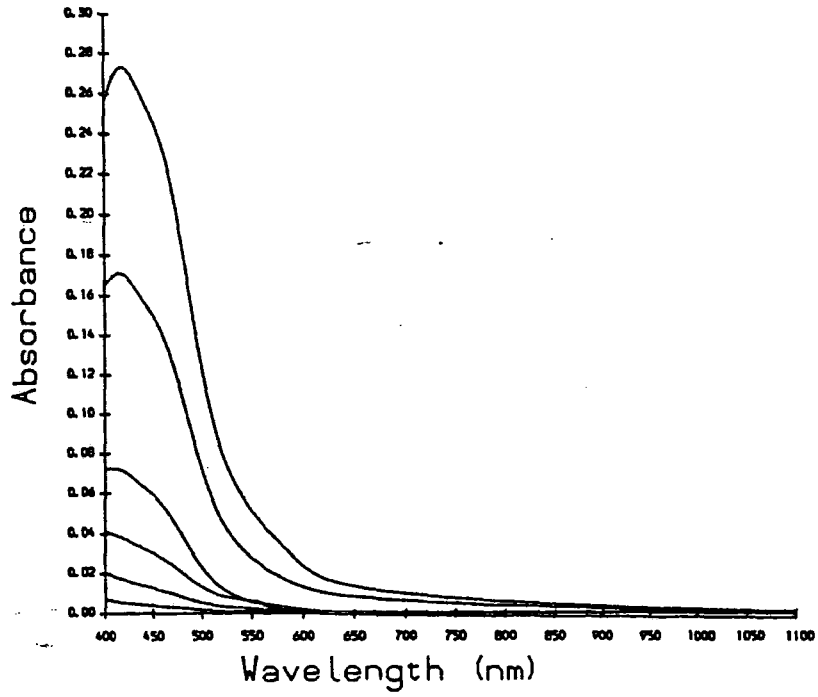

Figure 6.3 : Optical absorption of 2,6,10,20,40,60 Z-type monolayers of AMCR23 on soda glass

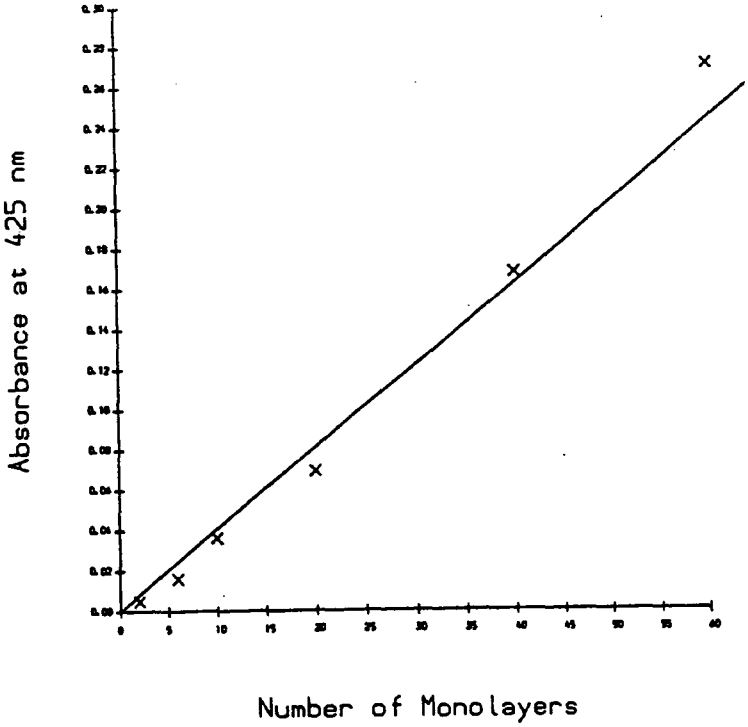

Figure 6.4 : Peak Absorbance of AMCR23 versus Number of Monolayers

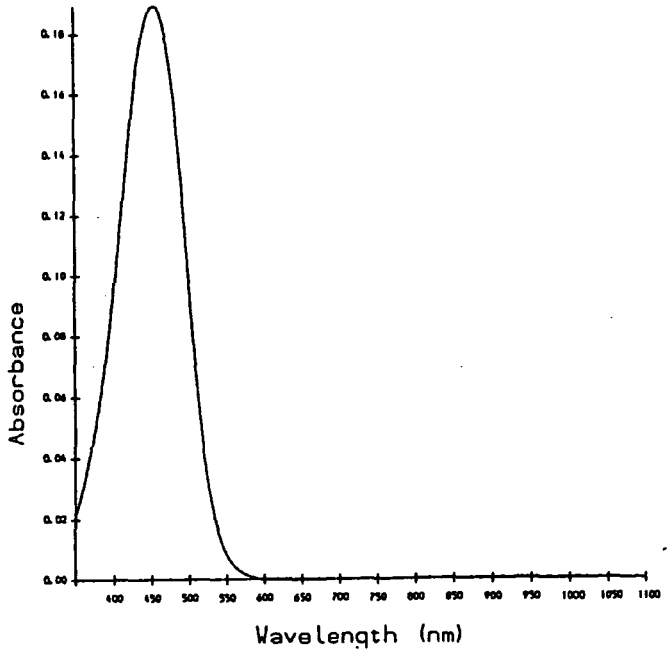

Figure 6.5 : Absorption Spectrum of 0.0098 mg ml^{-1} AMCR22 in Chloroform

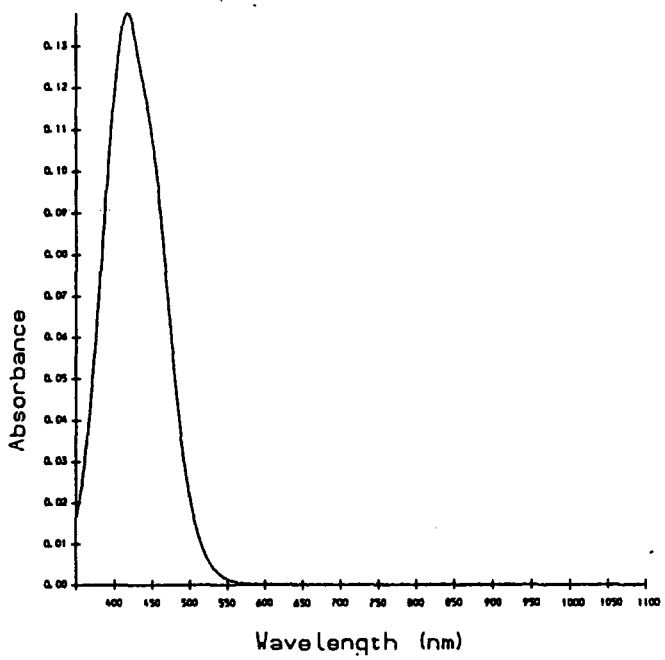

Figure 6.6 : Absorption Spectrum of 0.0114 mg ml^{-1} AMCR23 in Chloroform

Material	N	n	d (nm)	A	$\epsilon_i \equiv \frac{nA\lambda}{2\pi d \log_{10} e}$
AMCR22	20	1.62	31.3	0.0017	0.020
AMCR22	40	1.62	62.5	0.0094	0.055
AMCR22	60	1.62	93.8	0.0108	0.042
AMCR23	2	1.71	2.78	0.0020	0.279
AMCR23	6	1.71	8.34	0.0001	0.005
AMCR23	10	1.71	13.9	0.0005	0.014
AMCR23	20	1.71	27.8	0.0010	0.014
AMCR23	40	1.71	55.6	0.0170	0.119
AMCR23	60	1.71	83.4	0.0185	0.086
JT3	2	1.49	7.33	-0.0005†	-0.023
JT3	4	1.49	14.6	0.0042	0.097
JT3	8	1.49	29.3	0.004	0.050
JT3	20	1.49	73.3	0.0080	0.037
JT3	74	1.49	271.0	0.072	0.090

N = number of monolayers

n = averaged real part of LB film refractive index

d = film thickness from averaged thickness per monolayer

A = optical absorbance at 619nm

ϵ_i = imaginary part of film permittivity at 619nm

† this illustrates errors introduced in baseline subtraction

Table 6.1 : Permittivities of Several LB Film Materials from Optical Absorbance

of the excited and ground states respectively by the polar solvent. Moderately polar compounds, on the other hand, which tend to bond equalisation in the ground state, show very small solvent shifts. All materials examined here turned out to show no

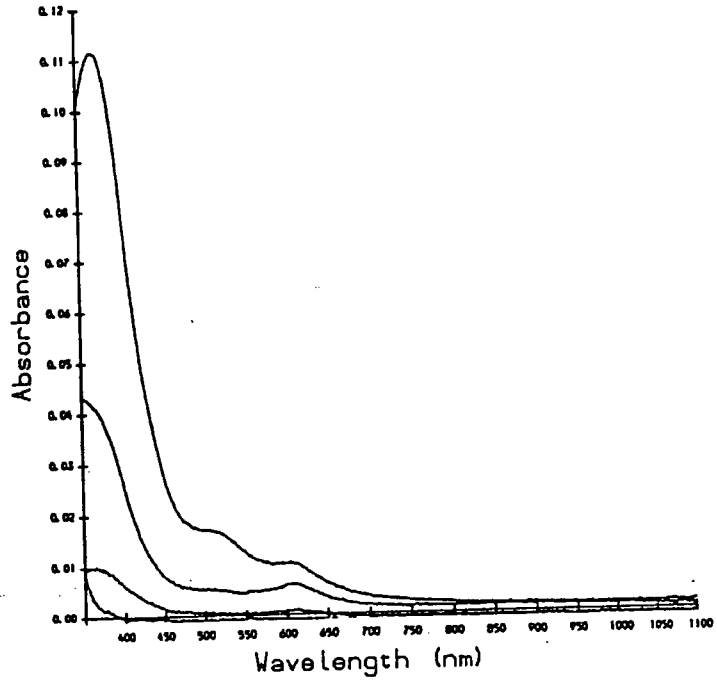

Figure 6.7 : Optical absorption spectrum of 2,4,8,20 Z-type JT3 monolayers in transmission

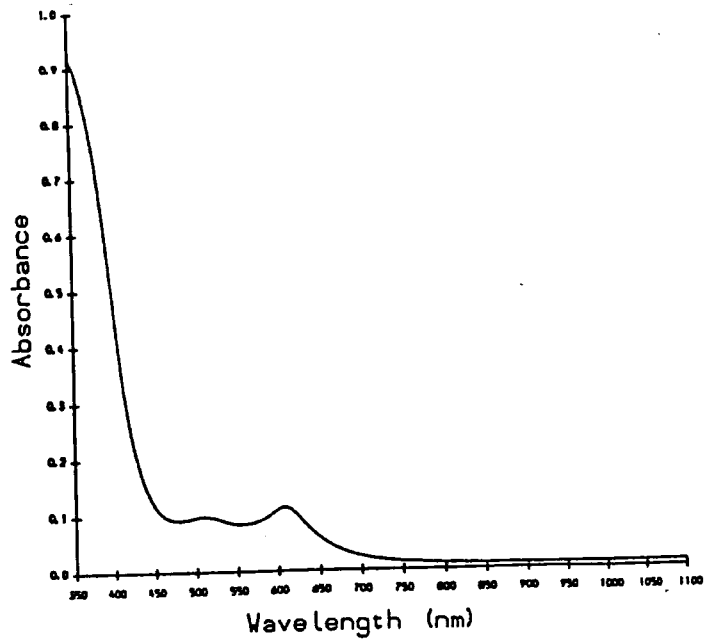

Figure 6.8 : Optical absorption spectrum of 74 Z-type JT3 monolayers in transmission

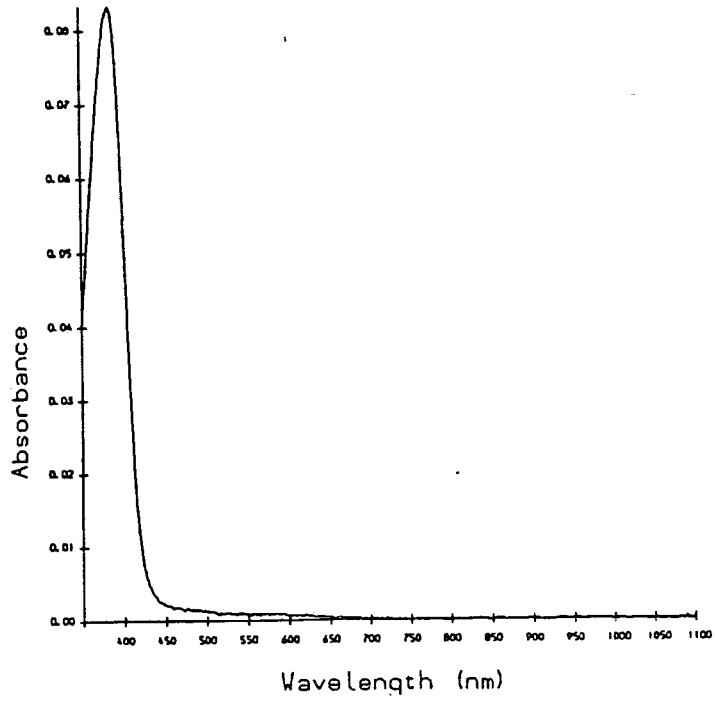

Figure 6.9 : Optical Absorption Spectrum of 0.01 mg ml^{-1} JT3 in $CHCL_3$

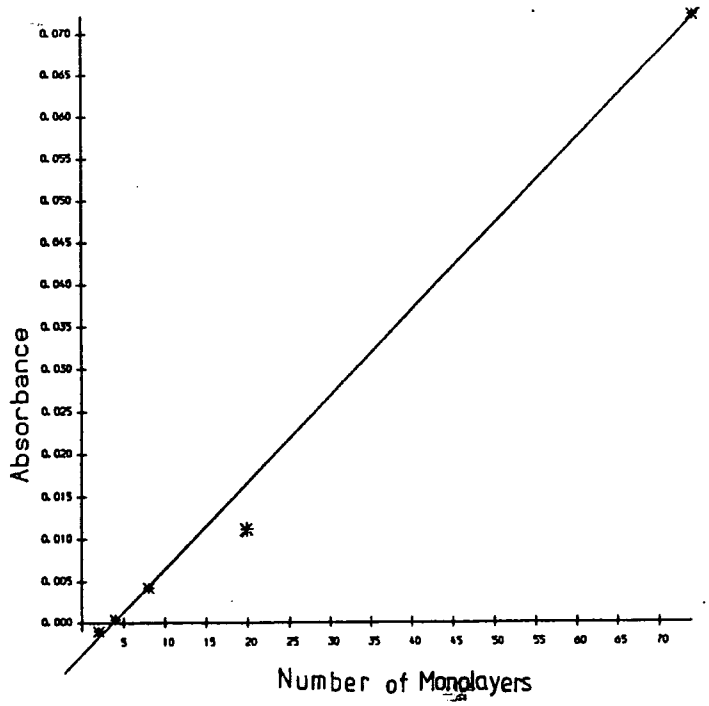

Figure 6.10 : JT3 Absorbance at 355 nm versus Number of Monolayers

discernible solvent shifts.

Bathochromic shifts may also be due to the formation of so-called J-aggregates [Nolte, 1975; Bücher, 1970; Penner, 1985]. None of the materials examined here displayed J-aggregation, and no further reference to the phenomenon will be made.

The spectra were recorded on either a Perkin-Elmer $\lambda 2$ spectrophotometer or a Cary 2300 spectrophotometer. The chosen wavelength range was usually 400-1100nm; the substrates were invariably Chance-Propper microscope slides.

It can easily be shown that

$$\epsilon_i = \frac{nA\lambda}{2\pi d \log_{10} e} \equiv -\frac{n\lambda}{2\pi d} \ln T \tag{6.1}$$

where A is optical absorbance, d is film thickness, n the real part of refractive index, T is the transmission coefficent and the other symbols have their usual meanings. The transmission coefficent and absorbance contain contributions from reflections at the glass/LB film interface and optical absorption and scattering in the LB film. The film thickness is calculated from the ellipsometric film thickness per monolayer, averaged over all samples. Similarly, the real part of refractive index is an average value taken from all the samples examined by ellipsometry. A baseline optical absorbance spectrum is recorded from an uncoated portion of the relevant sample and subtracted from the spectra of coated portions of the same sample. For comparison with the permittivity values derived from SPR, table 6.1 shows values for ϵ_i calculated from the above equation. The real part of refractive index, n, and the film thickness d are measured from ellipsometry (see sections 4.2 and 6.3). The ellipsometric measurements do not provide definitive measurements of thickness and refractive index. The ellipsometric data for ten-layer samples have been used for estimating the imaginary parts of permittivity on the grounds that the fewer LB monolayers, the greater the likelihood that the structural order is preserved from monolayer to monolayer.

Note that to provide meaningful comparison between ϵ_i values derived from SPR and the above method, the probe wavelengths have to be the same. In SPR, the probe beam free space wavelength λ is 633nm, at an angle of incidence θ of 42.5°, in a glass slide (refractive index, $n = 1.523$). The relevant wavelength is accordingly $\lambda/(n \sin\theta) = 619$nm. This is the wavelength at which the absorbance is measured for the purposes of equation 6.1.

6.2.2 Novel Materials

Absorption spectra of Z-type multilayers of AMCR22 and AMCR23 are shown in figures 6.1 and 6.3, respectively. The film samples are all brownish-orange to the naked eye and show no pronounced absorption beyond approximately 500nm. The maximum absorbance versus number of monolayers is plotted in figure 6.2 and 6.4 for AMCR22 and AMCR23 respectively. The linearity of both plots indicates the film quality does not deteriorate with increased number of monolayers. That the polymer molecules are essentially independent is shown by the solution absorption spectra in figures 6.5 and 6.6, which have the same features as the LB film spectra in figures 6.1 and 6.3. The derived values of imaginary part of permittivity in table 6.1 are of a similar order of magnitude to those derived from SPR in table 6.5.

Of the four JT materials, only LB films of JT3 could be deposited with sufficient consistency to justify further examination by spectrophotometry. Figure 6.10 indicates the consistency of monolayer deposition. Due to the low absorbance of individual monolayers, the subtraction of substrate absorbances has led to very small negative net absorbance for single monolayers. The substrate and gross absorbances are recorded from different areas of the sample. Figure 6.8 shows the absorbance of 74 Z-type JT3 monolayers in transmission. It has substantially the same features as all the other JT3 spectra: a broad peak centered on 420 nm followed by two shoulders at longer wavelengths.

The optical absorbances of all the samples examined here are quite low, and errors in measurement have led to a spread of permittivity values for each material. Comparison with the imaginary parts of permittivity listed in table 6.5 suggests that no firm conclusions can be drawn from table 6.1.

6.3 ELLIPSOMETRY

6.3.1 Introduction

Ellipsometric measurements are necessary because the SPR curve fitting procedure requires that one of the LB film parameters (thickness or real or imaginary part of permittivity) be fixed (see section 4.3.3). Silicon substrates, cleaned as described in section 2.1, were overcoated with multilayer LB films of each novel material, leaving a portion of the silicon uncoated for reference purposes. The uncoated sections were characterised by ellipsometry to estimate their optical constants, preparatory to measuring the thickness and refractive index of the LB overlayers. Generally, each

Material	N	n	l(nm)	l/N(nm)	t (nm)
AMCR22	10	1.539±0.006	15.6±0.2	1.56±0.02	2.6
AMCR22	20	1.638±0.003	31.5±0.3	1.58±0.01	ditto
AMCR22	30	1.677±0.003	46.6±0.1	1.55±0.01	ditto
AMCR23	10	1.921±0.011	18.1±0.4	1.81±0.04	2.4
AMCR23	20	1.610±0.001	24.7±0.3	1.24±0.02	ditto
AMCR23	30	1.603±0.001	36.4±0.9	1.12±0.03	ditto
JT1	10	1.499±0.008	35.2±0.5	3.52±0.05	4.1
JT2	-	-	-	-	3.5
JT3	10	1.474±0.005	37.4±0.4	3.74±0.04	4.2
JT3	20	1.478±0.010	73.2±1.2	3.66±0.06	ditto
JT3	30	1.521±0.002	107.7±1.2	3.59±0.04	ditto

N= number of LB monolayers

n = real part of film refractive index ± standard error

l = film thickness ± standard error

l/N = thickness per monolayer ± standard error

t = molecular length measured from space-filling models

Table 6.2 : Novel LB Film Material Optical Constants from Ellipsometry

measurement was repeated at least ten times to estimate the attached experimental error in substrate and LB film parameters.

Ellipsometry is feasable for LB monolayers deposited onto substrates having known optical constants. In practice, the ellipsometer calculation routines failed to converge on a single refractive index value for films thinner than approximately ten nanometres, or five monolayers. Films of at least ten monolayers yielded stable results, although the derived optical constants for ten-layer films differred considerably from those for thicker films, the latter tending to converge towards a fixed thickness per monolayer and refractive index with increasing film thickness. Generally, the film thickness per monolayer was the parameter held constant for SPR curve fitting procedures. The permittivities derived from the SPR curve fitting procedure were then compared to those calculated from ellipsometry.

6.3.2 Polysiloxanes and Diaryl Alkynes

The thicknesses and real parts of refractive index derived from ellipsometry are shown in table 6.2, which also includes, for comparison, the lengths of each of the molecules as measured from a CPK space-filling molecular modelling kit. The latter represent the largest possible film thickness per LB monolayer. All the measured film thicknesses were smaller than the product of molecular length and number of monolayers. The measured film thickness per monolayer, however, is an average over the entire film, and may not be representative of each monolayer. It is to be expected that the very first monolayer of a multilayer LB structure will be different from succeeding layers, if only because it is chemically bound to the substrate, whereas further layers are generally bound to each other. Furthermore, in many poorly-ordered films the in-plane structure deteriorates with rising thickness, hence it is feasable that the tilt angle increases and the thickness per monolayer falls from layer to layer.

For these reasons, the film thickness per monolayer is taken as a guide, not a definitive measurement. In succeeding sections where a film thickness per monolayer is required, the values deduced from ellipsometry have been used unless the resulting data made no sense. In those specific instances, this is indicated.

The real part of refractive index from ellipsometry, compared to the real part of refractive index derived from SPR curve fitting using film thicknesses from ellipsometry, is generally larger in the former instance. For monolayer samples, this may be due to the above difficulty in estimating the thickness of a single LB monolayer.

6.4 SURFACE PLASMON RESONANCE

6.4.1 Equipment Calibration

Unless the surface plasmon sensing apparatus is correctly adjusted before use, several effects can compromise the data acquisition. These, and the steps taken to eliminate them, are described in the following paragraphs.

As pointed out in chapter four, the laser beam divergence affects the shape of SPR curves as the beam wavefront, being curved, necessarily contains a spread of propagation vectors as well as a noise contribution from higher order laser beam modes due to imperfections in the laser resonator. To approach the perfect type of illumination for SPR, which is a monochromatic plane wave, the noise must be removed and the beam spatial profile altered to as nearly plane as possible. Measurements of beam spot size with distance indicated that it was very cleanly TEM_{00}, so there was no need to filter the beam with apertures or stops. Laser beam collimation is necessary if SEWs are to be examined in the infrared, where the halfwidth of the SPR curves is far smaller than in the visible region [Yang et. al., 1990]. The reasoning in appendix B suggests that beam collimation by a pair of appropriately-spaced lenses may improve the precision of curve fitted parameters. In practice, the silver substrates varied sufficiently in thickness and permittivity from sample to sample to swamp this improvement. The lenses were removed at an early stage in the research and all the measurements in this thesis were recorded without collimating lenses.

Any s-polarised components of the incident laser beam are not absorbed by surface plasmons. So, if the incident light is not purely p-polarised, the reflectivity at the SPR minimum will be higher than expected. The curve fitting procedure assumes purely p-polarised light and cannot compensate for this effect, which to first order looks like an overestimate of the film thickness. The laser selects output polarisation by a Brewster window. The laser orientation is selected by locating the angular minimum of the SPR and turning the laser until the reflected intensity is a minimum. This is repeated from time to time to compensate for wear and tear in the rotation stage and creep of the various components of the optical bench on which the SPR sensing system is mounted.

6.4.2 Silver Substrates

As mentioned in chapter four, to derive LB film optical constants, the thickness and permittivity of the silver substrate must first be known. Table 6.3 is a repre-

d(nm)	ϵ	d_n (nm)	TF(%)
44.3	-19.66+0.9011i	51.7	97
46.5	-18.96+0.5430i	50.7	97
48.5	-20.67+0.2000i	50.0	100
48.9	-18.63+0.3470i	51.2	100
49.3	-18.62+0.1680i	51.7	105
49.6	-18.74+0.3150i	49.7	95
51.1	-17.93+1.073i	51.7	97
52.7	-19.58+0.8330i	50.5	90
55.1	-19.16+0.7640i	50.5	90
54.5	-18.09+0.705i	50.7	97
64.6	-18.56+0.675i	50.0	100

d =fitted film thickness

ϵ = fitted permittivity

d_n = notional film thickness, as displayed by monitoring equipment

The TF is a geometrical correction for the difference in source and substrate locations

Table 6.3 : Fitted Thickness and Permittivity of Evaporated Silver Films

Thickness (nm)	ϵ	Method	Source
Not stated	-17.20+1.16i	Polarimetry	Winsemius et.al., 1976
62.3	≈-16+0.7i	SPR Curve Fitting	Kretschmann, 1971
40-70	-17.60+0.67i	SPR Curve Fitting	Schröder, 1981
30.0-37.5	-18.0+0.5i	Ellipsometry	Schröder, 1981
15-65	-19.2+0.89i	Transmission & Reflection	Schröder, 1981
49.6	-18.39+0.55i	SPR Curve Fitting	Pockrand, 1978
70	-19.02+0.624i	SPR Curve Fitting	Weber, 1975
48.1	-15.77+0.473i	SPR Curve Fitting	Wähling, 1978
30.4, 37.5	-17.08+0.474i	Transmission & Reflection	Johnson, 1972

d =curve fitted thickness

$\epsilon = \epsilon_r + i\epsilon_i$ = permittivity

d_n =notional thickness

The TF is a geometrical correction for the difference in source and substrate locations

Table 6.4 : Derived Thin Silver Film Optical Constants

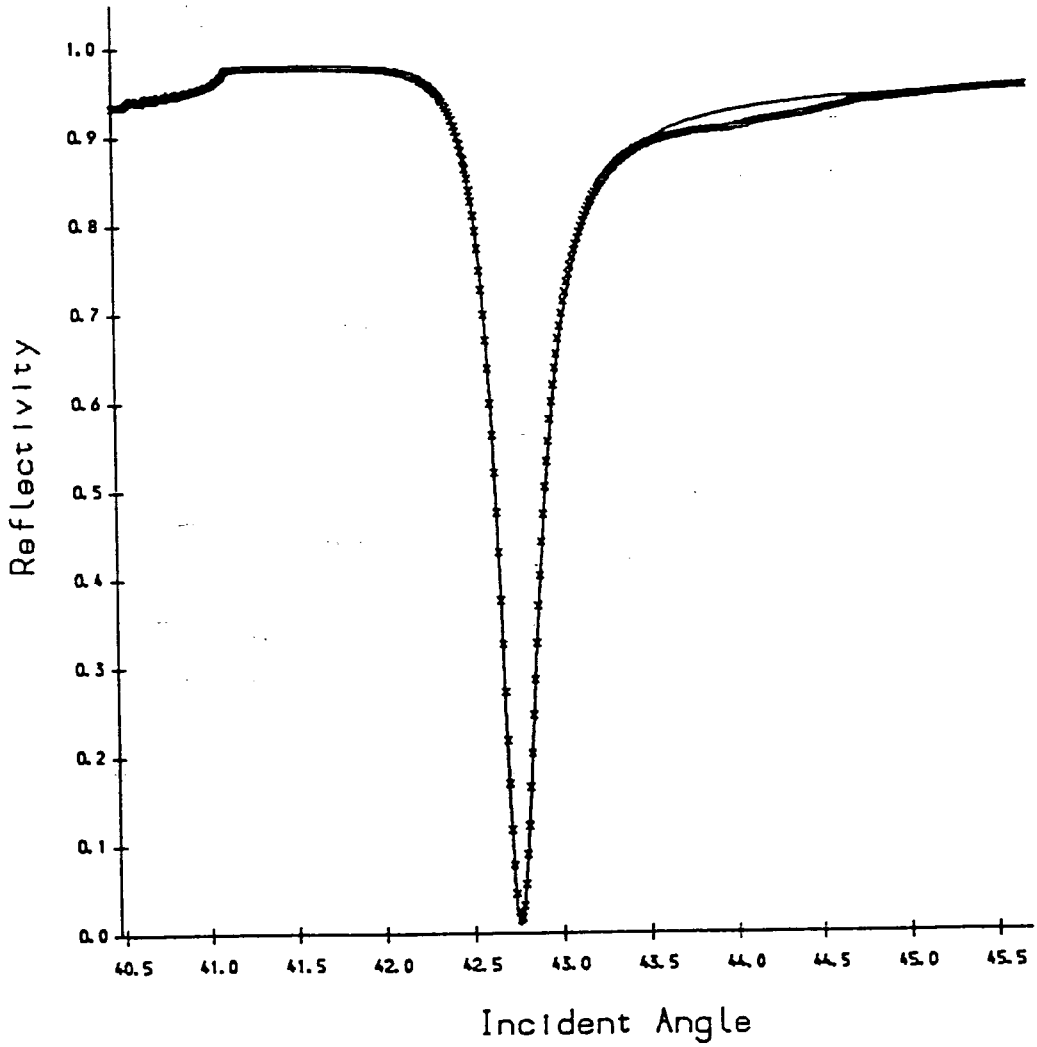

Figure 6.11 : Specimen SPR Curve of a Silver Film of Notional Thickness 50.7nm, Fitted Thickness 46.5nm

sentative set of data for silver films of approximately 50nm thickness on soda glass. All were deposited at pressures no greater than 2×10^{-5}mbar, with constant heating current and thickness set point 49nm using fresh silver wire on a source that had previously been baked clean in a vacuum. The notional thickness is the silver film thickness calculated by the film thickness monitor attached to the evaporator. The tooling factor (TF), described in chapter four, is an empirical geometrical correction compensating for the difference between boat-substrate and boat-detector separations and their different orientations. The fitted thickness is derived from fitting theoretical SPR data to the experimental curves. The fitted permittivities did not show any obvious dependence on fitted thicknesses, notional thickness or tooling factor. This suggests that slight variations in these quantities, within the limits of the evaporations listed above, are not as significant as the factors over which there is less control, such as evaporation rate, silver cleanliness/purity, water absorption and/or sulphide formation on the silver film once removed from the evaporator. The derived permittivities clearly do not match exactly with bulk values or values derived by other researchers in the field (*vide* table 6.4), although they do mostly fall between the extreme values measured by other researchers. On the other hand, the object is to characterise the silver substrates, not derive a definitive measurement of silver optical constants. Generally, a tooling factor of 97% with thickness set point 49.0nm was used. A sample SPR curve taken from a silver film of notional thickness 50.7nm, tooling factor 97% and fitted thickness 46.5nm is shown in figure 6.11.

6.4.3 Novel Materials

The permittivity of each novel material was estimated by first characterising the silver substrate, then fitting theoretical data to the SPR curve of the substrate plus LB film, holding the film thickness constant. The resulting SPR curves for monolayers of AMCR22, AMCR23 and JT3 are shown in figures 6.13, 6.14 and 6.15. For comparison, the SPR of a hemicyanine monolayer is shown in figure 6.12. The derived optical constants are shown in table 6.5. The reason for holding the film thickness constant, as opposed to the real part of permittivity, is that the real part of refractive index, derived from ellipsometry, also contains a component from the imaginary part of permittivity. It was not considered prudent to ignore this contribution, since it was found that ϵ_i/ϵ_r often took a value of approximately 0.1, and rose to 0.6 for one sample in particular.

The film thickness is derived from ellipsometry of multilayer films, and may not be representative of a monolayer sample of the same material (note that the same

Material	d(nm)	N	ϵ	$\sqrt{\epsilon}$
uncoated Ag	50	0	-17.01+0.581i	4.13-0.071i
22-TA	2.2	1	2.033+0.0297i	1.43+0.010i
hemicyanine	2.9	1	6.080+0.070i	2.47+0.013i
4HANS	2.9†	1	2.999+0.054i	1.73+0.015i
AMCR22	1.7†	1	1.990+0.0378i	1.41+0.013i
AMCR23	1.7	1	3.108+0.1204i	1.76+0.034i
JT1	3.5	1	1.932+0.368i	1.40+0.132i
JT3	3.7	1	1.439+0.1004i	1.20+0.042i
JT3	11.1	3	1.344+0.1162i	1.16+0.050i
JT3	18.5	5	1.294+0.2485i	1.14+0.109i
JT3	37.0	10	1.456+0.0981i	1.21+0.041i
JT3	74.0	20	1.408+0.1140i	1.19+0.048i

d = LB film thickness from ellipsometry

N =number of LB monolayers

$\epsilon = \epsilon_r + i\epsilon_i$ = fitted static permittivity

†estimated by varying d and searching for a good fitted SPR curve

Table 6.5 : Optical Constants of Several LB Materials from SPR

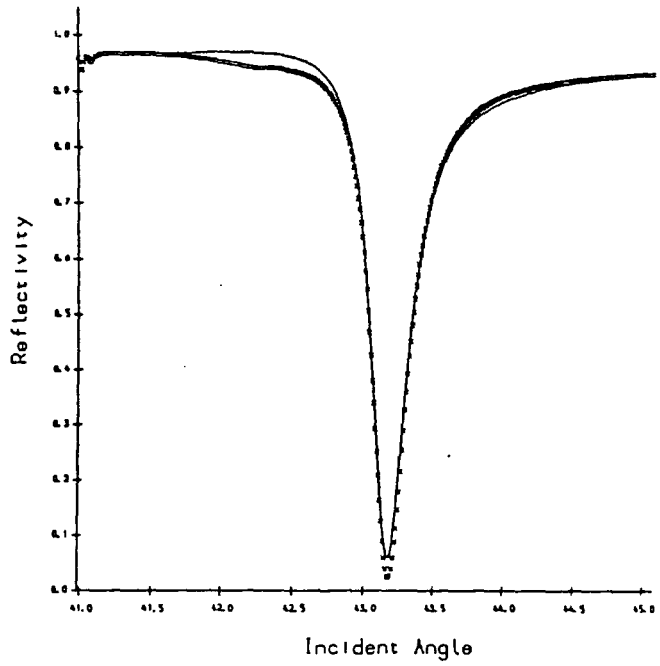

Figure 6.12 : SPR of a Hemicyanine Monolayer on a 50nm Silver substrate. The full line is theory; crosses are experimental

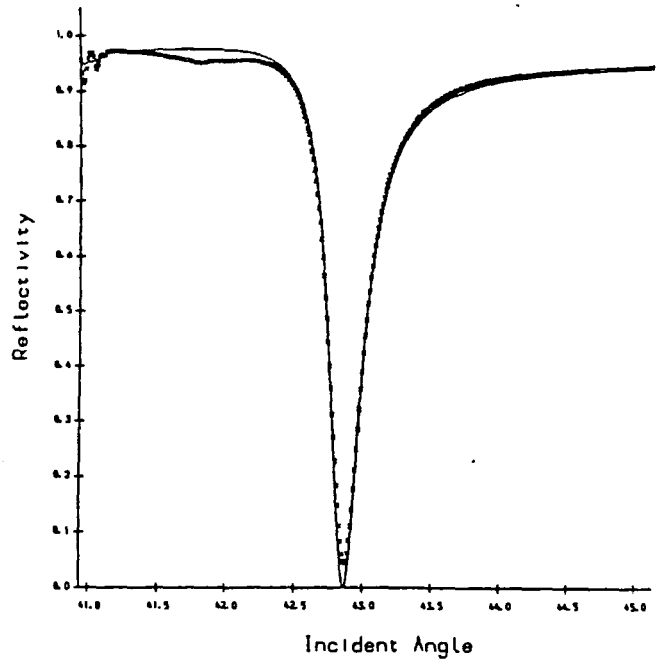

Figure 6.13 : SPR of an AMCR22 Monolayer on a 50nm Silver substrate. The full line is theory; crosses are experimental

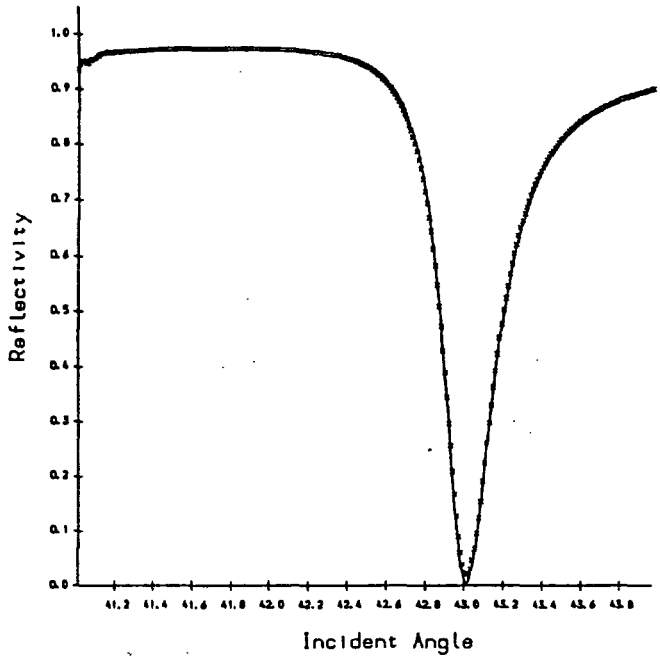

Figure 6.14 : SPR of an AMCR23 Monolayer on a 50nm Silver Substrate. The full line is theory; crosses are experimental

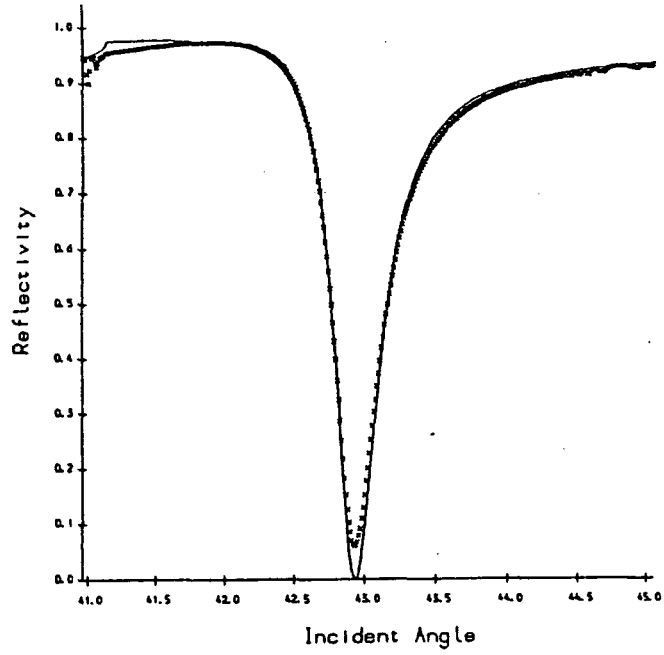

Figure 6.15 : SPR of a JT3 Monolayer on a 50nm Silver Substrate. The full line is theory; crosses are experiment

may be true of the permittivity). Where reasonable results have been achieved by this method, they have been included in table 6.5. The exception was AMCR22 which, according to the SPR curve fitting procedure, had a negative imaginary part of permittivity when the monolayer thicknesses derived from ellipsometry are presumed accurate. Instead, the thicknesses of AMCR22 monolayers were varied until the imaginary part of the permittivity of each took a positive value.

The real part of the square root of the derived permittivity in table 6.5 is generally smaller than the refractive index calculated from ellipsometry in table 6.2. This is presumably partly due to the difficulty of estimating precisely the thickness of a single LB monolayer and partly to the varying behaviour of LB materials deposited on different substrates - silver and silicon in this case.

6.5 ELECTRON AND X-RAY DIFFRACTION

Reflection high energy electron diffraction (RHEED) studies were performed at Durham using a JEM 120 transmission electron microscope equipped with a RHEED stage. Samples were held in a goniometer positioned below the projector lens. Electron diffraction indicates the arrangement of subcells within each LB monolayer; the more regular this is, the more orders are visible in the diffraction pattern. Image contrast is also improved by greater numbers of regularly-spaced subcells, hence RHEED produces better images for thicker LB films. Other requirements are that the substrate be sufficiently conducting to prevent the buildup of charge on the surface, which deflects the electron beam, and that the electron beam is not energetic enough to destroy the LB film. Dynamit Nobel silicon with its native oxide layer, overcoated with at least twenty LB monolayers generally fulfils the last two requirements when examined at 80KV.

Samples of 20 Z-type monolayers of AMCR22 and AMCR23, and a ten-layer sample of JT3 were deposited onto Dynamit Nobel silicon for examination by RHEED. The resulting photographs showed, at best, a broad fuzzy halo surrounding the central electron beam spot, indicating an amorphous film.

Small-angle X-ray diffraction scattering was performed by Dr. Y. Lvov, at the Institute of Crystallography, Moscow. Sample requirements for these experiments were that the LB overlayers be thick enough to allow diffraction from several crystal planes, so that the diffraction pattern contained several components of the electron density profile, which could be later extracted by numerical means. Samples ex-

amined included 20 layers of AMCR22, AMCR23 and JT3. All appeared to be amorphous.

6.6 SUMMARY

This chapter has described the linear optical properties of several novel polysiloxanes and diaryl alkynes in LB film form. The similarities between solution and LB film optical absorption spectra show that the LB films are essentially free of intramolecular interactions. The linearity of absorbance at fixed wavelength versus film thickness suggests uniform film deposition. Ellipsometric measurements confirm this supposition for thick (more than ten monolayer) AMCR22, AMCR23 and JT3 films, while also providing thickness data for use in SPR curve fitting and other data for estimation of the imaginary part of film permittivity independently of SPR. The imaginary parts of LB film permittivity derived from optical absorption are presented. X-ray and electron diffraction studies of several thick samples on silicon indicate that AMCR22, AMCR23 and JT3 formed amorphous films.

Silver substrates used extensively in the recording of SPR and Pockels' effect data have also been characterised. Their optical constants have been compared to those found in the literature and found to fall between the extremes of values obtained by several other workers in the field.

6.7 REFERENCES

Bücher, H., Kuhn, H. : Schiebe Aggregate Formation of Cyanine Dyes in Monolayers , *Chemical Physics Letters* **6** *3* , 1970 pp. 183- 5.

Johnson P. B., Christy R. W. : Optical Constants of the Noble Metals ,*Phys. Rev. B.* **6** *12* , 1972 pp. 4370-9.

Kretschmann, E. : The Determination of the Optical Constants of Metals by Excitation of Surface P lasmons (*in German*) ,*Z. Physik* **241** , 1971 pp. 313-24. publ. Springer-Verlag.

Nolte, H. J. : A Model of the Optically Active Schiebe- Aggregate of Pseudoisocyanine ,*Chem. Phys. Lett.* **31** *1* , 1975 pp. 134-9.

Penner, T. L. : The Formation of Mixed J Aggregates of Cyanine Dyes in Langmuir- Blodgett Monolayers ,*Thin Solid Films* **132** , 1985 pp. 185-92.

Pockrand, I. : Surface Plasma Oscillations at Silver Surfaces with Thin Transparent and Absorb ing Coatings ,*Surf. Sci.* **72** , 1978 pp. 577-88.

Schröder, U. : The Influence of Thin Metallic Overlayers on the Dispersion of Surface Plasma W aves in the Gold-Silver-Quartz System (*in German*) ,*Surf. Sci.* **102** , 1981 pp. 118-30. publ. North-Holland.

Weber, W. H., McCarthy, S. L. : Surface- Plasmon Resonance as a Sensitive Probe of Metal Film Properties ,*Phys. Rev. B.* **12** *12* , 1975 pp. 5643.

Winsemius, P., van Kampen, F. F., Lengkeek, H. P., van Went, C. G. : ,*J. Phys. F.* **6** , 1976 pp. 1583.

Wähling, G. : Arachidate Layers on Ag and Au Detected by the ATR Method ,*Z. Naturforsch* **33a** , 1978 pp. 536-39.

Yang, Bradberry, Sambles : Coupled Surface Plasmons at 3. 391μm ,*J. Mod. Optics* **37** *5* , 1990 pp. 993-1003.

Chapter VII

NONLINEAR OPTICAL TECHNIQUES: RESULTS AND DISCUSSION

7.1 INTRODUCTION

This chapter contains the results of second harmonic generation (SHG) and Pockels effect measurements on LB films of the JT and AMCR series molecules. Hemicyanine LB films are used as exemplary standards and for calibration purposes.

7.2 SECOND HARMONIC GENERATION

7.2.1 Background

Second harmonic generation experiments were performed at Plessy (Caswell) and at Durham. The Caswell apparatus (see chapter four) was used to rank the various materials in order of nonlinear susceptibility by normal-incidence SHG measurements of the p-polarised fundamental and second harmonic. The Durham SHG system was essentially identical but for a pair of polarisers, a half-wave plate and a rotatable sample mount which allowed measurement of SHG intensity in reflection. Given the second harmonic conversion efficiencies in reflection from s to p and from p to p polarisations, it is possible to estimate, in principle, the LB film tilt angle [Girling et. al., 1985]. This was attempted for monolayers of each material, but the results were inconclusive.

All the SHG data are normalised with respect to hemicyanine monolayers on soda glass.

7.2.2 Polysiloxanes

Normal incidence transmission SHG was used to examine the behaviour of mono- and multilayer LB films of the AMCR series molecules. All samples generally yielded consistent SH outputs and only suffered laser damage at the highest intensities of incident radiation ($\sim 10^{15}\mathrm{Wm}^{-2}$), at which the Nd:YAG laser was in Q-switched mode. Most measurements did not require Q-switching of the laser beam to generate adequate SHG. Within the AMCR series, the order of decreasing SHG output powers

Material	N	Structure	$I_{2\omega}/I_{2\omega}$(hemi)	$\lvert\chi^{(2)}/\chi^{(2)}_{\text{hemi}}\rvert$
AMCR22	1	Z	0.015	0.090
AMCR22	2	Z	0.030	0.064
AMCR22	4	Z	0.075	0.051
AMCR22	8	Z	0.115	0.031
AMCR23	1	Z	0.020	0.149
AMCR23	2	Z	0.028	0.086
AMCR23	4	Z	0.060	0.063
AMCR23	8	Z	0.108	0.042
AMCR24	1	Z	0.010	0.032†
AMCR22/22-TA	10	Alt. Y	0.070	0.004‡
AMCR23/22-TA	10	Alt. Y	0.090	0.005*
JT1	1	Z	0.013	0.036
JT3	1	Z	0.020	0.038
JT3	2	Z	0.035	0.032
JT3	4	Z	0.055	0.020
JT3	6	Z	0.075	0.016
JT3	10	Z	0.13	0.0043
JT4	1	Z	<0.01	<0.008**

N= number of monolayers

$\chi^{(2)}$ =sample susceptibility $\chi^{(2)}(-\omega;\omega,0)$ per monolayer

$\chi^{(2)}_{(hemi)}$ =hemicyanine monolayer susceptibility $\chi^{(2)}(-\omega;\omega,0)$

†using the permittivity and thickness of an AMCR22 monolayer

‡using the mean permittivity of AMCR22 and 22-TA and the individual monolayer thicknesses.

* using the mean permittivity of AMCR23 and 22-TA and the individal monolayer thicknesses

** using thickness and refractive index data for a JT4 monolayer

Table 7.1 : Net SHG intensities and susceptibilities per active monolayer

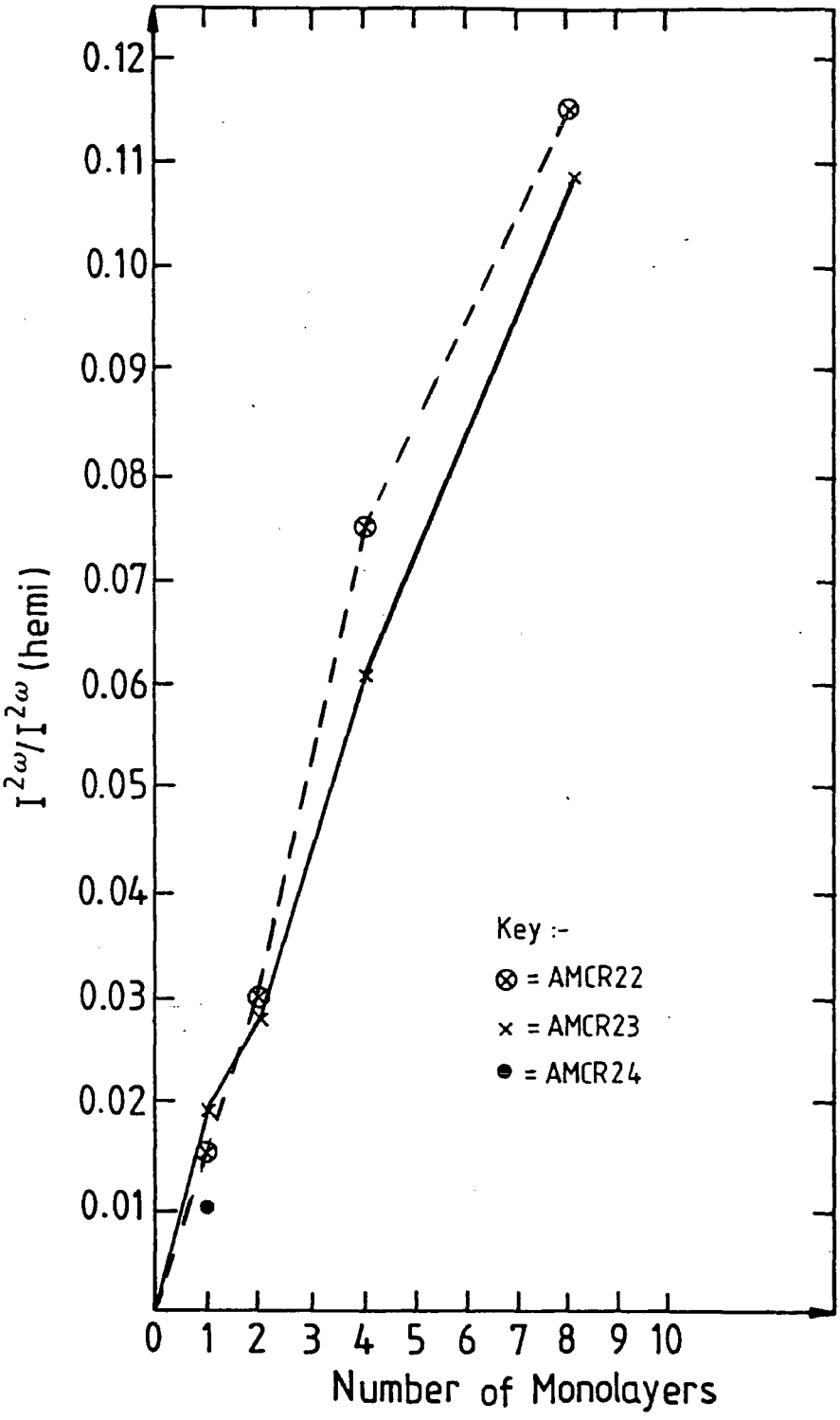

$I^{2\omega}$ = SHG intensity

$I^{2\omega}_{\text{hemi}}$ =hemicyanine monolayer SHG intensity

Figure 7.1 : AMCR series transmission SHG intensities

was AMCR23>AMCR22>AMCR24 for monolayer samples in transmission. The ranking of these materials in order of decreasing dipping ratio (see chapter five) is also AMCR23>AMCR22>AMCR24 , which bolsters the supposition that SHG increases with film uniformity. Section 7.3.3 commments on the relationship between optical nonlinearity and AMCR series molecular structure. Samples of AMCR24 provided poor SHG and multilayer films proved very difficult to deposit; that material was not examined further.

Theoretically, the normal-incidence SH output power of a film sufficently thin to ensure the fundamental and second harmonic remain phase-matched is given by equation 4.13. Equation 4.14 yields the second order susceptibility in terms of hemicyanine susceptibility, given certain calibration factors and ignoring dispersion.

Table 7.1 shows the SHG output intensities relative to a hemicyanine monolayer and the results of applying equation 4.14 The refractive indices and film thicknesses were extracted from curve fitted data in chapter six. SHG data for AMCR22 and AMCR23 are in rough agreement with the Pockels effect information. Despite their relatively weak SHG, monolayers of AMCR23 have a nonlinear susceptibility approaching that of hemicyanine. This is no doubt due to the relatively large refractive index and small thickness of AMCR23 monolayers compared to hemicyanine.

For LB films of N identical monolayers we may set $L = Nl$ where l is a thickness per monolayer and N the number of monolayers. Then, from equation 4.13 we may set

$$I_{2\omega} \propto \left(N\chi^{(2)}\right)^2 \tag{7.1}$$

Measurements of SHG power versus film thickness for Z-type multilayers of pure AMCR22 and AMCR23 (see figure 7.1) yielded an output power directly proportional to the number of deposited monolayers, $I_{2\omega} \propto N$. Thus, although the net measured susceptibility increased with film thickness, it appears that the susceptibility per monolayer decreased, with $\chi^{(2)} \propto 1/\sqrt{N}$, and the adjacent monolayers are not, as supposed above, identical.

Alternation of pure AMCR22 or AMCR23 with pure 22-TA in a ten-layer structure demonstrated that adjacent AMCR monolayers are not independent. The SHG output power per active monolayer was greatly reduced by alternation with passive

layers of 22-TA. Clearly, 22-TA monolayers make poorer substrates for LB deposition of AMCR material than do monolayers of AMCR material.

At the time of writing, no published studies of AMCR22, AMCR23 or AMCR24 exist, although Plessy (Caswell) have studied several similar molecules fairly extensively [Carr et. al., 1897] and derived a microscopic hyperpolarisability $\beta = 3.5 \times 10^{-49} C^3 m^3 J^{-2}$ by SHG. Hemicyanine, by comparison, has $\beta = (11.6 \pm 2.0 \times 10^{-49} C^3 m^3 J^{-2}$ [Neal et. al., 1986]. The materials studied at Caswell are sufficently similar to AMCR22 and AMCR23 in other respects to suggest that their nonlinear optical behaviour may also be similar. This has been confirmed by the above findings.

7.2.3 Diaryl alkynes

Normal incidence transmission SHG was used to probe the properties of pure mono- and multilayer structures of JT series molecules. In general, the JT materials have significantly lower laser damage thresholds than the AMCR series at the fundamental Nd:YAG wavelength. Consequently, it was rarely possible to obtain reproducible SHG data on isolated portions of the samples concerned before they disintegrated. This applied particularly to films of JT4 and, to a lesser extent, to JT1 . In the case of JT4, the damage threshold was such that film deterioration occurred at incident power levels too small to generate measurable SHG. The ranking of SHG output power within the JT series was found to be JT3>JT1>JT4 for monolayers in transmission. From chapter five, the ranking of dipping ratios of these materials is also JT3>JT1>JT4. All other things being equal, this would suggest that the films which failed to deposit uniformly lacked the noncentrosymmetry required for large SHG. Materials JT1 and JT3 differ only in that JT1 lacks a terminal methoxy (weak donor) group. Molecular structures following the broad design of donor/conjugated system/acceptor are widely regarded as optimal for nonlinear optical applications. Material JT1 has no such structure, whreas JT3, on the other hand, has. JT2 and JT1 are identical except for the shorter hydrocarbon tail of the JT2 molecule. The latter appears to be close to the minimum length, below which the molecule becomes soluble in water.

A JT1 monolayer yielded a slightly smaller SHG output than a JT3 monolayer; a ten-layer sample of Z-type JT3 yielded a SH output power approximately ten times that of a monolayer. The JT3 samples yielded results consistent with those previously reported for a JT3 monolayer [Tsibouklis, et. al., 1989], wherein the SHG output in transmission was recorded as $\sim$0.013 that of a hemicyanine monolayer.

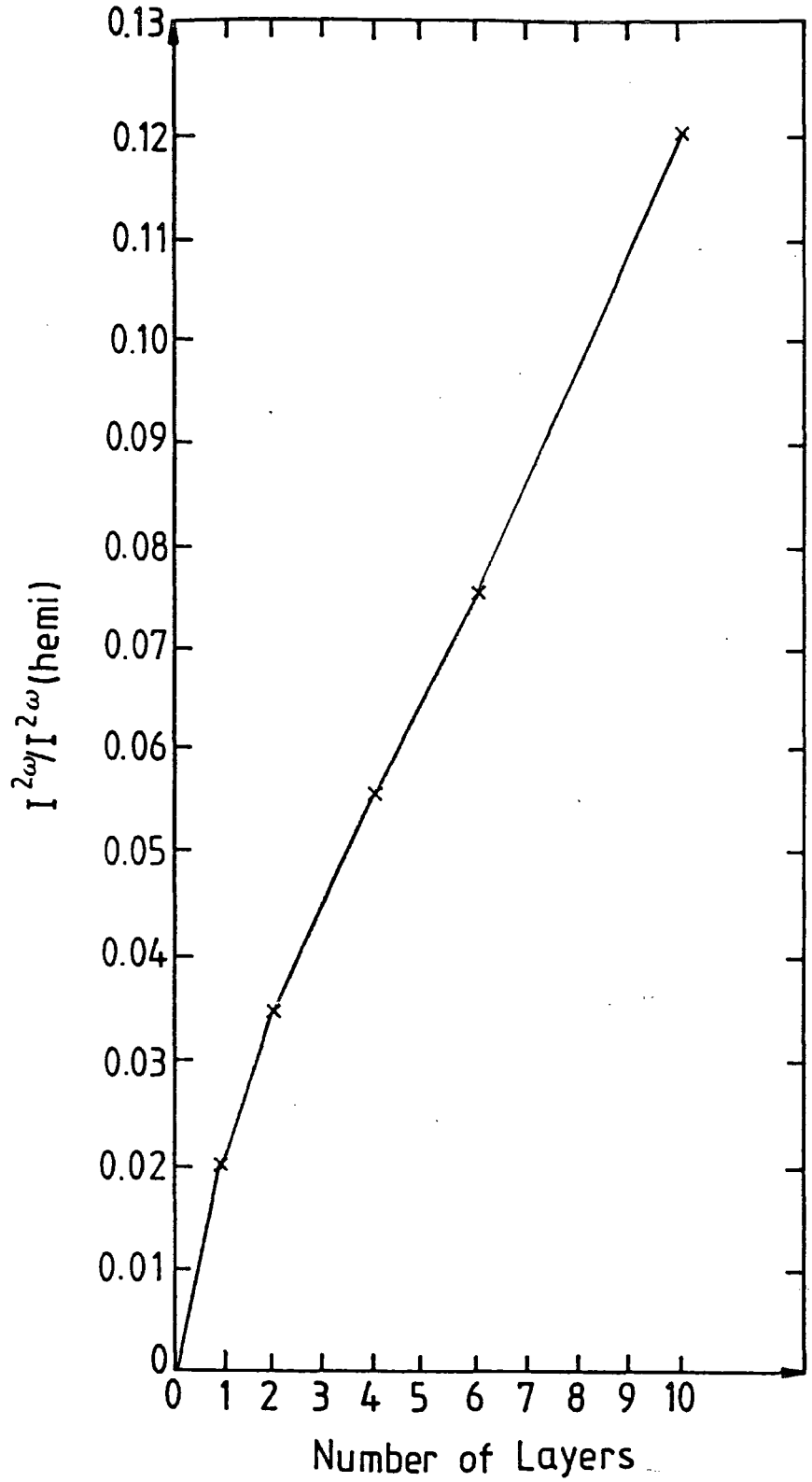

$I^{2\omega}$ =JT3 SHG intensity

$I^{2\omega}_{\text{hemi}}$ = hemicyanine monolayer SHG intensity

Figure 7.2 : JT3 transmission SHG intensity

Table 7.1 summarises these data and lists derived nonlinear susceptibilities relative to a hemicyanine monolayer, while figure 7.2 shows the dependence of SH output power on sample thickness for Z-type JT3 multilayers. The SH output power is quite linear with film thickness, which suggests that the susceptibility per monolayer $\chi^{(2)}(-2\omega;\omega,\omega)$ is inversely proportional to the square root of the film thickness - as for the AMCR series. Previous work at Durham on ten-layer samples of JT3 [Tsibouklis et. al., 1989] is consistent with this behaviour. Other workers have observed multilayer film behaviour that can only be ascribed to structural rearrangement of component molecules subsequent to deposition [Cresswell et.al., 1990; Young et. al., 1989; Novak et. al., 1987]. Also, scattering of second harmonic radiation from an imperfectly Z-type film may cause further reduction in the measured SHG. An alternative reason for the reduced SH output may be that absorption of the second harmonic is taking place in the film; this may, however, be ruled out on the grounds that the film absorbance at 532nm is $\sim$0.001, which is too small to greatly absorb the second harmonic signal.

7.3 THE POCKELS EFFECT

The permittivity changes of LB films under alternating electric fields have been known for several years [Cross, 1986; Loulergue et. al., 1988]. These changes have been measured in Durham using equipment described in chapter four. Hemicyanine monolayers have been used largely for calibration and reference purposes. Uncoated silver was also examined to evaluate the contributions from the substrate. No discernible signals were observed at twice the frequency of the applied electric field, indicating that cubic contributions to the nonlinear susceptibilities of all LB films concerned are negligible.

7.3.1 Hemicyanine monolayers

Monolayer samples of hemicyanine deposited onto 50nm silver films evaporated onto soda glass slides are used mainly for reference and calibration purposes. The Pockels' data indicate the orientation of the nonlinear susceptibility with respect to the silver substrate. This is illustrated by the contrast between in figures 7.3 and 7.4, which show the Pockels' signal from a hemicyanine and a nitrostilbene monolayer respectively, all other factors being equal. Monolayers of these dyes are known to deposit on silver with their dipole moments in opposite directions with respect to the substrate. So, the Pockels data gives a crude indication of the overall orientation of an LB film. A typical value for the nonlinear susceptibility of a hemicyanine monolayer

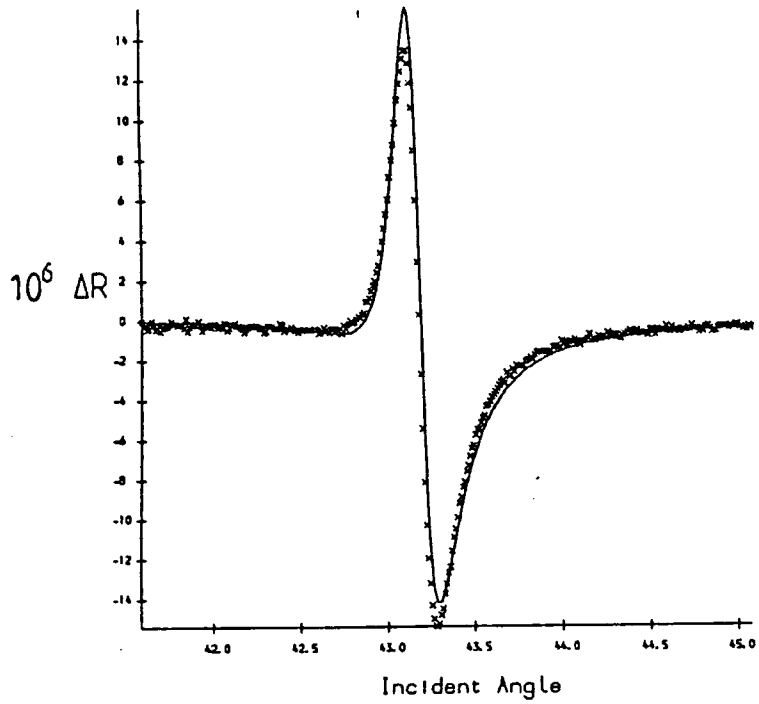

Figure 7.3 : Differential reflectivity of a hemicyanine monolayer

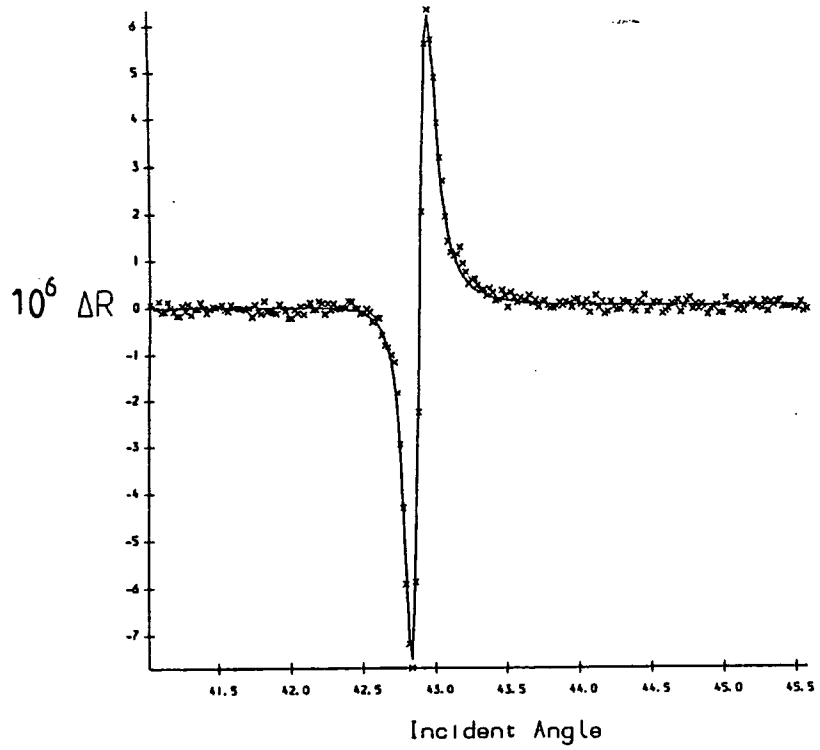

Figure 7.4 : Differential reflectivity of a nitrostilbene monolayer

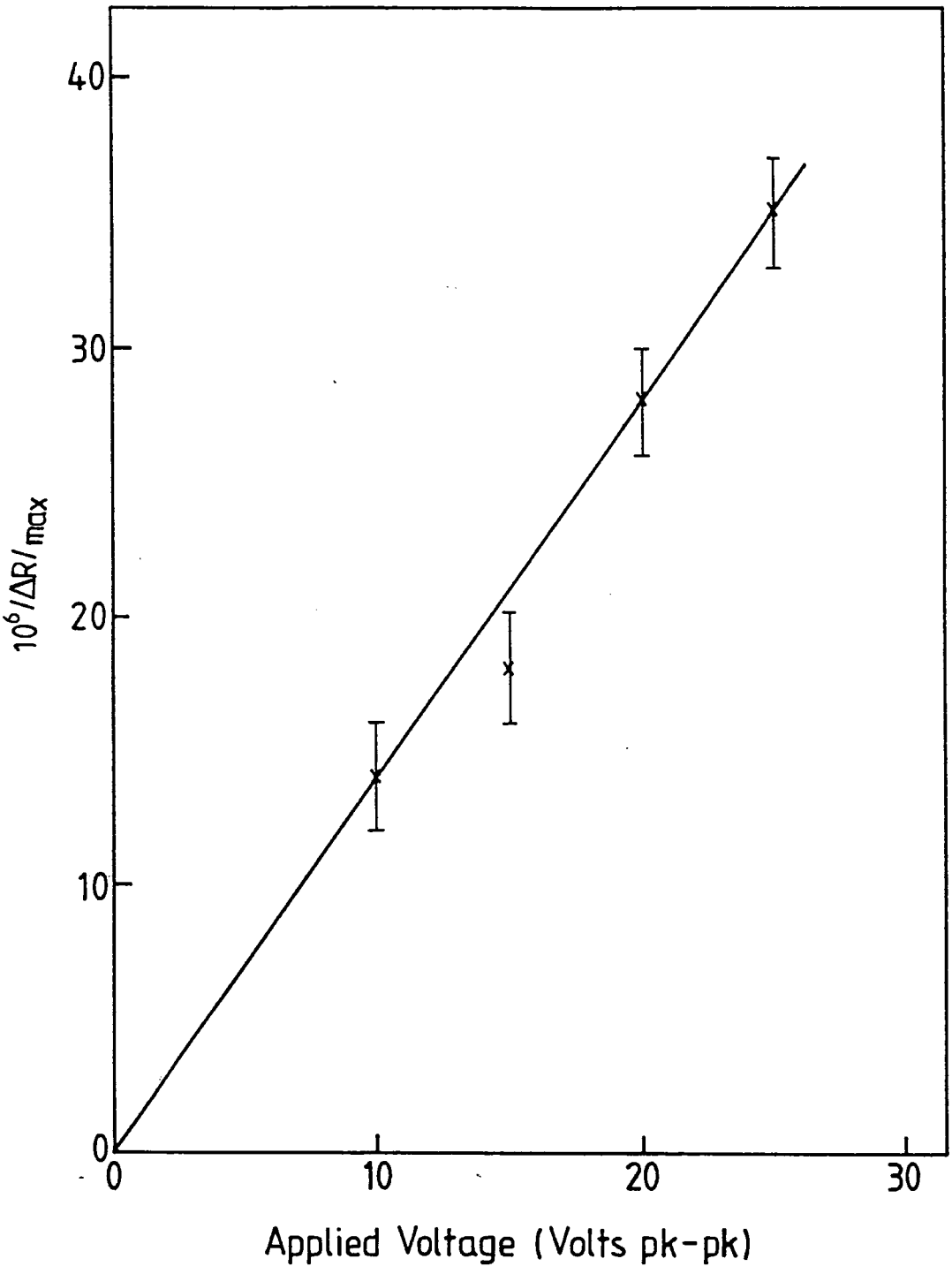

Figure 7.5 : Peak differential reflectivity of a hemicyanine monolayer versus applied voltage

was approximately 95+50i pm V^{-1} which is the same order of magnitude as the figure of 122+28.7i pmV^{-1} [Cross, 1986]. On account of this, the susceptibilities derived from differential reflectivity data are thought to be reliable provided the data are as clear as the experimental points shown in figures 7.3 and 7.4. For smaller signals (e.g. figures 7.6 and 7.7) with a poorer signal-to-noise ratio, the quality of curve fitting clearly deteriorates. It appears that experimental differential reflectivities approaching 10^{-6} can be fitted to quite accurately, while smaller differential reflectivities are less likely to show close correspondence between theory and experiment.

Measurement of the field-induced reflectivity change in hemicyanine showed the nonlinear susceptibility $\chi^{(2)}$ to be frequency-independent in the range 50Hz-5KHz. The measured reflectivity variation $|\Delta R|_{max}$ is the difference between maximum and minimum reflectivity changes. Figure 7.5 shows that for hemicyanine this quantity is proportional to the applied electric field. As mentioned in chapter four, this indicates that electroabsorption is not contributing to the Pockels data. By analogy, any LB film having optical absorption smaller than that of a hemicyanine monolayer should display no electroabsorption where the Pockels effect is expected.

7.3.2 Silver and Fatty Acids

As mentioned in chapter four, a silver surface will possess a second-order optical nonlinearity due to its lack of inversion symmetry [Shen, 1984]. Additionnal nonlinearities may arise from contamination by, for example, a surface layer of silver sulphide or particulate matter adhering to the surface. The equipment used for measuring the Pockels effect is sensitive enough to measure this nonlinearity. Figures 7.6 and 7.7 are the differential reflectivities of uncoated silver and a 22-TA monolayer deposited on silver. In both cases, the silver was 50nm thick, with an air gap of 6.8μm and an applied electric field of 35V pk at 3KHz. The difference between the peak-to-peak differential reflectivities is approximately 2×10^{-7}, which indicates that the nonlinearity arises mainly from the silver surface. The nonlinearity of the silver/fatty acid assembly has several sources: the noncentrosymmetrys at the silver/fatty acid and fatty acid/air interfaces and the intrinsic nonlinearity of fatty acid molecules. The former is comparable to the optical nonlinearity at any other interface, such as silver and air. Fatty acids have comparatively localised electronic structures, so their intrinsic nonlinearity is small. Thus in both cases the Pockels signal must be due to symmetry breaking at an interface: silver/air in uncoated silver and silver/fatty acid and/or fatty acid/air for a coated silver layer.

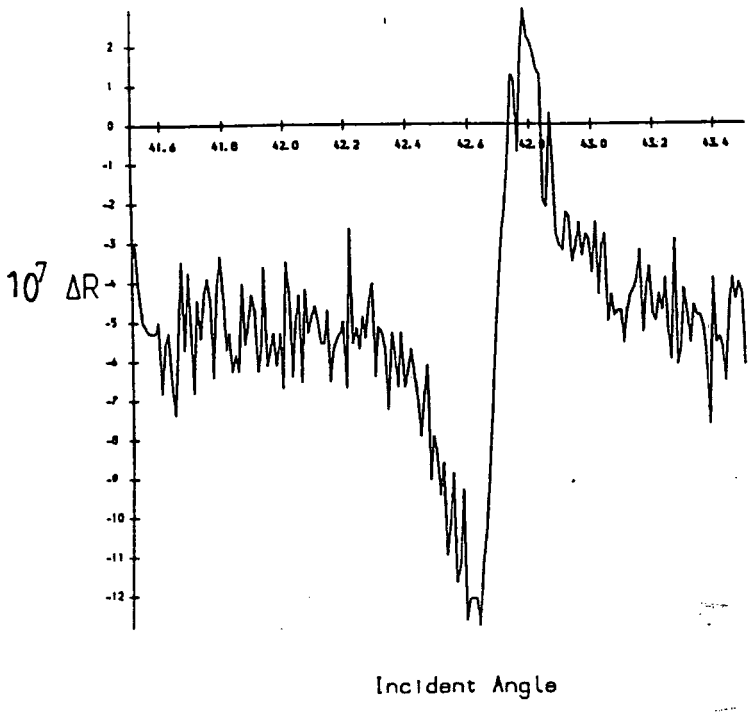

Figure 7.6 : Differential reflectivity of uncoated silver

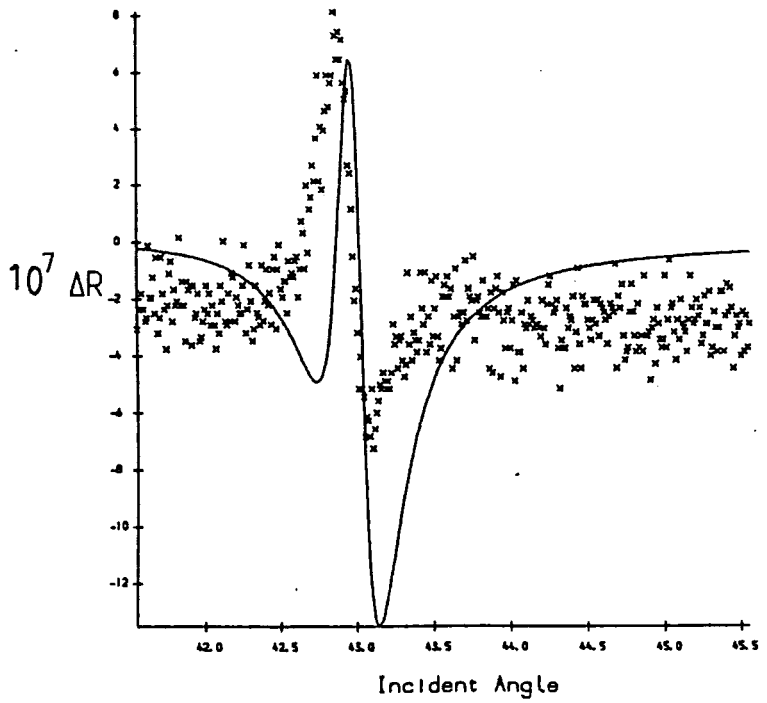

Figure 7.7 : Differential reflectivity of an ω-TA monolayer on a silver substrate

The curve fitting program presumes that nonlinear susceptibilities arise from intrinsic nonlinearities and is incapable of estimating $\chi^{(2)}$ at an interface. So, the surface susceptibility of silver cannot be estimated directly. Instead, it has to be compared to the fatty acid nonlinear susceptibility, taking the fatty acid as intrinsically nonlinear. That is, silver has a surface susceptibility corresponding approximately to the intrinsic susceptibility of a fatty acid monolayer. Curve fitted SPR and Pockels data for 22-TA are listed in table 7.2

This effect is present in all measurements of the Pockels effect in this thesis. So, the above contribution to the nonlinear susceptibility must be subtracted from the fitted susceptibility to obtain a true estimate of the LB film nonlinearity. This does not, of course, influence the nonlinear susceptibility of the structure as a whole.

7.3.3 Polysiloxanes

The AMCR materials are randomly-substituted polymers with no preferred orientation of the bipolar chromophores with respect to the polymer backbone; because of this, microscopic nonlinearities within each molecule largely cancel each other out and the molecules are essentially centrosymmetric. The LB deposition process, on the other hand, orients the molecules with respect to their substrate, which leads to an overall noncentrosymmetry within the LB film. The resulting nonlinearities are noticeable on the differential reflectivity plots in figures 7.8 and 7.9, which represent AMCR22 and AMCR23 respectively. AMCR24 did not adhere sufficently well to silver to produce SPR curves of sufficent quality to calculate the LB film optical constants. The permittivity changes in monolayers of AMCR22 and AMCR23 are comparable to those in twenty layers of JT3, but opposite in sign.

With reference to the structures of the AMCR molecules (see chapter five), the main acceptor groups (NO_2 and OH in AMCR22 and AMCR23, respectively) are at the ends of the chromophores most distant from the siloxane spines. The donor groups are in both cases the nitromethyl groups adjacent to the polymethylene spacer chains. This sets the direction of the conventional dipole moments, and by implication the second-order susceptibility, towards the siloxane spines, that is away from the substrate. This is reflected in the shape of the differential reflectivity plots in figures 7.8 and 7.9, which are in the opposite sense to that of a hemicyanine monolayer whose dipole moment points towards the silver substrate.

The strong NO_2 acceptor group in the AMCR22 molecule suggests that its ground state dipole moment is larger than that of AMCR23, which has no correspondingly

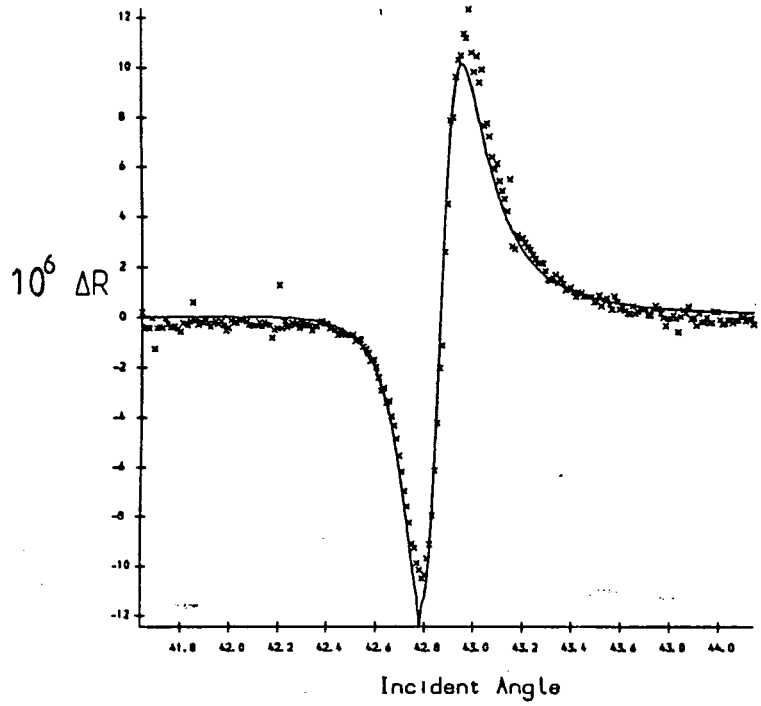

Figure 7.8 : Differential reflectivity of an AMCR22 monolayer on a 50nm silver substrate

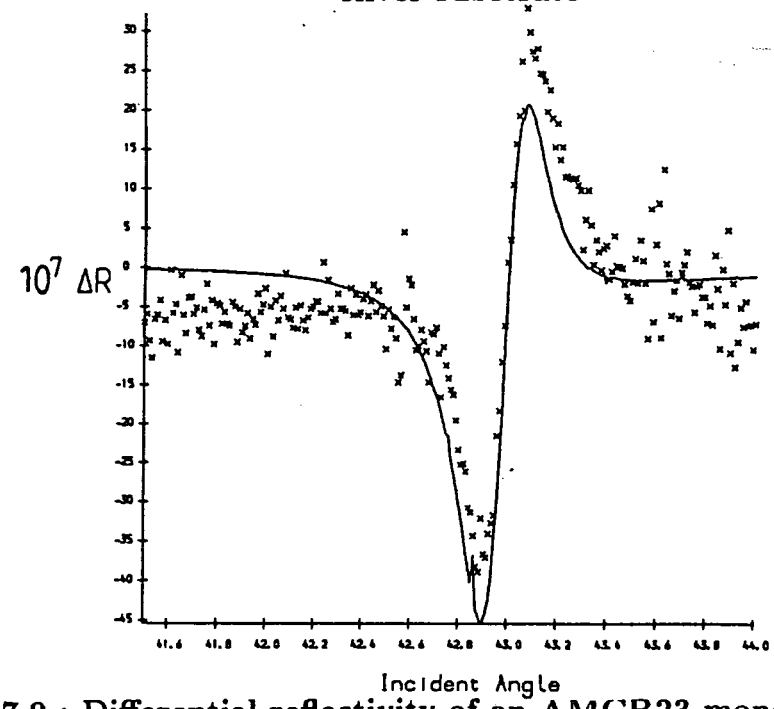

Figure 7.9 : Differential reflectivity of an AMCR23 monolayer on a 50nm silver substrate

strong acceptor. This, however, need not necessarily imply that AMCR22 has a larger nonlinear susceptibility because ground state dipole moments, like static polarisations, bear little relevance to nonlinear susceptibilities. In point of fact, a very large ground state dipole moment suggests a potential distribution that may not be easily deformed to display the transitions required for optical mixing. The relevant quantity is the difference in dipole moments between the ground and first excited states, which is likely to be large in a system consisting of a weak donor and acceptor separated by a conjugated system. The chromophores of AMCR23 are good examples of this, having a weak nitromethylene donor group and a weak alcohol acceptor group straddling a pair of phenyl rings separated by an azo bridge.

7.3.4 Diaryl Alkynes

Of the JT series, JT1 and JT4 showed low differential reflectivity changes per monolayer compared to JT3 and were not examined further. Pockels data consistent with the results presented here on JT3 monolayers have been reported [Tsibouklis et. al., 1989], and are listed in table 7.2 together with data on Z-type multilayers of JT3. Space-filling models of the JT series molecules suggested that JT3 was 4.2nm long when fully extended. As it is unlikely that the molecule will lie fully extended within LB films, the SPR curve fitting procedure was performed several times for a JT3 monolayer using different film thicknesses up to and including 4.2nm. The fit giving the smallest deviation between theory and experiment was taken as representative of the actual film thickness, taken as 3.7nm. Multilayer films were assumed to have thicknesses of integral multiples of 3.7nm. The derived permittivities show considerable variation in their real and imaginary parts, differing by up to about 40% from film to film, although the curve fitting procedure always converges to the same permittivity for a given film.

The nonlinear susceptibility is estimated from the formula

$$\chi^{(2)}(-\omega;\omega,0) = \frac{\epsilon d \Delta\epsilon}{V_a} \tag{7.2}$$

where ϵ is the film permittivity, $\Delta\epsilon$ is the permittivity change, d is the air gap, taken as much larger than the LB film thickness and $\chi^{(2)}(-\omega;\omega,0)$ is the bulk second order susceptibility, the tensor nature of which is ignored. Due to the limited accuracy of the program for fitting differential reflectivity data, the permittivity changes are not exact; figure 7.10 illustrates the difference between theoretical and measured values of differential reflectivities. Given this, the nonlinear susceptibilities derived

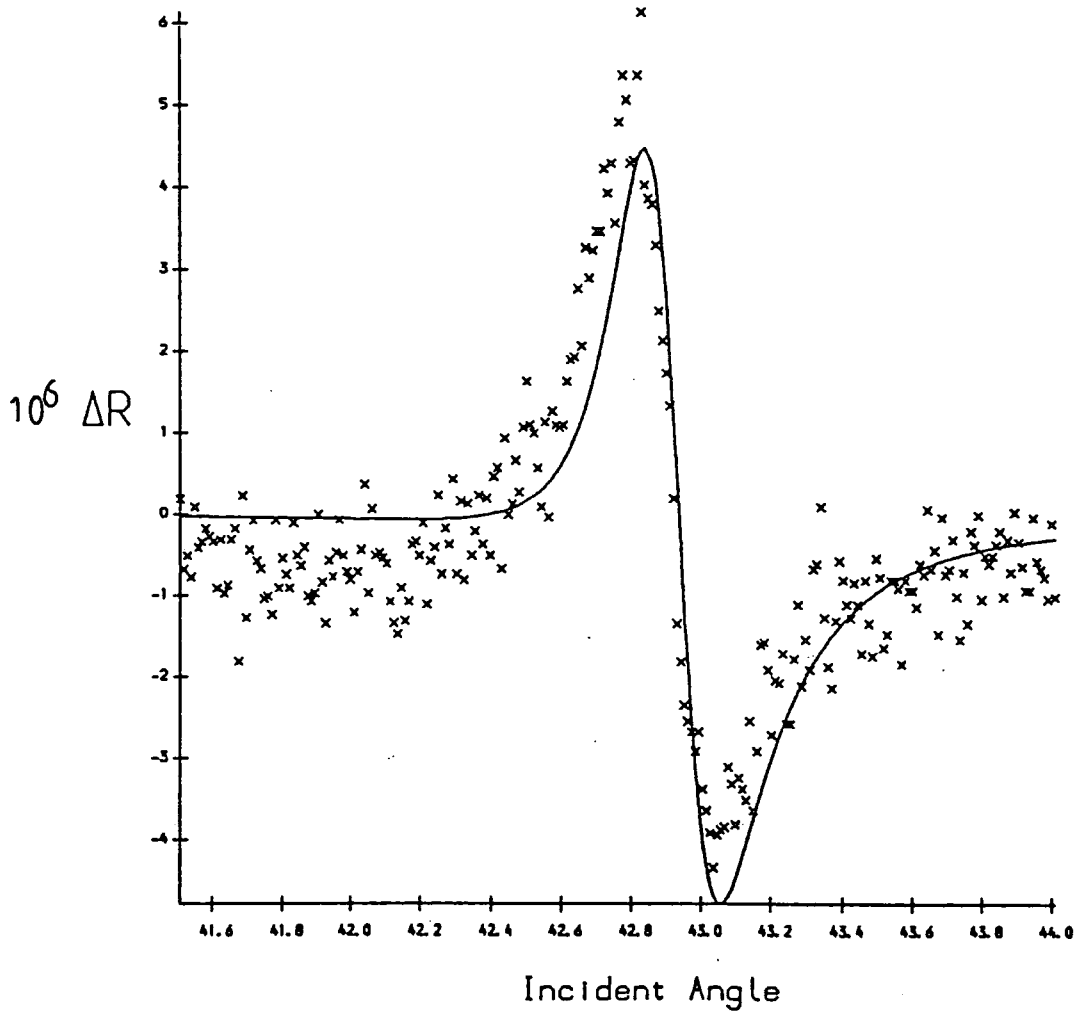

Figure 7.10 : Differential reflectivity of a JT3 monolayer on a 50nm silver substrate

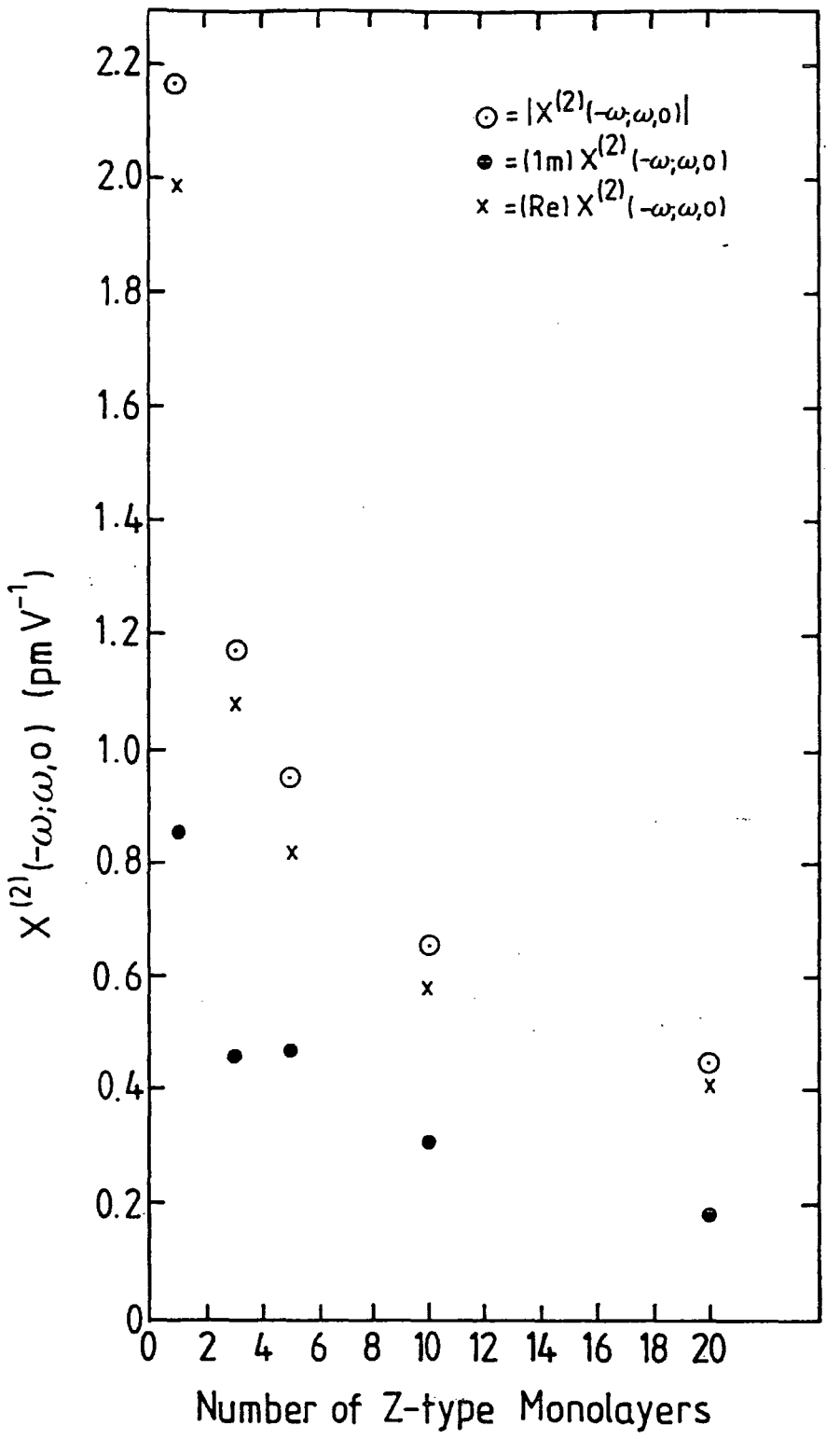

$\chi^{(2)}(-\omega;\omega,0)$ = JT3 LB film susceptibility per monolayer

Figure 7.11 : Nonlinear susceptibility of JT3 multilayers versus film thickness

Material	N	V_a (V)	$\Delta\epsilon/10^{-4}$	$\chi^{(2)}(-\omega;\omega,0)$ (pmV^{-1})	sense of $\chi^{(2)}$
22-TA	1	35	0.011+0.031i	0.653+1.90i	↑
hemicyanine	1	20	0.903+0.437i	94.5+49.9i	↑
4HANS	1	35	-0.249-0.0068i	-22.37-0.97i	↓
AMCR22	1	35	-0.329-0.037i	-1.08-1.42i	↓
AMCR23	1	25	-0.179+0.012i	-15+9.6i	↓
JT1	1	35	0.017+0.012i	0.95+0.70i	↑
JT3	1	35	0.047+0.017i	1.99+0.855i	↑
JT3	3	35	0.083+0.027i	1.08+0.459i	↑
JT3	5	35	0.113+0.039i	0.820+0.471i	↑
JT3	10	35	0.137+0.062i	0.581+0.313i	↑
JT3	20	35	0.201+0.072i	0.410+0.187i	↑
JT4	1	35	0.006+0.002i	0.32+0.22i	↑

l = LB film thickness

N =number of LB monolayers

V_a = applied voltage

$\Delta\epsilon = \Delta\epsilon_r + i\Delta\epsilon_i$ =field-induced permittivity change

$\chi^{(2)}(-\omega;\omega,0)$ = bulk susceptibility per monolayer

Air gap=10.5 micrometres The sense of $\chi^{(2)}$ is the direction of the macroscopic dipole moment with respect to the silver substrate. ↓ and ↑ represent towards and away from the silver, respectively.

Table 7.2 : Fitted Nonlinear Susceptibilities of several LB materials

by measurement of the Pockels effect are best taken as order-of-magnitude estimates. At the time of writing, no theoretical predictions of the polarisabilities of the JT series molecules were available.

The SHG data from the previous section indicate that the bulk susceptibility per monolayer fell as more JT3 monolayers were deposited. Curve fitted Pockels data show a rise in peak differential reflectivity and overall bulk susceptibility but the susceptibility per monolayer has been confirmed to decrease with increasing film thickness; the susceptibility per monolayer is quoted in table 7.2 and represented graphically in figure 7.11. Although Z-type JT3 monolayers are readily deposited onto solid substrates, rearrangement towards a Y-type structure and/or progressive deterioration of in-plane order in subsequent monolayers leads to cancellation of the optical nonlinearity, to the point where JT3 structures have a susceptibility over two orders of magnitude smaller than that of a hemicyanine monolayer. A recent notable exception is the family of $C_mH_{2m+1}-Q3CNQ$ ($m > 15$), molecules and their analogues which have been shown to consistently deposit up to fifty stable Z-type monolayers with a second harmonic conversion efficency per monolayer comparable to that of a hemicyanine monolayer [Ashwell et. al., 1990].

Several methods have been recently developed in an attempt to overcome the lack of optical nonlinearity inherent in Y-type LB film structures. Alternation of the optically nonlinear material with a comparatively inert spacer layer (e.g. 22-TA) may reduce interactions between adjacent monolayers, thus improving in-plane order at the price of halving the susceptibility. Better still, alternation of two optically nonlinear species such that their dipole moments add constructively produces an organic superlattice with ehnanced optical nonlinearity [Young et. al., 1990; Neal et. al., 1986; Cross et. al., 1987]. Also, should the nonlinear susceptibility be in the same plane as the dipping direction and invariant from monolayer to monolayer [Bosshard et. al., 1989], nonlinear Y-type films become feasable and the deposition method assumes secondary importance. Alternation of JT3 with another material was not attempted, although in the light of the above information, such an experiment may shed light on the structure of multilayer JT3 assemblies and lead to enhanced nonlinear behaviour of LB films containing those molecules.

The Pockels data resemble those of a hemicyanine monolayer to the extent that the differential reflectivity is positive below the SPR minimum and negative above it. This indicates that the orientation of the nonlinear susceptibility $\chi^{(2)}(-\omega;\omega,0)$ is similar to that of a hemicyanine monolayer: towards the silver substrate. Conversely,

if the differential reflectivity were negative below the SPR minimum and positive above it, the nonlinear susceptibility would be taken as pointing away from the silver substrate. The JT series molecules each have an azophenyl group, which is a strong acceptor, next to their hydrocarbon tails; JT3 and JT4 also have a weak methoxy donor group at the other end of the chromophore. So, the direction of the conventional dipole moment in the JT series is from the hydrocarbon chain along the chromophore. Similar comments apply to hemicyanine monolayers. Accordingly, Z-type layers of all JT molecules should display a dipole moment in the same direction as a Z-type hemicyanine monolayer. As shown in table 7.2, this has been confirmed experimentally.

7.4 SUMMARY

The nonlinear susceptibilites of AMCR series monolayers and JT3 mono- and multilayers have been measured by the Pockels effect. Of the novel materials, a monolayer of AMCR23 possessed the highest nonlinear susceptibility, being approximately two orders of magnitude smaller than that of a hemicyanine monolayer. Z-type multilayers of JT3 showed a nonlinear susceptibility directly proportional to film thickness.

Much of the data has been corroborated by transmission SHG experiments. The SHG of monolayers of each novel material is approximately two orders of magnitude smaller than that of a hemicyanine monolayer. The SHG of multilayers of Z-type AMCR22, AMCR23 and JT3 rises linearly with film thickness. This indicates that the average nonlinear susceptibility per monolayer falls rapidly with increasing film thickness.

7.5 REFERENCES

Ashwell, G. J., Dawnay, E. J. C., Kuczynski, A. P., Szablewski, M., Sandy, I. M., Bryce, M. R., Grainger, A. M., Hasan, M. : Langmuir- Blodgett Alignment of Zwitterionic Optically Non-linear D-π-A Materials ,*J. Chem. Soc. Farady Trans.* **86** *7* , 1990 pp. 1117-21.

Bosshard, Ch., Tieke, B., Seifert, M., Günter, P. : Nonlinear Optical Y-type Langmuir-Blodgett Films of 2-docosylamino-5- nitropyridine (Presented at Int. Conf. Materials for Non-linear and Electro- optics, Cambridge, UK) ,*Inst. Phys. Conf. Ser. No 103 Section 2.3* , 1989 pp. 181-6. publ. IOP Publishing.

Cresswell, J. P., Tsibouklis, J., Petty, M. C., Feast, W. J., Carr, N., Goodwin, M. J., Lvov, Y. M. : Langmuir- Blodgett Alternate Layer Structures for Second-Order Nonlinear Optics , *SPIE conf. on Nonlinear Optical Properties of Organic Materials III* , 1990

Cross, G. H. : Linear Pockels Response of a Monolayer Langmuir-Blodgett Film , *Electron. Letters* **22** *21* , 1986 pp. 1111-3.

Cross, G. H., Peterson, I. R., Girling, I. R. : Nonlinear Optics and Electro-Optics in Langmuir-Blodgett Films ,*Proc. 31st SPIE Int. Conf. Optoelectronics, San Diego* , 1987

Carr, N., Goodwin, M. J., McRoberts, A. M., Gray, G. W., Marsden, R., Scrowston, R. M. : Second Harmonic Generation in a Monomolecular Langmuir-Blodgett Film of a Preformed Polymer ,*Makromol. Chem. Rapid. commun.* **8** , 1987 pp. 487-93.

Girling, I. R., Cade, N. A., Kolinsky, P. V., Montgomery, C. M. : Observation of Second-Harmonic Generation from a Langmuir- Blodgett Monolayer of a Merocyanine Dye ,*Electron. Letts.* **21** *5* , 1985 pp. 169-70.

Loulergue, J. C., Dumont, M., Levy, Y. : Linear Electro- Optic Properties of Langmuir-Blodgett Multilayers of an Organic Azo Dye , *Thin Solid Films Proc. 3rd Int. Conf. LB Films, Göttingen.* **160** , 1988 pp. 399-405.

Neal, D. B., Petty, M. C., Roberts, G. G., Ahmad, M. M., Feast, W. J. : Second Harmonic Generation from LB Superlattices Containing two Active Componen ts ,*Electron. Letters* **22** *9* , 1985 pp. 460-462.

Novak, V. R., Lvov, Y. M., Myagkov, I. V., Teternik, G. A. : Bilayer-Structure Langmuir Films without an Inversion Center , *JETP Lett.* **45** *11* , 1987 pp. 698-9. publ. American Institute of Physics.

Shen, Y. R. : The Principles of Nonlinear Optics , 1984 publ. Wiley.

Tsibouklis, J., Cresswell, J. P., Kalita, N., Pearson, C., Maddaford, P. J., Ancelin, H., Yarwood, J., Goodwin, M. J., Carr, N., Feast, W. J., Petty, M. C. : Functionalised Diarylalkynes : A New Class of Langmuir-Blodgett Film Materials for Non-Linear Optics , *J. Phys. D.: Appl. Phys.* **22** , 1989 pp. 1608-12. publ. IOP.

Young, M. C. J., Jones, R., Tredgold, R. H., Lu, W. X., Ali-Adib, Z., Hodge, P., Abbasi, F. : Optical and Structural Characterisation of Langmuir- Blodgett Multilayers of Non-Polymeric and Polymeric Hemicyanines , *Thin Solid Films* **182** , 1989 pp. 319-32. publ. Elsevier.

Young, M. C. J., Lu, W. X., Tredgold, R. H., Hodge, P., Abbasi, F., : Optical Second Harmonic- Generation from Laminated Polymeric LB Multilayers , *Electronics Letters* **26** *14* , 1990 pp. 993-5.

Chapter VIII

CONCLUSIONS

Several novel Langmuir-Blodgett (LB) film-forming materials have been extensively characterised in floating monolayer form. The depostion characterisitics of each material into Langmuir-Blodgett mono- and multilayers on solid substrates have also been examined. Of the monomeric materials, $CH_3(CH_2)_{21}Py^+C{\equiv}CPhOCH_3$, or JT3, formed the most consistent LB films. Of several polymeric materials having siloxane spines approximately sixteen Si atoms long with randomly-substituted bipolar chromophores as side groups, AMCR22 and AMCR23 showed promising film-forming properties as well as the unusual characteristics of extreme stability as floating monolayers and no apparent damage on compression to very small apparent areas per molecule.

Experimental apparatus and associated software were designed to estimate the second-order nonlinear susceptibility $\chi^{(2)}(-\omega;\omega,0)$ of ultrathin (2 nm approx) LB films. The equipment exploited the well-known phenomena of surface plasmon resonance and the Pockels' effect: a high-strength, low-frequency electric field ($\sim 10^7$ V m^{-1} at 3KHz) applied to the LB film modulated the film permittivity via the Pockels' effect. This permittivity change was measured and, given the LB film and substrate thicknesses and optical constants (which were be estimated using the same equipment), was used to calculate one component of the LB film second order nonlinear susceptibility: $\chi^{(2)}_{zzz}(-\omega;\omega,0)$. This was done for a variety of materials in mono- and multilayer form, and the results corroborated by second-harmonic generation.

The data derived by this technique appear to be genuine estimates of the nonlinear susceptibility. In chapter two various effects which may have influenced the estimation of LB film and substrate optical constants derived from SPR were shown to be negligible. These included material parameters, thermal effects and piezoelectricity. Similarly, spurious effects which may have influenced the Pockel's effect have also been shown to be negligible for the materials examined here. These were electroabsorbtion (Stark effect), substrate contributions, cubic behaviour, piezoelectricity and resonant nonlinearities. Thus, it has been shown that the Pockels' effect, as described in this thesis, is an effective alternative to second harmonic generation for estimating the second-order nolinear susceptibility of Langmuir-Blodgett films.

Compared to a hemicyanine monolayer, none of the materials examined here showed a high nonlinear susceptibility in monolayer form. The largest were those of AMCR23 and AMCR22, whose susceptibilities were approximately one tenth and one hundredth that of a hemicyanine monolayer. Given the chemical similarity between AMCR22 and AMCR23, the exact structure of the chromophoric sidegroups obviously greatly influenced the nonlinear susceptibility. Second-harmonic generation (SHG) experiments, however, suggested that the structural order of AMCR22 and AMCR23 multilayers deteriorated with increasing film thickness, since the SHG output power did not rise quadratically with film thickness.

In monolayer form, material JT3 showed a nonlinear susceptibility approximately two orders of magnitude smaller than that of a hemicyanine monolayer. While JT3 produced Langmuir-Blodgett films up to 37 monolayers in thickness, the nonlinear susceptibility per monolayer fell drastically with increasing film thickness: SHG and Pockels' effect data indicated that the susceptibility per monolayer was inversely proportional to the square root of the number of deposited monolayers.

Chapter IX

SUGGESTIONS FOR FURTHER WORK

Given that monolayers of material AMCR23 displayed a nonlinear susceptibility approximately an order of magnitude smaller than hemicyanine monolayers, it seems reasonable to further examine the nonlinear optical behaviour of AMCR23 multilayer structures and the effects of alterations in the structures of the AMCR23 chromophores. The justification for this lies in the fact that polymeric Langmuir-Blodgett (LB) films are generally more mechanically and thermally stable than monomeric films. Polymeric multilayer LB films with high optical nonlinearities may ultimately form the basis for a variety of devices such as hybrid optical communication devices and variable phase retarders.

The dc Kerr effect is a refractive index change proportional to the square of a low-frequency applied electric field and the third-order nonlinear susceptibility $\chi^{(3)}$. In contrast to the Pockels' effect, this refractive index variation appears at twice the frequency of the low-frequency applied electric field. It may be possible to measure this susceptibility in a manner analogous to the measurements of $\chi^{(2)}_{zzz}(-\omega;\omega,0)$ performed in this thesis. The improvements required of the apparatus are a larger applied electric field and greater sensitivity of detection apparatus.

More broadly, the apparatus described here for measurement of the Pockels' effect amounts to a specialised method of prism coupling radiation into an electromagnetic surface mode. As such it may be feasable to adapt the equipment to examine a broader range of guided electromagnetic waves and provide more detailed information on the bulk and surface porperties of polymeric and monomeric materials.

Appendix A

Derivation of the Relationship between Permittivity and the Piezoelectric Coefficent

A collection of variables may be defined which specify the thermodynamic state of any system: **E**, **D**, σ, ε, S and T which are electric field, electric displacement, stress, strain, entropy and temperature respectively. Then, choosing **E**, ε and T as independent gives

$$\mathbf{D} = \mathbf{D}(\mathbf{E}, \varepsilon, T) \tag{A.1}$$

$$\sigma = \sigma(\mathbf{E}, \varepsilon, T) \tag{A.2}$$

$$S = S(\mathbf{E}, \varepsilon, T) \tag{A.3}$$

As we have no interest in identities involving entropy and all changes are assumed isothermal, the dependences on T and S may be dropped. Expanding the displacement and strain as perfect differentials gives, in cartesian tensor notation:

$$dD_i = \left(\frac{\partial D_i}{\partial E_k}\right)_{\varepsilon} dE_k + \left(\frac{\partial D_i}{\partial \varepsilon_{kl}}\right)_{E} d\varepsilon_{kl} \tag{A.4}$$

and

$$d\sigma_{ij} = \left(\frac{\partial \sigma_{ij}}{\partial E_k}\right)_{\varepsilon} dE_k + \left(\frac{\partial \sigma_{ij}}{\partial \varepsilon_{kl}}\right)_{E} d\varepsilon_{kl} \tag{A.5}$$

As the electric field and displacement are related by

$$D_i(E_j) = \epsilon_{ij} E_j \tag{A.6}$$

and

$$D_i(E_j + \Delta E_j) = (\epsilon_{ij} + \Delta\epsilon_{ij})(E_j + \Delta E_j) \approx \epsilon_{ij} E_j + \epsilon_{ij} \Delta E_j \tag{A.7}$$

so

$$\epsilon_{ij} = \lim_{\Delta E_j \to 0} \frac{D_i(E_j + \Delta E_j) - D_i(E_j)}{\Delta E_j} = \frac{\partial D_i}{\partial E_j} \tag{A.8}$$

So the permittivity at constant strain is given by

$$\left(\frac{\partial D_i}{\partial E_k}\right)_\varepsilon = \epsilon^\varepsilon_{ik} \tag{A.9}$$

The Maxwell relation

$$\left(\frac{\partial \sigma_{ij}}{\partial E_k}\right)_\varepsilon = \left(\frac{\partial D_k}{\partial \varepsilon_{ij}}\right)_E = -d_{kij} \tag{A.10}$$

states that the piezoelectric coefficent d_{kij} is the same for the direct and converse piezoelectric effects. The derivative of stress with respect to strain may be identified with the compliance tensor:

$$\left(\frac{\partial \sigma_{ij}}{\partial \varepsilon_{kl}}\right)_E = s_{ijkl} \tag{A.11}$$

After appropriate substitutions the expansions A.4 and A.5 can be rewritten as

$$dD_i = \epsilon^\varepsilon_{ik} dE_k - d_{ikl} d\varepsilon_{kl} \tag{A.12}$$

and

$$d\sigma_{ij} = -d_{ijk} dE_k + s_{ijkl} d\varepsilon_{kl} \tag{A.13}$$

If a vector f_j can be found, the indices of the compliance tensor may be contracted to give

$$d_{ikl} = s_{ijkl} f_j \tag{A.14}$$

so we may put

$$dD_i = \epsilon^\varepsilon_{ik} dE_k - s_{ijkl} f_j d\varepsilon_{kl} = \epsilon^\varepsilon_{ik} dE_k - f_j (d\sigma_{ij} + d_{ijk} dE_k) \tag{A.15}$$

that is

$$\frac{\partial D_i}{\partial E_k} = \epsilon_{ik}^{\varepsilon} - f_j \frac{d\sigma_{ij}}{dE_k} - d_{ijk} f_j \qquad (A.16)$$

Under constant stress ($d\sigma = 0$), A.16 becomes

$$\left(\frac{\partial D_i}{\partial E_k}\right)_{\sigma} = \epsilon_{ik}^{\varepsilon} - d_{ijk} f_j = \epsilon_{ik}^{\sigma} \qquad (A.17)$$

where ϵ^{σ} is the permittivity at constant stress. The last equation means that the refractive index of a clamped thin film (constant strain) is not the same as the refractive index of a free film (constant stress). To highlight this difference, ignoring the tensor nature of all these quantities for the moment by dropping all subscripts gives, for the last equation

$$\epsilon^{\sigma} = \epsilon^{\varepsilon} - \frac{d^2}{s} \qquad (A.18)$$

we note that since the units of piezoelectric coefficent are CN^{-1}, those of compliance are Nm^{-2} and those of permittivity are $CV^{-1}m^{-1}$, the last equation is dimensionally correct.

Appendix B

Laser Beam Collimation

The He-Ne laser used in all SPR and Pockels effect experiments here contains one planar and one concave mirror. These act as an optical resonator. At the surface of each mirror, the radii of curvature of mirror and wavefront must be equal. It has been shown in several standard texts on Gaussian optics that a laser resonator is formally equivalent to a suitable arrangement of thin lenses operating in the paraxial regime. Therefore, it is possible to focus a Gaussian mode to a planar wavefront using only thin lenses. More formally, the wave equation

$$\nabla^2 \mathbf{E} = -\frac{1}{c^2}\frac{\partial^2 \mathbf{E}}{\partial t^2} \qquad (B.1)$$

solved using the slowly varying amplitude approximation to yield the electric field of a Gaussian TEM_{00} mode:-

$$E(z) = \frac{E_0 w_0}{w(z)} \exp\left[\frac{-\rho^2}{R(z)}\right] \exp[-itan^{-1}(z/z_0)] \exp\left[\frac{-ik(z+\rho^2)}{2R(z)}\right] \qquad (B.2)$$

in cylindrical coordinates. z is the axial distance from the beam waist, which has diameter $2w_0$; $w(z)$ is the beam spot size given by $w^2(z) = w_0^2(1 + z^2/z_0^2)$ where $z_0 = \pi w_0/\lambda$ is the Rayleigh distance. The wavefronts are defined by the final exponential term, where

$$k\left(\frac{z+\rho^2}{2R(z)}\right) = constant \qquad (B.3)$$

which represents parabolic wavefronts. For $\rho^2 << z^2$, the wavefronts are effectively spherical with a radius of curvature $R(z)$. As $\rho \sim$1mm and $z \sim$1m in the existing experimental arrangement, this approximation is generally valid. The apparent centre of curvature is at z_0 when examined from $z >> z_0$. The beam divergence angle is $\tan(\theta/2) = \rho/z$. Thus, if the propagation vector on the beam axis is k, the projection of the TEM_{00} mode onto the z plane is a travelling wave with wavevector

$$k_\rho = k\sin(\theta/2) = \frac{k}{\sqrt{1+z^2/\rho^2}} \tag{B.4}$$

and phase given by

$$\exp\left[\frac{-k\rho^2}{2R(z)}\right] \tag{B.5}$$

from B.2. If this radial behaviour can be cancelled, the spread of k vectors in the z plane may in principle be reduced to zero and the beam becomes perfectly collimated. Now consider a thin lens in the ρ plane with its centre on the z axis. Any incident wavefront is modified by a phase shift

$$\exp\left[\frac{ik\rho^2}{2f}\right] \tag{B.6}$$

which increases with distance from the axis. $k = 2\pi n/\lambda$ and f is the focal length. Clearly, passing a TEM_{00} mode through a lens of focal length equal to half the beam radius of curvature acts to collimate the beam.

This approach works well in principle, but the radius of curvature of a laser beam is not easily measured without extensive preparation. Furthermore, as the beam radius of curvature varies with propagation distance, using a single lens limits the experimenter to locating it at one position on the beam axis. A collimated output can be obtained from a pair of lenses of arbitrary focal lengths, provided that their separation and distance from the beam waist are chosen correctly. This is explained in the following paragraphs.

It is a well-known result of geometrical optics that two lenses separated a distance equal to the sum of their focal lengths will alter the diameter of an incident plane wave light beam. Laser beams, however, do not have plane wavefronts, and a Gaussian optics approach must be taken to derive the conditions necessary for their collimation. Standard ABCD matrix formalism, as found in many Gaussian optics texts (e.g. Yariv, 1985), is well suited to the task. The ABCD matrix of the lens system shown overleaf in figure B.1 is

$$\begin{pmatrix} (1-\frac{l_3}{f_2})(1-\frac{l_2}{f_1})-\frac{l_3}{f_1} & l_1((1-\frac{l_3}{f_2})(1-\frac{l_2}{f_1})-\frac{l_3}{f_1})+l_2(1-\frac{l_3}{f_2})+l_3 \\ -\frac{1}{f_2}(1-\frac{l_2}{f_1})-\frac{1}{f_1} & -l_1(\frac{1}{f_2}+\frac{1}{f_1}-\frac{l_2}{f_1 f_2})+1-\frac{l_2}{f_2} \end{pmatrix} \tag{B.7}$$

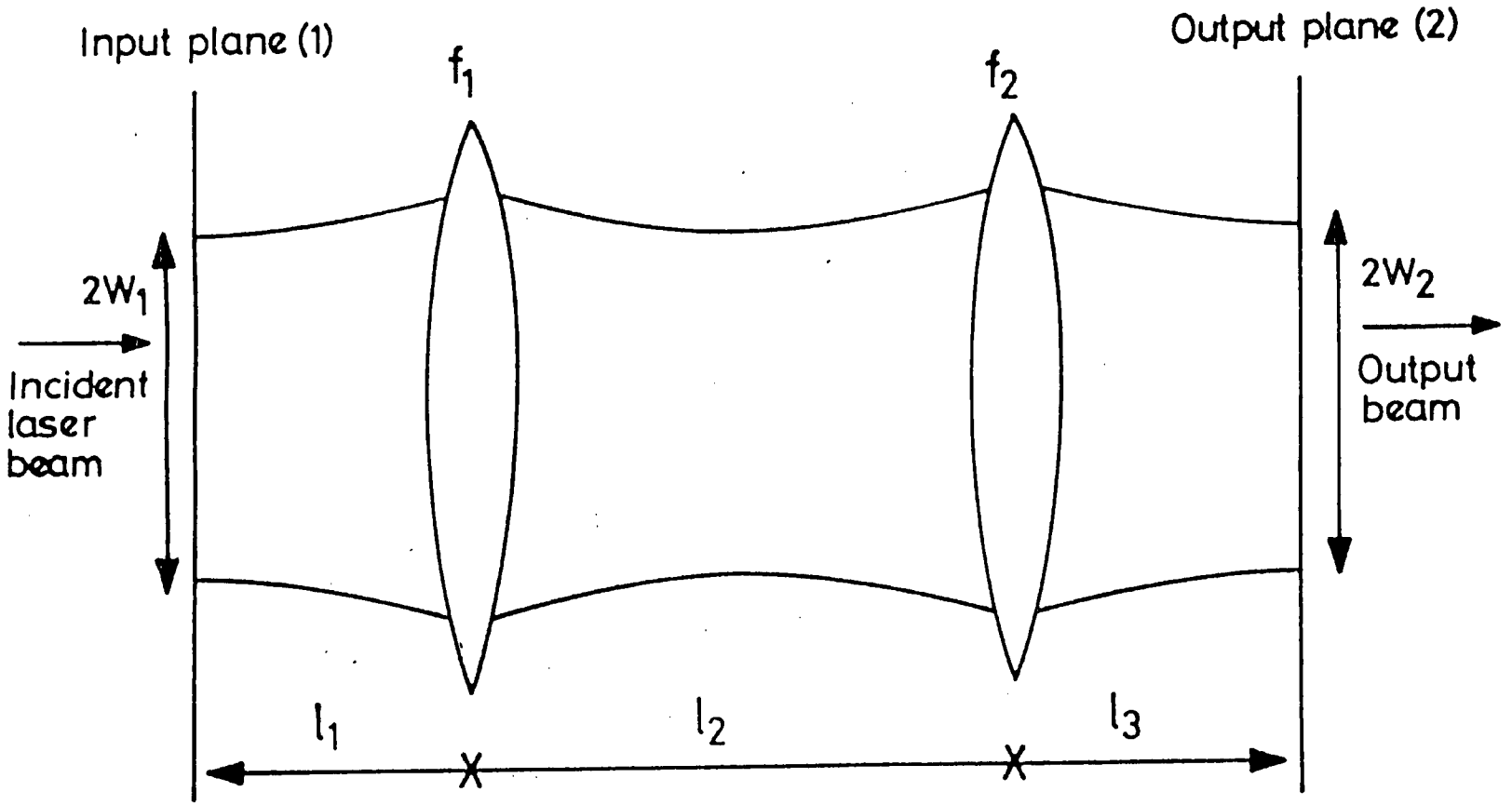

Figure B.1 : Laser Beam Collimating Lenses

According to the ABCD law,

$$\frac{1}{q_2} = \frac{Aq_1 + B}{Cq_1 + D} \tag{B.8}$$

where

$$\frac{1}{q} = \frac{1}{R} - \frac{i\lambda}{\pi w^2} \tag{B.9}$$

where R and $2w$ represent the radius of curvature and beam diameter respectively at any given position.Inserting appropriate expressions for q and R at planes 1 and 2 into B.8 gives

$$(\frac{1}{R_2} - \frac{i\lambda}{\pi w_2^2})(C + D(\frac{1}{R_1} - \frac{i\lambda}{\pi w_1^2})) = A + B(\frac{1}{R_1} - \frac{i\lambda}{\pi w_1^2})) \tag{B.10}$$

The conditions that the output beam from plane 2 be collimated are

$$R_2 = \infty \tag{B.11}$$

and

$$\frac{\partial w_2}{\partial l_3} = 0 \tag{B.12}$$

The latter is equivalent to requiring the output beam diameter to be a minimum. Inserting B.11 then B.12 in B.10 and separating the real and imaginary parts gives

$$l_2 = f_1 + f_2 \tag{B.13}$$

and

$$l_1 f_1 = (f_1 - l_1)(f_2 - l_2) \tag{B.14}$$

which are the conditions that the output beam divergence be zero.Note that B.13 and B.14 may not be simultaneously valid. The former is normally used when aligning

lenses approximately in the laboratory. Accurate alignment of the lens system relies on eq. B.12 i.e. the spacing between the lenses is adjusted until the output beam diameter is a minimum.

Inserting either B.13 or B.14 into B.10 and solving for w_2 yields

$$w_2^2 = w_1^2(l_2 - f_1 - f_2)\frac{1}{f_2(f_1 l_1 - l_1 l_2 + f_1 l_2)} \qquad (B.15)$$

which, though cumbersome, is independent of l_3. Inserting $\lambda = 632$ nm, $f_1 = f_2 = 15$ cm, $l_1 = 20$ cm, $l_2 = 25$ cm and $w_1 = 2$ mm gives w_2 as 80 microns. The limitations on the beam diameter are, firstly, that it occupies a relatively small area of the sample under examination and, secondly, that the heating of the illuminated area be insignificant. The former condition is amply fulfilled experimentally, since most of the samples under examination are larger than 1 cm square. As to the latter, researchers in surface plasmon resonance almost without exception assume that the silver coating forms an adequate heat sink.

Appendix C

Listing of the SPR and Pockels Data Acquisition Program Source Code

```
{ $D+,$F+,$G+,$I5000,$L+,$R+,$W+,$X+ }{ Compiler options }
PROGRAM Autorig(input,output);
 CONST
  len = 38; { string length }
  pi = 3.14159265;
 TYPE
  string = PACKED ARRAY[1..len] OF char;
  byte = 0..&FF;
 VAR
  extcritangle : real; { prism assembly's external critical angle }
  prismindex : real; { Crown BK - 7 glass R.I }
  scandir : boolean; { TRUE for aclock, FALSE for clock }
  slideindex : real; { Chance - Propper slide R.I }
  data,cmd,dmm,psd : integer; { IEEE device channels }
 { Various "housekeeping" procedures & functions follow }
 FUNCTION answer(request : PACKED ARRAY [low..high : integer] OF char) :
boolean;
{ returns true on keying "Y"/"y",false on keying "N"/"n" }
  VAR
   i : integer;
   reply : boolean;
   retcode : integer;
  BEGIN { answer }
   oscli( 'FX201,0');
   { enable keyboard }
   oscli( 'FX15,0');
   { flush all buffers }
   vdu(134);
   i := low;
    WHILE (request[i] <> '?') AND (i <= high) DO BEGIN
     write(request[i]);
     i := i + 1
    END; { while }
   write( ' < Y/N >');
   vdu(13);
    REPEAT
     oscli( 'FX21,0'); { flush keyboard buffer }
     retcode := inkey(32767);
      CASE retcode OF
       &79,&59 : reply := true;
       &6E,&4E : reply := false
      END; { case }
```

```
      OTHERWISE ; { do nothing }
    UNTIL (retcode = &79) OR (retcode = &59) OR (retcode = &6E) OR (retcode = &4E);
   answer := reply
  END; { answer }
PROCEDURE pause(delay : integer);
{ delay some centiseconds }
  BEGIN { pause }
    settime(0);
     REPEAT UNTIL (time = delay)
  END; { pause }
FUNCTION arccos(value : real ) : real;
  BEGIN { arccos }
    arccos := arctan(sqrt(1 - value * value)/value)
  END; { arccos }
FUNCTION arcsin(value : real ) : real;
{ Returns inverse sin of value in radians, principal value only }
  BEGIN { arcsin }
    arcsin := arctan(value/(sqrt(1 - value * value)))
  END; { arcsin }
FUNCTION criticalangle : real;
{ Returns external critical angle of incidence (degrees), being }
{ angle w.r.t. hypoteneuse face normal, for bare prism or }
{ prism + slide, whilst ignoring index - matching fluid, if any. }
{ Requires externally defined prismindex and slideindex }
  CONST
    pi = 3.1416;
  VAR
    thetacrit : real;
  BEGIN { criticalangle }
    criticalangle := (180/pi) * (pi/4 - arcsin(prismindex * sin(pi/4 - arcsin(1/prismindex))))
  END; { criticalangle }
FUNCTION internalangle(angle : real ) : real;
{ Returns internal angle of incidence in degrees given ext. }
{ angle in degrees. Requires externally defined prismindex }
{ and slideindex }
  CONST
    pi = 3.1416;
  VAR
    theta : real;
  BEGIN { internalangle }
    { Convert to radians }
    angle := angle * pi/180;
    theta := pi/4 - arcsin(sin(pi/4 - angle)/prismindex);
     IF slideindex <> 1 THEN theta := arcsin(prismindex * sin(theta)/slideindex);
    internalangle := 180 * theta/pi
  END; { internalangle }
```

```
PROCEDURE page;
{ Clear screen }
 CONST
   clscode = 12;
 BEGIN { page }
  vdu(clscode)
 END; { page }
PROCEDURE rotate(angle : real);
{ Stepper motor driver.Compensates backlash by reversing rotation twice }
{ whenever one reversal asked for }
{ Treats clockwise rotation as − ve, anticlockwise as + ve. }
{ Handles any angle of TYPE REAL }
 CONST
  backlash = 2; { excess steps to cancel backlash }
  minangle = 0.004; { angle per unit step of motor }
 TYPE
  dirrange = −1..1;
  { motor can turn + vely or − vely. 0 used to indicate initialisation }
 VAR
  newdirection : dirrange;
  steps : integer; { steps corresponding to angle }
 FUNCTION olddirection : integer;
 { Returns previous direction 0 if not initialised, −1 for clock, 1 for aclock }
  CONST
   osbyte = &FFF4;
  TYPE
   dirrange = −1..1;
  VAR
   bits : integer;
   olddir : dirrange;
  BEGIN { olddirection }
  { if unconfigured, remedy it }
    IF (code0(osbyte, &96, &62, &00)DIV&10000)MOD&100 <> &FF THEN BEGIN
     oscli( 'FX&97, &62, &FF');
     olddir := 0;
    END; { if }
    ELSE BEGIN
     { already initialised, read old direction }
     bits := code0(osbyte, &96, &60, &00);
     { extract B5 of Y in &PYXA }
     bits := (bits DIV &10000) MOD &100;
     bits := (bits MOD 128) DIV 64;
      IF bits = 1 THEN olddir := 1 ELSE olddir := −1
    END; { else }
   olddirection := olddir
  END; { olddirection }
                                                PROCEDURE turn;
```

```
{ turn stepper motor given no.of steps in either direction }
{ Requires external integer steps }
 VAR
  j : integer;
 BEGIN { turn }
   IF steps > 0 THEN BEGIN
     FOR j := 0 TO steps - 1 DO BEGIN
      oscli( 'FX&97,&60,&C0');
      oscli( 'FX&97,&60,&40')
     END; { for }
   END; { IF steps > 0..... }
   ELSE BEGIN
     FOR j := 0 DOWNTO steps + 1 DO BEGIN
      oscli( 'FX&97,&60,&80');
      oscli( 'FX&97,&60,&00')
     END; { for }
   END; { ELSE.... }
 END; { turn }
BEGIN { rotate }
{ take angle as integer multiple of minium step by dividing it }
{ by angle per unit step }
 steps := trunc(angle/minangle);
  IF steps <> 0 THEN { i.e.if no rotation,do nothing }BEGIN
  { decide which way to turn }IF steps < 0 THEN newdirection := -1 ELSE newdirection :=
1;
    IF olddirection = newdirection THEN turn ELSE BEGIN
     steps := newdirection * (abs(steps) + backlash);
     turn;
     steps := -newdirection * backlash;
     turn
    END; { else }
  END; { if }
END; { rotate }
PROCEDURE tab(x,y : integer);
{ tabulation }
 CONST
   tabcode = 31;
 BEGIN { tab }
  vdu(tabcode,x,y)
 END; { tab }
{ $S 'IEEELIB' }
{ IEEELIB }
{ IEEE procedure and function library follows }
PROCEDURE IEEEb(devno : integer);
{ Equiv. to BASIC's PRINT# < command channel >,"BBC DEVICE NO",< devno > }
 TYPE
```

```
    byte = 0..&FF;
    block = PACKED RECORD
      block : PACKED ARRAY[1..3] OF byte;
      num : integer
    END;
  VAR
    parblk : block;
    retcode : integer;
  BEGIN { IEEEb }
    parblk.block[1] := &04;
    parblk.block[2] := 0;
    parblk.block[3] := &40;
    parblk.num := devno;
    { call OSWORD with A = &80 for IEEEFS commands }
    retcode := code1(&FFF1,&80,parblk)
  END; { IEEEb }
PROCEDURE IEEEc;
{ Equiv. to BASIC's PRINT# < command channel >,"CLEAR" }
  TYPE
    byte = 0..&FF;
    block = PACKED ARRAY[1..3] OF byte;
  VAR
    parblk : block;
    retcode : integer;
  BEGIN { IEEEc }
    parblk[1] := &03;
    parblk[2] := &00;
    parblk[3] := &50;
    { call OSWORD with A = &80 for IEEEFS commands }
    retcode := code1(&FFF1,&80,parblk)
  END; { IEEEc }
PROCEDURE IEEEclose(handle : integer);
{ Equiv. to BASIC's CLOSE# < handle > }
  VAR
    retcode : integer;
  BEGIN { IEEEclose }
    { call OSFILE with A = X = 0, Y = handle to shut file }
    retcode := code0(&FFCE,0,0,handle)
  END; { IEEEclose }
PROCEDURE IEEEe(eos1,eos2 : char);
{ Equiv. to BASIC PRINT# < command channel >,"END; OF STRING",eos1(+eos2) }
  TYPE
    byte = 0..&FF;
    block = PACKED ARRAY[1..5] OF byte;
  VAR
    parblk : block;
    retcode : integer;
```

```
  BEGIN { IEEEe }
    IF eos2 = ' ' THEN parblk[1] := 4 ELSE parblk[1] := 5;
   parblk[2] := 0;
   parblk[3] := &81;
   parblk[4] := ord(eos1);
   parblk[5] := ord(eos2);
   { call OSWORD with A = &80 for IEEEFS commands }
   retcode := code1(&FFF1,&80,parblk)
  END; { IEEEe }
PROCEDURE IEEEg(chan : integer);
{ Equiv. to BASIC's }
{ PRINT# < command channel >,"GO TO LOCAL",< device channel >,"EXECUTE" }
{ with the restriction that only one channel can be dealt with at a time }
  TYPE
   byte = 0..&FF;
   block = PACKED RECORD
     param : PACKED ARRAY[1..3] OF byte;
     channel : integer
   END;
  VAR
   parblk : block;
   retcode : integer;
  BEGIN { IEEEg }
   parblk.param[1] := &04;
   parblk.param[2] := 0;
   parblk.param[3] := &22;
   parblk.channel := chan;
   { call OSWORD with A = &80 for IEEEFS commands }
   retcode := code1(&FFF1,&80,parblk)
  END; { IEEEg }
FUNCTION IEEEinput(channel : integer) : real;
{ Equiv. to BASIC's INPUT# < data channel >,< real > }
{ All input is done in binary by repeated calls to OSBGET with A = X = 0, Y = channel }
  CONST
   len = 255;
  TYPE
   string = PACKED ARRAY[1..len] OF char;
   digits = SET OF &30..&39;
  VAR
   i : integer;
   retcode,nbytes : integer;
   datastr : string;
   data : digits;
  BEGIN { IEEEinput }
   { find data type }
   retcode := code0(&FFD7,&00,&00,channel) MOD &100;
    IF retcode <> 0 THEN writeln( 'not string data type in IEEEinput');
```

```
    { find no. of bytes, exclusive of the following one }
    nbytes := code0(&FFD7,&00,&00,channel) MOD &100;
   { deal w/ leading (terminator) bytes. Provision is made for no terminators }data := [&30..&39];
     REPEAT
      retcode := code0(&FFD7,&00,&00,channel) MOD &100;
      nbytes := nbytes - 1;
     UNTIL (retcode IN data) OR (retcode = &2D) OR (retcode = &2E) OR (retcode =
&2B);
    { input data bytes. retcode already contains the first }
    datastr[nbytes + 1] := chr(retcode);
     FOR i := nbytes DOWNTO 1 DO BEGIN
      retcode := code0(&FFD7,&00,&00,channel) MOD &100;
      datastr[i] := chr(retcode);
     END; { for }
    { convert to real }
    IEEEinput := rval(datastr)
  END; { IEEEinput }
 PROCEDURE IEEEl(channo : integer);
 { Equiv.to BASIC's }
 { PRINT# < command channel >,"LISTEN",< device channel >,"EXECUTE" }
 { with restriction that only one channel can be listened at a time }
  TYPE
   byte = 0..&FF;
   block = PACKED RECORD
    param : PACKED ARRAY[1..3] OF byte;
    channel : integer
   END;
  VAR
   parblk : block;
   retcode : integer;
  BEGIN { IEEEl }
   parblk.param[1] := &04;
   parblk.param[2] := 0;
   parblk.param[3] := &20;
   parblk.channel := channo;
   { call OSWORD with A = &80 for IEEEFS commands }
   retcode := code1(&FFF1,&80,parblk)
  END; { IEEEl }
 PROCEDURE IEEElo;
 { Equiv. to BASIC's PRINT# < command channel >,"LOCAL LOCKOUT" }
  TYPE
   byte = 0..&FF;
   block = PACKED ARRAY[1..3] OF byte;
  VAR
   parblk : block;
   retcode : integer;
  BEGIN { IEEElo }
```

```
    parblk[1] := &03;
    parblk[2] := 0;
    parblk[3] := &61;
    retcode := code1(&FFF1, &80, parblk)
  END; { IEEElo }
FUNCTION IEEEopenin(astring : PACKED ARRAY[low..high : integer] OF char) :
integer;
  { Equiv. to BASIC's < channel no >= OPENIN(filename). }
  { Requires external astring as filename }
  { WARNING : truncates filenames longer than strlen! }
  { This may cause crash in some circumstances }
  CONST
    strlen = 10; { max. string length necessary }
  TYPE
    byte = 0..&FF;
    bytestr = PACKED ARRAY[1..strlen] OF byte;
  VAR
    retcode, i : integer;
    byteline : bytestr;
  BEGIN { IEEEopenin }
    i := 1;
      { convert file name to string of bytes }
      REPEAT
        byteline[i] := ord(astring[low + i - 1]);
        i := i + 1;
      UNTIL (astring[low + i - 1] = ' ') OR (low + i - 1 = high) OR (i - low = strlen - 1);
    { terminator to byte string has to be carriage return = &0D }
    byteline[i] := &0D;
    { pass over to OS. Call OSFIND with A = &C0 to OPENIN a file }
    retcode := (code1(&FFCE, &C0, byteline) MOD &100);
      { check channel has opened }
      IF retcode = 0 THEN writeln( 'This channel cannot be opened!');
    IEEEopenin := retcode
  END; { IEEEopenin }
FUNCTION IEEEp : integer;
{ Equiv. to BASIC PRINT# < command channel >,"PARALLEL POLL REQUEST" }
{ followed by INPUT# < command channel >, < poll response > }
  TYPE
    byte = 0..&FF;
    block = PACKED ARRAY[1..4] OF byte;
  VAR
    parblk : block;
    retcode : integer;
  BEGIN { IEEEp }
    parblk[1] := 3;
    parblk[2] := 4;
    parblk[3] := &02;
```

```
    { call OSWORD with A = &80 for IEEEFS commands }
    retcode := code1(&FFF1, &80, parblk);
    IEEEp := parblk[4]
  END; { IEEEp }
PROCEDURE IEEEparallel_poll_d(channel : integer);
{ Equiv. to BASIC }
{ PRINT# < command channel >."PARALLEL POLL DISABLE", < channel >,"EXECUTE" }
{ with restriction that only one channel can be dealt with at a time }
  TYPE
    byte = 0..&FF;
    block = PACKED ARRAY[1..4] OF byte;
  VAR
    parblk : block;
    retcode : integer;
  BEGIN { IEEEparallel_poll_d }
    parblk[1] := 4;
    parblk[2] := 0;
    parblk[3] := &21;
    parblk[4] := channel;
    { call OSWORD with A = &80 for IEEEFS commands }
    retcode := code1(&FFF1, &80, parblk)
  END; { IEEEparallel_poll_d }
PROCEDURE IEEEparallel_poll_e(channel, message : integer);
{ Equiv. to }
{ BASIC PRINT# < command channel >,"PARALLEL POLL ENABLE", < channel >, < message > }
  TYPE
    byte = 0..&FF;
    block = PACKED ARRAY[1..5] OF byte;
  VAR
    parblk : block;
    retcode : integer;
  BEGIN { IEEEparallel_poll_e }
    parblk[1] := 5;
    parblk[2] := 0;
    parblk[3] := &48;
    parblk[4] := channel;
    parblk[5] := message;
    { call OSWORD with A = &80 for IEEEFS commands }
    retcode := code1(&FFF1, &80, parblk)
  END; { IEEEparallel_poll_e }
PROCEDURE IEEEprint(channel : integer; string : PACKED ARRAY[low..high :
integer] OF char);
{ Equiv. to BASIC's PRINT# < data channel >, < string > }
{ All writing is done in binary by repeated calls to OSBGET with A = type, then }
{ no.of bytes, then bytes; X = 0; Y = channel }
  TYPE
```

```
    byte = 0..&FF;
  VAR
    datum : byte;
    i : integer;
    retcode : integer;
  BEGIN { IEEEprint }
    { Prepare for binary write }
    retcode := code0(&FFD4, &00, &00, channel);
    retcode := code0(&FFD4, high - low + 1, &00, channel);
    { now send data byte by byte }
    FOR i := high DOWNTO low DO BEGIN
      datum := ord(string[i]);
      retcode := code0(&FFD4, datum, &00, channel)
    END;
  END; { IEEEprint }
PROCEDURE IEEEparallel_poll_u;
{ Equiv. to BASIC PRINT# < command channel >,"PARALLEL POLL UNCONFIGURE" }
  TYPE
    byte = 0..&FF;
    block = PACKED ARRAY[1..3] OF byte;
  VAR
    parblk : block;
    retcode : integer;
  BEGIN { IEEEparallel_poll_u }
    parblk[1] := 3;
    parblk[2] := 0;
    parblk[3] := &60;
    { call OSWORD with A = &80 for IEEEFS commands }
    retcode := code1(&FFF1, &80, parblk);
  END; { IEEEparallel_poll_u }
PROCEDURE IEEEr(datachan : integer; VAR byteline : PACKED ARRAY[low..high :
integer] OF integer);
{ Equivalent to BASIC's PRINT# < command channel >,"READ BINARY",< high - low + 1 > }
{ followed by FOR I = low to high : byteline(I) = BGET# < data channel >: NEXT }
  CONST
    osword = &FFF1;
    osbget = &FFD7;
  TYPE
    byte = 0..&FF;
    block = PACKED ARRAY[1..7] OF byte;
  VAR
    parblk : block;
    retcode : integer;
  BEGIN { IEEEr }
    parblk[1] := &07;
    parblk[2] := 0;
    parblk[3] := &14;
```

```
    parblk[4] := (high - low + 1) DIV &1000000;
    parblk[5] := ((high - low + 1) DIV &10000) MOD &100;
    parblk[6] := ((high - low + 1) DIV &100) MOD &100;
    parblk[7] := (high - low + 1) MOD &100;
    retcode := code1(osword, &80, parblk);
    FOR retcode := low TO high DO byteline[retcode] := code0(osbget, &00, &00, datachan) MOD &100
  END; { IEEEr }
PROCEDURE IEEErem;
{ Equiv. to BASIC's PRINT# < command channel >,"REMOTE ENABLE" }
  TYPE
    byte = 0..&FF;
    block = PACKED ARRAY[1..3] OF byte;
  VAR
    parblk : block;
    retcode : integer;
  BEGIN { IEEErem }
    parblk[1] := &03;
    parblk[2] := 0;
    parblk[3] := &70;
    { call OSWORD with A = &80 for IEEEFS commands }
    retcode := code1(&FFF1, &80, parblk)
  END; { IEEErem }
PROCEDURE IEEEremote_d;
{ Equiv. to BASIC's PRINT# < command channel >,"REMOTE DISABLE" }
  TYPE
    byte = 0..&FF;
    block = PACKED ARRAY[1..3] OF byte;
  VAR
    parblk : block;
    retcode : integer;
  BEGIN { IEEEremote_d }
    parblk[1] := &03;
    parblk[2] := 0;
    parblk[3] := &71;
    { call OSWORD with A = &80 for IEEEFS command }
    retcode := code1(&FFF1, &80, parblk)
  END; { IEEEremote_d }
FUNCTION IEEEs : integer;
{ Equiv. to BASIC PRINT#cmd,"STATUS" followed by INPUT#cmd, < status bytes > }
  TYPE
    byte = 0..&FF;
    block = PACKED ARRAY[1..7] OF byte;
    retstr = PACKED ARRAY[1..4] OF char;
  VAR
    parblk : block;
    i : integer;
```

```
    str : retstr;
  BEGIN { IEEEs }
    parblk[1] := &03;
    parblk[2] := &07;
    parblk[3] := &01;
    { call OSWORD with A = &80 for IEEEFS commands }
    i := code1(&FFF1, &80, parblk);
    i := parblk[4];
    i := i + parblk[5] * &100;
    i := i + parblk[6] * &10000;
    IEEEs := i + parblk[7] * &100000
  END; { IEEEs }
FUNCTION IEEEse(instrchan : integer) : integer;
{ Equiv. to BASIC PRINT# < command channel >,"SERIAL POLL",< channel >,1 }
{ as very few devices return more than one serial poll status byte }
  TYPE
    byte = 0..&FF;
    block = PACKED ARRAY[1..6] OF byte;
  VAR
    parblk : block;
    i : integer;
  BEGIN { IEEEse }
    parblk[1] := &05;
    parblk[2] := 6;
    parblk[3] := &44;
    parblk[4] := instrchan;
    parblk[5] := 1;
    { call OSWORD with A = &80 for IEEEFS command }
    i := code1(&FFF1, &80, parblk);
    IEEEse := parblk[6]
  END; { IEEEse }
PROCEDURE IEEEsel(channo : integer);
{ Equiv. to }
{ BASIC's PRINT# < command channel >,"SELECTED DEVICE CLEAR",< channo >,"EXECUTE"
{ with restriction that only one channel can be cleared at a time }
  TYPE
    byte = 0..&FF;
    block = PACKED RECORD
      param : PACKED ARRAY[1..3] OF byte;
      channel : integer
    END;
  VAR
    parblk : block;
    retcode : integer;
  BEGIN { IEEEsel }
    parblk.param[1] := &04;
```

```
    parblk.param[2] := 0;
    parblk.param[3] := &24;
    parblk.channel := channo;
    { call OSWORD with A = &80 for IEEEFS commands }
    retcode := code1(&FFF1,&80,parblk)
  END; { IEEEsel }
PROCEDURE IEEEt(channo : integer);
{ Equiv. to BASIC's PRINT# < command channel >,"TALK",< device channel > }
{ with restrction that only one channel can be talked at a time }
  TYPE
    byte = 0..&FF;
    block = PACKED RECORD
      param : PACKED ARRAY[1..3] OF byte;
      channel : integer;
    END;
  VAR
    parblk : block;
    retcode : integer;
  BEGIN { IEEEt }
    parblk.param[1] := &04;
    parblk.param[2] := 0;
    parblk.param[3] := &41;
    parblk.channel := channo;
    { call OSWORD with A = &80 for IEEEFS commands }
    retcode := code1(&FFF1,&80,parblk)
  END; { IEEEt }
FUNCTION IEEEtest : boolean;
{ Uses OSARGS = &FFDA to return TRUE if IEEEFS current, FALSE otherwise }
  VAR
    retcode : integer;
  BEGIN { IEEEtest }
    retcode := (code0(&FFDA,0,0,0)MOD&100);
      IF retcode = &07 THEN IEEEtest := true ELSE IEEEtest := false
  END; { IEEEtest }
PROCEDURE IEEEtr(nbytes : integer);
{ Equiv. to BASIC's PRINT# < command channel >,"TRANSFER",< nbytes > }
  TYPE
    byte = 0..&FF;
    block = PACKED ARRAY[1..7] OF byte;
  VAR
    parblk : block;
    retcode : integer;
  BEGIN { IEEEtr }
    parblk[1] := &07;
    parblk[2] := &00;
    parblk[3] := &10;
    parblk[4] := nbytes DIV &FFFFFF;
```

```
    parblk[5] := (nbytes DIV &FFFF) MOD &100;
    parblk[6] := (nbytes DIV &FF) MOD &100;
    parblk[7] := nbytes MOD &100;
    { call OSWORD with A = &80 for IEEEFS commands }
    retcode := code1(&FFF1,&80,parblk)
  END; { IEEEtr }
PROCEDURE IEEEu;
{ Equiv. to BASIC's PRINT# < command channel >,"UNTALK" }
  TYPE
    byte = 0..&FF;
    block = PACKED ARRAY[1..3] OF byte;
  VAR
    parblk : block;
    retcode : integer;
  BEGIN { IEEEu }
    parblk[1] := &03;
    parblk[2] := 0;
    parblk[3] := &58;
    { call OSWORD with A = &80 for IEEEFS commands }
    retcode := code1(&FFF1,&80,parblk)
  END; { IEEEu }
PROCEDURE IEEEunl;
{ Equiv. to BASIC's PRINT# < command channel >,"UNLISTEN" }
  TYPE
    byte = 0..&FF;
    block = PACKED ARRAY[1..3] OF byte;
  VAR
    parblk : block;
    retcode : integer;
  BEGIN { IEEEunl }
    parblk[1] := &03;
    parblk[2] := 0;
    parblk[3] := &54;
    { call OSWORD with A = &80 for IEEEFS commands }
    retcode := code1(&FFF1,&80,parblk)
  END; { IEEEunl }
{ Initialisation and any relevant measurement procedures/functions follow }
PROCEDURE IEEEinit;
{ Sets up IEEEFS & BBC }
  TYPE
    str = PACKED ARRAY[1..8] OF char;
  VAR
    cmdstr : str;
  BEGIN { IEEEinit }
    oscli( 'IEEE');
    cmdstr := 'DATA    ';
```

```
    data := IEEEopenin(cmdstr);
    cmdstr := 'COMMAND ';
    cmd := IEEEopenin(cmdstr);
    IEEEb(0);
    IEEEc;
    IEEEe(chr(&0D), ' ');
  END; { IEEEinit }
 PROCEDURE IEEEshut;
 { close down IEEEFS and return to ADFS }
  BEGIN { IEEEshut }
    oscli( 'IEEE');
    IEEEe(chr(&0A), ' ');
    IEEEclose(data);
    IEEEclose(cmd);
    oscli( 'ADFS')
  END; { IEEEshut }
{ $S 'IEEE/5208' }
 { IEEE/5208 }
 { IEEEFS control procedures for Keithley 195A dmm. Requires global definition }
 { of integer data, cmd, dmm and real reading. Also requires external IEEE }
 { procedure library }
 PROCEDURE dmminit;
 { Initialise and configure Keithley 195A dmm }
  TYPE
    str = PACKED ARRAY[1..27] OF char;
  VAR
    cmdstr : str;
    statusword : integer;
  BEGIN { dmminit }
    IEEErem;
    cmdstr := '16                    ';
    dmm := IEEEopenin(cmdstr);
    IEEEsel(dmm);
    IEEElo;
    IEEEu;
    IEEEl(dmm);
    { send command string }
    cmdstr := 'R0XF0XS2XZ0XQ00XB0X       ';
    IEEEprint(data, cmdstr);
    cmdstr := 'G1XT0XY(13)X              ';
    IEEEprint(data, cmdstr);
    IEEEunl;
    IEEEt(dmm);
    IEEEu
  END; { dmminit }
 FUNCTION dmmread : real;
```

```
{ Take a single reading from dmm }
 CONST
  accuracy = 0.001; { s.d. of result }
 VAR
  count, err, mean, sig, sqtot, reading : real;
 BEGIN { dmmread }
    { first ensure IEEEFS active and dmm configured }
    IF NOT(IEEEtest) THEN BEGIN
     IEEEinit;
     dmminit
    END; { if }
  { Pause for dmm to settle down }
  pause(100);
  IEEEt(dmm);
  count := 2;
  reading := IEEEinput(data);
  sqtot := reading * reading;
  mean := reading;
  reading := IEEEinput(data);
  sqtot := sqtot + reading * reading;
  mean := (mean + reading)/count;
    REPEAT
      err := (sqtot - count * mean * mean)/(count + 1);
      reading := IEEEinput(data);
      sqtot := sqtot + reading * reading;
      mean := (mean * count + reading)/(count + 1);
      count := count + 1;
    { iterate until error on mean result < desired s.d. }
    UNTIL sqrt(abs(err/count)) < accuracy;
  IEEEu;
  dmmread := mean
 END; { dmmread }
PROCEDURE dmmshut;
{ shut dmm channel }
 BEGIN { dmmshut }
  IEEEremote_d;
  IEEEg(dmm);
  IEEEclose(dmm)
 END; { dmmshut }
{ IEEEFS control procedures for Brookdeal 5208 psd. }
{ Requires IEEE proc. library }
{ ABSOLUTELY REQUIRES external definition of }
{ integer data, command, psd and a real voltage }
PROCEDURE reopenpsd;
 TYPE
  string = PACKED ARRAY[1..2] OF char;
 VAR
```

```
  str : string;
 BEGIN { reopenpsd }
  str := '5 ';
  psd := IEEEopenin(str);
  IEEElo
 END; { reopenpsd }
FUNCTION psdread(chan : boolean) : real;
{ Read voltage from one of the psd channels }
{ CH1 is taken as TRUE, CH2 as FALSE }
 CONST
  accuracy = 0.0000005; { error of result }
 TYPE
  string = PACKED ARRAY[1..3] OF char;
 VAR
  str : string;
  count, err, mean, sig, sqtot, reading : real;
 FUNCTION voltage(psdreading : real) : real;
 { convert psd 'sensitivity' to a voltage }
  CONST
   psdfsd = 2000;
  TYPE
   str = PACKED ARRAY[1..2] OF char;
  VAR
   cmdstr : str;
   sensitivity : integer;
   reading : real;
  BEGIN { voltage }
   IEEEl(psd);
   cmdstr := 'S';
   IEEEprint(data, cmdstr);
   IEEEt(psd);
   reading := IEEEinput(data);
   IEEEu;
   sensitivity := round(reading);
   { use look - up table for conversion }
    CASE sensitivity OF
     0 : reading := 5;
     1 : reading := 2;
     2 : reading := 1;
     3 : reading := 0.5;
     4 : reading := 0.2;
     5 : reading := 0.1;
     6 : reading := 0.05;
     7 : reading := 0.02;
     8 : reading := 0.01;
     9 : reading := 0.005;
    10 : reading := 0.002;
    11 : reading := 0.001;
```

```
      12 : reading := 0.0005;
      13 : reading := 0.0002;
      14 : reading := 0.0001;
      15 : reading := 0.00005;
      16 : reading := 0.00002;
      17 : reading := 0.00001;
      18 : reading := 0.000005;
      19 : reading := 0.000002;
      20 : reading := 0.000001
    END; { case }
    OTHERWISE; { do nothing }
  { voltage reading = fraction of f.s.d. * f.s.d. in volts }
  voltage := (psdreading/psdfsd) * reading
 END; { voltage }
BEGIN { psdread }
  { If IEEEfs inactive, restart it & open psd channel }
  IF NOT(IEEEtest) THEN BEGIN
    IEEEinit;
    reopenpsd
  END; { IF NOT(IEEE..... }
 { Wait a few seconds to ensure psd settles down }
 pause(400);
 { main body of sampling procedure }
 count := 2;
 IEEEl(psd);
  IF chan THEN str := 'Q1 ' ELSE str := 'Q2 ';
 IEEEprint(data, str);
 IEEEt(psd);
 reading := IEEEinput(data);
 IEEEu;
 reading := voltage(reading);
 sqtot := reading * reading;
 mean := reading;
 IEEEl(psd);
 IEEEprint(data, str);
 IEEEt(psd);
 reading := IEEEinput(data);
 IEEEu;
 reading := voltage(reading);
 sqtot := sqtot + reading * reading;
 mean := (mean + reading)/count;
  REPEAT
    err := (sqtot - count * mean * mean)/(count + 1);
    IEEEl(psd);
    IEEEprint(data, str);
    IEEEt(psd);
    reading := IEEEinput(data);
```

```
      IEEEu;
      reading := voltage(reading);
      sqtot := sqtot + reading * reading;
      mean := (mean * count + reading)/(count + 1);
      count := count + 1;
    { iterate until error on mean reading < desired s.d. }
    UNTIL sqrt(abs(err/count)) < accuracy;
  psdread := mean
 END; { psdread }
PROCEDURE psdinit;
{ Initialise psd }
 CONST
  strlen = 59;
 TYPE
  str = PACKED ARRAY[1..strlen] OF char;
 VAR
  cmdstr : str;
  i : integer;
  Xvolts, Yvolts : real;
 PROCEDURE poll;
  BEGIN { poll }
    REPEAT UNTIL (IEEEse(psd) MOD 2) = 1;
  END; { poll }
 BEGIN { psdinit }
  { lock in on signal and read phase }
  cmdstr := '5                                                    ';
  psd := IEEEopenin(cmdstr);
  IEEEsel(psd);
  pause(500);
  IEEEl(psd);
  cmdstr := 'D 0;M 0;P 2,200;X 0;O 0,0;F 1;J 100,6;T 5,0;S 13;R 0        ';
  IEEEprint(data, cmdstr);
  pause(500);
  IEEEunl;
 END; { psdinit }
PROCEDURE psdshut;
{ shut psd channel }
 BEGIN { psdshut }
  oscli( 'IEEE');
  IEEEremote_d;
  IEEEg(psd);
  IEEEclose(psd);
 END; { psdshut }
{ $S 'MAINBODY' }
{ MAINBODY }
{ Main control procedures follow }
```

```
PROCEDURE locatecriticalangle;
{ Note refractive indices defined globally }
 CONST
  datalen = 1000;
  { Max. number of points permitted in critical angle location scan }
  minangle = 0.032;
  { Minimum angular step in degrees used to find critical angle }
  retcode = &0D; { ASCII value of carriage return }
 TYPE
  datastr = PACKED ARRAY[1..datalen] OF real;
 VAR
  angle : real; { scan angle used to locate critical angle }
  calvolts : datastr; { Use this for locating critical angle }
  i : integer;
  Imax : integer; { Index of array element containing maxgrad }
  keycode : integer;
  maxgrad : real; { highest gradient in critical angle scan }
  npoints : integer; { Number of points in critical angle scan }
  newvolts,oldvolts : real; { dmm readings }
  smooth : datastr; { Smoothed critical angle scan }
 FUNCTION gradient(j : integer) : real;
 { Interpolates gradient between 3 adjacent points of smooth }
 { curve, j being central }
  VAR
   a,b,c : real;
  BEGIN { gradient }
   a := smooth[j - 1];
   b := smooth[j];
   c := smooth[j + 1];
   gradient := j * (a - 2 * b + c) + (-a * (2 * j + 1) + 4 * j * b - c * (2 * j - 1))/2
  END; { gradient }
 BEGIN { locatecriticalangle }
 { Rough location of critical angle & calibration here }
   REPEAT
    page;
     IF answer( 'Default prism index 1.517?          ') THEN BEGIN
      prismindex := 1.517;
      tab(0,1)
     END;
     ELSE BEGIN
      tab(0,1);
      vdu(134);
      write( 'Enter prism refractive index ');
      oscli( 'FX201,0');
      read(prismindex);
      oscli( 'FX201,1')
```

```
      END;
      IF answer( 'Default slide index 1.523?          ') THEN BEGIN
        slideindex := 1.523;
        tab(0,3)
      END;
      ELSE BEGIN
        tab(0,3);
        vdu(134);
        writeln( 'Enter slide refractive index ');
        vdu(134);
        write( '(Unit slide index is taken as no slide)');
        oscli( 'FX201,0');
        read(slideindex);
        oscli( 'FX201,1')
      END;
    UNTIL (prismindex > 1) AND (prismindex < 2) AND (slideindex >= 1) AND (slideindex <
2);
    vdu(134);
    writeln( 'Prism External Critical Angle');
    vdu(134);
    extcritangle := criticalangle;
    writeln( 'w.r.t.back face = ',extcritangle : 5 : 2, ' degrees');
    vdu(134);
    writeln( 'Prism Internal Critical Angle');
    vdu(134);
    writeln( 'w.r.t. back face = ',internalangle(extcritangle) : 5 : 2, ' degrees');
    writeln;
    vdu(134);
    writeln( 'Use the two cursor keys to move');
    vdu(134);
    writeln( 'near to a critical angle');
    vdu(32,130,93,134);
    writeln( 'To move clockwise');
    vdu(32,130,91,134);
    writeln( 'To move counterclockwise');
    vdu(134);
    writeln( ' < RETURN >  to continue');
    oscli( 'FX201,0');
    { define angle now in case diode need not be moved later }
    angle := 0.5;
     REPEAT
      keycode := inkey(1000);
       CASE keycode OF
        136 : BEGIN { caseindex }
              angle := 0.5;
              { turn aclock }
```

```
            rotate(angle)
          END; { caseindex }
        137 : BEGIN { caseindex }
            angle := -0.5;
            { turn clock }
            rotate(angle)
          END; { caseindex }
      END; { case }
      OTHERWISE { do nothing };
    UNTIL (keycode = retcode);
  oscli( 'FX201,1');
  page;
  vdu(134);
    IF answer( 'Locate critical angle precisely?') THEN BEGIN
      { Pick a region covering critical angle }
      page;
      tab(5,12);
      vdu(141);
      vdu(131);
      writeln( 'Locating Critical Angle');
      tab(5,13);
      vdu(141);
      vdu(131);
      writeln( 'Locating Critical Angle');
      npoints := 0;
      newvolts := dmmread;
      oldvolts := newvolts;
      WHILE (datalen > npoints) AND (abs((oldvolts-newvolts)/(oldvolts+newvolts)) <
0.2) DO BEGIN
        oldvolts := newvolts;
        IF angle < 0 THEN angle := 0.5 - angle ELSE angle := -(angle + 0.5);
        rotate(angle);
        npoints := trunc(abs(angle)/minangle);
        newvolts := dmmread
      END; { WHILE (datalen..... }
      IF angle < 0 THEN angle := minangle ELSE angle := -minangle;
      FOR i := 1 TO npoints DO BEGIN
        calvolts[i] := dmmread;
        rotate(angle)
      END; { FOR i := ... }
    writeln;
    writeln;
    { Apply 5 - point smoothing }
    smooth[1] := calvolts[1];
    smooth[2] := calvolts[2];
      FOR i := 3 TO npoints - 2 DO BEGIN
```

```
        smooth[i] := (calvolts[i - 2] + calvolts[i + 2])/16 + (calvolts[i - 1] + calvolts[i + 1])/4 +
6 * calvolts[i]/16
          END; { FOR 1 := 2.... }
        smooth[npoints - 1] := calvolts[npoints - 1];
        smooth[npoints] := calvolts[npoints];
        { Interpolate gradients }
          FOR i := 2 TO npoints - 1 DO BEGIN
            calvolts[i] := gradient(i)
          END; { FOR i := 2 TO npoints.... }
        { Find highest gradient }
        maxgrad := abs(calvolts[2]);
        Imax := 2;
          FOR i := 3 TO npoints - 1 DO BEGIN
            IF abs(calvolts[i]) > maxgrad THEN BEGIN
              maxgrad := abs(calvolts[i]);
              Imax := i
            END; { IF abs... }
          END; { FOR i := 2 TO.... }
        { Return diode to critical angle }
        rotate(-angle * (npoints - Imax));
      { shut down dmm & IEEEfs to return to original state }
      dmmshut;
      IEEEshut
    END; { IF answe.... }
  { Fix direction for later scans. }
  { Ignore possibility that diode may have }
  { been moved to the other side of the laser beam }
  scandir := true
END; { locatecriticalangle }
PROCEDURE scancurve(pock : boolean);
{ This is the business bit that records baselines and gross reflectivities }
CONST
  datalength = 1499;
  minangle = 0.004; { minimum possible external angular interval }
  len = 20;
TYPE
  results = PACKED ARRAY[1..datalength] OF real; { result of one scan }
  string = PACKED ARRAY[1..len] OF char;
VAR
  ACX, ACY : results; { In - phase & quadrature components of Pockels signal }
  acxfile, acyfile : string; { fnames for AC results }
  baseline : boolean; { flag indicating whether to record DC baseline }
  DC : results; { SPR baselines and gross reflectivities }
  dcfile : string; { fname for DC results }
  minstep : real; { smallest angular interval required }
  npoints : integer; { no. of points in scan }
```

```
  offset : real; { difference between critical angle and starting angle }
  retcode : integer; { INKEY code }
  scanrange : real; { region covered by scan }
  startangle : real; { angle at which scan begins }
PROCEDURE setscanparams;
  BEGIN { setscanparams }
    REPEAT
      writeln;
      vdu(134);
      writeln( 'How many degrees should the ');
      vdu(134);
      write( 'scan cover? ');
      readln(scanrange);
      writeln;
      vdu(134);
      writeln( 'What is the angular step in');
      vdu(134);
      writeln( 'degrees between readings? ');
      vdu(134);
      writeln( '(must be a multiple of 0.004)');
      vdu(134);
      readln(minstep);
        IF minstep < 0 THEN minstep := -minstep;
      npoints := trunc(scanrange/minstep);
  UNTIL ((npoints <= datalength) AND (trunc(minstep/minangle) = minstep/minangle))
  END; { setscanparams }
PROCEDURE recordangles;
{ Creates spool file of internal angles of incidence used in scan }
  VAR
    i : integer;
    theta : real;
  BEGIN { recordangles }
    oscli( ' - ADFS - SPOOL angles');
      FOR i := 1 TO npoints DO writeln(internalangle(startangle + i * minstep) : 7 : 4, ',');
    oscli( ' - ADFS - SPOOL');
    page
  END; { recordangles }
PROCEDURE saveresults;
  VAR
    i : integer;
  BEGIN { saveresults }
    oscli(dcfile);
      FOR i := 1 TO npoints DO writeln(DC[i] : 6 : 3);
    oscli( 'SPOOL');
      IF pock THEN BEGIN
        oscli(acxfile);
```

```
      FOR i := 1 TO npoints DO writeln(ACX[i]);
     oscli( 'SPOOL');
     oscli(acyfile);
      FOR i := 1 TO npoints DO writeln(ACY[i]);
     oscli( 'SPOOL')
    END; { IF pock... }
   { oscli commands take system back to ADFS }
   IEEEinit;
   dmminit;
    IF pock THEN reopenpsd
 END; { saveresults }
PROCEDURE getcurve;
 VAR
  i : integer;
 BEGIN { getcurve }
    FOR i := 1 TO npoints DO BEGIN
     DC[i] := dmmread;
      IF pock THEN BEGIN
       ACX[i] := psdread(true);
       ACY[i] := psdread(false)
      END; { IF pock... }
     rotate(minstep)
    END; { FOR i := .... }
    { Take diode back to start position }
    IF minstep < 0 THEN rotate(abs(scanrange)) ELSE rotate(-abs(scanrange));
   saveresults
 END; { getcurve }
PROCEDURE shutdown;
{ Close dmm, psd IEEEFS and reboot }
 BEGIN { shutdown }
   dmmshut;
    IF pock THEN psdshut;
   IEEEshut;
   { reboot totally to free all memory for next run }
   oscli( 'BACK');
   oscli( 'EXEC !BOOT')
 END; { shutdown }
PROCEDURE findSPRmin;
 VAR
   Imin : integer; { i value at which min. reflectivity happens }
   i : integer;
   Rmin : real; { minimum reflectivity }
 BEGIN { findSPRmin }
   page;
   tab(4, 14);
   vdu(141);
```

```
vdu(134);
writeln( 'Finding SPR Minimum');
tab(4,15);
vdu(141);
vdu(142);
writeln( 'Finding SPR Minimum');
{ set angular directions & range }
minstep := 0.128;
scanrange := 11;
npoints := trunc(scanrange/minstep);
{ do crude scan }
 FOR i := 1 TO npoints DO BEGIN
  DC[i] := dmmread;
  rotate(minstep)
 END; { FOR i : ..... }
rotate(-abs(scanrange));
Imin := 1;
Rmin := DC[1];
 FOR i := 1 TO npoints DO BEGIN
    IF DC[i] < Rmin THEN BEGIN
      Rmin := DC[i];
      Imin := i
    END; { IF DC[... }
 END; { FOR i := 1 ..... }
offset := Imin * minstep;
rotate(offset);
startangle := extcritangle + offset;
{ SPR minimum must be within minstep of Imin }
{ so back off more than one step and do detailed scan }
offset := -2 * minstep;
rotate(offset);
startangle := startangle + offset;
{ now spot minimum more accurately, searching over 4 * minstep }
scanrange := 4 * minstep;
minstep := minangle;
npoints := trunc(scanrange/minstep);
 FOR i := 1 TO npoints DO BEGIN
  DC[i] := dmmread;
  rotate(minstep)
 END; { FOR i := ... }
rotate(-abs(scanrange));
Rmin := DC[1];
Imin := 1;
 FOR i := 1 TO npoints DO BEGIN
    IF DC[i] < Rmin THEN BEGIN
      Rmin := DC[i];
```

```
        Imin := i
      END; { IF DC[... }
    END; { FOR... }
  offset := Imin * minangle;
  rotate(offset);
  startangle := startangle + offset;
  offset := 0;
  { adjust offset accordingly }
  { and set psd phase to maximise quadrature component }
  { then shut down all IEEE gear and re - initialise later }
  psdinit;
  psdshut;
  dmmshut;
  IEEEshut
END; { findSPRmin }
BEGIN { scancurve }
 { Arrange scan start points and parameters }
 REPEAT
  page;
  tab(7,3);
  vdu(141);
  vdu(131);
  writeln( 'Available options : -');
  tab(7,4);
  vdu(141);
  vdu(131);
  writeln( 'Available options : -');
  tab(0,6);
  vdu(134);
  writeln( '1 - scan from the present location');
  writeln;
  vdu(134);
  writeln( '2 - offset the diode some angle');
  writeln;
  vdu(134);
  writeln( '3 - scan the region of the SPR minimum');
  vdu(134);
  writeln( '(baseline cannot be recorded');
  vdu(134);
  writeln( 'with this option)');
  writeln;
  vdu(134);
  writeln( '4 - Exit');
  writeln;
  retcode := inkey(500);
  page;
```

```
CASE retcode OF
 &21,&31 : BEGIN { caseindex }
          writeln;
          vdu(134);
         IF answer( 'record baseline?') THEN baseline := true ELSE baseline := false;
          writeln;
          setscanparams;
          startangle := extcritangle;
          { Record angles for scan }
          recordangles;
          IEEEinit;
          dmminit;
           IF pock THEN psdinit;
           { record baseline if required }
           IF baseline THEN BEGIN
            page;
            tab(6,12);
            vdu(133);
            vdu(141);
            writeln( 'Taking Baseline');
            tab(6,13);
            vdu(130);
            vdu(141);
            writeln( 'Taking Baseline');
            dcfile := ' - ADFS - SPOOL br      ';
            acxfile := ' - ADFS - SPOOL acxbr   ';
            acyfile := ' - ADFS - SPOOL acybr   ';
            getcurve
           END; { IF baseline.... }
          { Record total reflectivities }
          page;
          vdu(134);
          writeln( 'Continue to take gross');
          vdu(134);
          writeln( 'reflectivity curves');
           REPEAT UNTIL answer( '? ');
          dcfile := ' - ADFS - SPOOL tr      ';
          acxfile := ' - ADFS - SPOOL acxtr   ';
          acyfile := ' - ADFS - SPOOL acytr   ';
          page;
          tab(6,12);
          vdu(133);
          vdu(141);
          writeln( 'Taking gross curves');
          tab(6,13);
          vdu(130);
```

```
        vdu(141);
        writeln( 'Taking gross curves');
        getcurve
      END; { caseindex }
&22,&32 : BEGIN { caseindex }
        writeln;
        vdu(134);
        writeln( 'How many degrees off');
        vdu(134);
        writeln( 'the critical angle ?');
        readln(offset);
        { Turn diode }
        rotate(offset);
        setscanparams;
        writeln;
        vdu(134);
      IF answer( 'record baseline?') THEN baseline := true ELSE baseline := false;
        { record angles used for scan }
        startangle := extcritangle + offset;
        recordangles;
        { Record baseline if required, then do scan }
        IEEEinit;
        dmminit;
          IF pock THEN psdinit;
          { record baseline if required }
          IF baseline THEN BEGIN
            page;
            tab(6,12);
            vdu(133);
            vdu(141);
            writeln( 'Taking Baseline');
            tab(6,13);
            vdu(130);
            vdu(141);
            writeln( 'Taking Baseline');
            dcfile := ' - ADFS - SPOOL br     ';
            acxfile := ' - ADFS - SPOOL acxbr  ';
            acyfile := ' - ADFS - SPOOL acybr  ';
            getcurve
          END; { IF baseline.... }
        { record total reflectivities }
        page;
        vdu(134);
        writeln( 'Continue to take gross');
        vdu(134);
        writeln( 'reflectivity curves');
```

```
        REPEAT UNTIL answer( '? ');
        dcfile := ' – ADFS – SPOOL tr     ';
        acxfile := ' – ADFS – SPOOL acxtr  ';
        acyfile := ' – ADFS – SPOOL acytr  ';
        page;
        tab(6,12);
        vdu(133);
        vdu(141);
        writeln( 'Taking gross curves');
        tab(6,13);
        vdu(130);
        vdu(141);
        writeln( 'Taking gross curves');
        getcurve
      END; { caseindex }
&23,&33 : BEGIN { caseindex }
        { find SPR minimum & reset psd if Pockels scan }
        findSPRmin;
        { Allow user to adjust air gap by hand }
        REPEAT
          page;
          tab(4,14);
          vdu(134);
          vdu(141);
          writeln( 'Adjust air gap by hand');
          tab(4,15);
          vdu(134);
          vdu(141);
          writeln( 'Adjust air gap by hand');
          tab(6,18);
        UNTIL answer( 'Continue?');
        { back off a few degrees }
        offset := -2;
        startangle := startangle + offset;
        rotate(offset);
        setscanparams;
        { record angles of scan }
        recordangles;
        { Scan. Baseline cannot be recorded with this option }
        IEEEinit;
        dmminit;
        IF pock THEN reopenpsd;
        dcfile := ' – ADFS – SPOOL tr     ';
        acxfile := ' – ADFS – SPOOL acxtr  ';
        acyfile := ' – ADFS – SPOOL acytr  ';
        page;
```

```
            tab(6,12);
            vdu(133);
            vdu(141);
            writeln( 'Taking gross curves');
            tab(6,13);
            vdu(130);
            vdu(141);
            writeln( 'Taking gross curves');
            getcurve
          END; { caseindex }
    &24,&34 : shutdown
  END; { CASE retcode..... }
  OTHERWISE retcode := &0D;
 UNTIL retcode <> &0D
END; { scancurve }
PROCEDURE MainMenu;
{ Choose from all rig options }
VAR
 pock : boolean; { flag as to whether to do Pockels scan }
 retcode : integer;
 str : string;
 PROCEDURE helpuser(astring : string);
 { Ensure user knows what's going on by presenting help files }
  PROCEDURE selectdir;
  { User may choose the directory containing results files }
   CONST
    strlen = 50;
   TYPE
    string = PACKED ARRAY[1..strlen] OF char;
   VAR
    astr : string;
    i : 1..strlen;
   BEGIN { selectdir }
    astr := 'DIR :                                    ';
    page;
    vdu(134);
    writeln( 'Enter directory for result files');
    vdu(134);
    writeln( '(include requisite drive)');
    vdu(134);
    i := 6;
     WHILE NOT(eoln(input)) AND (i <= strlen) DO BEGIN
      astr[i] := input ↑;
      get(input);
      i := i + 1
     END; { WHILE NOT(eol..... }
    oscli(astr);
```

```
    END; { selectdir }
  BEGIN { helpuser }
  { Ensure user knows what's going on }
   page;
   tab(0,13);
    IF NOT(answer( 'Are you familiar with this rig?      )) THEN
     BEGIN
      page;
      tab(7,24);
      vdu(136);
      vdu(133);
      write( ' < SHIFT >  to continue');
      vdu(28,0,22,39,0);
      vdu(14);
      oscli(astring);
      vdu(15);
      vdu(28,0,24,39,24);
      page;
      vdu(136);
       IF answer( 'Hard copy?                    ') THEN
        BEGIN
        { print notes }
         vdu(28,0,24,39,0);
         page;
         vdu(2);
         oscli(astring);
         vdu(3)
        END; { if }
     END; { if }
    selectdir;
    vdu(28,0,24,39,0)
  END; { helpuser }
BEGIN { MainMenu }
 mode(7);
 oscli( 'ADFS');
 vdu(23,1,0,0,0,0,0,0,0,0); { cursor off }
 oscli( 'FX4,1'); { disable cursor editing & assign ASCII codes }
 tab(8,2);
 vdu(141,131);
 write( 'Main Menu');
 tab(8,3);
 vdu(141,131);
 writeln( 'Main Menu');
 writeln;
 vdu(134);
```

```
writeln( '1 - Surface Plasmon Resonance');
writeln;
vdu(134);
writeln( '2 - Pockels Spectroscopy');
writeln;
oscli( 'FX21,0'); { flush keyboard buffer }
 REPEAT
  retcode := &0D;
  retcode := inkey(100);
   CASE retcode OF
    &21,&31 : BEGIN { caseindex }
              str := '-ADFS-TYPE:0.$.HELP.SPRcurve        ';
              helpuser(str);
              locatecriticalangle;
              pock := false;
              scancurve(pock);
              MainMenu
             END; { caseindex }
    &32,&22 : BEGIN { caseindex }
              str := '-ADFS-TYPE:0.$.HELP.Pockels         ';
              helpuser(str);
              locatecriticalangle;
              pock := true;
              scancurve(pock);
              MainMenu
             END; { caseindex }
   END; { case }
   OTHERWISE retcode := &0D;
 UNTIL retcode <> &0D;
END; { mainmenu }
BEGIN { Autorig }
 MainMenu
END. { Autorig }
```

Appendix D

Publications

. Phys. D: Appl. Phys. 22 (1989) 1608–1612. Printed in the UK

Functionalised diarylalkynes: a new class of Langmuir–Blodgett film materials for non-linear optics†

J Tsibouklis‡§, J P Cresswell‡, N Kalita‡, C Pearson‡, P J Maddaford§, H Ancelin§, J Yarwood§, M J Goodwin‖, N Carr‖, W J Feast§ and M C Petty‡

‡ Molecular Electronics Research Group, School of Engineering and Applied Science, University of Durham, Science Laboratories, South Road, Durham DH1 3LE, UK
§ Department of Chemistry, University of Durham, Science Laboratories, South Road, Durham DH1 3LE, UK
‖ Plessey Research (Caswell) Ltd, Allen Clark Research Centre, Caswell, Towcester, Northants NN12 8EQ, UK

Received 2 June 1989

Abstract. A number of novel, functionalised, diarylalkynes have been prepared which are capable of forming non-centrosymmetric Langmuir–Blodgett films by Z-type deposition. The non-linear optical behaviour of these layers has been investigated using both second-harmonic generation and surface plasmon resonance techniques.

1. Introduction

The basic requirements for an organic material to exhibit significant second-order non-linear optical (NLO) behaviour are now well understood. In general NLO materials are comprised of molecules that possess a large difference in dipole moment between their ground and excited states and which are organised in a non-centrosymmetric manner. A number of approaches have been tried in attempts to control the molecular packing in NLO materials. Although, in principle, one can change the packing properties by making subtle modifications on the molecule, the problem of obtaining a crystal with a predefined structure from a specifically designed organic molecule has yet to be solved.

The Langmuir–Blodgett (LB) technique represents one of the most elegant methods available for 'engineering' thin organic films. However, the most common, Y-type, deposition mode results in centrosymmetric packing of the molecules. In previous work, Girling *et al* (1985a, b, c) have overcome this problem by alternating layers of organic dyes with optically inert fatty acids. Subsequently, Neal *et al* (1986) reported the fabrication of multilayer arrays containing two 'active' NLO components. Nevertheless, the construction of these superlattices is time consuming and requires specialised equipment. An alternative approach is to find a single LB NLO material that readily deposits in the non-centrosymmetric X or Z-type modes. In contrast to Y-type deposition, these modes are not very common and can lead to films of poor quality. However, a number of workers have reported some progress using the method (Allen *et al* 1987, Kowel *et al* 1987).

In this work we report some preliminary studies of the LB film formation and the NLO properties of a class of functionalised diarylalkynes. Z-type deposition is observed for a number of these compounds.

2. Experimental details

2.1. Synthesis

1-(4′-Pyridyl)-2-phenylethyne and 1-(4′-Pyridyl)-2-(4′-methoxyphenyl)ethyne were synthesised from the corresponding phenyl- or 4-methoxyphenylethynes (Allen and Cook 1963) using a method analogous to that described by Takahashi (1980) for the synthesis of tolans, see below.

Bis(triphenylphosphine)palladium(II) chloride (0.35 g, 0.005 mol) was added to a mixture of 4-bromopyridine hydrochloride (9.7 g, 0.05 mol) and phenylethyne (6 g, 0.06 mol) suspended in diethyl-

† Based on work presented at a Meeting on Molecular Electronics organised by The Dielectrics Society and The Molecular Crystals Discussion Group, held at The University College of Wales, Bangor, UK, on 3–5 April 1989.

0022-3727/89/111608 + 05 $02.50

MULTILAYER ASSEMBLIES FOR NON-LINEAR OPTICS

D. B. Neal[a], N. Kalita, C. Pearson, M. C. Petty, J. P. Lloyd and G. G. Roberts[b]
Molecular Electronics Research Group, School of Engineering and Applied Science, University of Durham, Durham, DH1 3LE, U.K.
M. M. Ahmad[c] and W. J. Feast
Department of Chemistry, University of Durham, Durham, DH1 3LE, U.K.

ABSTRACT

Langmuir-Blodgett films of hemicyanine and amidonitrostilbene derivatives which are of interest for non-linear optical applications have been investigated. The optical absorption spectra of multilayers of the two dyes and of alternate-layer films are reported. Surface plasmon resonance has also been used to study the linear and non-linear optical properties of these films.

INTRODUCTION

The possibility of exploiting Langmuir-Blodgett (LB) multilayer assemblies for non-linear optical applications is currently receiving considerable attention [1]. In the case of second-order non-linear effects, a large number of materials have already been investigated. These include long-chain dye derivatives based on merocyanine [2], hemicyanine [3,4], nitrostilbene [5] and azobenzene [6]. Some of the chromophores of such systems have been incorporated into pre-formed polymers; these can also be deposited by the LB technique [7,8]. The non-linearities of all these materials are associated with the hyperpolarizabilities of the constituent molecules, which invariably consist of donor and acceptor groups separated by a conjugated electron system. However, in order for the LB film to exhibit second order non-linear optical effects, the individual molecules must be deposited in a non-centrosymmetric manner.One way of achieving this is to

---

[a] current address: Department of Physical Sciences, Trent Polytechnic, Nottingham, NG11 8NS, U.K.
[b] current address: Department of Engineering Science, University of Oxford, Oxford, OX1 3PJ, U.K.
[c] current address: BP Research Centre, Sunbury-on-Thames, Middlesex, TW16 7LN, U.K.

0379-6779/89/$3.50

build up an alternating-layer structure with two different types of materials. Recent developments in LB deposition equipment now make this relatively straightforward [9,10]. An active dye layer may be alternated with an inert "spacer" layer (e.g. a long chain fatty acid) [2]. Alternatively, two "active" dye layers, chosen so that their individual molecular hyperpolarizabilities are additive, may be alternated [11].

We have previously discussed the properties of a multilayer system in which a long-chain hemicyanine dye is alternated with an amidonitrostilbene derivative [11,12]. It was interesting to note that the non-linear response of one bilayer of this structure was found to be greater than that expected from the simple addition of the contributions arising from the individual (separated) monolayers. Another important fact to arise from our studies was that the non-linear response of the hemicyanine was considerably enhanced if the dye was diluted with a fatty acid [12,13].

In this paper we present some further data for LB layers of the hemicyanine and amidonitrostilbene systems. We concentrate on the optical absorption spectra of various types of multilayers and we also discuss the use of the technique of surface plasmon resonance (SPR) to investigate both the linear and non-linear optical properties of the thin films.

EXPERIMENTAL

Details concerning the LB deposition of the dye materials have been given previously and will not be repeated here [5, 11-13]. For optical absorption work, the substrates used were either spectrosil B vitreous silica (for measurements on weakly absorbing films to 180 nm) or Corning 7059 glass (where measurements below 340 nm were not required, or to 250 nm for films with absorbance > 0.1). The optical absorption spectra were recorded in transmission using a Cary 2300 spectrophotometer.

Surface plasmon resonance studies were undertaken using a custom built experimental system based on the Kretschmann configuration [14]. For this work, the LB films were deposited onto glass microscope slides that had previously been coated with a 50 nm silver layer by vacuum evaporation. Surface plasma waves were excited at the silver/air or silver/LB film interface by directing a p-polarized laser beam (1mW, HeNe, 632.8 nm) onto the back surface of the silver film. Neutral density filters were used to reduce the laser power so as to avoid local heating effects in the sample.

RESULTS AND DISCUSSION

Optical absorption studies

Optical absorption spectra for the nitrostilbene and hemicyanine dyes, in both solution and LB film form, are shown in figure 1; the molecular structures of the two materials are given as insets in the respective diagrams. In the case of the nitrostilbene material (figure 1(a)), the absorption spectrum for the multilayer is very similar to that of the solution. The effect of using a different (non-polar) solvent is also found to be quite small; the details of this are given elsewhere [15]. In contrast, the data for the hemicyanine dye (figure 1(b)) reveal a marked difference between the LB film and solution spectra.

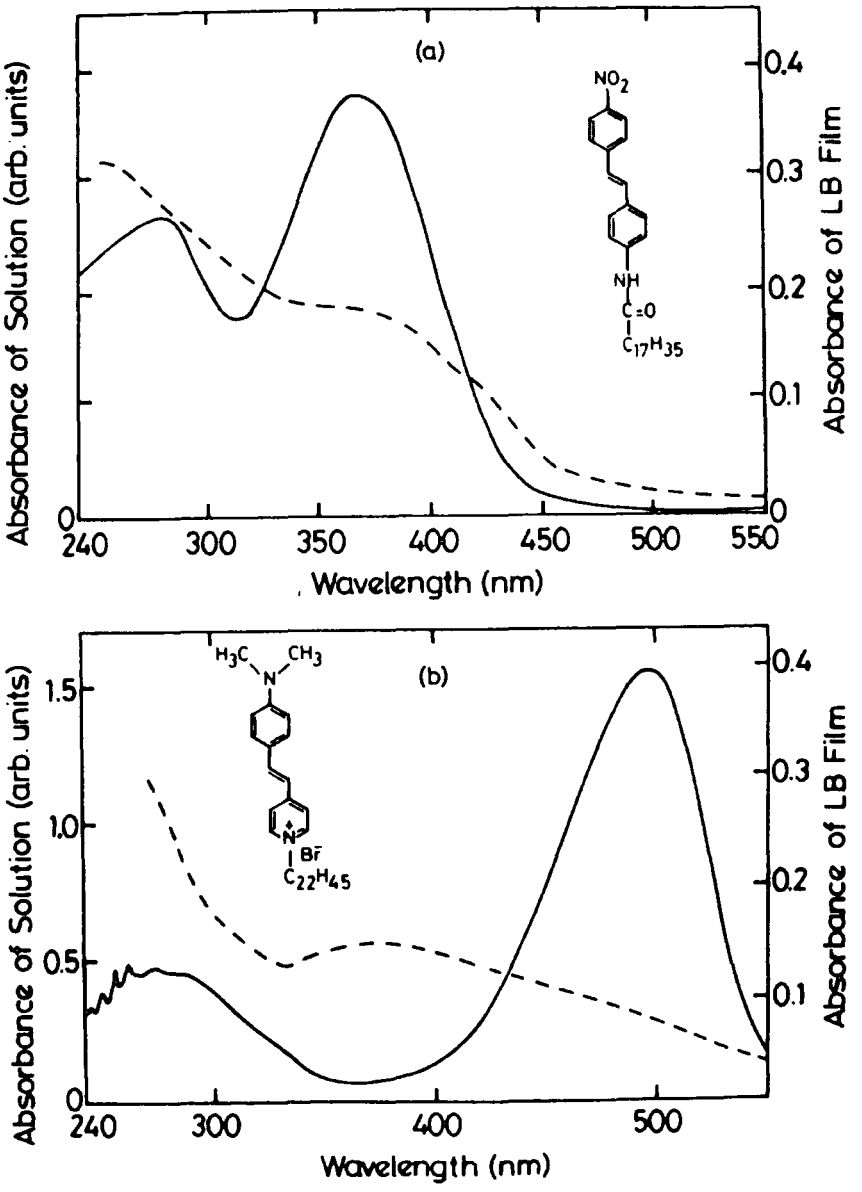

Figure 1. U.V/visible absorption spectra for (a) nitrostilbene and (b) hemicyanine dyes in chloroform (solid line) (approx. conc. $\sim 10^{-5}$ M) and in LB film form (broken line). Insets show molecular structure. For (a) LB film thickness = 60 layers; for (b) 36 layers.

The first absorption band is broadened and considerably blue-shifted in the multilayer relative to the solution. This is possibly the result of the formation of aggregates in the LB film structure [15,16]. Indeed, if the monolayer is diluted with a long chain fatty acid, then the absorption band moves back towards that observed for the solution spectrum [15,16]. The mixed hemicyanine/fatty acid system now exhibits significant absorption at 532nm, the second-harmonic wavelength resulting from an incident 1.064 μm Nd:YAG laser. It has been suggested that this effect is directly responsible for the enhanced second-order non-linear behaviour for these mixed layers [15,16]. This phenomenon is not, however, seen in the case of the nitrostilbene material : the absorption spectra of the diluted monolayers all possess the same profile as the pure material and the enhanced non-linearity is not observed [15].

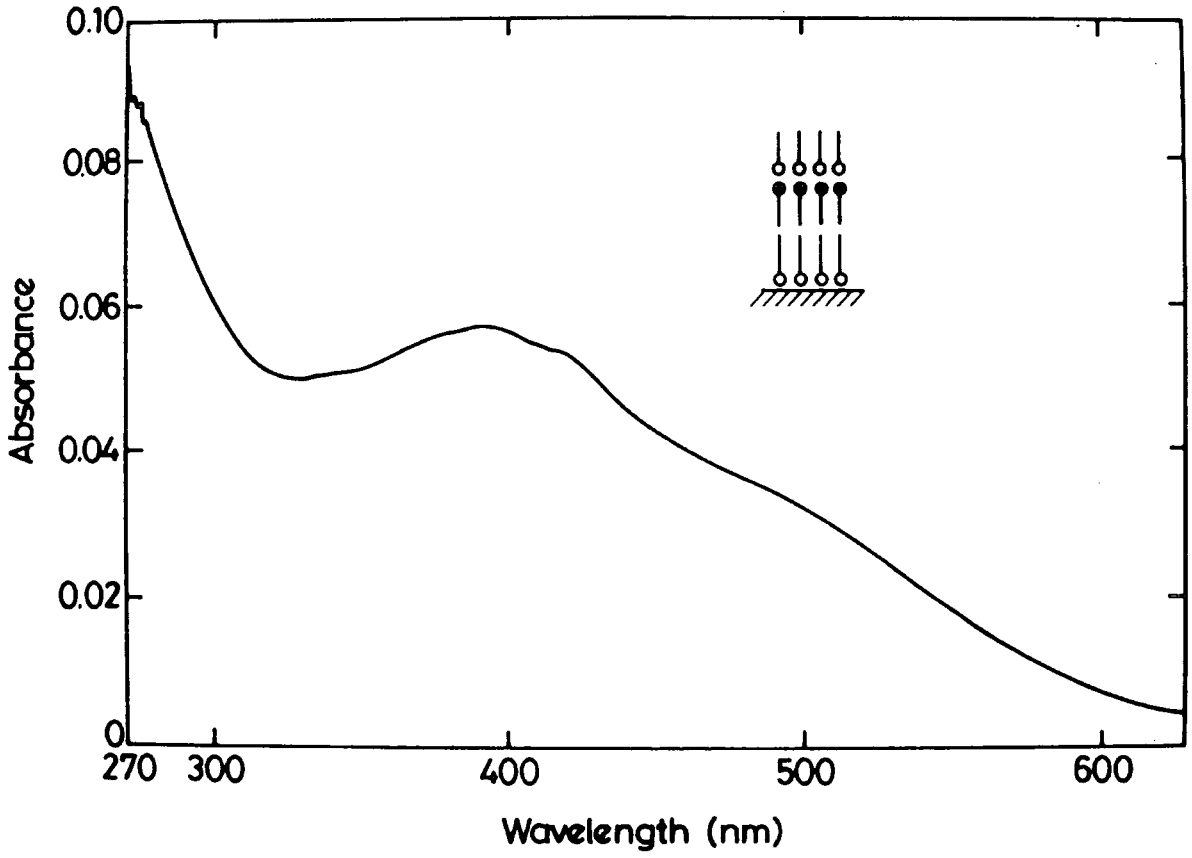

Figure 2. U.V/visible absorption spectrum of alternating hemicyanine (11-layers)/ nitrostilbene (10-layers) structure.

The hemicyanine/nitrostilbene alternate-layer structure is particularly important from the non-linear optical viewpoint [11,12]. Figure 2 shows the optical absorption spectrum of a sample consisting of 11-layers of the hemicyanine alternated with 10-layers of the nitrostilbene (the hemicyanine was deposited first on withdrawal of the substrate through the subphase). The spectrum is clearly not the result of a simple weighted addition of the spectra

of multilayers of the nitrostilbene (figure 1(a)) and hemicyanine (figure 1(b)). This can be seen from the fact that the first absorption band of the hemicyanine is at 376nm, whilst the first and second bands of the nitrostilbene give rise to an absorbance which increases with decreasing wavelength, over the entire range 500-200nm; thus any linear combination of the two will produce a first absorption peak below 376nm, whereas the alternate-layer system displays a distinct peak at 393nm. A possible explanation for this phenomenon may lie in the opposite direction of the first excited state dipoles (with respect to the hydrocarbon tails) for the nitrostilbene compared to the hemicyanine. Although the direction of charge transfer is unchanged in going from the ground to the first excited state in either molecule, the degree of this transfer is much greater in the excited state. Thus, when the molecules are placed head to head in the multilayer structure, the positive end of the hemicyanine will be adjacent to the negative end of the nitrostilbene. In this situation, the excited state of either molecule will be more stable than in a conventional Y-type LB multilayer in which the ends of adjacent dipoles possess the same polarity. This stabilization of the excited states is likely to produce a bathochromic shift in the first absorption bands of both molecules, in accordance with the observed peak at 393nm in figure 2.

Surface plasmon resonance

SPR curves obtained from a stepped-thickness LB structure of the nitrostilbene material are presented in figure 3; the fatty acid layer (22-tricosenoic acid) between the nitrostilbene and the silver was simply used to improve the deposition of the dye layer. The almost constant depth of resonance with increasing film thickness indicates that the dye layer is not highly scattering or absorbing at the wavelength of the laser (632.8nm); this was expected from the absorption spectrum shown in figure 1(a). The data shown in figure 3 may be fitted using a computer model in order to obtain the refractive index of the amidonitrostilbene, given the film thickness. We have used ellipsometry to measure the latter parameter, obtaining a value of 3.2 nm per monolayer. Treating the layers as homogeneous, non-absorbing, isotropic media (the data fit is not usually improved with a uniaxial model [17]) we calculate a value of 1.6 ± 0.05 for the real part of the refractive index [15], which agrees with the ellipsometric figure (1.55±0.05). SPR curves were also measured using a stepped thickness LB film structure of the hemicyanine dye. Unfortunately the curves tended to be rather irreproducible (especially for larger numbers of monolayers) reflecting the poorer deposition quality observed in multilayers of pure hemicyanine, and no attempt was made to analyse these data in detail. In contrast, we note that the deposition quality of the hemicyanine when deposited in alternate layers (bilayer form) with the nitrostilbene is excellent.

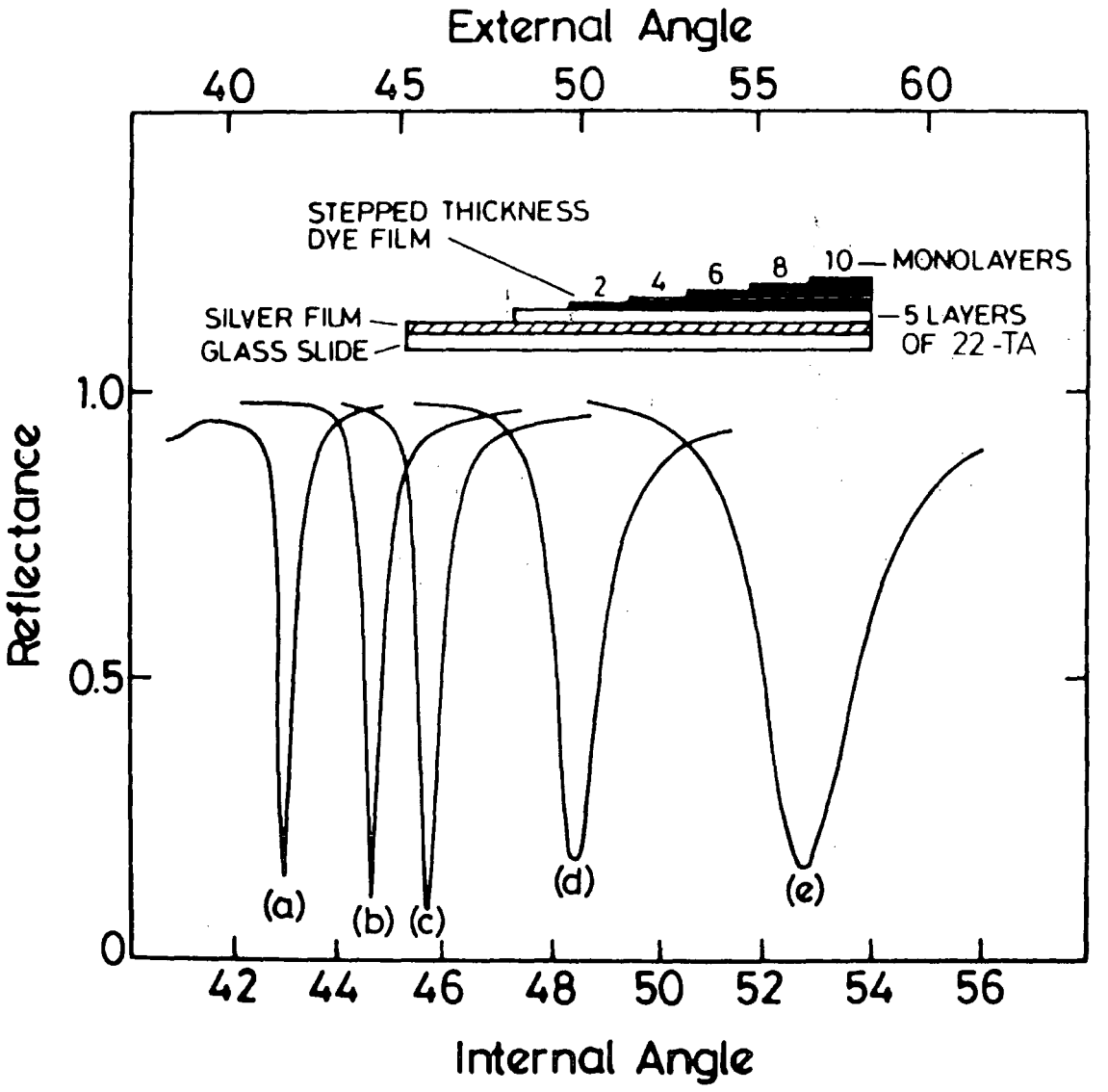

Figure 3. SPR curves of a silvered slide (a) with a fatty acid overcoating (b) and subsequent further overcoatings of 2, 6 and 10 layers of nitrostilbene ((c), (d) and (e)). Inset shows schematic diagram of sample.

The SPR configuration may also be used to directly measure the second-order non-linear susceptibility of the LB layer. This is accomplished by applying an electric field to the organic layer and simultaneously monitoring the change in reflectivity that is a result of the Pockels effect [18,19]. Figure 4 shows the SPR curve and the angular dependence of the differential reflectance for a film consisting of six alternate-layers of pure hemicyanine and pure nitrostilbene. The differential reflectance was measured using a potential of 25V (peak value, 4.8 KHz) applied across a nominal 3μm air gap. As expected, the curve takes the form of the derivative of the SPR curve. The magnitude of this signal was found to scale approximately linearly with applied field. Preliminary measurements have

also been undertaken using bilayers where the hemicyanine was diluted with a fatty acid (i.e. alternate layers of nitostilbene and diluted hemicyanine). No enhancement of the signal was observed in this case. This observation is consistent with the hypothesis (mentioned earlier) that the enhanced second-order non-linear behaviour of diluted films is a resonant effect due to absorption at the wavelength of interest. In the case of the SPR measurements, the films do not absorb at the laser wavelength of 632.8 nm (see Figure 2) and hence no resonant enhancement is expected.

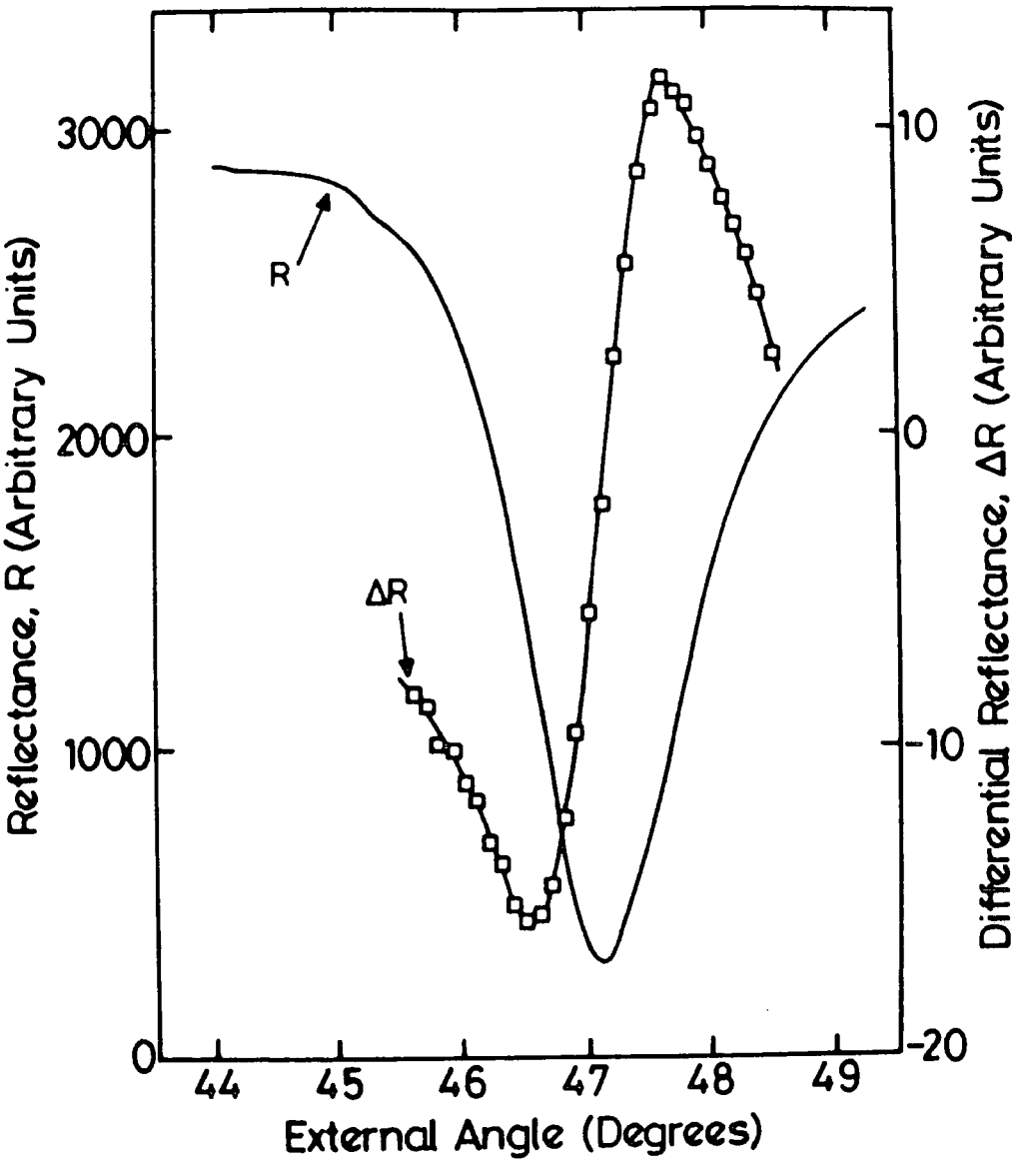

Figure 4. Angular dependence of the reflectance (R) and the differential reflectance (ΔR) of a 3-bilayer film of pure hemicyanine and pure nitrostilbene

CONCLUSIONS

LB films of hemicyanine and nitrostilbene derivatives have been investigated in both multilayer and alternate-layer structures. Shifts have been observed in the optical absorption spectra of hemicyanine multilayers relative to the solution absorption which may be due to aggregate formation in the films. The absorption spectra of alternate layer films were found not to be the result of a simple weighted addition of the spectra of the individual multilayers. This has been explained in terms of the stabilisation of excited state dipoles due to the film structure. Finally, surface plasmon resonance measurements have been used to study the linear and non-linear optical properties of some films. In contrast to previous reports, at the wavelength used, no enhancement of the non-linear optical properties of alternate layer structures was observed on dilution of the hemicyanine with a fatty acid.

ACKNOWLEDGEMENTS

We wish to thank Mr. G. Briody for undertaking the ellipsometric studies. DBN and NK wish to thank the SERC and Plessey Ltd. for financial support. Part of this work was funded under a Joint Opto-Electronic Research Scheme (JOERS).

REFERENCES

1 J. Zyss, J. Mol. Electron., 1 (1985) 25.

2 I. R. Girling, P. V. Kolinsky, N. A. Cade, J. D. Earls and I. R. Peterson, Optics Commun. 1 (1985) 289.

3 G. H. Cross, I. R. Peterson, I. R. Girling, N. A. Cade, M. J. Goodwin, N. Carr, R. S. Sethi, R. Marsden, G. W. Gray, D. Lacey, A. M. McRoberts, R. M. Scrowston and K. J. Toyne, Thin Solid Films, 156 (1988) 39.

4 L. M. Hayden and S. T. Kowel, Opt. Commun., 61 (1987) 351.

5 M. M. Ahmad, W. J. Feast, D. B. Neal, M. C. Petty and G. G. Roberts, J. Mol. Electron, 2 (1986) 129.

6 S. Allen, R. A. Hann, S. K. Gupta, P. F. Gordon, B. D. Bothwell, I. Ledoux, P. Vidakovic, J. Zyss, P. Robin, E. Chastaing and J. C. Dubois, SPIE 1986, 682, 97.

7 R. H. Tredgold, M. C. J. Young, P. Hodge and E. Khoshdel, Thin Solid Films, 151 (1987) 441.

8 N. Carr, M. J. Goodwin, A. M. McRoberts, G. W. Gray, R. Marsden and R. M. Scrowston, Makromol. Chem., Rapid Commun., 8 (1987) 487.

9 B. Holcroft, M. C. Petty, G. G. Roberts and G. J. Russell, Thin Solid Films, 134 (1985) 83.

10 M. F. Daniel, J. C. Dolphin, A. J. Grant, K. E. N. Kerr and G. W. Smith, Thin Solid Films 133 (1985) 235.

11 D. B. Neal, M. C. Petty, G. G. Roberts, M. M. Ahmad, W. J. Feast, I. R. Girling, N. A. Cade, P. V. Kolinsky and I. R. Peterson, Elec. Lett, 22 (1986) 460.

12 D. B. Neal, M. C. Petty, G. G. Roberts, M. M. Ahmad, W. J. Feast, I. R. Girling, N. A. Cade, P. V. Kolinsky and I. R. Peterson, Proc. 6th Int. Symp. Applic. Ferroelectrics, IEEE, New York (1986) 89.

13 I. R. Girling, N. A. Cade, P. V. Kolinsky, R. J. Jones, I. R. Peterson, M. M. Ahmad, D. B. Neal, M. C. Petty and G. G. Roberts, J. Opt. Soc. Am. B, 4 (1987) 950.

14 E. Kretzchmann and H. Raether, Z. Naturforsch, A23 (1968) 2135.

15 D. B. Neal, Ph.D. thesis, University of Durham, U.K. (1987).

16 J. S. Schildkraut, T. L. Penner, C. S. Willand and A. Ulman, Optics Letts., 13 (1988) 134.

17 I. Pockrand, J. D. Swalen, J. G. Gordon II and M. R. Philpott, Surface Science, 74 (1977) 237.

18 G. H. Cross, I. R. Girling, I. R. Peterson and N. A. Cade, Elec.Lett., 22 (1986) 1111.

19 G. H. Cross, I. R. Peterson, I. R. Girling, N. A. Cade, M. J. Goodwin, N. Carr, R. S. Sethi, R. Marsden, G. W. Gray, D. Lacey, A. M. McRoberts, R. M. Scrowston and K. J. Toyne, Thin Solid Films, 156 (1988) 39.

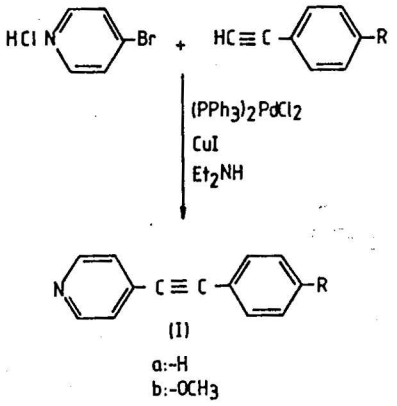

amine (100 cm^3) in a 250 cm^3 two-necked flask. The mixture was stirred (magnetic follower) at room temperature and maintained under an atmosphere of dry nitrogen. After 30 min, copper(I) iodide (50 mg, 0.0004 mol) was added and the stirring continued for 60 h. Diethylamine was removed by rotary evaporation, water (50 cm^3) was added to the residue and the resulting mixture was extracted with diethyl ether (3 × 50 cm^3). Residual palladium salts were removed by passage of the dried (magnesium sulphate) ether extract through a column of alumina (4 cm × 2 cm^2; neutral, activity I). Evaporation of the ether gave the crude product which was purified by sublimation (90 °C/4 × 10^{-2} mbar) to give the following.

1-(4'-Pyridyl)-2-phenylethyne (Ia), (7.34 g, 0.041 mol, 82%) was obtained as a white crystalline solid, MP = 95 °C; found C, 87.41; H, 5.01; N, 7.73%; $M^+_{(massspec.)}$ 179; $C_{13}H_9N$ requires C, 87.12; H, 5.06; N, 7.82%; M, 179; $\bar{\nu}$ 2222 cm^{-1} (—C≡C—); ^{1}H–NMR ($CDCl_3$), (PPM WRT internal TMS) 8.6 (d, 2H), 7.8–7.2 (m, 7H).

1-(4'-Pyridyl)-2-(4'-methoxyphenyl)ethyne (Ib), (9.1 g, 0.043 mol, 87%) was similarly obtained from methoxyphenylethyne (7.8 g, 0.06 mol) as a white crystalline solid, MP = 102 °C; found C, 80.09; H, 5.24; N, 6.81%; $M^+_{(massspec.)}$ 209; $C_{14}H_{11}NO$ requires C, 80.36; H, 5.30; N, 6.70%; M, 209; $\bar{\nu}$ 2225 cm^{-1} (—C≡C—); ^{1}H–NMR ($CDCl_3$), (PPM WRT internal TMS) 8.6 (d, 2H), 7.5 (d, 2H), 7.0 (d, 2H), 3.9 (s, 3H).

Functionalised diarylalkynes (JT), Ia or Ib (0.01 mol) was mixed with the appropriate 1-bromoalkane (0.03 mol) in a 50 cm^3 flask and the mixture warmed in a steam bath for five hours. The crude product was cooled to room temperature, washed with ether (3 × 100 cm^3), and recrystallised from chloroform/ether (10:1, v/v). The yields and some spectroscopic parameters for the compounds made are given in table 1.

2.2. Film deposition and characterisation

Monolayer studies were conducted using a constant-perimeter trough which has been described previously (Petty 1987). The materials were spread from solutions (about 1 mg cm^{-3}) in chloroform (Aristar grade) on to a water subphase at approximately 20 °C. The water was purified by reverse osmosis followed by deionisation and UV sterilisation. During the measurement of isotherms and monolayer deposition, the water pH was 5.6–5.8.

A variety of different substrates were used, including single-crystal silicon wafers and glass slides. Surface plasmon resonance studies were performed with LB layers deposited onto silver-coated glass slides. Infrared spectra were recorded for films deposited onto a silicon attenuated total reflection (ATR) crystal using a Mattson Sirius 100 Fourier transform spectrometer.

The NLO coefficients of monolayer structures were measured using an ATR cell (Cross *et al* 1987). An applied AC field (3 kHz) modulated the cell reflectivity by varying the permittivity of the monolayer. The second-order nonlinear susceptibility $\chi^{(2)}$ $(-\omega; \omega, 0)$ was determined by fitting the experimental results to theoretical reflectivity changes.

Second harmonic generation (SHG) studies of mono- and multilayers were performed at Plessey (Caswell). The apparatus used consisted essentially of a Nd:YAG laser plus appropriate focusing and filtering optics

Table 1. Compounds prepared. All new compounds gave satisfactory microanalyses: C, ±0.35; H, ±0.25; N, ±0.25. The purity of all compounds was checked by HPLC, all displayed single narrow peaks.

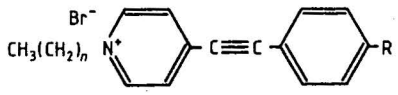

Number	Compound n	Compound R	Yield (%)	λ_{max} (nm)	ν(C≡C) (cm^{-1})	^{1}H–NMR($CDCl_3$) δ(PPM)
JT1	21	H	68	353	2218	9.4d, 7.9d, 7.6–7.9m, 4.9t, 2.0t, 1.2b, 0.8t
JT2	17	H	81	352	2220	9.4d, 7.9d, 7.6–7.2m, 4.8t, 2.0t, 1.2b, 0.8t
JT3	21	OCH_3	75	388	2215	9.3d, 7.9d, 7.5d, 6.9d, 4.8t, 3.8s, 2.1b, 2.0b, 1.2b, 0.8t
JT4	17	OCH_3	76	386	2217	9.4d, 7.9d, 7.5d, 6.9d, 4.8t, 3.8s, 2.0b, 1.9b, 1.2b, 0.8t
JT5	9	OCH_3	78	386	2218	9.3d, 7.9d, 7.5d, 6.9d, 4.9t, 3.9s, 1.9b, 1.8b, 1.2b, 0.8t

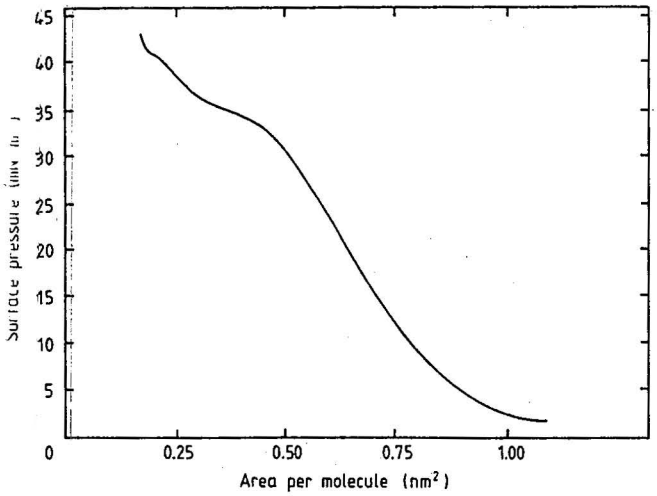

Figure 1. Typical isotherm plot for material JT4.

(Carr *et al* 1987). Trigger pulses were derived from the 1.06 μm fundamental and second-harmonic pulses were detected using a photomultiplier tube. All measurements were taken in reflection mode from samples dipped on Corning 7059 glass.

3. Discussion

3.1. Film formation

All the materials investigated formed reasonably condensed monolayers at the air–water interface. Figure 1 shows an example of a pressure versus area plot for JT4 (compression rate $\simeq 2\,cm^2\,s^{-1}$). This isotherm was fairly representative of all those studied. An exception was that from JT5: in this case no plateau was observed in the pressure–area curve and a very large amount of material needed to be spread on the water surface in order to produce a condensed monolayer—this result is perhaps not surprising in view of the relatively short aliphatic chain for this molecule. The plateau observed in figure 1 is almost certainly related to some molecular rearrangement taking place in the monolayer. Very similar isotherms have been reported by Neal (1987) for a wide variety of LB dye materials. It should be noted that the diarylalkyne moiety in our materials will be fairly rigid. At large molecular areas this group may well be lying on the water surface. As the area is reduced the group would then 'flip' into the upright position to give the condensed area per molecule (above the plateau) of approximately 0.3 nm^2 observed in figure 1.

A summary of the LB deposition characteristics of the materials is given in table 2. These data were obtained for film thicknesses ranging from 1 to 10 layers. Film transfer from the water surface to a variety of solid substrates (dipping speed $\simeq 2\,mm\,min^{-1}$) could be readily effected for most of the materials (again, JT5 was an exception). Mixed deposition modes were

Table 2. Summary of dipping characteristics. Z→ Y: initially Z-type but becomes more Y-type in character as the number of layers increases. Substrates: Al and glass.

Compound	Monolayer formation	Multilayer deposition
JT1	Yes	Y → Z
JT2	Yes	Z → Y
JT3	Yes	Z
JT4	Yes	Z
JT5	Yes	No

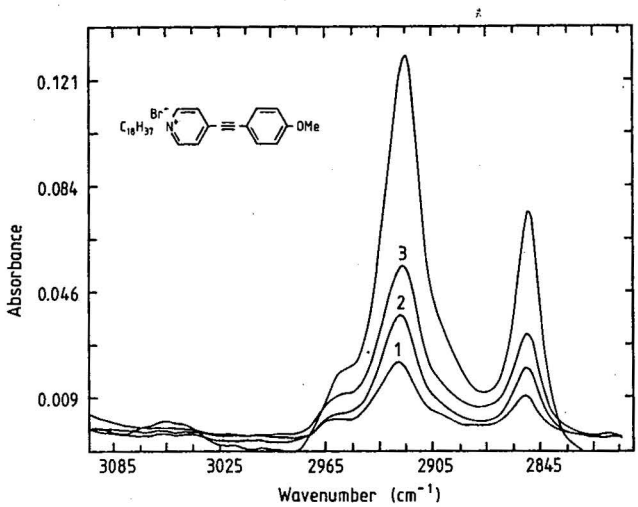

Figure 2. FTIR spectrum for different number of layers of JT4 deposited on silicon ATR crystal.

invariably encountered (Z→ Y in table 2 refers to the deposition of the first few layers being Z-type, but progressively becoming Y-type as further layers are deposited). The most reproducible films (from the viewpoint of deposition) were obtained from JT3 and JT4. These materials exhibited Z-type deposition over the thickness range investigated (1–10 layers) with a deposition ratio of 1.0 ± 0.1.

Figure 2 shows some infrared data for different numbers of monolayers of JT4 deposited onto the silicon ATR crystal; a similar set of spectra was obtained for JT3. The two main absorption peaks, at 2917 cm^{-1} and 2850 cm^{-1}, may be assigned to the asymmetric and symmetric stretching frequencies of the CH_2 groups in the hydrocarbon chains. The intensities of these absorptions scale reasonably well with the number of monolayers, indicating reproducible monolayer deposition in this thickness range.

3.2. NLO characterisation

A preliminary study of the linear and non-linear optical properties of monolayers and multilayers of JT3 was undertaken using the techniques of surface plasmon resonance and second-harmonic generation.

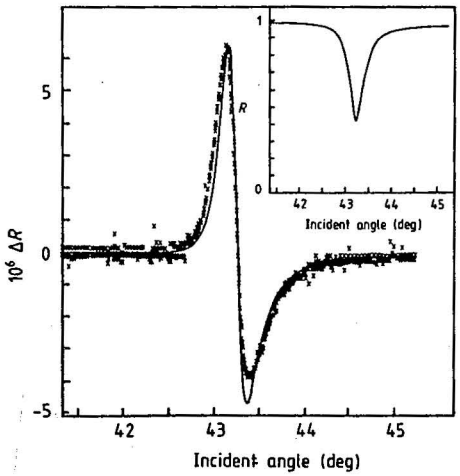

Figure 3. Differential reflectivity measured for one monolayer of JT3 for an applied voltage of 30 V and air gap 1.5 μm. Crosses are the experimental points, full curve is the theoretical fit. The inset shows the DC SPR curve.

The differential reflectivity obtained from the SPR experiment is shown in figure 3: the full curve represents the best (least-squares) fit to the experimental points. The DC resonance curve is given in the inset to figure 3. Values for the permittivity, ε, and film thickness, d, obtained from this are:

$$\varepsilon = 2.33 + 0.54\mathrm{i}$$

$$d = 4.3\ \mathrm{nm}.$$

The finite imaginary component of the permittivity may well be the result of scattering losses in the ATR experiment as JT3 was not found to absorb significantly at the HeNe laser frequency. The measured monolayer thickness agrees well with the overall length of the JT3 molecule (4.3 nm from a space-filling model).

The differential reflection curve in figure 3 yields the following values for the DC-induced changes in the real and imaginary parts of the dielectric constant

$$\Delta\varepsilon = 1.9 \times 10^{-5} + 1.3 \times 10^{-5}\mathrm{i}.$$

When the thickness of the air gap, d, in the ATR cell is much larger than the LB film thickness, then the complex second-order susceptibility $\chi^{(2)}(-\omega;\ \omega,\ 0)$ may be evaluated

$$\chi^{(2)}(-\omega;\ \omega, 0) = \frac{\Delta\varepsilon d\varepsilon_s}{V}$$

where ε_s is the static dielectric constant. Taking experimental values of $V = 30$ V, $d = 1.5\ \mu$m and using $\varepsilon_s = 2.3$ (i.e. the value calculated at 633 nm), then

$$\chi^{(2)}(-\omega;\ \omega, 0) = (1.9 \times 10^{-12} + 1.3 \times 10^{-12}\mathrm{i})\ \mathrm{mV}^{-1}.$$

Although the above figure is approximately two orders of magnitude less than that reported for monolayers of a hemicyanine dye (Cross *et al* 1986) it still represents a significant NLO effect (hemicyanine has one of the largest coefficients for LB materials).

The order of magnitude of the above result has been confirmed using SHG. Taking one layer of the hemicyanine dye as a reference, the second-harmonic signal from one layer of JT3 was found to be approximately 0.02 of that of the hemicyanine. The SHG technique was also used to explore the effect of film thickness on the non-linear optical coefficients of our films. Ideally, the SHG signal strength should be directly proportional to the square of the number of non-centrosymmetrically deposited LB layers. We have observed no such effect for JT3. The largest signal obtained was that for a 10-layer film; this exhibited a second-harmonic signal approximately 0.13 that of the reference hemicyanine monolayer. Many of our multilayer films of JT3 (up to 30 layers) showed second-harmonic intensities that were comparable with single monolayer structures. Such effects have been noted by other workers of Z-type LB layers (Loulergue *et al* 1988) and attributed to some sort of structural reorganisation in the deposited multilayer. Although monolayers of JT3 appear to transfer well to solid substrates in the Z-type deposition mode, subsequent rearrangement of the molecules leads to cancellation of much of the NLO activity.

4. Conclusions

In this work we have reported Z-type LB film deposition for a number of novel diarylalkynes. Although some of these materials exhibited a modest second-order non-linear susceptibility in monolayer form, the expected increase in the intensity of the second-harmonic generation with increasing film thickness was not observed. It is likely that some rearrangement has taken place within the film, giving rise to a more centrosymmetric packing of the molecules.

Z-type LB film deposition is a simple method of building up the non-centrosymmetric structure to exhibit second-order non-linear optical effects. However, it is clear from this work and that of others that much more work is required in order to understand, and ultimately control, the crystal structure of these types of layers.

Acknowledgment

We should like to thank the Science and Engineering Research Council for supporting this work.

References

Ahmad M M, Feast W J, Neal D B, Petty M C and Roberts G G 1986 *J. Mol. Electron.* **2** 129

Allen A D and Cook C D 1963 *Can. J. Chem.* **41** 1084
Allen S, Hann R A, Gupta S K, Gordon P F, Bothwell B D, Ledoux I, Vidakovic P, Zyss J, Robin P, Chastaing E and Dubois J C 1987 *Proc. Soc. Photo-Opt. Eng.* **682** 97
Carr N and Goodwin M J 1987 *Makromol. Chem. Rapid Commun.* **8** 487
Cross G H, Girling I R, Peterson I R and Cade N A 1986 *Electron. Lett.* **22** 1112
Cross G H, Girling I R, Peterson I R, Cade N A and Earls J D 1987 *J. Opt. Soc. Am.* B **4** 962
Earls J D, Peterson I R, Russell G J, Girling I R and Cade N A 1986 *J. Mol. Electron.* **2** 85
Girling I R, Cade N A, Kolinsky P V and Montgomery C M 1985 *Electron. Lett.* **21** 169
Girling I R, Kolinsky P V, Cade N A, Earls J D and Peterson I R 1985 *Opt. Commun.* **55** 289
Kowel S T, Hayden L M and Selfridge R H 1987 *Proc. Soc. Photo-Opt. Eng.* **682** 103
Loulergue J C, Dumont M, Levy Y, Robin P, Pocholle J P and Papuchon M 1988 *Thin Solid Films* **160** 399
Neal D B 1987 *PhD thesis* University of Durham
Neal D B, Petty M C, Roberts G G, Ahmad M M, Feast W J, Girling I R, Cade N A, Kolinsky P V and Peterson I R 1986 *Electron. Lett.* **22** 460
Petty M C 1987 *Polymer Surfaces and Interfaces* ed. W J Feast and H S Munro (New York: Wiley) p 163
Takahashi S, Kuroyama Y, Sonogashira K and Hagihara N 1980 *Synthesis* 627